Spatio-temporal pattern of root exudation and enzyme activities in the rhizosphere

Dissertation

in fullfilment of the requirements for the degree of

Dr. rer. nat.

of the faculty of Mathematics and Natural Sciences

at Kiel University

submitted by

Nataliya Bilyera

born in Sonyachne, Ukraine

Kiel, February 2022

First examiner:	Jun.-Prof. Dr. Bahar S. Razavi
Second examiner:	Prof. Dr. Eva Stukenbrock
Date of the oral examination:	09.05.2022

Summary

Due to the interaction of plants and microorganisms in the rhizosphere, the soil around roots differs greatly in its bio-geochemical composition and activity from bulk soil. Plants can secrete root exudates (e.g., enzymes, benzoxazinoids) to mine nutrients or defend against pathogens. The intensity of rhizosphere processes, such as the release of root exudates, depends on environmental conditions and root properties, such as root hairs. 2-D chemical imaging techniques enable the visualization of enzymes, pH levels, nutrient gradients and water levels around the root. These non-destructive methods can be applied *in situ* and combined to image the soil-root system, and are therefore promising instruments for investigating the interaction of individual rhizosphere processes.

This thesis aims at studying the role of root hairs, benzoxazinoids, soil texture and drought on the spatio-temporal pattern of root exudates and enzyme activities in the rhizosphere. The following 2-D imaging methods were combined to visualize enzyme activity, ^{14}C exudates, soil water, pH values and dissolved nutrients: zymography, phosphor imaging, neutron radiography, planar optodes and diffusive gradients in thin films (DGT). The images were then analyzed for co-localization of the measured parameters. In addition, soil samples were taken locally to measure enzyme kinetics and to conduct microbiome analysis using DNA sequencing. This multi-imaging approach coupled with co-localization analyses was applied for the first time in the laboratory in rhizobox experiments and in the field using root windows.

This thesis revealed, that root hairs enlarged the rhizosphere extent for β-glucosidase, promoted higher leucine aminopeptidase and acid phosphatase activity, inducing the formation of phosphorus depletion zones in three-week-old maize grown in rhizoboxes. Under field conditions, root hairs of 12-week-old maize plants had no significant effect on the level of phosphatase or its activity in the rhizosphere, but soil texture played a more important role, resulting in larger rhizospheres in sandy soil than in loamy soil. Under drought, root hairs widen the rhizosphere to ensure better nutrient mining and water uptake.

Benzoxazinoids are secreted by roots to defend against pathogenic fungi (eg, genus *Fusarium* and *Gibberella*). In this study, benzoxazinoids suppressed the activities of microorganisms in the rhizosphere, resulting in a 30% lower β-glucosidase activity. Increased exudation and activity of enzymes with a plant protection function (e.g. chitinase, β-glucosidase) could not compensate the deficiency of benzoxazinoids used to defend against fungi.

Generally, this thesis showed for the first time that gene knock-out often substantially alters the process-network in the rhizosphere, including its spatial localization along and across the roots. Plant breeding towards increasing the content of benzoxazinoids and the presence of root hairs is a promising tool for better plant protection and improving nutrients acquisition, especially under drought and on sandy soils.

Zusammenfassung

Durch die Interaktion von Pflanzen und Mikroorganismen in der sogenannten Rhizosphäre unterscheidet sich der Boden rund um Wurzeln stark in seiner bio-geochemischen Zusammensetzung und Aktivität vom wurzel-freien Boden. Pflanzen können Wurzelexsudate (z.B. Enzyme, Bezoxazinoiden) ausscheiden, um Nährstoffe aufzunehmen oder sich gegen Krankheitserreger zu wehren. Die Intensität von Rhizosphärenprozessen, wie der Ausscheidung von Wurzelexsudaten, hängt von Umweltbedingungen und Wurzeleigenschaften, wie beispielsweise Wurzelhaaren, ab. Chemische 2D-Bildgebungsverfahren ermöglichen die Visualisierung von Enzymen, pH-Werten, Nährstoffgradienten und Wassergehalten rund um die Wurzel. Diese Verfahren können in situ angewandt werden, zerstören das Boden-Wurzelsystem nicht, sind kombinierbar und somit vielversprechende Instrumente, um das Zusammenspiel einzelner Rhizosphärenprozesse zu untersuchen.

Diese Dissertation zielt darauf ab, den Einfluss von Wurzelhaaren, Benzoxazinoiden, Bodentextur und Wasserstress auf die räumliche und zeitliche Verteilung und Zusammensetzung von Wurzelexsudaten und Enzymaktivitäten in der Rhizosphäre zu untersuchen. Zur Visualisierung von Enzymen, ^{14}C Wurzelexsudate , Wasserhaushalt, pH-Werten und gelösten Nährstoffen wurden folgende 2D-Bildgebungsverfahren kombiniert: Zymographie, Phosphorimaging, Neutronenradiographie, Planare Optoden und Diffusive Gradients in thin films (DGT). Anschließend wurden die Bilder auf Co-Lokalisierung der gemessenen Parameter analysiert. Zusätzlich wurden lokal Bodenproben zu Bestimmung der Enzymkinetik und Mikrobiom-Analyse mittels DNA-Sequenzierung entnommen. Dieser Multi-Imaging-Ansatz gekoppelt mit Co-Lokalisierungsanalysen wurde zum ersten Mal im Labor in Rhizobox-Experimenten und im Feld mit Hilfe von Wurzelfenstern angewendet.

Diese Dissertation zeigte, dass in Rhizoboxen 3-Wochen alte Maispflanzen mit Wurzelhaaren eine größere die Rhizosphäre für β-Glucosidase ausbildeten und eine höhere Aktivität von Leucinaminopeptidase und saurer Phosphatase hatten und breitere Phosphorverarmungszonen als Maispflanzen ohne Wurzelhaare ausbildeten. Unter Feldbedingungen hatten Wurzelhaare von 12-Wochen alten Maispflanzen aber keine signifikante Auswirkung auf das Ausmaß der Phosphatase oder ihrer Aktivität in der Rhizosphäre, sondern die Bodentextur spielte eine bedeutendere Rolle und führte zu größeren Rhizosphären im sandigen Boden als im lehmigen Boden. Bei Trockenheit erweitern Wurzelhaare die Rhizosphäre, um eine höhe Menge von Nährstoffe und Wasser aufzunehmen

Benzoxazinoiden werden von Wurzeln ausgeschieden, um sich gegen pathogene Pilze (z. B. genus *Fusarium* und *Gibberella*) zu wehren. In dieser Studie unterdrückten Benzoxazinoiden die Aktivitäten von Mikroorganismen in der Rhizosphäre, was zu einer um 30 % niedrigeren β-Glucosidase-Aktivität führte. Eine erhöhte Exsudation und Aktivität von Enzymen

mit Pflanzenschutzfunktion (z. B. Chitinase, β-Glucosidase) konnten den Mangel an Benzoxazinoiden von Pilzen nicht kompensieren.

Allgemein zeigte diese Dissertation zum ersten Mal, dass Gen-Knock-out das Prozess-Netzwerk in der Rhizosphäre oft wesentlich verändert, einschließlich seiner räumlichen Lokalisierung entlang und über den Wurzeln. Die Pflanzenzüchtung zur Erhöhung des Gehalts an Benzoxazinoiden und das Vorhandensein von Wurzelhaaren ist ein vielversprechendes Instrument für einen besseren Pflanzenschutz und eine verbesserte Nährstoffaufnahme, insbesondere bei Trockenheit und auf sandigen Böden.

Table of Contents

List of Figures VI
List of Tables XVI
Abbreviations XIX
1 Extended summary 1
General introduction 1
1.1 The influence of rhizosphere traits (root hairs and exudate composition) on rhizosphere processes and microbiome 1
1.2 Abiotic factors (soil texture, drought) 2
1.3 Soil imaging approaches 3
1.4 Objectives 5
1.5 Experiments, materials and methods 7
1.5.1 Plant genotypes 7
1.5.2 Rhizobox experiments 7
1.5.3 Field experiment 7
1.5.4 Labelling method to trace ^{14}C exudates distribution 7
1.5.5 Soil imaging methods 8
1.5.6 Image analysis 9
1.5.7 Enzyme assay 11
1.5.8 Microbiome analysis 11
1.6 Results and discussion 12
1.6.1 Methodological innovations to study the rhizosphere processes 12
1.6.2 Effect of root hairs on rhizosphere processes 14
1.6.3 The influence of benzoxazinoids on soil microbiome and its enzyme activities 18
1.6.4 Effect of drought on for the spatial distribution of microbial activities 20
1.6.5 Effect of soil texture on P mobilization processes 22
1.7 Summary of the main results of the studies 24
1.8 Conclusions and perspectives 27
1.9 References 28
1.10 Contribution to the included manuscripts 32
2 Publications and manuscripts 34
2.1 Study 1. Soil zymography: Simple and reliable? Review of current knowledge and optimization of the method 34
2.2 Study 2: How “hot” are hotspots: Statistically localizing the high-activity areas on soil and rhizosphere images 61

2.3 Study 3. Maize genotype-specific exudation strategies: an adaptive mechanism to increase microbial activity in the rhizosphere....90

2.4 Study 4. Root hairs and protein addition to soil promote leucine aminopeptidase activity of *Hordeum vulgare L.*....122

2.5 Study 5. Co-localised phosphorus mobilization processes in the rhizosphere of field-grown maize jointly contribute to plant nutrition....139

2.6 Study 6. Water availability is more important than exudation for the spatial distribution of microbial activities under drought....188

2.7 Study 7. Effect of root hairs and benzoxazinoids on maize microbiome and its enzymatic activity in the rhizosphere hot- and coldspots....211

3 Acknowledgements....240

4 Declarations....242

List of Figures

Extended abstract:

Figure ES1. Schematic overview of the main research questions and general objectives of the individual studies in this PhD thesis. 6

Figure ES 2. An overview of the imaging methods applied (A) in the rhizobox laboratory experiment or (B) in the root window field experiment. *Taken from Bilyera et al. (2021b) and Bilyera et al. (2022).* 9

Figure ES 3. Steps of image analysis and data integration for obtaining qualitative data from soil images. *Taken from Bilyera et al. (2022)*.....10

Figure ES 4. The main steps of hotspots visualization by soil and plant imaging techniques and the basic principle of statistically localizing hotspots. *Taken from Bilyera et al (2020).* 12

Figure ES 5. The rhizosphere extent for β-glucosidase activity (a) and ^{14}C-labeled root exudates (b). Data are means for each genotype (WT, *rth3* and *bx1*) (n = 4), error bars indicate standard deviations. Letters within one root type mark significant differences among the genotypes at $P < 0.05$. Asterisks on the bracket at the right side indicate significant differences between root sections ('***' $P < 0.001$; '**' $P < 0.01$; '*' $P < 0.05$). *Taken from Bilyera et al. (2021).* 15

Figure ES 6. Rhizosphere extent of leucine aminopeptidase activity (distance from the root surface, mm), for barley genotypes with and without roots hairs and with protein or control (sterile water) addition. Values represent mean ± SE ($n = 90$). Different lowercase letters indicate a significant difference between the protein and control treatments and different uppercase letters indicate a significant difference between the root hair genotype ($p < 0.05$). *Taken from Greenfield et al. (2021).*.....16

Figure ES 7. Average pH, acid phosphatase activity, P and Mn flux as a function of distance to the root surface of two maize genotypes (wild-type (WT) and root hair defective mutant (*rth3*)) grown in loam (L) and sand (S). Coloured error bars represent standard error of $n=6$ (L-WT) or $n=5$ (L-*rth3*, S-WT, S-*rth3*) for pH and acid phosphatase activity; $n=3$ (L-WT, L-*rth3*) or $n=2$ (S-WT, S-*rth3*) for P and Mn flux. The average rhizosphere extent is shown as dark grey areas and was determined from individual concentration-distance plots with a threshold value (mean concentration at distance >2.5mm (*i.e.*, bulk soil +/- 2xSD); light grey areas indicate standard error for the average rhizosphere extent. No rhizosphere extent was defined for P flux. *Taken from Bilyera et al. (2022).* 17

Figure ES 8. Scheme of the main phosphorus mobilization processes in the rhizosphere of wild type maize created based on the results of Study 5. 18

Figure ES 9. Maximum enzyme activity (V_{max}) of β-glucosidase, acid phosphatase, chitinase and leucine aminopeptidase. Data are means for each genotype (*bx1,* WT, and *rth3)* (n=4), error bars indicate standard error. Different capital letters indicate significant difference among the genotypes in coldspots, while lower case letters indicate significant differences among the genotypes in hotspot at $P<0.05$. Asterisks above the bars indicate significant differences between

cold- and hotspot for each genotype ('***' P<0.001; '**' P<0.01; '*' P<0.05, '(*)' P<0.1). *Taken from Bilyera et al. (in preparation).* 19

Figure ES 10. Relative abundance of top soil bacterial (a) and fungal (b) communities at genus level in the soil from the cold- and hotspots of three maize genotypes (WT, *rth3, bx1*). Data are mean of four replicates, except two replicates for *bx1* coldspots. *Taken from Bilyera et al (in preparation).* 20

Figure ES 11 (a) Hotspot (%) and (b) bidirectional rhizosphere extent of β-glucosidase activity for two maize genotypes (wild type and mutant *rth3*) under optimal water content and drought conditions. *p* values were obtained after two-way ANOVA. η^2: effect size; genotype: wild type and mutant *rth3*; water: drought and optimal water content. Data are mean (n=3) and error bars represent standard deviation (SD). *Taken from Zhang et al. (under review).*.....21

Figure ES 12. Michaelis–Menten kinetic parameters, i.e. (a) β-glucosidase activity (V_{max}, nmol g^{-1} h^{-1}) and (b) substrate affinity (K_m, µmol g^{-1} soil), of rhizosphere soil for two maize genotypes (wild type and mutant *rth3*) under optimal water content and drought conditions. *p* values were obtained after two-way ANOVA. η^2: effect size; genotype: wild type and mutant *rth3*; water: drought and optimal water content. Data are mean (n=3) and error bars represent standard deviation (SD). *Taken from Zhang et al. (under review).*.....21

Figure ES 13 Summary of the main findings obtained in individual studies of the PhD thesis ...26

Study 1

Figure 1. Schematic illustration of soil zymography setup and its main steps: a. shows root position and membrane attachment. The inset shows laser scanning for soil surface topography; b. Performance of soil zymography under the initial environmental conditions of the samples; c. Balance between saturating substrate concentration of soil and selected substrate concentration; d. Proper calibration standards; e. Fixed camera settings and photography conditions. *Art work: Tahoora Emam.* 37

Figure. 2. Examples of calibration line: a) when the correlation of gray values and concentrations are linear; b) when the correlation is not linear. When the calibration line shows non-linear behavior, the safe zone of the curve according to the concentration and gray values should be identified and only the linear range of the calibration should be used. -.....41

Figure 3. Intensity of MUF and AMC standard curves with and without NaOH, as well as trend of leucine aminopeptidase activity with and without buffer. 42

Figure 4. Four possible positions of root in soil: i) completely out of the soil surface, ii) partly buried in soil and positioned partly outside of the soil surface, iii) partly buried in soil and positioned at the same level as the soil surface, iv) completely buried in the soil. The eliminated zones around the lupine root (a) corresponding to the similar root position as position (i). (b), shows eliminated zones around the maize root covered by 1 mm gel plate when the root is at a similar position as (i). A clear imprint of enzyme activity on the root and surrounding soil (c) corresponding to the similar root position as (iii). All images are in true color without image processing. 44

Figure 5. Top: a, b and c presenting three different load levels around a soil column. The sub figure of a, shows real soil column. All images are in true color without image processing. Bottom: four incubation durations. The radial diffusion on the membrane after 26 h is clearly detectable.. 46

Figure 6. Detected false signals on membrane saturated by sterile water under UV light. Not a single pixel refers to spot with enzyme activity. (a) Shows the original zymogram in true color and (b) shows the same zymogram after image processing.....48

Figure 7. (a) Example of zymogram (true color), and (b) shows segmented root in green, while blue is root and noise which should be excluded from the analysis (when the whole root is not visible or the contrast between root and background is not sufficient). 50

Figure 8. a) Example of detecting the boundaries of different categories of enzyme activities in the specific gradient (biopores). Percentage of the area of MUF/AMC concentration in the total image is considered as a function of color intensity. Asterisks indicate significant differences between the mean values (modified from Hoang et al., 2016). b) Example of spatial distribution of hotspots in soil treated with and without fertilizer. Long-term N fertilization leads to formation of aggregate hotspots while no fertilization caused dispersed distribution of hotspots. The dotted quadrates represent symbolic applied quadrat counts method on images.....52

Figure 9. a: an example of overlapped ^{14}C image and zymography. The red color corresponds to β-glucosidase activity and white represents ^{14}C release (root exudate). b: An illustrative example of phosphatase activity (blue) and changes of pH (red) along the maize root. In (a) and (b) background (soil) is converted to black to improve the visibility. c: an example of three overlapped images: real root, zymogram, and CO_2 changes. The green color represents the area where leucine-aminopeptidase activity and CO_2 release overlapped. Sub-figures shows: i. roots, ii. leucine-aminopeptidase imprint, and iii. CO_2 release. There are areas where microbial respiration is visible while imprint of enzyme activity is not detectable (or the activity is low). 53

Study 2

Figure 1. An example of the grey value distribution (from 0 to 255) for leucine aminopeptidase activity in soil (data extracted from the 8-bit image in Fig. 6b in Razavi et al., 2017). The dashed curve reflects the normal distribution of the grey values of the soil background for enzyme activity with its mean + 2 standard deviations (presented as vertical dashed lines). The hotspot area (S) thresholded by the Mean+2SD approach corresponds to 12% of the whole image. Because the Top-25% approach is strongly biased by the highest grey value (here 255), only 0.2% of the total area are highlighted as hotspots. 67

Figure 2. Original soil zymograms of leucine aminopeptidase (Razavi et al., 2017) and hotspots (red) identified using Top-25%, Mean+2SD and Mean+3SD approaches (compare Fig. 1). Numbers on top left show the percentage of the total image area belonged to the hotspots. 68

Figure 3. Original and binarized images of roots and exudates in soil after labeling the plants with $^{14}CO_2$ (Holz et al., 2018). The hotspots (red) were identified using Top-25%, Mean+2SD and

Mean+3SD approaches. Numbers on top left show the percentage of the total image area belonged to the hotspots. 68

Figure 4. Original and binarized images of ^{14}C-labeled glyphosate in plants (Fig 5 D, Pereira et al., 2019). The hotspots (red) were identified using Top-25%, Mean+2SD and Mean+3SD approaches. Numbers on top left show the percentage of the total image area belonged to the hotspots. 69

Figure 5. Hotspots in % of the total area thresholded by 17 thresholding built-in methods in ImageJ and Mean+2SD, Mean+3SD or Top-25% for three test images: a) soil zymogram for leucine aminopeptidase (Razavi et al., 2017); b) ^{14}C image for $^{14}CO_2$-labeled root and exudates in soil and c) ^{14}C image of ^{14}C-labeled glyphosate in plants (Pereira et al., 2019). 72

Figure 6. Normalized grey value activities for mean and standard deviation values for background and hotspots separated by 17 thresholding built-in methods in ImageJ and Mean+2SD, Mean+3SD or Top-25% for three test images: a) soil zymogram for leucine aminopeptidase (Razavi et al., 2017); b) ^{14}C image for $^{14}CO_2$-labeled root and exudates in soil (Holz et al., 2018) and c) ^{14}C image of ^{14}C-labeled glyphosate in plants (Pereira et al., 2019). 74

Figure S1. An example of the original grey value distribution (bars) for a) leucine aminopeptidase activity in soil (data extracted from the 8-bit image in Fig. 6b in Razavi et al., 2017); b) ^{14}C image for $^{14}CO_2$-labeled root and exudates in soil (Holz et al., 2018) and c) ^{14}C image of ^{14}C-labeled glyphosate in plants (Pereira et al., 2019) and two fitted normal distributions using the normalmixEM function in R. Red and green lines denote comp 1 and comp 2 distributions in the summary table. As shown at a) red (comp 1) normal distribution covers (lambda (λ)) 89% of the values, while green covers only 11%. Mean values (mu (μ)) and SD (sigma (σ)) were 39 and 81, and 9 and 40 for red and green distribution, respectively. 84

Figure S2. Montage image with results from all built-in thresholding methods in ImageJ (Schindelin et al., 2012) applied to the soil zymogram for leucine aminopeptidase (Razavi et al., 2017). 85

Figure S3. Montage image with results from all built-in thresholding methods in ImageJ (Schindelin et al., 2012) applied to a ^{14}C image of ^{14}C-labeled glyphosate in plants (Pereira et al., 2019). 86

Figure S4. Montage image with results from all built-in thresholding methods in ImageJ (Schindelin et al., 2012) applied to a ^{14}C image for $^{14}CO_2$-labeled roots and exudates in soil (Holz et al., 2018). 87

Study 3

Figure 1. Root images (real light photos) (a,b,c), zymograms of β-glucosidase activity (d,e,f), ^{14}C phosphor images (g,h,i), and neutron radiographs (j,k,l) of three maize genotypes (WT, *rth3* and *bx1*). Side color or gray scales are proportional to β-glucosidase activity (pmol cm^{-2} h^{-1}), ^{14}C activity (MBq) and to volumetric water content. Always one representative replicate out of four was chosen. WT: wild-type maize, *rth3:* root-hair defective mutant*; bx1:* mutant with reduced benzoxazinoids in root exudates. 101

Figure 2. The rhizosphere extent for β-glucosidase activity (a) and ^{14}C-labeled root exudates (b). Data are means for each genotype (WT, *rth3* and *bx1*) (n = 4), error bars indicate standard deviations. Letters within one root type mark significant differences among the genotypes at $P < 0.05$. Asterisks on the bracket at the right side indicate significant differences between root sections ('***' $P < 0.001$; '**' $P < 0.01$; '*' $P < 0.05$).....102

Figure 3. Mean of *β*-glucosidase activity in bulk soil (shaded) and in the rhizosphere along the mature root and root tips. Data are means for each genotype (WT, *rth3* and *bx1*) (n = 4), error bars indicate standard deviations. Letters within one root section mark significant differences among the genotypes at $P < 0.05$. Capital letters refer to bulk soil, while lower case letters refer to rhizosphere soil. Relative increase (fold, times) in β-glucosidase activity along mature root and at root tip compared to bulk soil is marked over arrow at each column. The vertical thin dashed line separates the bars for bulk and rhizosphere activities. 103

Figure 4. Region of interest (ROIs) images of hotspots for (a) exudates and β-glucosidase activity; and (b) β-glucosidase activity and water content, and their overlap image for three maize genotypes (WT, *rth3, bx1*). The results of co-localization analysis are given as means of four replicates and presented by overlap coefficient (r) and two Manders coefficients (M1 and M2, see detailed explanation in Fig. S3). Asterisks on the values indicate significant difference between genotypes ('*' $P < 0.05$; '**' $P < 0.01$; '***' $P < 0.001$). 105

Figure 5. General pattern of the effects of maize mutations (root-hair defective *rth3* and benzoxazinoids (BX) deficient *bx1* as compared to wild-type *(*WT) on the rhizosphere extent, hotspots, enzyme activity gradient and overlap of β-glucosidase with exudates. Significant increase and decrease indicated by ↑ and ↓, respectively. 110

Figure S1. Linear correlation between the gray values of the calibration membranes incubated for one hour and methylumbelliferone (MUF) concentrations. 111

Figure S2. Sketch of rhizosphere thresholding methodology: a) an example of zymogram with five rectangles (B1-B5) which represent the areas of background β-glucosidase activity; b) gray values plotted against the distance.....112

Figure S3. Schematic illustration of quantitative co-localization of activities/hotspots on two images A (Hotspot 1 – red) and B (Hotspot 2 – green) hotspots. Yellow part indicates 48% of overlap between two hotspot images (r=0.48); Manders coefficient 1 indicates that 44% of Hotspot 1 (yellow fraction of red hotspot) is considered as co-localized with Hotspot 2 (M1=0.44); Manders coefficient 2 indicates that 65 % of Hotspot 2 (yellow fraction of green hotspot) is considered as co-localized with Hotspot 1 (red hotspot) (M2=0.65). 113

Figure S4. Hotspots for *β*-glucosidase activity and ^{14}C exudation. Data are means for each genotype (WT, *rth3* and *bx1*) (n=4), error bars indicate standard deviations. Letters within one hotspot type marks significant differences among the genotypes at $P<0.05$.....114

Study 4

Figure 1. Rhizobox set-up showing the position of the protein and control (sterile water) horizontal bands in soil.....126

Figure. 2. Examples of barley roots grown in rhizoboxes (A) and the spatial distribution of leucine aminopeptidase activity in the soil and rhizosphere of barley roots (B) with and without root hairs. Side colour bar is proportional to the enzyme activity (pmol mm^{-2} h^{-1}) and protein (P) and control (C) band positions are indicated on the right-hand side of the zymograms.....130

Figure 3. Rhizosphere extent of leucine aminopeptidase activity (distance from the root surface, mm), mean leucine aminopeptidase activity (LAP) across the rhizosphere and maximum leucine aminopeptidase activity of the rhizosphere (pmol AMC mm^{-2} h^{-1}) for barley genotypes with and without roots hairs and with protein or control (sterile water) addition. Values represent mean ± SE (n = 90). Different lowercase letters indicate a significant difference between protein and control treatments and different uppercase letters indicate a significant difference between root hair genotype (p < 0.05).....131

Figure 4. The kinetic parameters V_{max} (nmol AMC g^{-1} h^{-1}) and K_m (µmol AMC g^{-1}) of soil leucine aminopeptidase activity for barley genotypes with and without roots hairs and with protein or control (sterile water) addition. Values represent mean ± SE (n = 3). Different lowercase letters indicate a significant difference between protein and control treatments and different uppercase letters indicate a significant difference between root hair genotype (p < 0.05).....132

Study 5

Figure 1. Custom designed root window construction at the experimental field site of the DFG priority program 2089 “Rhizosphere Spatiotemporal Organisation – A Key to Rhizosphere Functions”. (a) Experimental plot (loam) with newly installed root window construction and observation pit at the short end of the plot. (b) Close-up of the root window construction, with observation window being covered by two removable PVC boards that are pressed against the soil plot with aluminium bars and wing bolts for stability and protection against light. (c) Root window observation area (60 x 60 cm) of a loam plot planted with *Zea mays* L. wild-type (B73) at growth stage BBCH 59. (d) Root window pits covered by wooden boards in between sampling campaigns. 145

Figure 2. Exemplary root images, pH, acid phosphatase activity (pmol mm^{-2} h^{-1}), P flux and Mn flux (pg cm^{-2} s^{-1}) images (overlaid on the corresponding root image with 50% transparency) of two maize genotypes (wild-type (WT) and root hair defective mutant (*rth3*)) grown in root windows on loam (L) and sand (S) in the field. The identification number of each field plot (FP) is indicated in the top part of root images. Dotted circles highlight actively growing roots during method application. Red arrows highlight P hotspots at actively growing root tips and white arrows indicate possible P depletion zones around older roots.....151

Figure 3. Average pH, acid phosphatase activity, P and Mn flux as a function of distance to the root surface of two maize genotypes (wild-type (WT) and root hair defective mutant (*rth3*)) grown in loam (L) and sand (S). Coloured error bars represent standard error of n=6 (L-WT) or n=5 (L-*rth3*, S-WT, S-*rth3*) for pH and acid phosphatase activity; n=3 (L-WT, L-*rth3*) or n=2 (S-WT, S-*rth3*) for P and Mn flux. The average rhizosphere extent is shown as dark grey areas and was determined from individual concentration-distance plots with a threshold value (mean

concentration at distance >2.5mm (*i.e.*, bulk soil +/- 2xSD); light grey areas indicate standard error for the average rhizosphere extent. No rhizosphere extent was defined for P flux.....153

Figure 4. Averaged (a) pH, (b) acid phosphatase activity, (c) P and (d) Mn fluxes of bulk soil (area excluding root surface mask enlarged by 2.5 mm), rhizosphere (individual rhizosphere extent) and root surface (area of image covered by root tissue only) of two maize genotypes (wild-type (WT) and root-hair defective mutant (*rth3*)) grown in loam (L) and sand (S). Error bars represent SE of n = 6 (L-WT), or n = 5 (L-*rth3*, S-WT, S-*rth3*) for pH and acid phosphatase; n = 3 (L-WT, L-*rth3*) or n = 2 (S-WT, S-*rth3*) for P and Mn flux*. Note: P rhizosphere flux was measured within the area of Mn rhizosphere extent, as no P rhizosphere extent could be defined.* Letters above the bars indicate significant differences between treatments according to two-way ANOVA for each spatial domain according to Tukey post-hoc test, *i.e.,* root surface (a), rhizosphere (k-m), and bulk (x-y). Asterisks indicate significant differences between the spatial domains (bulk, rhizosphere, root surface) within one treatment (one-way ANOVA, '.' *p<0.10*, '*' *p<0.05*, '**' *p<0.01, '***' p<0.001*). 154

Figure 5. Hotspot coverage of pH (a), acid phosphatase activity (b), P flux (c), and Mn flux (d) on the root surface, in the individual rhizosphere and in the bulk soil expressed as relative percentage based on the total area of respective spatial domain. Bars and error bars represent mean and standard error of L-WT (n = 6), L-*rth3* (n = 5), S-WT (n = 5), S-*rth3* (n = 5) for pH and phosphatase, for P and Mn flux, L-WT and L-*rth3* (n = 3); and S-WT and S-*rth3* (n=2). Note that P rhizosphere flux was measured in the Mn rhizosphere. Asterisks indicate significant differences between root surface, rhizosphere, bulk hotspot coverage according to one way-ANOVA (' ' n.s., '.' *p* <0.10, '*' *p < 0.05*, '**' *p< 0.01*). 155

Figure 6. Spatial differences along root axis: Root surface pH (a), and acid phosphatase activity (b), P (c) and Mn flux (d) of young (< 2 cm from root cap) and older root tissue (> 4 cm from root cap). Number below each bar represents replicates (individual root sections on which the parameter was measured). Asterisks indicate significant differences between young and older tissues (*t-test* with '.' p < 0.10, '*' *p < 0.05*, '**' *p< 0.01*). Letters indicate significant differences between the treatments for young tissues (a-c) and old tissues (k) (two-way ANOVA *p < 0.05*, Tukey post-hoc test).....157

Figure S1. Image analysis workflow on the example of a ROI image of acid phosphatase activity. Step 1 shows the photograph of ROI in the window of field plot 15 (S-WT) and the corresponding zymogram. Step 2 depicts the concentration-distance plot of this ROI: the black line represents the average phosphatase activity for each distance class (*i.e.* 1 pixel = 0.038 mm) as a function of distance to the root mask, the light grey error bars show the standard deviation within each distance class. The blue line represents the bulk average phosphatase activity at a distance >2.5mm from the root surface, while the dotted lines represent the standard deviation. The red line represents the threshold (bulk + 2x SD) for determining the rhizosphere extent and hotspots. Step 3 shows the areas to measure the average activity within each spatial domain, *i.e.,* the root surface in black, the rhizosphere in grey and bulk soil in white. Step 4 shows how much of each spatial domain is covered by hotspots (*i.e.*, areas of phosphatase activity > threshold, in red colour). Step 5 shows the hotspot area of two parameters (here pH-only in red, phosphatase-only in green) and the common area of both hotspot areas in yellow for the root surface and the standardized rhizosphere (2.5 mm from the root surface). The overlap coefficient (r) gives the

share of common hotspot area within the cumulative area of the pH and phosphatase activity hotspot area. Step 6 refers to the assessment of spatial changes along the root axis, *i.e.*, measurements at young root tissues (< 2 cm from the root cap) and older root sections (> 4 cm from the root cap).....175

Figure S2. pH replicate regions of interest (ROI) used for image analysis.....176

Figure S3. Acid phosphatase activity replicate regions of interest (ROI) used for image analysis (a) and an exemplary of the entire zymograms for each treatment (b). 177

Figure S4. P flux (left side) and Mn flux (right side) replicate regions of interest (ROI) used for image analysis. 178

Figure S5. Labile calcium (Ca) net intensity in DGT replicate regions of interest (ROI). Note: high Ca concentration in the elongation zone of roots that grew during method application, i.e., middle root in FP15-O2, and both roots in FP15-O3 (red arrows).....179

Figure S6. Labile zink (Zn) accumulated on DGT gels. Circles highlight root tips with a diameter > 1mm (orange) and ~0.5 mm (green). Red arrows show root tips that grew out of the ROI during DGT application. 180

Study 6

Figure 1. Spatial distribution of β-glucosidase activity for two maize genotypes (wild type and mutant *rth3*) under optimal water content (a & b) and drought conditions (c & d). The color scale is proportional to β-glucosidase activity (nmol cm^{-2} h^{-1}). *Note*: for Fig. 1d, a root photo was overlapped with zymogram to link root compartments with enzymatic hotspots, and the small figure in the upper left corner is original zymogram. 196

Figure 2 (a) Hotspot (%) and (b) bidirectional rhizosphere extent of β-glucosidase activity for two maize genotypes (wild type and mutant *rth3*) under optimal water content and drought conditions. *p* values were obtained after two-way ANOVA. η^2: effect size; genotype: wild type and mutant *rth3*; water: drought and optimal water content. Data are mean (n=3) and error bars represent standard deviation (SD). 197

Figure 3 Michaelis–Menten kinetic parameters, i.e. (a) β-glucosidase activity (V_{max}, nmol g^{-1} h^{-1}) and (b) substrate affinity (K_m, µmol g^{-1} soil), of rhizosphere soil for two maize genotypes (wild type and mutant *rth3*) under optimal water content and drought conditions. *p* values were obtained after two-way ANOVA. η^2: effect size; genotype: wild type and mutant *rth3*; water: drought and optimal water content. Data are mean (n=3) and error bars represent standard deviation (SD). ..
.....197

Figure 4 Spatial distribution of root exudates for two maize genotypes (wild type and mutant *rth3*) under optimal water content (a & b) and drought conditions (c & d). *Note:* different scales for drought and optimal water content. 198

Figure 5 (a) Percentage of hotspot and (b) bidirectional rhizosphere extent of root exudates for two maize genotypes (wild type and *rth3* mutant) under optimal water content and drought conditions. *p* values were obtained after two-way ANOVA. η^2: effect size; genotype: wild type and

mutant *rth3*; water: drought and optimal water content. Data are mean (n=3) and error bars represent standard deviation (SD).....199

Figure 6. Region of interest (ROIs) of soil water spatial distribution for two maize genotypes (wild type and mutant *rth3*) under optimal water content (a & b) and drought conditions (c & d). Side color scale is proportional to volumetric water content. 200

Figure 7 Bidirectional rhizosphere extent of soil water content for two maize genotypes (wild type and mutant *rth3*) under optimal water content and drought conditions. *p* values were obtained after two-way ANOVA. η^2: effect size; genotype: wild type and mutant *rth3*; water: drought and optimal water content. Data are mean (n=3) and error bars represent standard deviation (SD). ..
.....200

Figure 8 Colocalization analysis for region of interest (ROIs) of (a) hotspots between β-glucosidase activity (Enzyme) and ^{14}C exudates (Exudates), or (b) hotspots between β-glucosidase activity (Enzyme) and water content (Water). M1: Manders' coefficient, the fraction of Enzyme overlapping with Exudates or Water; M2: Manders' coefficient, the fraction of Exudates or Water overlapping with Enzyme; *p* values were obtained after two-way ANOVA. genotype: wild type and mutant *rth3*; water: drought and optimal water content. Upper case letters in (a): significant differences for M1 between optimal and drought conditions after two-way ANOVA and Student's t-test at $p < 0.05$. Upper case letters in (b): significant differences for M1 among four treatments after two-way ANOVA analysis and Tukey's HSD test at $p < 0.05$. Lower case letters in (a) and (b): significant differences for M2 between optimal and drought conditions after two-way ANOVA and Student's t-test at $p < 0.05$.....201

Figure 9 Root hairs induced larger hotspot area and broader rhizosphere extent of β-glucosidase activities, as well as higher potential β-glucosidase activities (V_{max}) than that for the maize mutant. Drought widened the rhizosphere extent of root exudates and soil water. Co-localization analysis showed that enzymatic hotspots are more co-localized with hotspots of root exudates under optimal water conditions. In contrast, enzyme hotspots showed higher dependency on water hotspots under the scarcity of both water and root exudates.....205

Figure S1. (a) root images and (b) total root length on the soil surface for two maize genotypes (wild type and mutant *rth3*) under optimal water content and drought conditions. *p* values were obtained after Scheirer-Ray-Hare test. genotype: wild type and mutant *rth3*; water: drought and optimal water content. Data are mean (n=3) and error bars represent standard deviation (SD). ..
.....210

Study 7

Figure 1. Maximum enzyme activity (V_{max}) of β-glucosidase, acid phosphatase, chitinase and leucine aminopeptidase. Data are means for each genotype (*bx1,* WT, and *rth3)* (n=4), error bars indicate standard error. Different capital letters indicate significant difference among the genotypes in colspots, while lower case letters indicate significant differences among the genotypes in hotspot at *P<0.05*. Asterisks above the bars indicate significant differences between cold- and hotspot for each genotype ('***' *P*<0.001; '**' *P*<0.01; '*' *P*<0.05, '(*)' *P*<0.1).....220

Figure 2. K_m values of β-glucosidase, acid phosphatase, chitinase and leucine aminopeptidase. Data are means for each genotype (*bx1,* WT, and *rth3)* (n=4), error bars indicate standard error. Different capital letters indicate significant difference among the genotypes in coldspots, while lower case letters indicate significant differences among the genotypes in hotspot at *P<0.05*. Asterisks above the bars indicate significant differences between cold- and hotspot for each genotype (‘***’ *P*<0.001; ‘**’ *P*<0.01; ‘*’ *P*<0.05, ‘(*)’ *P*<0.1). 221

Figure 3. Catalytic efficiency (K_a) of β-glucosidase, acid phosphatase, chitinase and leucine aminopeptidase. Data are means for each genotype (*bx1,* WT, and *rth3)* (n=4), error bars indicate standard error. Different capital letters indicate significant difference among the genotypes in colspots, while lower case letters indicate significant differences among the genotypes in hotspot at *P<0.05*. Asterisks above the bars indicate significant differences between cold- and hotspot for each genotype (‘***’ *P*<0.001; ‘**’ *P*<0.01; ‘*’ *P*<0.05, ‘(*)’ *P*<0.1).....222

Figure 4. Turnover time at the lack of substrate of four enzymes: β-glucosidase, acid phosphatase, chitinase and leucine aminopeptidase. Data are means for each genotype (*bx1,* WT, and *rth3)* (n=4), error bars indicate standard error. Different capital letters indicate significant difference among the genotypes in colspots, while lower case letters indicate significant differences among the genotypes in hotspot at *P<0.05*. Asterisks above the bars indicate significant differences between cold- and hotspot for each genotype (‘***’ *P*<0.001; ‘**’ *P*<0.01; ‘*’ *P*<0.05, ‘(*)’ *P*<0.1). 224

Figure 5. Microbial biomass carbon (C_{mic}) (a) and Shannon diversity for bacterial and fungal diversity (b). Data are means for each genotype (*bx1,* WT, and *rth3)* (n=4), error bars indicate standard error. Different capital letters indicate significant difference among the genotypes in colspots, while lower case letters indicate significant differences among the genotypes in hotspot at *P<0.05*. Asterisks above the bars indicate significant differences between cold- and hotspot for each genotype (‘***’ *P*<0.001; ‘**’ *P*<0.01; ‘*’ *P*<0.05, ‘(*)’ *P*<0.1).....225

Figure S1. An exemplary image of the hot- and coldspot localization of β-glucosidase activity in the rhizosphere. 237

Figure S2. Rarefaction analysis of the soil hot- and coldspot fungal (a) and bacterial (b) microbiome. The sampling intensity plot shows the detected ASVs number (y-axis) depending on the sequencing depth-(x-axis). When the curves reach plateau at sequencing depth, they were sufficiently deeply sequenced. Vertical black line marks the sample with the smallest number of sequences across all samples. 238

Figure S3. Non-metric multidimensional scaling (NMDS) plot of the bacterial and fungal community structure associated with rhizosphere hot or coldspots of the maize genotypes (WT, *rth3, bx1*).....239

List of Tables

Extended abstract:

Table ES 1. Summary of the *in situ* soil imaging techniques applied in the studies of PhD thesis. ……..
Error! Bookmark not defined.

Table ES 2. Summary of the approaches applied for image analysis 9

Table ES 3. Synthesis of methodological innovations and main conclusions 13

Study 1:

Table 1. Enzymes commonly imaged in environmental samples, and their organic matter constituents and substrates.....40

Table 2. Summary of abiotic and biotic factors which may distort results. 55

Study 2:

Table 1. Approaches to hotspot determination of selected soil parameters in 2-D images 65

Table 2. Comparison of hotspot areas on three images of activity distribution in soils or plants calculated by Mean+2SD, Mean+3SD and Top-25% approaches. 71

Table S1. Results of two-samples t-Test for hotspot mean values between statistical approaches (Mean+2/3SD) and standard methods in ImageJ and Top-25% 88

Study 3:

Table S1. Degrees of co-localization as fuzzy linguistic variables and the respective ranges of values of popular coefficients used to estimate co-localization, such as PC, r, and M1(M2), (Zinchuk *et al.*, 2013). 115

Table S2. Result of co-localization analysis for the whole image of water content at neutron image (Water), ^{14}C exudates (Exudates) and *β*-glucosidase activity (Enzyme). The co-localization parameters are overlay coefficient (r), Mander's coefficient 1 (M1) and 2 (M2). Data are means for each genotype and parameter (n=4) ± standard deviations. Capital letters mark significant differences among the genotypes at *P<0.1.* Asterisks on the p-values indicate significant differences between root type ('(*)'*P<0.1;* '*' *P<0.05*; '**' *P<0.01;* '***' *P<0.001*). 116

Study 4:

Table 1. General properties of the soil used in the experiments. Values are expressed on a dry weight basis and represent mean ± SE (*n = 3*).....125

Table 2. Root area and leucine aminopeptidase hotspot of the two barley genotypes per plant. Values represent mean ± S.E (*n = 3*). Different lowercase letters indicate a significant difference between genotypes ($p < 0.05$).....129

Table 3. Two-way ANOVA results for each of the measured variables using $p < 0.05$ as the cut-off for statistical significance (as indicated by values in bold). 130

Study 5:

Table 1. General substrate characteristics before fertilization. Data are represent mean ± standard error (*n*=12) (from Vetterlein et al. (2021).....143

Table 2. Application sequence of imaging techniques including number of zymograms, optodes and DGT gels applied, number of regions of interest (ROI) used for image analysis with corresponding position (distance from the soil surface) within the root window. Biological replicates are represented by the root system grown in individual root window from different field plots Note that analysed DGT replicates were limited due to application challanges in the field (cavities, poor contact).....148

Table 3. Top: Overlap coefficients for co-localized hotspots of acidification (pH), acid phosphatase, P and Mn flux in two spatial domains (root surface and rhizosphere) across treatments. Data represent means ± SE, following by the number of replicates for pairs of parameters in parentheses (n). Bottom: *p-values* from two-way ANOVA comparing the effect of substrate, genotype, and their interaction across treatments within each parameter combination. Significant effects ($p<0.05$) are marked in bold. Different letters in each column indicate significant ($p<0.05$) difference between treatments within each parameter combination as revealed by the corresponding Tukey post-hoc test. 156

Table S1. Two-way ANOVA and post-hoc Tukey test results for averaged rhizosphere extents (corresponding to data shown in Fig. 3) across treatments within each parameter (pH, phosphatase, P-flux, Mn-flux). Different letters in columns indicate significant (*p<0.05*) difference between treatments within each parameter.....181

Table S2. Two-way ANOVA and post-hoc Tukey test results for average bulk, rhizosphere and root surface pH, acid phosphatase, P and Mn fluxes across treatments within each spatial domain (corresponding to data shown in Fig. 4). Different letters in column indicate significant (*p<0.05*) difference between treatments within spatial domain. *P-values* are given *in italics* for each factor (Substrate, Genotype) and their interaction. Asterisks on the *P-values* indicate significant differences between soils, genotypes or their interactions. Significant factors (*p<0.05*) are marked in bold.....182

Table S3. Two-way ANOVA results comparing hotspot coverage (corresponding to data shown in Fig. 5) across treatments within each parameter (pH, phosphatase, P-flux, Mn-flux) and spatial domain (root surface, individual rhizosphere, bulk soil). Significant factors ($p<0.05$) are marked in bold.....183

Table S4. The results of one-way ANOVA and Tukey post-hoc test for comparison of hotspot coverage in spatial domains (root surface, individual rhizosphere, and bulk soil) within each treatment (corresponding to data shown in Fig. 5). *P-values* in bold indicate significant (*p<0.05*)

difference between spatial domains. Different letters in rows indicate significant (*p<0.05*) differences between hotspot coverage of root surface, rhizosphere and bulk soil in each treatment.....184

Table S5. The results of *t-test* for paired means comparison of overlap coefficient on root surface and in the standardized rhizosphere (corresponding to data shown in Table 3). *P-values* in bold indicate significant (*p<0.05*) difference between overlap coefficients at root surface and in the rhizosphere in each treatment. 185

Table S6. The results of t-test for paired means comparison of root surface young (< 2cm from root cap) and older root tissue (> 4 cm from root cap), and older root tissues and bulk soil pH, acid phosphatase activity, P and Mn-fluxes (corresponding to data shown in Fig. 6). Significant differences (*p<0.1*) are shown in bold. 186

Study 7:

Table 1. Root traits of the maize genotypes (wild-type (WT), *rth3* and *bx1*) and their role for microbial activity in the rhizosphere and plant nutrition..... Error! Bookmark not defined.214

Table 2. Vector length and vector angle for the ration of enzyme activities in the hotspot and coldspot of three maize genotypes (WT, *rth3* and *bx1*). Different capital letters indicate significant difference among the genotypes in the colspots, while lower case letters indicate significant differences among the genotypes in the hotspots at *P<0.05*. Asterisks indicate significant differences between cold- and hotspot for each genotype ('***' *P*<0.001; '**' *P*<0.01; '*' *P*<0.05, '(*)' *P*<0.1; 'ns' *P*>0.1). ..... Error! Bookmark not defined.

Table S1. Barcode to sample assignments 235

Table S2. Beta diversity by PERMANOVA analysis. Significant (Pr<0.1) values are marked in bold. 236

Abbreviations

2-D	Two dimensional
ANOVA	Analysis of Variance
BBCH	**B**iologische **B**undesanstalt, Bundessortenamt und **CH**emische Industrie
BSA	Bovine serum albumin
BX	Benzoxazinoids
C	Carbon
CEC	Cation exchange capacity
CO_2	Carbon dioxide
df	degrees of freedom
DGT	Diffusion in thin films
EM	Expected
FP	Field plot
JACoP	Just another co-localization plug-in
K_a	Substrate efficiency
K_m	substrate affinity, a concentration at half-maximum rate
LA-ICPMS	Laser ablation Inductively coupled plasma mass-spectroscopy
LAP	leucine aminopeptidase activity
M1 and M2	Manders' coefficient
Mn	Manganese
MUF	methylumbelliferone
N	Nitrogen
P	Phosphorus
p	*p* value
PC	Pearson's correlation coefficient
P_i	Inorganic phosphorus
P_o	Organic phosphorus
PVC	Polyvinyl chloride
r	Overlap coefficient
ROI	Region of interest
SD	Standard deviation
SOM	Soil organic matter
UV	Ultraviolet

V_{max}	Maximum potential enzyme activitiy
WHC	Water holding capacity
WT	Wild type
η2	Effect size

1 Extended summary

General introduction

The simultaneous increase of the world's population and the shortage of non-renewable resources for production of fertilizers combined with limited area appropriate for cropping require a revision of fertilization and crop breeding strategies in modern agriculture. Rhizosphere management is one of the promising practices to build nutrient-efficient agroecosystems using a full potential of crops including their ability to resist against soil-born phytopathogens (Canarini et al., 2019; Zhang et al., 2010). Rhizosphere engineering allows increasing crop productivity with restricted resource availability and ensures environmental protection (Zhang et al., 2010). However, prior to implementation of rhizosphere management, detailed knowledge of multiple rhizosphere processes is needed. Despite many efforts to study rhizosphere since Hiltner's definition (Hiltner, 1904), a holistic picture of rhizosphere functioning still remains restricted (York et al., 2016).

1.1 The influence of rhizosphere traits (root hairs and exudate composition) on rhizosphere processes and microbiome

Plants and microorganisms interact in the rhizosphere, accelerating the process rates of nutrient mining beyond those in bulk soil (Koranda et al., 2011, Berg and Smalla, 2009; Philippot et al., 2013; Yang et al., 2017). Rhizosphere traits such as root morphology and exudates' composition are essential for these interactions in the rhizosphere.

Root morphology plays a major role in determining the quality, quantity and distribution of exudates on the surface of the root. A key root morphological trait, which is known to increase carbon (C) substrate availability for microorganisms, is the presence of root hairs (Holz et al., 2018; Jones et al., 2009). Root hairs enable higher root surface area coming in direct contact with rhizosphere (Haling et al., 2013; Silberbush and Barber, 1983), and hence the zone of root hairs has the greatest potential for nutrient and water uptake (Brown et al., 2013 Itoh and Barber, 1983).

Roots exude primary metabolites ensure plant nutrition and secondary metabolites to defend the plant against pathogenic microorganisms (Erb and Kliebenstein, 2020; Jones et al., 2009; Vives-Peris et al., 2020). The primary metabolites induce rhizosphere acidification, facilitate higher microbial activity and promote the mineralization of soil organic matter (SOM). Enzyme activity is crucial for the process of SOM decomposition, which is also responsible for C (i.e., glucose), phosphorus (P) and nitrogen (N) mining in the rhizosphere. Enzymes are either released directly from the roots into the soil (Cairns and Esen, 2010) or produced by microorganisms often

facilitated by plants via releasing easily available organic substances (Bertin et al., 2003). The exudation of protons promote rhizosphere acidification, which provides favourable conditions for nutrient (e.g. P) mobilization in soil (Bertrand et al., 1999). Rhizosphere acidification alone with carboxylate anions from organic acids may also increase P availability and contribute to ligand-promoted mineral P dissolution (Oburger et al., 2011, 2009). Besides, protons released by roots shift the pH optimum in favour of increased acid phosphatase activity (Dick et al., 2000), thus indirectly promoting P mineralization and SOM decomposition.

During the growing period, plant experiences not only nutrients limitation, but also face herbivores damage. In response to this damage, some plants (i.e., maize) release benzoxazinoids (BXs) – the defensive secondary metabolites (Erb and Kliebenstein, 2020; Frey et al., 1997). Despite their important plant protective function, BXs were found to reduce maize yield in a field experiment (Hu et al., 2018), probably due to the inhibition of beneficial microorganisms, which in turn decrease nutrients availability (Berendsen et al., 2012). Thus, the inhibitory effects of BXs could, on one hand, promote higher demand for nutrients and formation of enzymatic hotspots, and, on the other hand, BXs may inactivate some part of enzyme-producing microorganisms. Besides, some enzymes (i.e., chitinase or leucine aminopeptidase) are released by plants, acting as natural plant protection substances to defend against fungal and insect pathogens (Flach et al., 1992; Henrissat, 1991) and may partly compensate for BXs deficiency in plants.

Still, we have a limited knowledge of the role of root hairs in the spatial distribution of root exudates and the role of exudates' composition on enzymatic activities, which define the intensity, and extent of rhizosphere processes attributed to nutrients mining and plant protection.

1.2 Abiotic factors (soil texture, drought)

Not only roots, but also soil properties (i.e., soil texture) and the changing environmental conditions (i.e., drought) influence the rates and intensity of the rhizosphere processes. For instance, soils with contrasting textures differ in available and total nutrients due to contrasting clay and soil organic matter content, water regime, soil mineralogy, etc. For example, frequently observed lower nutrient availability on sandy than on loamy soils (Lang et al., 2016) may induce higher rates of mobilizing process in the rhizosphere in order to overcome nutrient deficiency. Furthermore, higher buffering capacity (Vogel et al., 2020) and lower ion leaching in loam (Gaines and Gaines, 1994) enables less mobility of H^+ ions released from the root, and thus maintaining lower pH and greater extent of acidification around the root. The efficiency of nutrient, e.g., P uptake by the plants, which contributes to the depletion zone formation, also depends on soil

texture (Baldovinos and Thomas, 1967; Zheng et al., 2003). Although P sorption on clay than on sand particles may decrease P availability, it may also prevent P losses (Gaines and Gaines, 1994). Thus, it remains unclear to which extend higher rates of nutrient mobilization processes in sand may compensate for more favourable nutrition properties of loam at the rhizosphere level.

Drought, as one possible consequence of global warming, may affect the quantity of root exudates (Preece and Peñuelas, 2016). Drought, likely up-regulates the belowground allocation of assimilated C to compensate negative effects of water limitation (Preece and Peñuelas, 2016). For example, an increase in the release of mucilage, a gel exuded at the root tip, not only facilitates root water uptake but also eases the root growth into dry soil (Holz et al., 2020) However, the amount of root exudation is also projected to decline under severe drought, probably due to a lower photosynthetic activity as result of stomata closure or the C redirection to other vital processes (Gargallo-Garriga et al., 2018). The presence of root hairs (e.g., more root exudates) may magnify the uncertainty in our understanding of how drought affects root exudation and microbial functionality (e.g., enzyme activities). Apart from alterations in root exudation caused by drought, water depletion directly imposes osmotic pressure on both root and microbial cells, disconnects enzymes from substrates as well as microorganisms from nutrients, which can lead to microbial death and thus impair enzyme activities (Turner et al., 2003). This suggests that the spatial distribution of enzyme activities may also shift based on the pattern of water content, especially if plants are exposed to drought stress. It is still unknown whether a higher root exudation can offset the direct negative impacts of water stress. Therefore, a process-based understanding is urgently needed to identify the role of root exudates and water content in the distribution of enzyme activities.

1.3 Soil imaging approaches

The rapid development of non-destructive methods allows obtaining images of the spatial distribution of various properties and processes in the rhizosphere. For instance, root exudates with phosphor imaging, enzyme activity with soil zymography, water content with neutron radiography, pH with planar optodes and nutrient fluxes with diffusive gradients in thin films (DGT). Furthermore, the combination of th ese imaging techniques allow unique insights into the interaction of individual rhizosphere processes.

In laboratory conditions soil zymography was successfully combined with the planar optodes method (Ma et al., 2019), DGT (Hummel et al., 2021) or neutron radiography (Holz et al., 2019); the planar optodes method was simultaneously used with DGT (Hoefer et al., 2017).

However, to study the spatial distribution of phosphatase activities and acidification zones in the rhizosphere in relation to their effects on available P distribution and vice versa, application of all three methods (zymography, planar optodes, DGT) simultaneously is required. All three methods are non-destructive and may be applied during the whole vegetation period several times, giving insights into the dynamic changes of the soil process and their rates.

Rhizoboxes provide easy access to roots and rhizosphere soil and facilitate the application of imaging techniques in the laboratory. However, such laboratory-based studies are often limited to early-plant developmental stages and consequently spatiotemporal information on rhizosphere parameters of mature plants is scarce. Permanently installed flat root windows enable non-destructive sampling across plant development *in situ* under field conditions.

1.4 Objectives

The main objective of this thesis was to study the processes of nutrient acquisition and plant defence in the rhizosphere (Fig. ES 1). To achieve this objective we aimed to develop and apply multi-imaging approaches combined with the measurements of soil microbiome and enzyme activities to study the rhizosphere processes of SOM decomposition, as well as P mobilization at laboratory and field scales.

The specific objectives were:

1) Optimization and improvement of the protocol of *in situ* imaging method soil zymography for mapping activities of different enzymes (Study 1).

2) Development and testing of an approach for separating hotspot activities from the surrounding activities in soil (Study 2) and development of a stepwise data integration for image analysis (Study 5).
3) Implementation of multi-imaging approaches and the development of co-localization analysis of soil images to link several rhizosphere processes aimed to identify the role of:
    a) root hairs for exudates and enzyme activities and their spatial distribution in the rhizosphere (Studies 3 and 4),
    b) benzoxazinoids on microbial activity and rhizosphere extent (Study 3)
    c) exudation and root hairs on P mobilization processes in the rhizosphere of maize at a late developmental stage (Study 5);
    d) soil texture and root hairs for P mobilization processes of maize under field conditions (Study 5);
    e) drought for the exudation, rhizosphere extent and microbial activity (Study 6).

4) Assessment of the effects of root morphology and exudates composition on the bacterial and fungal microbial communities, enzyme kinetics and nutrients limitation in the rhizosphere hot- and coldspots revealed by soil imaging (Studies 4 and 7).

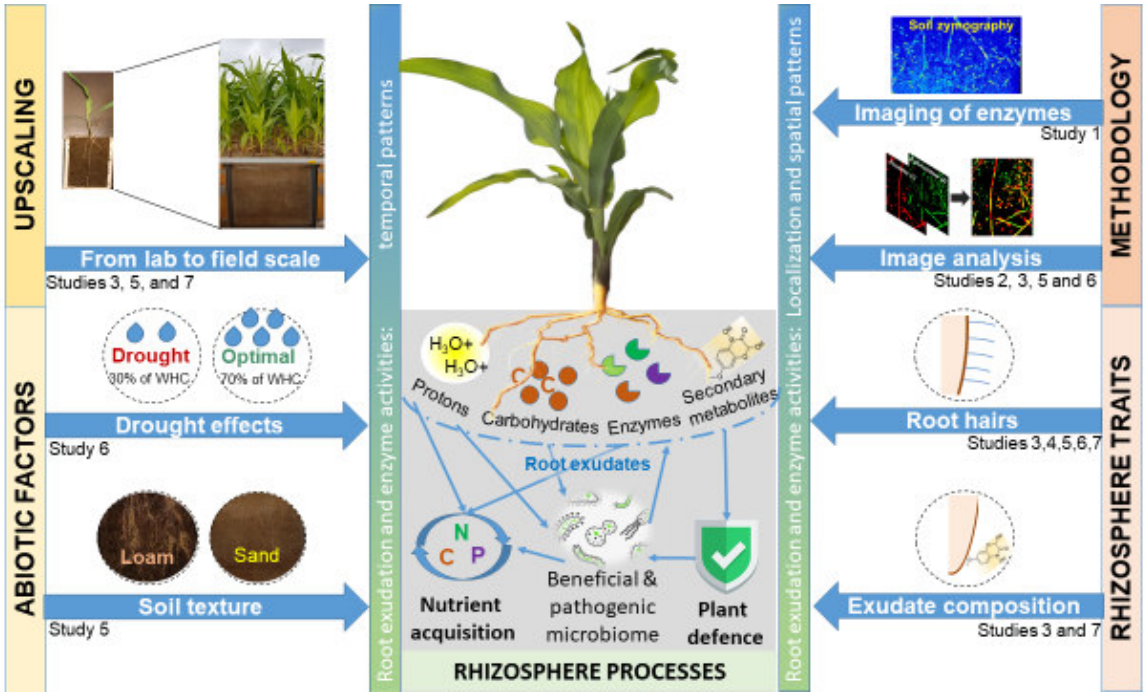

Figure ES1. Schematic overview of the main research questions and general objectives of the individual studies in this PhD thesis.

1.5 Experiments, materials and methods

1.5.1 Plant genotypes

To test the effect of root hairs, we compared a wild type with a root-hair defective mutant *rth3* (Wen & Schnable, 1994; Hochholdinger *et al.*, 2008, 2018) for maize (*Zea mays* L.) and a wild type and a root-hair defective mutant *rhb* (Brown et al. 2012) for barley (*Hordeum vulgare* L.).

The effect of benzoxazinoids (BXs) was determined by comparing a wild type with a BXs deficit mutant *bx1* (Frey et al., 1997).

1.5.2 Rhizobox experiments

In the laboratory experiments, we planted maize (Studies 3, 6 and 7) and barley (Study 4) in the rhizoboxes with inner dimensions of 12.5 × 12.5 × 2.5 cm (Study 4) or 10 × 21.2 × 0.6 cm Studies 3, 6 and 7) filled with soil (Eutric Cambisol or Haplic Phaeozem, respectively). The rhizoboxes were kept at an angle of 45° to make sure the roots grow along the lower side. The soil water content was maintained at 70% water holding capacity (WHC) (Studies 3, 4, 6 and 7), and also adjusted to 30% WHC (Study 6). All plants were grown under controlled conditions in a climate chamber with a constant temperature of 22 °C. The photoperiod was 12 h; the light intensity was 350 µM m^{-2} s^{-1}.

1.5.3 Field experiment

Field experiment (Study 5) was conducted at the experimental field in Bad Lauchstädt, Germany (N 51.390424, E 11.875933). Briefly, maize was grown on two substrates of different texture (loam L; and sand S). The substrate 'loam' originated from the 0-50 cm depth of a Haplic Phaeozem near Schladebach, Germany (51°18′31.41″ N; 12°6′16.31″ E) which had been under agricultural use before excavation. The substrate 'sand' was obtained by sieving and mixing 16.7% of the already mentioned loam with 83.3% quartz sand (WF 33, Quarzwerke Weferlingen, Germany). Both substrates were sieved < 4mm and filled into the plots. Custom designed root windows were installed in three individual replicate plots per substrate and maize genotype combination, resulting in a total number of 12 root windows. Root windows were constructed on site in April 2019, prior to the first cultivating of the plants in the experimental pots.

1.5.4 Labelling method to trace ^{14}C exudates distribution

To trace the spatial patters of ^{14}C exudation in the rhizotron experiment, after 21 days of growth, the plants were labelled with $^{14}CO_2$ (0.5 MBq per plant) at a target CO_2 concentration of

500 ppm, following the procedure described by Kuzyakov et al. (2006). Briefly, six plants (two replicates of each of three genotypes) were put in an airtight chamber (120 L volume) for two consecutive days. Before labelling, the CO_2 inside the labelling chamber was reduced by cycling the air through 1 M NaOH for 8 h with the grow light off. For the labelling, Na_2CO_3 solution containing 3 MBq of $Na_2{}^{14}CO_3$ was dissolved in 10 ml phosphoric acid (100%). During the labelling, all plants were kept under a grow light (350 µmol m^{-2} s^{-1}) to enable a maximum photosynthetic activity. After 6 h, not assimilated $^{14}CO_2$ in the chamber was trapped by pumping the air through 1 M NaOH for 2 h. The ^{14}C imaging was done as described in Holz et al. (2018).

1.5.5 Soil imaging methods

The summary of imaging methods applied in this thesis are given in Table ES 1, and are described in detail in the materials and methods of the respective study or its supplementary. In the Studies 3 and 6, the imaging methods were applied in the following order: ^{14}C imaging – zymography – neutron radiography (Fig. ES. 2a). In the field experiment of Study 5 (Fig. ES 2b), there were several orders of methods applied to be able to conduct image analysis in all 12 root windows within one week. The triple method application was used to ensure the minimum time interval between the imaged parameters to co-localize them pairwise quantitatively.

Table ES 1. Summary of the *in situ* soil imaging techniques applied in the studies of this PhD thesis.

Measured parameter	**Method**	**Equipment**	**Reference**	**Study**
Spatial distribution of enzyme activity	Soil zymography	Camera, UV light, substrates, membrane.	Spohn et al., 2013 Razavi et al., 2019	Studies 3, 4, 5, 6 and 7
Spatial distribution of ^{14}C exudates	Phosphor imaging	Laser scanner for phosphorimaging (650 nm excitation, FLA-7000, GE Healthcare, U.S.A.)	Holz et al., 2018	Studies 3 and 6
Spatial distribution of soil water content	Neutron radiography	Neutron beam, scintillator, CCD camera	Ahmed et al., 2016; Moradi et al., 2009	Studies 3 and 6
Spatial distribution of soil pH	Planar optodes	Sensor foils SF-HP5R, VisiSens TD imaging system	Blossfeld and Gansert, 2007	Study 5
Spatial distribution of nutrients	Diffusion in thin films (DGTs)	DGT gels, LA-ICPMS	Kreuzeder et al. 2013	Study 5

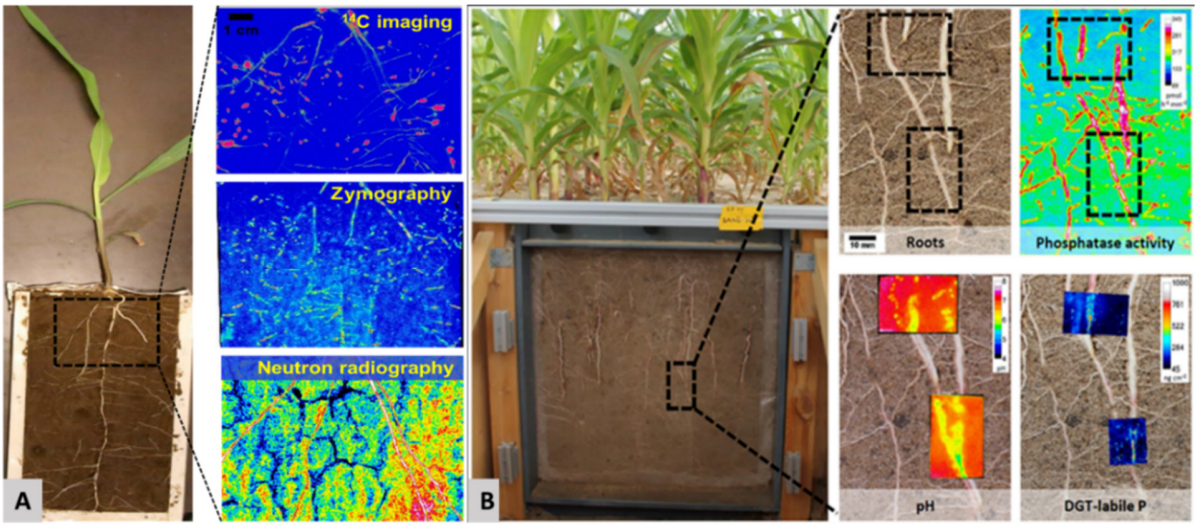

Figure ES 2. An overview of the imaging methods applied (A) in the rhizobox laboratory experiment or (B) in the root window field experiment. *Taken from Bilyera et al. (2021b) and Bilyera et al. (2022).*

1.5.6 Image analysis

Soil images were all analysed by the Imagej software. The overview of the approaches applied for image analysis or developed in this thesis (Study 2) are shown in Table ES 2. In order to obtain maximum information from the restricted amount of regions of interest (ROIs) obtained in a challenging filed imaging campaign (Study 5), a stepwise data integration analysis was applied, which includes 6 steps of detailed and spatially resolved analysis. The steps and their sequence are shown in Fig. ES. 3.

Table ES 2. Summary of the approaches applied for image analysis

Parameters/methods	**Approach/Type of analysis**	**Reference**	**Study**
Rhizosphere gradients	Euclidian distance	Lucas et al., 2019	Study 5
Hotspot thresholding	Mean +/- 2 SD of background activities	Bilyera et al., 2020 (Study 2)	Study 3 and 5
Hotspot co-localization	Co-localization analysis with JaCoP (just another co-localization plugin)	Bolte and Cordelières, 2006	Study 3, 5, 6

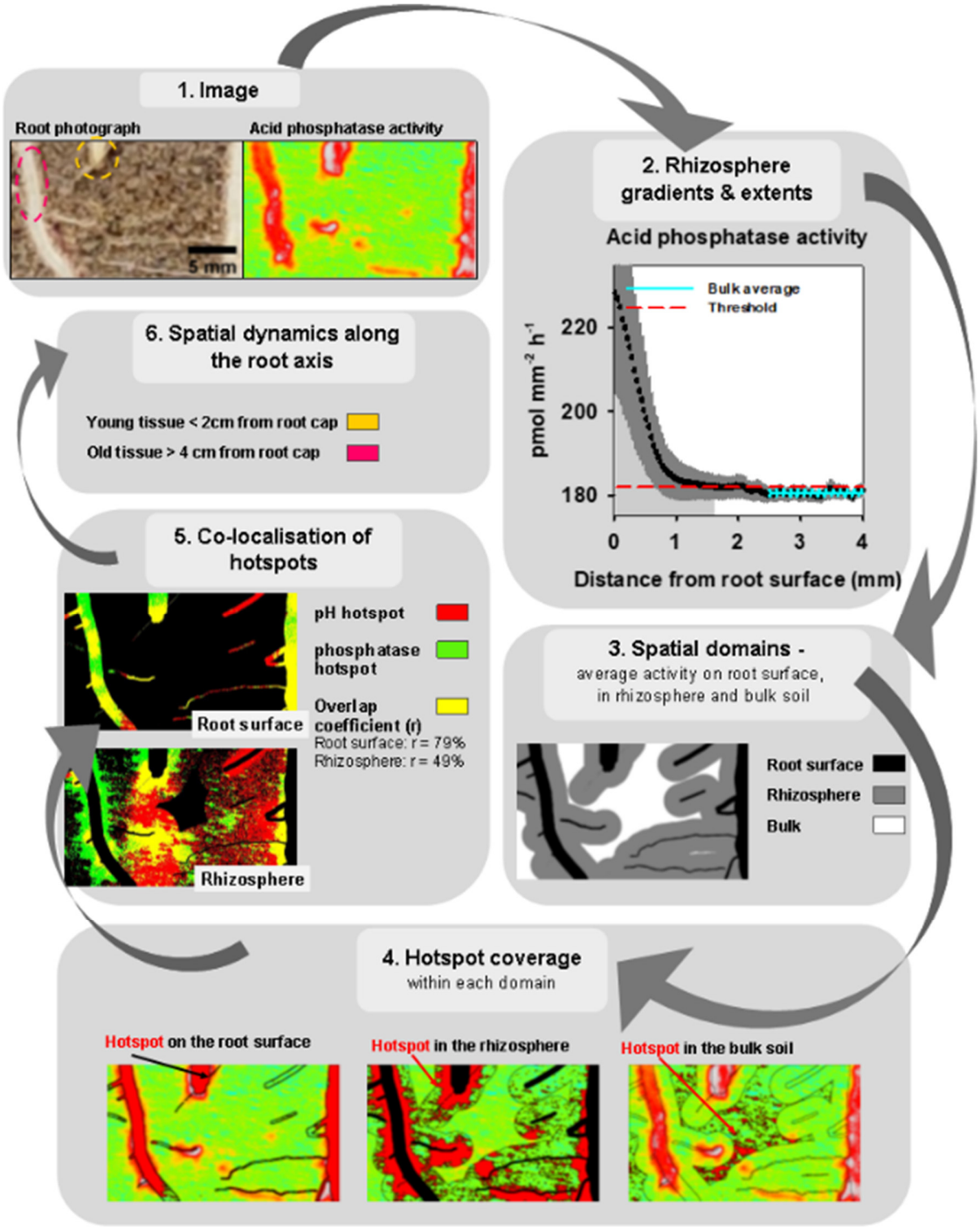

Figure ES 3. Steps of image analysis and data integration for obtaining qualitative data from soil images. *Taken from Bilyera et al. (2022)*.

1.5.7 Enzyme assay

Activities of enzymes in the destructive soil samples were measured using fluorogenically labelled substrates as described in Razavi et al. (2016). The kinetics parameters presented in this PhD thesis were maximum potential enzyme activity (V_{max}), substrate concentration at half-maximal rate (K_m), catalytic efficiency of enzyme (K_a), and substrate turnover time (T).

1.5.8 Microbiome analysis

DNA was extracted using the QIAGEN DNeasy PowerSoil Pro kit (QIAGEN, Germany) for soil following the manufacturer's instructions with 200 mg rhizosphere soil from hot and coldspots as input material. DNA was quantified using an AccuClear™ Ultra High Sensitivity dsDNA Quantitation Kit with 7 DNA standards (Biotium, CA USA) on Tecan spectrometer (Tecan group AG, Switzerland).

We sequenced several different experiments in a single MiSeq run and the qPCR products of this study were included in a run of which the sequences were deposited previously (Hu et al., 2018). The V3–V4 region of 16S rRNA was amplified with the primers 515F (Parada) and 806R (Apprill).

Firstly, the raw read data were quality checked with FastQC (Andrews, 2010) and demultiplexed using cutadapt (Martin, 2011). Then, we followed the DADA2 pipeline from Callahan et al., (2016) using the R package dada2 (v3.10). Instead of clustering the sequences in operational taxonomic units (OTUs), the DADA2 pipeline produces amplicon sequence variants (ASVs), which replace OTUs as the units of analysis (Callahan et al., 2017).

1.6 Results and discussion

1.6.1 Methodological innovations to study the rhizosphere processes

The presented thesis advanced the earlier developed imaging method zymography (Study 1) and included novel first time field zymography application (Study 5). An important step forward has been done with the development of the standardized thresholding method for hotspots on various soil images (Study 2, Fig. ES 4). The application of multi-imaging approach in the rhizobox experiments (Studies 3 and 6) and at the root windows in a field (Study 5), as well as adaptation of pairwise co-localization analysis for hotspots of various soil parameters were successfully done in several studies of this thesis. The detailed description of methodological innovations and their main outcomes are given in Table ES 3, and discussed in detail in Studies 1-7. All these methodological innovations allowed studying the processes in the rhizosphere, its spatial organization and microbiome functioning including enzymatic activities.

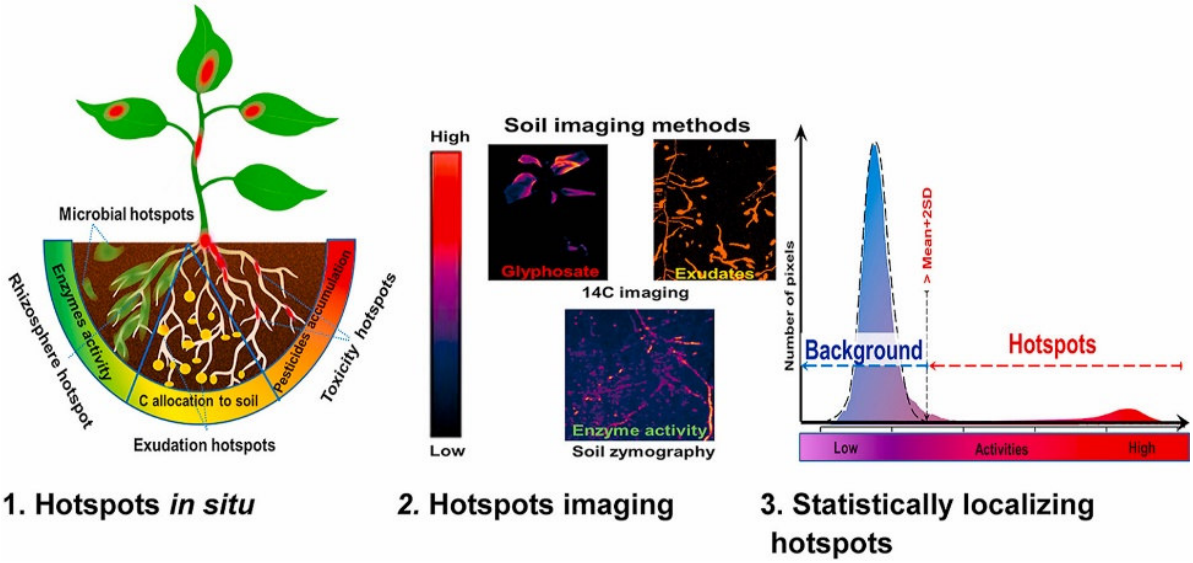

Figure ES 4. The main steps of hotspots visualization by soil and plant imaging techniques and the basic principle of statistically localizing hotspots. *Taken from Bilyera et al (2020).*

Table ES 3. Synthesis of methodological innovations and main conclusions

Study	Type of study	Methodological innovations	Main results
Study 1	Method review	Advancement of the direct soil zymography	Full improved protocol was provided for the whole process of zymography and image analysis thereafter
Study 2	Methodological	Statistical approach for hotspot thresholding on soil images	Mean + 2SD approach (supplied with R script) was developed as most reliable for hotspots thresholding on various soil images
Study 3	Laboratory / Growth chamber /Rhizobox	1) Multi-imaging approach for laboratory experiment (three consequently applied imaging methods to link exudation, enzyme activity and water availability) 2) Implementation of the co-localization analysis to multi-imaging method	1). First study to provide evidence of maize genotype-specific exudation strategies (via root tips or from whole root), including their implications for microbial functions 2). An equal dependence of β-glucosidase activity on water and ^{14}C exudate availability in the rhizosphere, as revealed by co-localization analysis.
Study 4	Laboratory / Growth chamber / Rhizobox	1) Localized protein addition to study its mineralization by root- and microbially derived proteases 2) Combination of *in situ* /zymography) and *ex situ* (enzyme survey) rhizosphere sampling methods	1. Combination of root hairs and protein addition allows producing the highest leucine aminopeptidase activity in the rhizosphere creating an advantage for plants with root hairs to access protein hotspots in soil. 2. Clear evidence on the disparity between *in situ* and *ex situ* rhizosphere sampling methods for leucine aminopeptidase activity.
Study 5	Field / Root windows	1) First study on field zymography in the stationary installed root windows in maize field 2) Multi-imaging approach at field experiment 3) Stepwise image analysis and data integration	1. Rhizosphere acidification was linked to root growth and created a pH optimum for acid phosphatase activity able to mineralize organic P, especially at young root tissues which are major sites of P uptake 2. The combined imaging revealed that individual P solubilizing processes co-localized and interacted in the rhizosphere.
Study 6	Laboratory / Growth chamber/ Rhizobox	Combination of multi-imaging approach with enzyme kinetics to reveal the influence of several parameters on enzymes of C-cycles.	Optimal water content contributed more to an increase in hotspot area, a broader rhizosphere extension and overall higher activities of β-glucosidase than root hairs did.
Study 7	Laboratory / Growth chamber/ Rhizobox	Combination of non-destructive hotspots detection by zymography with enzyme assay and microbiome analysis in destructive samples of hot- and coldspots	The presence of benzoxazinoids strongly supported the plant defense against pathogenic fungi (i.e., *Fusarium* and *Gibberella*), which, however, could not be fully substituted by an increased exudation and activities of enzymes (chitinase, β-glucosidase) with plant protection function in *bx1*.

1.6.2 Effect of root hairs on rhizosphere processes

Root hairs are usually abundant only 1-5 cm above the root tip (Jungk, 2001), but rhizodeposits formed when such hairs break and lyse promote microbial activity in the rhizosphere of the root region above 5-6 cm from the root tip, as the root continues growing. These root-hair rhizodeposits, along with the released exudates, increase the active portion of microbial biomass in the rhizosphere (Zhang et al., 2020) and therefore stimulate β-glucosidase production (Wang and Lu, 2006).

Generally, the presence of root hairs enlarged the enzymatic activity of the rhizosphere by up to 50% (Ma et al., 2018b), as also confirmed in our study for β-glucosidase activity (+35% of rhizosphere extent) (Fig. ES 5). Thus, plants with root hairs exploit larger volumes of soil to acquire available C sources via enzymatic hydrolysis. However, root-hair defective *rth3* could compensate for its up to 70 % smaller root surface area (Raghothama and Karthikeyan, 2005; Segal et al., 2008) by increasing the total amount of exudates distributed longitudinally along the roots (Lagos et al., 2015) and not restricted to root tips, as in wild type. Thus, *rth3* performed a plant strategy to maintain high microbial activity and thus enzyme activity (including β-glucosidase) by releasing easily available C into the entire rhizosphere (Cotton et al., 2019). This might also reflect the higher membrane permeability in the absence of root hairs. Additional release of primary metabolites and β-glucosidase (Gramss et al., 1999) from the mature root zone in *rth3* could not fully compensate for the absence of root hairs. Therefore, root hairs are an important root traits for maintaining hotspot activities of C-cycle enzymes (here β-glucosidase) in a larger soil volume, and thus, providing better conditions for microbial activities and SOM decomposition.

It is very probable that the increase in leucine aminopeptidase activity due to root hairs induces greater rhizosphere priming thereby enhancing the release of N from SOM required to fuel microbial growth (Brzostek et al., 2013; Dijkstra et al., 2013). The rhizosphere extent of leucine aminopeptidase activity in the rhizosphere was largest when soluble protein was applied (Fig. ES 6) but this enhancement was observed for both barley genotypes irrespective of the presence of root hairs. This contradicted our expectations, that root hairs would increase the area of high leucine aminopeptidase activity in the rhizosphere compared to roots without hairs via an increased surface area of the root for microbial colonisation (Gilroy and Jones, 2000; Haling et al., 2013).

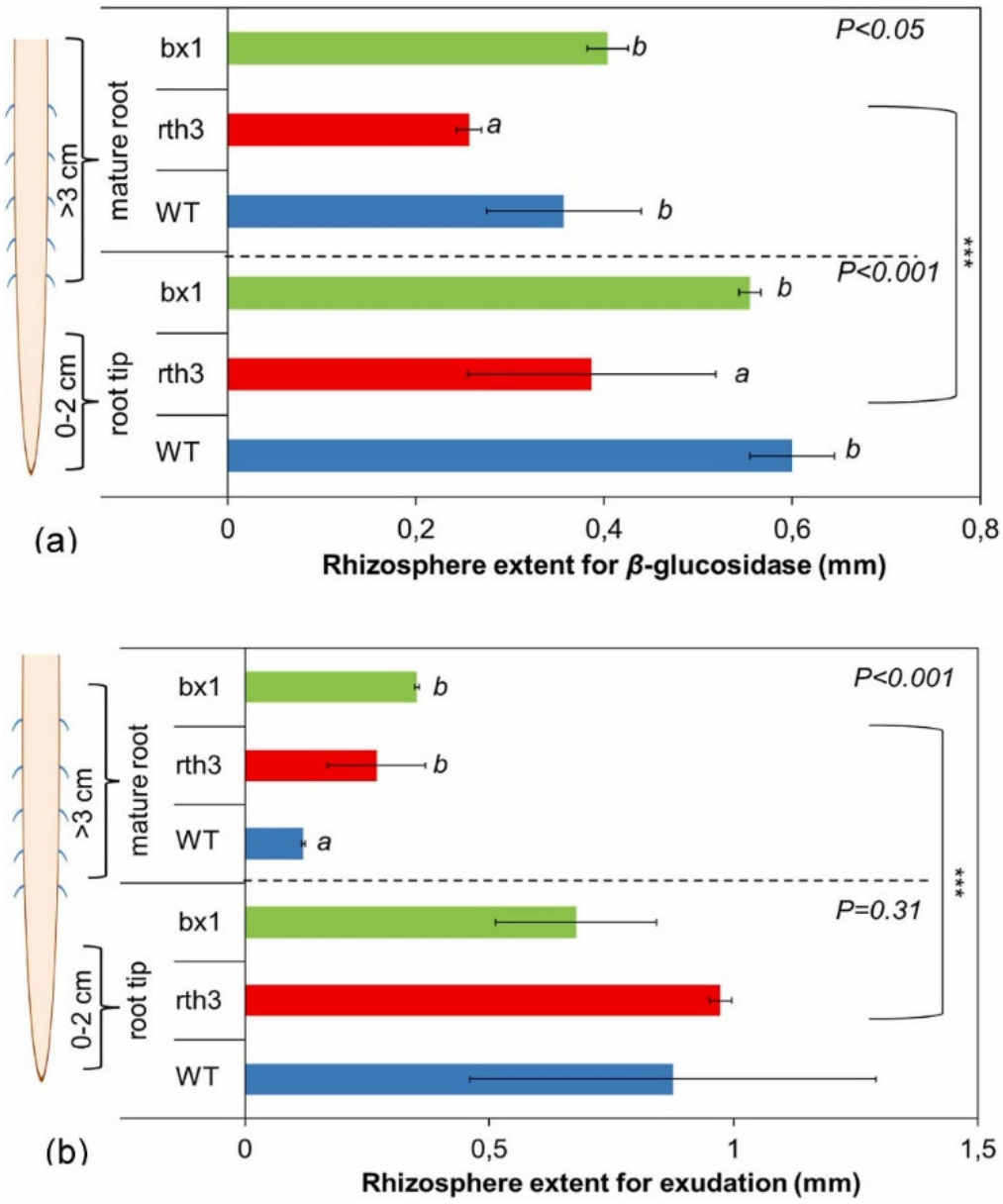

Figure ES 5. The rhizosphere extent for β-glucosidase activity (a) and ^{14}C-labeled root exudates (b). Data are means for each genotype (WT, *rth3* and *bx1*) (n = 4), error bars indicate standard deviations. Letters within one root type mark significant differences among the genotypes at $P < 0.05$. Asterisks on the bracket at the right side indicate significant differences between root sections ('***' $P < 0.001$; '**' $P < 0.01$; '*' $P < 0.05$). *Taken from Bilyera et al. (2021).*

Leucine aminopeptidase activity was higher in the rhizosphere with root hairs and protein addition compared to the other treatment combinations (Fig. ES 6). This suggests that microorganisms and plant roots in the rhizosphere of barley genotype with root hairs have a greater advantage in utilising protein hotspots in the soil. The ability to obtain more N is particularly important in agricultural soils where crops tend to be more N limited (Rütting et al., 2018).

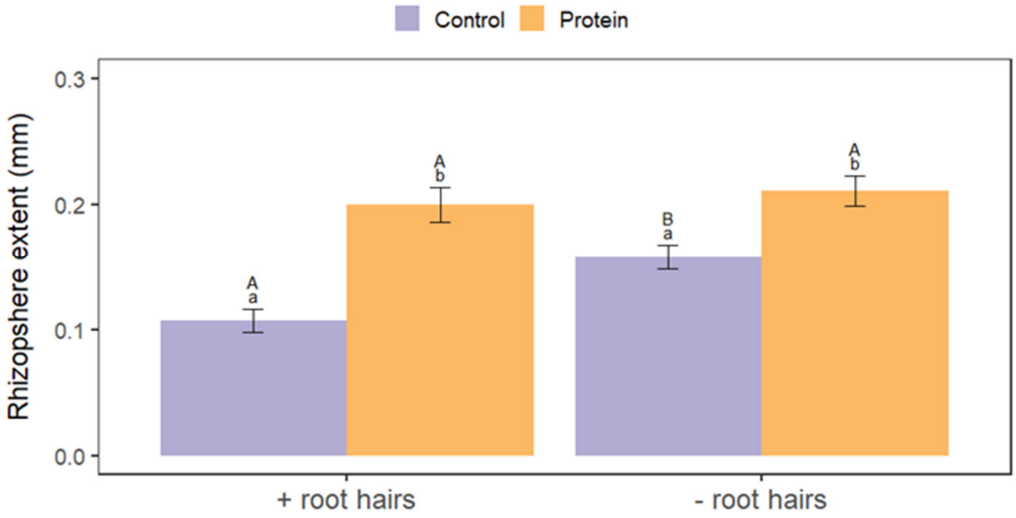

Figure ES 6. Rhizosphere extent of leucine aminopeptidase activity (distance from the root surface, mm), for barley genotypes with and without roots hairs and with protein or control (sterile water) addition. Values represent mean ± SE (n = 90). Different lowercase letters indicate a significant difference between the protein and control treatments and different uppercase letters indicate a significant difference between the root hair genotype (p < 0.05). *Taken from Greenfield et al. (2021).*

In contrast to the other enzymes (β-glucosidase and leucine aminopeptidase), we did not find a significant effect of root hairs on phosphatase activity and its related rhizosphere extent in field conditions (Fig. ES 7). Similar acid phosphatase rhizosphere extents of around 1 mm were found by Kandeler et al. (2002) after soil slicing (resolution 0.2 mm) or by Ma et al. (2018) (1-2 mm measured with zymography from the root center) and Razavi et al. (2016) for younger maize plants (7-21 days old). Nevertheless, our results are comparable to these zymography studies when adding the root radii (ranging from 0.1-1.0 mm) to the rhizosphere extents. Furthermore, the activity of the P cycle enzyme (acid phosphatase) increased in the hotspots due to the presence of root hairs in the rhizobox experiment (Study 7). The formation of the P depletion zones around the root and especially with the presence of root hairs (Hummel et al., 2021) induced up to 80% higher acid phosphatase activity (Fig. ES 8) to mineralize organic P to plant available forms. It should be noted, that microorganisms themselves did not experience evident P limitation (Study 7) and the P mobilization processes were probably induced by an increased plant P demand.

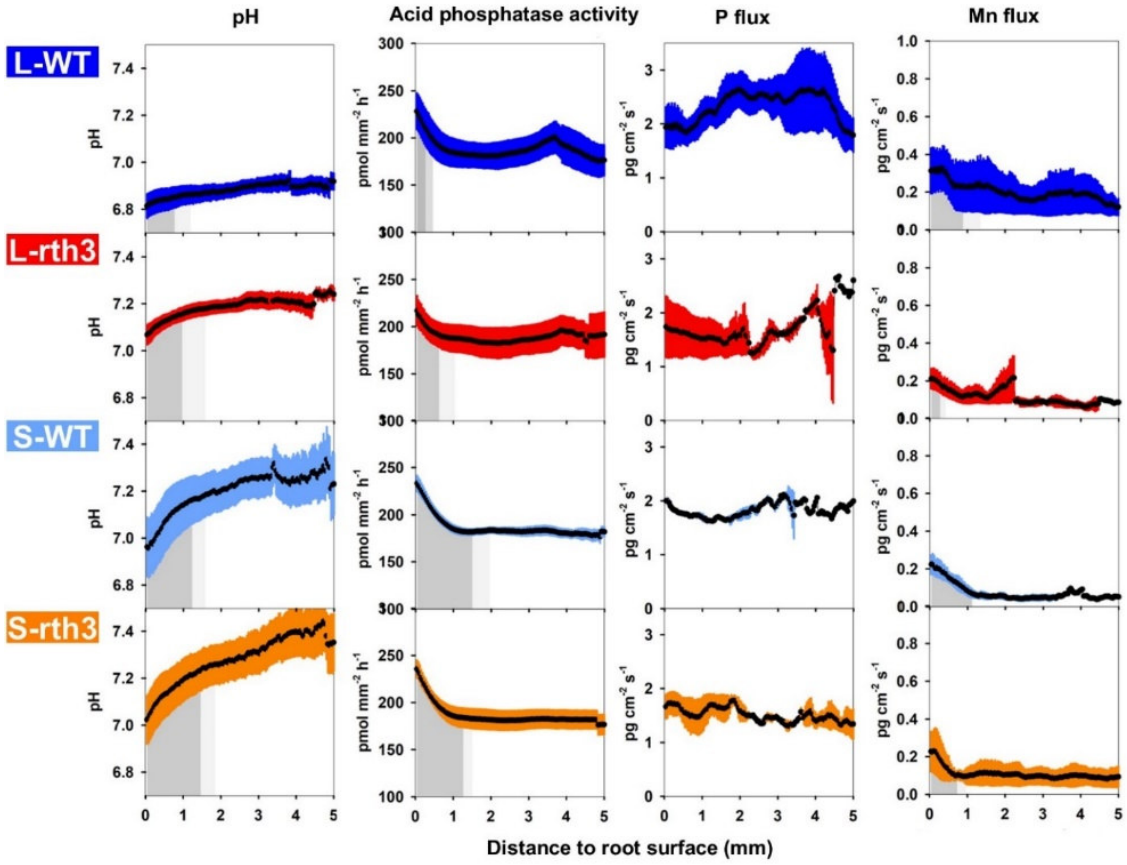

Figure ES 7. Average pH, acid phosphatase activity, P and Mn flux as a function of distance to the root surface of two maize genotypes (wild-type (WT) and root hair defective mutant (*rth3*)) grown in loam (L) and sand (S). Coloured error bars represent standard error of *n*=6 (L-WT) or *n*=5 (L-*rth3*, S-WT, S-*rth3*) for pH and acid phosphatase activity; *n*=3 (L-WT, L-*rth3*) or *n*=2 (S-WT, S-*rth3*) for P and Mn flux. The average rhizosphere extent is shown as dark grey areas and was determined from individual concentration-distance plots with a threshold value (mean concentration at distance >2.5mm (*i.e.*, bulk soil +/- 2xSD); light grey areas indicate standard error for the average rhizosphere extent. No rhizosphere extent was defined for P flux. *Taken from Bilyera et al. (2022).*

More spatially resolved analysis revealed that WT root tips were more acidic than root-hair defective *rth3* tips, potentially contributing to locally increased P solubility and uptake. As we could not observe increased P fluxes in WT (Fig. ES 7), the higher P contents in WT compared to *rth3* are most likely related to the higher absorption surface due to the presence of root hairs leading to greater P uptake despite similar extent and intensity of P solubilizing processes in the rhizosphere of both maize genotypes. Overall, the combined imaging of phosphatase activity, soil pH and nutrient gradients *in situ* revealed that individual P solubilizing processes co-localized and interacted in the rhizosphere (Fig. ES 8). Our results also demonstrate the challenge to find

significant and clear trends under field conditions as several processes occur simultaneously, *i.e.*, mobilization, solubilisation, desorption, enzymatic conversion of organic (P_o) to mineral P (P_i), microbial mobilization, and immobilization as well as P uptake.

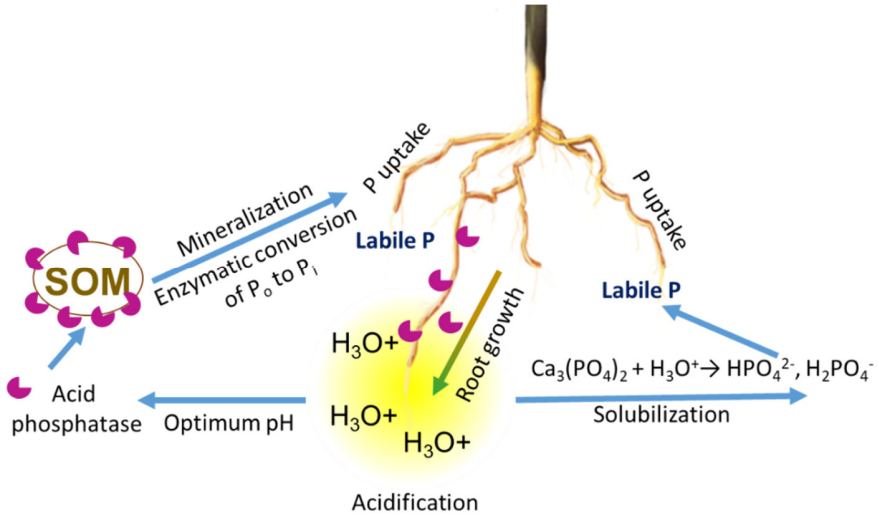

Figure ES 8. Scheme of the main phosphorus mobilization processes in the rhizosphere of wild type maize created based on the results of Study 5.

1.6.3 The influence of benzoxazinoids on soil microbiome and its enzyme activities

The altering of exudates composition towards the decrease of secondary metabolite benzoxazinoids induces significant changes in the rhizosphere of maize. Thus, the *bx1* maize did not need to invest high energy in synthesizing benzoxazinoids and therefore probably produced more primary metabolites (Pott et al., 2019). Consequently, microbes being very close to the root are less inhibited by defensive secondary metabolites (10-40% lower amount) but instead have 20-30% more primary (soluble protein, amino acids, sugars) metabolites (Hu et al., 2018). More available C released further from the root surface presumably enlarges the rhizosphere extent for β-glucosidase activity in *bx1,* but this was not demonstrated in our results. Instead, excluding benzoxazinoids from exudates resulted in a sharp gradient of β-glucosidase activity (2.4-fold) between the rhizosphere and bulk soil (Study 3, Fig. 3). The two-times larger area of non-rhizosphere β-glucosidase hotspots away from the root surface in *bx1* supports the indirect influence of the inhibitory effect of benzoxazinoids (Hu et al., 2018) or other secondary metabolites (Banerjee et al., 2018). Moreover, the 30% higher β-glucosidase activity in the rhizosphere along the root axis of *bx1* (Study 3, Fig. 3) may reflect the absence of the fungicidal

effect of benzoxazinoids in *bx1* (Kudjordjie et al., 2019). Overall, the release of benzoxazinoids by roots of WT suppressed the activities of rhizosphere microorganisms, which led to 30% lower β-glucosidase activity on root surface and in the rhizosphere, but did not change the rhizosphere extent.

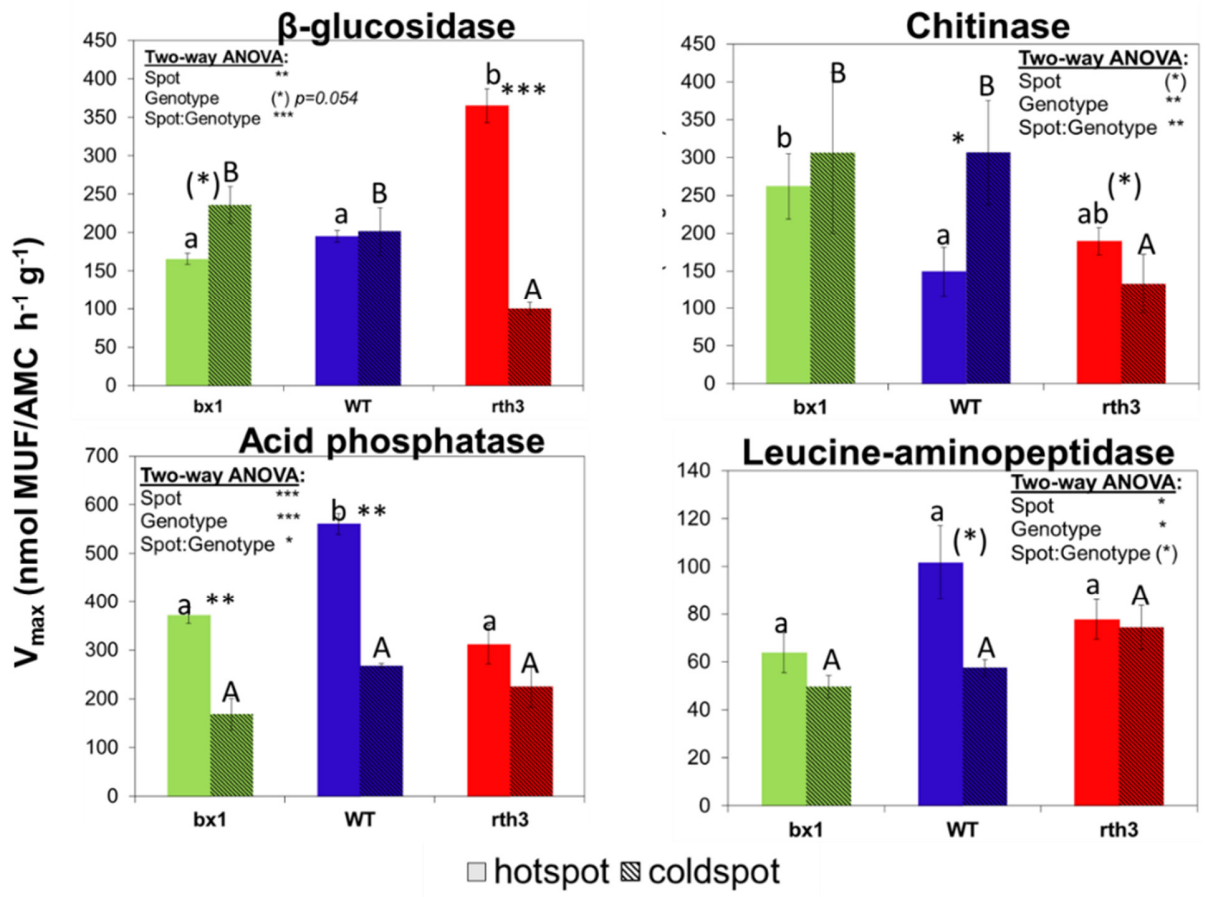

Figure ES 9. Maximum enzyme activity (V_{max}) of β-glucosidase, acid phosphatase, chitinase and leucine aminopeptidase. Data are means for each genotype (*bx1,* WT, and *rth3)* (n=4), error bars indicate standard error. Different capital letters indicate significant difference among the genotypes in coldspots, while lower case letters indicate significant differences among the genotypes in hotspot at *P<0.05*. Asterisks above the bars indicate significant differences between cold- and hotspot for each genotype ('***' *P*<0.001; '**' *P*<0.01; '*' *P*<0.05, '(*)' *P*<0.1). *Taken from Bilyera et al. (in preparation).*

In the further *ex situ* measurements of enzyme activities, we detected significantly higher chitinase activity in *bx1* (Fig. ES 9). Chitinase may acts as a natural plant protection substance to defend plant against fungal and insect pathogens (Flach et al., 1992; Henrissat, 1991; Scranton et al., 2012). Therefore, such an increase in chitinase activity may partly compensate for benzoxazinoids evadeficiency. Nevertheless, it seems that chitinases were not as effective

against pathogenic fungi as benzoxazinoids. The latter was proved by dramatically increased abundance of plant pathogenic fungi of genus *Fusarium* and *Gibberella* (Fig. ES 10), which cause Gibberella stalk and ear rot or root rot diseases on maize (Goswami and Kistler, 2004; Okello et al., 2019; Zhao et al., 2021). Typically, plants regulate the release of BXs based on the media, they grow in, and thus modify its concentration in the rhizosphere (Hazrati et al., 2020), which is not relevant for BXs deficient genotype *bx1*.

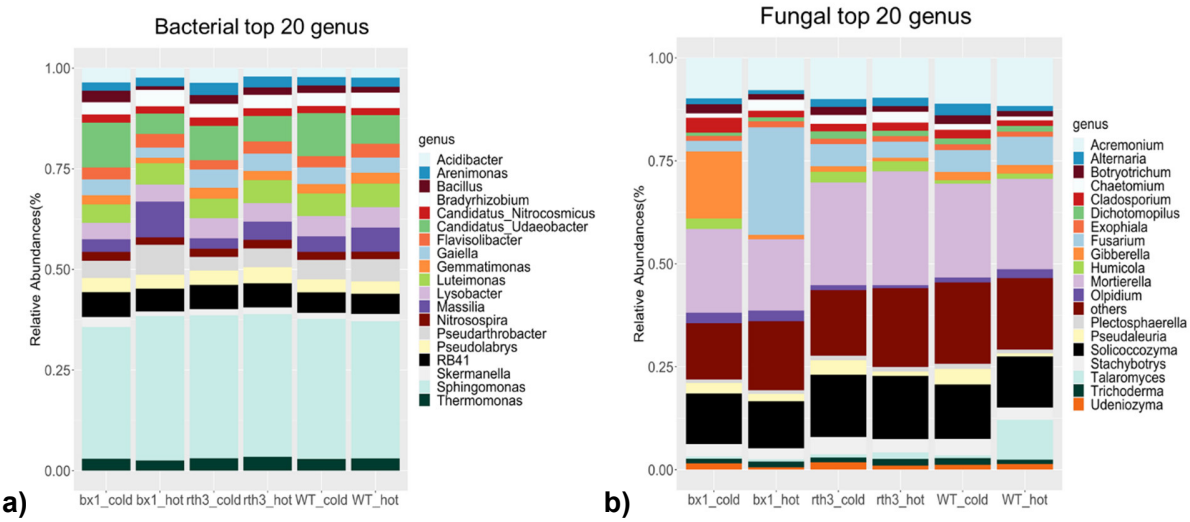

Figure ES 10. Relative abundance of top soil bacterial (a) and fungal (b) communities at genus level in the soil from the cold- and hotspots of three maize genotypes (WT, *rth3, bx1*). Data are mean of four replicates, except two replicates for *bx1* coldspots. *Taken from Bilyera et al (in preparation).*

To conclude, the presence of BXs in root exudates decreased the enzymatic activity by 30%, did not significantly reduce microbial biomass, but strongly supported the plant defence against pathogenic fungi (i.e., genus *Fusarium* and *Gibberella*), which, however, could not be fully substituted by an increased exudation and activities of enzymes with plant protection function (i.e., chitinase, β-glucosidase) in *bx1*.

1.6.4 Effect of drought on for the spatial distribution of microbial activities

Although root exudates directly relieved microbial C limitation, the importance of soil moisture offset root hairs in regulating the occurrence of enzyme hotspots. Drought reduced the hotspot area (Fig. ES 11a) and narrowed the rhizosphere extent of β-glucosidase activity (Fig. ES 11b). The larger hotspots area and wider rhizosphere extent of β-glucosidase activity are concurrent with optimal water content because the proper soil moisture is a prerequisite for higher root biomass. It has been strongly suggested as a compelling explanation for higher rhizodeposition (Preece and Peñuelas, 2016). Additionally, the optimal water content provides a

suitable growth environment for microorganisms, and increased microbial access to nutrients and energy (Ahmed et al., 2018) as well as an improved diffusion of root exudates into the extended soil volume (Holz et al., 2019). Consequently, β-glucosidase activities in the wet soil were higher than under the drought conditions (Fig. ES 12a). Such higher β-glucosidase activities were sufficient to maintain microbial activities and crucial functions, and thus the enzyme systems in the dry soil were more efficient (Fig. ES 12b).

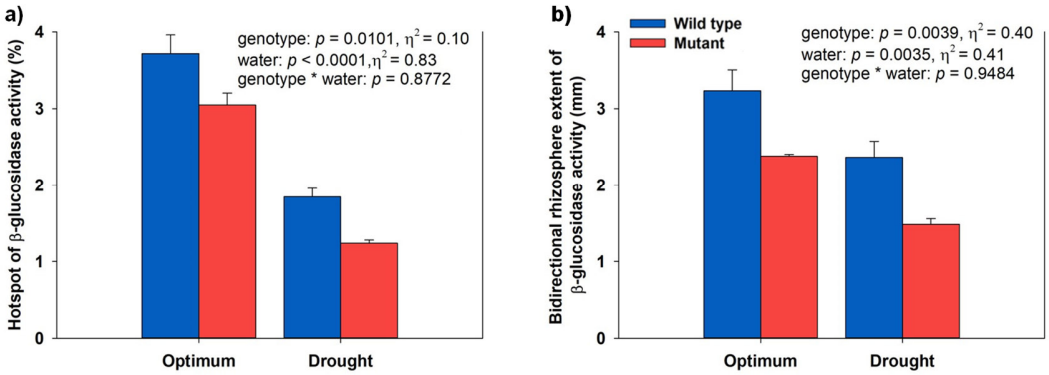

Figure ES 11 (a) Hotspot (%) and (b) bidirectional rhizosphere extent of β-glucosidase activity for two maize genotypes (wild type and mutant *rth3*) under optimal water content and drought conditions. *p* values were obtained after two-way ANOVA. η^2: effect size; genotype: wild type and mutant *rth3*; water: drought and optimal water content. Data are mean (n=3) and error bars represent standard deviation (SD). *Taken from Zhang et al. (under review).*

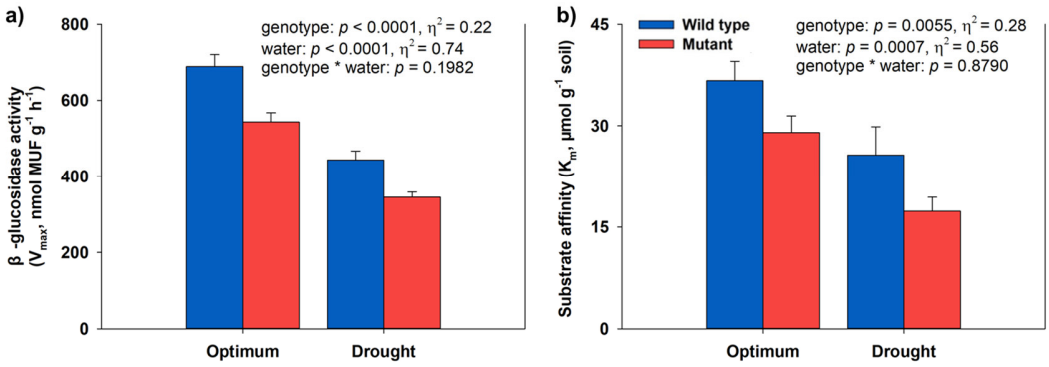

Figure ES 12. Michaelis–Menten kinetic parameters, i.e. (a) β-glucosidase activity (V_{max}, nmol g^{-1} h^{-1}) and (b) substrate affinity (K_m, µmol g^{-1} soil), of rhizosphere soil for two maize genotypes (wild type and mutant *rth3*) under optimal water content and drought conditions. *p* values were obtained after two-way ANOVA. η^2: effect size; genotype: wild type and mutant *rth3*; water: drought and optimal water content. Data are mean (n=3) and error bars represent standard deviation (SD). *Taken from Zhang et al. (under review).*

Thus, soil moisture is likely to contribute more than root morphology such as root hairs in controlling enzymatic hotspot and their distribution in the rhizosphere, as water activates microbial biomass and mediate solute transport in soil. Despite this, root hairs still play extremely important roles when plants face droughts. For example, root hairs tend to increase the hotspot area of root exudates, as well as significantly widen the rhizosphere extension of root exudates and water under drought meaning 24% - 37% increase of proportion of soil which can be mined by plant – a crucial root trait considering that the efficiency of gaining water and nutrients from a defined soil volume may strongly decrease under drought.

1.6.5 Effect of soil texture on P mobilization processes

Soil texture had a significant effect on the acidification features in the rhizosphere. The lower pH buffer capacity of sand compared to loam due to the less presence of secondary minerals, clay, and organic matter resulted in the steeper rhizosphere gradients of pH in sand compared to loam (Fig. ES 7). Moreover, the effective diffusion coefficient of protons is larger in sand compared to loam (Olesen et al., 2001) contributing to ~0.45 mm larger rhizosphere extents in sand (on average 1.35 mm) than in loam (on average 0.89 mm, Fig. ES 7). Such an increased rhizosphere acidification facilitated the higher activity of acid phosphatase. Thus, an average rhizosphere acidification was ~0.1 pH units stronger in sand than in loam and caused ~1 mm larger average rhizosphere extents for acid phosphatase activity there.

The maize derived root exudates (*i.e.*, C-containing primary and secondary metabolites released by roots) (Bilyera et al., 2021, Santageli et al., in preparation) are more strongly sorbed in loam than in sand hence limiting exudate diffusion and consequently the extent of their microbial stimulation effect in loam. As enzyme diffusion in soil is negligible (Guber et al., 2018), the larger rhizosphere extent in the rhizosphere of sand-grown maize was due to a greater activity of phosphatase-releasing microbes. However, the efficacy of phosphatases generally depends on P_o availability and P esters might strongly sorb to the soil solid-phase (Huang et al., 2005), which limits hydrolysis by phosphatases (Gerke, 2015). In loam, P_o was nearly 6-times higher compared to sand. Hence, in loam, similar phosphatase activities in the rhizosphere could have mobilized a larger amount of phosphate from P_o compared to sand. The higher presence of organic P suggests that, in loam, acid phosphatase activity played a more prominent role in plant P nutrition compared to the sand. Moreover, the contents of total P, clay and organic C were found to be important for extraction efficacy (Bilyera et al., 2018). Since all of the listed parameters were

higher in loam than in sand, we may assume that organic P stock as well as intracellular enzyme activities in loam could be underestimated if compared to sand.

In sand, co-localisation coefficients of acidification and acid phosphatase activity were higher than in loam which was in line with the slightly higher hotspot coverage and (slightly) larger rhizosphere extents of both parameters in sand compared to patchier distribution along the roots in loam. The higher hotspot coverage of pH, acid phosphatase activity and Mn on the root surface in sand may indicate more pronounced root processes in response to P-limitation or may be a result of less sorption or improved detection due to better sensor-soil contact in sand. Due to the higher amount of Ca-phosphates deriving from the fertilization in sand, acidification might be more important in terms of P solubilisation because the solubility of Ca-phosphates increases with lower pH (Penn and Camberato, 2019). But the effect of fertilization was likely restricted to the upper parts of the plots as the P fertilizer was surface-applied and was limited as reflected by the generally lower P contents in maize grown on sand.

Overall, more pronounced diffusion of solutes in the sand compared to loam resulted in greater extent of acidification mainly around young root tissues. High P flux also co-localized with acidification at root tips. Acidification was likely linked to root growth and created a pH optimum for acid phosphatase activity, (i.e., transformation of P_o to available phosphate) and P uptake especially at the root tips and within the elongation zone, which are the major sites of P uptake. This calls for application of phosphorus fertilizers at early stages and preferably cultivate maize on loamy soils with increasing of SOM by which maize plants will be able to mobilize available P at later stages.

1.7 Summary of the main results of the studies

In this thesis, we improved the protocol of soil zymography - *in situ* imaging method of enzyme activity (Study 1), and applied soil zymography under field conditions (Study 5) for the first time. Besides, soil zymography was combined with phosphor imaging and neutron radiography to study the role of root exudation and water content for spatial distribution of enzyme activity in the rhizosphere (Study 3). In a field, we challenged to combine soil zymography, optodes and diffusive gradients in thin films (DGT) to study phosphorus mobilization processes in the rhizosphere of maize at later growing period (tassel emergence) (Study 5). The obtained images of high resolution give an important insight into the spatial distribution of hotspot enzyme activities, ^{14}C exudates release, soil water distribution, acidification features and nutrients in the rhizosphere. However, to obtain the maximum quantitative data of hotspots area, their co-localization and the gradients in the rhizosphere, we developed an approach for statistically localizing hotspots on soil images (Study 2), implement co-localization analysis for hotspots of different origin (Studies 3, 5 and 6) and developed the stepwise data integration for image analysis (Study 5). These methodological advancements allowed to reveal the influence of rhizosphere traits (root hairs, exudates composition) and abiotic factors (soil texture, drought) on the rhizosphere processes of nutrient acquisition and plant defence as summarized in Fig. ES13.

Our results showed that root hairs:

a) enlarge rhizosphere extent for β-glucosidase by 35 % and thus, providing better conditions for microbial activities and SOM decomposition. While the absence of root hairs in *rth3* induced higher abundance of *Candidatus* Udaeocacter, which able to acquire more energy demanding amino acids and vitamins as C (=energy) source from the environment instead of soil organic carbon;
b) promote higher leucine aminopeptidase activity and thus ensures a greater advantage in utilising protein hotspots in the soil for roots and microorganisms ;
c) induce formation of the P depletion zones in the 3-weeks-old maize in a rhizobox, which resulted in up to 80 % higher acid phosphatase activity to mineralize organic P to plant available mineral forms;
d) do not have significant effect on the rhizosphere extent of phosphatase activity in the rhizosphere of field-grown 12-weeks-old maize;
e) widen the rhizosphere extension of root exudates and water under drought meaning 24% - 37% increase of proportion of soil which can be mined by plant.

Co-localization analysis revealed that both available carbon (^{14}C exudates) and available soil water equally contributed to β-glucosidase activity, but soil moisture is likely to contribute more than root morphology such as root hairs in controlling enzymatic hotspot and their distribution in the rhizosphere.

Benzoxazinoids suppressed the activities of rhizosphere microorganisms, which led to 30% lower β-glucosidase activity on root surface and in the rhizosphere. On the other hand, the presence of benzoxazinoids strongly supported plant defence against pathogenic fungi (i.e., genus *Fusarium* and *Gibberella*), which, however, could not be fully substituted by an increased exudation and activities of enzymes (chitinase, β-glucosidase) with plant protection function in *bx1*.

Soil texture plays a significant role for the intensity and effectiveness of P mobilizing processes. Maize grown in sand had ~0.45 mm larger rhizosphere extents of acidification being also ~0.1 pH units stronger than in loam. This larger and stronger acidification caused ~1 mm larger average rhizosphere extents for acid phosphatase activity in sand, which however did not have preference over loam with nearly 6 times higher amount of soil organic matter. Thus, higher amount of organic substrate for acid phosphatase in loam was more important for P mobilization in the rhizosphere of maize that the stronger acidification or broader enzymatic extent in sand.

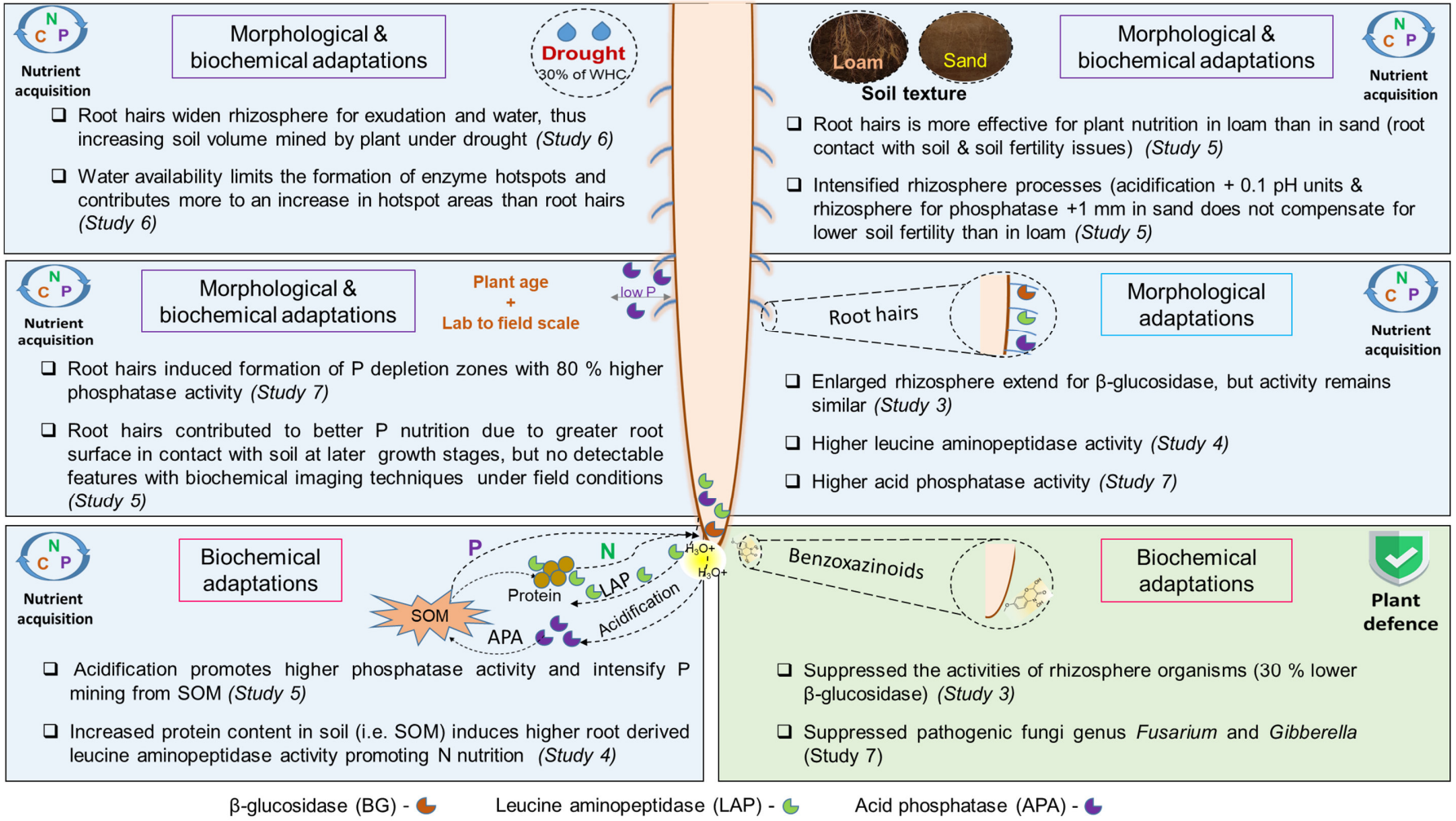

Figure ES 13 Summary of the main findings obtained in individual studies of the PhD thesis

1.8 Conclusions and perspectives

Generally, this thesis showed for the first time that multi-imaging techniques when combined with *ex-situ* enzyme kinetics and DNA sequencing for microbiome analysis are a powerful tool to study simultaneously occurred rhizosphere processes of nutrients' mining and plant defence. The proposed complex approach enables revealing the role of root exudates composition, root morphology and environmental factors on the rhizosphere processes as well as key players inducing them.

We conclude that the shape and extent of the rhizosphere for enzyme activities are genotype-specific and depend on the spatial distribution of the released rhizodeposits. Soil conditions (i.e., soil texture) play an important role for intensities of the enzymatic process of nutrient mobilization. Therefore, sandy soils should be amended with organic matter (i.e. manure, crop residues, etc.) to facilitate enzymatic decomposition of organic substrates over a longer growing period in field for better nutrient supply to crops in a long-term perspective. Our studies show that gene knock-out often substantially alters the process-network in the rhizosphere, including its spatial localization along and across the roots. Thus, plant breeding towards increasing the presence of root hairs is a promising tool for an effective rhizosphere management to improve plant-soil-microbe interactions leading to better nutrients acquisition and especially phosphorus as a finite resource on the planet. In the current threat of global warming, maize will be benefited from root hairs to overcome drought conditions. Manipulation of root exudation composition is another breeding strategy for improving plant ability to acquire nutrients from soil. By aiming at higher content of benzoxazinoids, maize breeding also reinforces the natural ability of plant to protect itself against pathogens and thus perform environmentally friendly and sustainable crop production.

1.9 References

Ahmed, M.A., Sanaullah, M., Blagodatskaya, E., Mason-Jones, K., Jawad, H., Kuzyakov, Y., Dippold, M.A., 2018. Soil microorganisms exhibit enzymatic and priming response to root mucilage under drought. Soil Biology and Biochemistry 116, 410–418. doi:10.1016/j.soilbio.2017.10.041

Andrews, S., 2010. FASTQC. A quality control tool for high throughput sequence data.

Baldovinos, F., Thomas, G.W., 1967. The Effect of Soil Clay Content on Phosphorus Uptake. Soil Science Society of America Journal 1, 2–4. doi:https://doi.org/10.2136/sssaj1967.03615995003100050020x

Banerjee, S., Schlaeppi, K., van der Heijden, M.G.A., 2018. Keystone taxa as drivers of microbiome structure and functioning. Nature Reviews Microbiology 16, 567–576. doi:10.1038/s41579-018-0024-1

Berendsen, R.L., Pieterse, C.M.J., Bakker, P.A.H.M., 2012. The rhizosphere microbiome and plant health. Trends in Plant Science 17, 478–486. doi:10.1016/j.tplants.2012.04.001

Bertin, C., Yang, X., Weston, L.A., 2003. The role of root exudates and allelochemicals in the rhizosphere. Plant and Soil 256, 67–83. doi:10.1023/A:1026290508166

Bertrand, I., Hinsinger, P., Jaillard, B., Arvieu, J.C., 1999. Dynamics of phosphorus in the rhizosphere of maize and rape grown on synthetic, phosphated calcite and goethite. Plant and Soil 211, 111–119. doi:10.1023/A:1004328815280

Bilyera, N., Blagodatskaya, E., Yevdokimov, I., Kuzyakov, Y., 2018. Towards a conversion factor for soil microbial phosphorus. European Journal of Soil Biology 87, 1–8. doi:10.1016/j.ejsobi.2018.03.002

Bilyera, N., Kuzyakova, I., Guber, A., Razavi, B.S., Kuzyakov, Y., 2020. How “hot” are hotspots: Statistically localizing the high-activity areas on soil and rhizosphere images. Rhizosphere 16, 100259. doi:doi.org/10.1016/j.rhisph.2020.100259

Bilyera, N., Zhang, X., Duddek, P., Fan, L., Banfield, C.C., Schlüter, S., Carminati, A., Kaestner, A., Ahmed, M.A., Kuzyakov, Y., Dippold, M.A., Spielvogel, S., Razavi, B.S., 2021. Maize genotype-specific exudation strategies: an adaptive mechanism to increase microbial activity in the rhizosphere. Soil Biology and Biochemistry 162, 108426. doi:10.1016/j.soilbio.2021.108426

Blossfeld, S., Gansert, D., 2007. A novel non-invasive optical method for quantitative visualization of pH dynamics in the rhizosphere of plants. Plant, Cell and Environment 30, 176–186. doi:10.1111/j.1365-3040.2006.01616.x

Bolte, S., Cordelières, F.P., 2006. A guided tour into subcellular colocalization analysis in light microscopy. Journal of Microscopy. doi:10.1111/j.1365-2818.2006.01706.x

Brown, L.K., George, T.S., Dupuy, L.X., White, P.J., 2013. A conceptual model of root hair ideotypes for future agricultural environments: what combination of traits should be targeted to cope with limited P availability? Annals of Botany 112, 317–330. doi:10.1093/aob/mcs231

Cairns, J.R.K., Esen, A., 2010. β-Glucosidases. Cellular and Molecular Life Sciences 67, 3389–3405. 10.1007/s00018-010-0399-2

Callahan, B.J., McMurdie, P.J., Holmes, S.P., 2017. Exact sequence variants should replace operational taxonomic units in marker-gene data analysis. The ISME Journal 11, 2639–2643. doi:10.1038/ismej.2017.119

Callahan, B.J., McMurdie, P.J., Rosen, M.J., Han, A.W., Johnson, A.J.A., Holmes, S.P., 2016. DADA2: High-resolution sample inference from Illumina amplicon data. Nature Methods 13, 581–583. doi:10.1038/nmeth.3869

Canarini, A., Kaiser, C., Merchant, A., Richter, A., Wanek, W., 2019. Root exudation of primary metabolites: Mechanisms and their roles in plant responses to environmental stimuli. Frontiers in Plant Science 10. doi:10.3389/fpls.2019.00157

Cotton, T.E.A., Pétriacq, P., Cameron, D.D., Meselmani, M. Al, Schwarzenbacher, R., Rolfe, S.A., Ton, J., 2019. Metabolic regulation of the maize rhizobiome by benzoxazinoids. The ISME Journal 13, 1647–1658. doi:10.1038/s41396-019-0375-2

Curtin, D., Trolove, S., 2013. Predicting pH buffering capacity of New Zealand soils from organic matter content and mineral characteristics. Soil Research 51, 494. doi:10.1071/SR13137

Daly, K.R., Keyes, S.D., Masum, S., Roose, T., 2016. Image-based modelling of nutrient movement in and around the rhizosphere. Journal of Experimental Botany 67, 1059–1070. doi:10.1093/jxb/erv544

Dick, R., Rattei, T., Haslbeck, M., Schwab, W., Gierl, A., Frey, M., 2012. Comparative analysis of benzoxazinoid biosynthesis in monocots and dicots: Independent recruitment of Stabilization and activation functions. Plant Cell 24, 915–928.

Dick, W.A., Cheng, L., Wang, P., 2000. Soil acid and alkaline phosphatase activity as pH adjustment indicators. Soil Biology and Biochemistry 32, 1915–1919. doi:doi.org/10.1016/S0038-0717(00)00166-8

Erb, M., Kliebenstein, D.J., 2020. Plant Secondary Metabolites as Defenses, Regulators, and Primary Metabolites: The Blurred Functional Trichotomy. Plant Physiology 184, 39–52. doi:10.1104/pp.20.00433

Farrar, J., Hawes, M., Jones, D., Lindow, S., 2003. How roots control the flux of carbon to the rhizosphere. Ecology 84, 827–837. doi:10.1890/0012-9658(2003)084[0827:HRCTFO]2.0.CO;2

Flach, J., Pilet, P.-E., Jollès, P., 1992. What's new in chitinase research? Experientia 48, 701–716. doi:10.1007/BF02124285

Frey, M., Chomet, P., Glawischnig, E., Stettner, C., Grün, S., Winklmair, A., Eisenreich, W., Bacher, A., Meeley, R.B., Briggs, S.P., Simcox, K., Gierl, A., 1997. Analysis of a chemical plant defense mechanism in grasses. Science 277, 696–699. doi:10.1126/science.277.5326.696

Gaines, T.P., Gaines, S.T., 1994. Soil texture effect on nitrate leaching in soil percolates. Communications in Soil Science and Plant Analysis 25, 2561–2570. doi:10.1080/00103629409369207

Gargallo-Garriga, A., Preece, C., Sardans, J., Oravec, M., Urban, O., Peñuelas, J., 2018. Root exudate metabolomes change under drought and show limited capacity for recovery. Scientific Reports 8, 12696. doi:10.1038/s41598-018-30150-0

Gerke, J., 2015. The acquisition of phosphate by higher plants: Effect of carboxylate release by the roots. A critical review. Journal of Plant Nutrition and Soil Science 178, 351–364. doi:10.1002/jpln.201400590

Gianfreda, L., 2015. Enzymes of importance to rhizosphere processes. Journal of Soil Science and Plant Nutrition 0–0. doi:10.4067/S0718-95162015005000022

Goswami, R.S., Kistler, H.C., 2004. Heading for disaster: Fusarium graminearum on cereal crops. Molecular Plant Pathology 5, 515–525. doi:10.1111/j.1364-3703.2004.00252.x

Gramss, G., Voigt, K.-D., Kirsche, B., 1999. Oxidoreductase enzymes liberated by plant roots and their effects on soil humic material. Chemosphere 38, 1481–1494. doi:10.1016/S0045-6535(98)00369-5

Greenfield, L.M., Razavi, B.S., Bilyera, N., Zhang, X., Jones, D.L., 2021. Root hairs and protein addition to soil promote leucine aminopeptidase activity of Hordeum vulgare L. Rhizosphere 18, 100329. doi:10.1016/j.rhisph.2021.100329

Guber, A., Kravchenko, A., Razavi, B.S., Uteau, D., Peth, S., Blagodatskaya, E., Kuzyakov, Y., 2018. Quantitative soil zymography: Mechanisms, processes of substrate and enzyme diffusion in porous media. Soil Biology and Biochemistry 127, 156–167. doi:10.1016/j.soilbio.2018.09.030

Haling, R.E., Brown, L.K., Bengough, A.G., Young, I.M., Hallett, P.D., White, P.J., George, T.S., 2013. Root hairs improve root penetration, root–soil contact, and phosphorus acquisition in soils of different strength. Journal of Experimental Botany 64, 3711–3721. doi:10.1093/jxb/ert200

Hazrati, H., Fomsgaard, I.S., Kudsk, P., 2020. Root-Exuded Benzoxazinoids : Uptake and Translocation in Neighboring Plants.

Henrissat, B., 1991. A classification of glycosyl hydrolases based on amino acid sequence similarities. Biochemical Journal 280, 309–316. doi:10.1042/bj2800309

Hiltner, L., 1904. Über neuere Erfahrungen und Probleme auf dem Gebiete der Bodenbakteriologie unter besonderer Berücksichtigung der Gründüngung und Brache. Arbeiten Der Deutschen Landwirtschaftlichen Gesellschaft 98, 59–78.

Hinsinger, P., Bengough, A.G., Vetterlein, D., Young, I.M., 2009. Rhizosphere: Biophysics, biogeochemistry and ecological relevance. Plant and Soil 321, 117–152. doi:10.1007/s11104-008-9885-9

Hoefer, C., Santner, J., Borisov, S.M., Wenzel, W.W., Puschenreiter, M., 2017. Integrating chemical imaging of cationic trace metal solutes and pH into a single hydrogel layer. Analytica Chimica Acta 950, 88–97. doi:10.1016/j.aca.2016.11.004

Holz, M., Zarebanadkouki, M., Carminati, A., Becker, J.N., Spohn, M., 2020. The effect of root hairs on rhizosphere phosphatase activity. Journal of Plant Nutrition and Soil Science 000, 1–7. doi:10.1002/jpln.201900426

Holz, M., Zarebanadkouki, M., Carminati, A., Hovind, J., Kaestner, A., Spohn, M., 2019. Increased water retention in the rhizosphere allows for high phosphatase activity in drying soil. Plant and Soil 443, 259–271. doi:10.1007/s11104-019-04234-3

Holz, M., Zarebanadkouki, M., Kuzyakov, Y., Pausch, J., Carminati, A., 2018. Root hairs increase rhizosphere extension and carbon input to soil. Annals of Botany 121, 61–69. doi:10.1093/aob/mcx127

Hu, L., Robert, C.A.M., Cadot, S., Zhang, X., Ye, M., Li, B., Manzo, D., Chervet, N., Steinger, T., Van Der Heijden, M.G.A., Schlaeppi, K., Erb, M., 2018. Root exudate metabolites drive plant-soil feedbacks on growth and defense by shaping the rhizosphere microbiota. Nature Communications 9, 1–13. doi:10.1038/s41467-018-05122-7

Huang, Q., Liang, W., Cai, P., 2005. Adsorption, desorption and activities of acid phosphatase on various colloidal particles from an Ultisol. Colloids and Surfaces B: Biointerfaces 45, 209–214. doi:10.1016/j.colsurfb.2005.08.011

Hummel, C., Boitt, G., Santner, J., Lehto, N.J., Condron, L., Wenzel, W.W., 2021. Co-occurring increased phosphatase activity and labile P depletion in the rhizosphere of Lupinus angustifolius assessed with a novel, combined 2D-imaging approach. Soil Biology and Biochemistry 153. doi:10.1016/j.soilbio.2020.107963

Itoh, S., Barber, S.A., 1983. A numerical solution of whole plant nutrient uptake for soil-root systems with root hairs. Plant and Soil 70,

403–413. doi:10.1007/BF02374895

Jones, D.L., 1998. Organic acids in the rhizosphere – a critical review. Plant and Soil 205, 25–44. doi:10.1023/A:1004356007312

Jones, D.L., Nguyen, C., Finlay, R.D., 2009. Carbon flow in the rhizosphere: carbon trading at the soil–root interface. Plant and Soil 321, 5–33. doi:10.1007/s11104-009-9925-0

Jungk, A., 2001. Root hairs and the acquisition of plant nutrients from soil. Journal of Plant Nutrition and Soil Science 164, 121–129. doi:10.1002/1522-2624(200104)164:2<121::AID-JPLN121>3.0.CO;2-6

Jungk, A., Seeling, B., Gerke, J., 1993. Mobilization of different phosphate fractions in the rhizosphere. Plant and Soil 155–156, 91–94. doi:10.1007/BF00024991

Kandeler, E., Marschner, P., Tscherko, D., Singh Gahoonia, T., Nielsen, N.E., 2002. Microbial community composition and functional diversity in the rhizosphere of maize. Plant and Soil 238, 301–312. doi:10.1023/A:1014479220689

Koranda, M., Schnecker, J., Kaiser, C., Fuchslueger, L., Kitzler, B., Stange, C.F., Sessitsch, A., Zechmeister-Boltenstern, S., Richter, A., 2011. Microbial processes and community composition in the rhizosphere of European beech – The influence of plant C exudates. Soil Biology and Biochemistry 43, 551–558. doi:10.1016/j.soilbio.2010.11.022

Kreuzeder, A., Santner, J., Prohaska, T., Wenzel, W.W., 2013. Gel for simultaneous chemical imaging of anionic and cationic solutes using diffusive gradients in thin films. Analytical Chemistry 85, 12028–12036. doi:10.1021/ac403050f

Kudjordjie, E.N., Sapkota, R., Steffensen, S.K., Fomsgaard, I.S., Nicolaisen, M., 2019. Maize synthesized benzoxazinoids affect the host associated microbiome. Microbiome 7, 1–17. doi:10.1186/s40168-019-0677-7

Kumar, A., Singh, V.P., Pandey, D.S., Kumar, R., 2019. Rhizosphere Management: A Novel Approach for Improving the Crop Productivity. International Journal of Current Microbiology and Applied Sciences 8, 2143–2155. doi:10.20546/ijcmas.2019.803.257

Kuzyakov, Y., Shevtzova, E., Pustovoytov, K., 2006. Carbonate re-crystallization in soil revealed by 14C labeling: Experiment, model and significance for paleo-environmental reconstructions. Geoderma 131, 45–58. doi:10.1016/j.geoderma.2005.03.002

Lagos, M.L., Maruyama, F., Nannipieri, P., Mora, M.L., Ogram, A., Jorquera, M.A., 2015. Current overview on the study of bacteria in the rhizosphere by modern molecular techniques: A mini-review. Journal of Soil Science and Plant Nutrition 15, 504–523. doi:10.4067/s0718-95162015005000042

Lang, F., Bauhus, J., Frossard, E., George, E., Kaiser, K., Kaupenjohann, M., Krüger, J., Matzner, E., Polle, A., Prietzel, J., Rennenberg, H., Wellbrock, N., 2016. Phosphorus in forest ecosystems: New insights from an ecosystem nutrition perspective. Journal of Plant Nutrition and Soil Science 2015, 129–135. doi:10.1002/jpln.201500541

Liu, Y., Shahbaz, M., Ge, T., Zhu, Z., Liu, S., Chen, L., Wu, X., Deng, Y., Lu, S., Wu, J., 2020. European Journal of Soil Biology Effects of root exudate stoichiometry on CO 2 emission from paddy soil. European Journal of Soil Biology 101, 103247. doi:10.1016/j.ejsobi.2020.103247

Lucas, M., Schlüter, S., Vogel, H., Vetterlein, D., 2019. Roots compact the surrounding soil depending on the structures they encounter. Scientific Reports 9, 16236. doi:10.1038/s41598-019-52665-w

Ma, X., Mason-Jones, K., Liu, Y., Blagodatskaya, E., Kuzyakov, Y., Guber, A., Dippold, M.A., Razavi, B.S., 2019. Coupling zymography with pH mapping reveals a shift in lupine phosphorus acquisition strategy driven by cluster roots. Soil Biology and Biochemistry 135, 420–428. doi:10.1016/j.rhisph.2020.100198

Ma, X., Zarebanadkouki, M., Kuzyakov, Y., Blagodatskaya, E., Pausch, J., Razavi, B.S., 2018. Spatial patterns of enzyme activities in the rhizosphere: Effects of root hairs and root radius. Soil Biology and Biochemistry 118, 69–78.

Martin, M., 2011. Cutadapt removes adapter sequences from high-throughput sequencing reads. EMBnet.Journal 17, 10.

McDougall, B.M., Rovira, A.D., 1970. Sites of exudation of 14C-labelled compounds from wheat roots. New Phytologist 69, 999–1003. doi:10.1111/j.1469-8137.1970.tb02479.x

Nannipieri, P., Johnson, R.L., Paul, E.A., 1978. Criteria for measurement of microbial growth and activity in soil. Soil Biology and Biochemistry 10, 223–229. doi:10.1016/0038-0717(78)90100-1

Neumann, G., Römheld, V., 1999. Root excretion of carboxylic acids and protons in phosphorus-deficient plants. Plant and Soil 211, 121–130. doi:10.1023/A:1004380832118

Oburger, E., Jones, D.L., Wenzel, W.W., 2011. Phosphorus saturation and pH differentially regulate the efficiency of organic acid anion-mediated P solubilization mechanisms in soil. Plant and Soil 341, 363–382. doi:10.1007/s11104-010-0650-5

Oburger, E., Kirk, G.J.D., Wenzel, W.W., Puschenreiter, M., Jones, D.L., 2009. Interactive effects of organic acids in the rhizosphere. Soil Biology and Biochemistry 41, 449–457. doi:10.1016/j.soilbio.2008.10.034

Okello, P.N., Petrović, K., Kontz, B., Mathew, F.M., 2019. Eight species of Fusarium cause root rot of corn (Zea mays) in South

Dakota. Plant Health Progress 20, 38–43. doi:10.1094/PHP-11-18-0075-RS

Olesen, T., Moldrup, P., Yamaguchi, T., Rolston, D.E., 2001. Constant slope impedance factor model for predicting the solute diffusion coefficient in unsaturated soil. Soil Science 166, 89–96. doi:10.1097/00010694-200102000-00002

Penn, C.J., Camberato, J.J., 2019. A critical review on soil chemical processes that control how soil ph affects phosphorus availability to plants. Agriculture 9, 1–18. doi:10.3390/agriculture9060120

Pott, D.M., Osorio, S., Vallarino, J.G., 2019. From Central to Specialized Metabolism: An Overview of Some Secondary Compounds Derived From the Primary Metabolism for Their Role in Conferring Nutritional and Organoleptic Characteristics to Fruit. Frontiers in Plant Science 10. doi:10.3389/fpls.2019.00835

Preece, C., Peñuelas, J., 2016. Rhizodeposition under drought and consequences for soil communities and ecosystem resilience. Plant and Soil 409, 1–17. doi:10.1007/s11104-016-3090-z

Raghothama, K.G., Karthikeyan, A.S., 2005. Phosphate Acquisition. Plant and Soil 274, 37–49. doi:10.1007/s11104-004-2005-6

Razavi, B.S., Blagodatskaya, E., Kuzyakov, Y., 2016a. Temperature selects for static soil enzyme systems to maintain high catalytic efficiency. Soil Biology and Biochemistry 97, 15–22. doi:10.1016/j.soilbio.2016.02.018

Razavi, B.S., Zarebanadkouki, M., Blagodatskaya, E., Kuzyakov, Y., 2016b. Rhizosphere shape of lentil and maize: Spatial distribution of enzyme activities. Soil Biology and Biochemistry 79, 229–237. doi:10.1016/j.soilbio.2016.02.020

Ruiz, S., Koebernick, N., Duncan, S., Fletcher, D.M., Scotson, C., Boghi, A., 2020. Significance of root hairs at the field scale – modelling root water and phosphorus uptake under different field conditions 281–304.

Scranton, M.A., Yee, A., Park, S., Walling, L.L., 2012. Plant Leucine Aminopeptidases Moonlight as Molecular Chaperones to Alleviate Stress-induced Damage * □. Journal of Biological Chemistry 287, 18408–18417. doi:10.1074/jbc.M111.309500

Segal, E., Kushnir, T., Mualem, Y., Shani, U., 2008. Water Uptake and Hydraulics of the Root Hair Rhizosphere. Vadose Zone Journal 7, 1027–1034. doi:10.2136/vzj2007.0122

Silberbush, M., Barber, S.A., 1983. Sensitivity of simulated phosphorus uptake to parameters used by a mechanistic-mathematical model. Plant and Soil 74, 93–100. doi:10.1007/BF02178744

Tachibana, Y., Ohta, Y., 1983. Root surface area, as a parameter in relation to water and nutrient uptake by cucumber plant. Soil Science and Plant Nutrition 29, 387–392. doi:10.1080/00380768.1983.10434642

Turner, B.L., Driessen, J.P., Haygarth, P.M., Mckelvie, I.D., 2003. Potential contribution of lysed bacterial cells to phosphorus solubilisation in two rewetted Australian pasture soils. Soil Biology and Biochemistry 35, 187–189. doi:10.1016/S0038-0717(02)00244-4

Vetterlein, D., Lippold, E., Schreiter, S., Phalempin, M., Fahrenkampf, T., Hochholdinger, F., Marcon, C., Tarkka, M., Oburger, E., Ahmed, M., Javaux, M., Schlüter, S., 2021. Experimental platforms for the investigation of spatiotemporal patterns in the rhizosphere—Laboratory and field scale. Journal of Plant Nutrition and Soil Science 184, 35–50. doi:10.1002/jpln.202000079

Vives-Peris, V., de Ollas, C., Gómez-Cadenas, A., Pérez-Clemente, R.M., 2020. Root exudates: from plant to rhizosphere and beyond. Plant Cell Reports 39, 3–17. doi:10.1007/s00299-019-02447-5

Vogel, S., Bönecke, E., Kling, C., Kramer, E., Lück, K., Nagel, A., Philipp, G., Rühlmann, J., Schröter, I., Gebbers, R., 2020. Base neutralizing capacity of agricultural soils in a quaternary landscape of northłeast Germany and its relationship to best management practices in lime requirement determination. Agronomy 10. doi:10.3390/agronomy10060877

Voothuluru, P., Braun, D.M., Boyer, J.S., 2018. An in vivo imaging assay detects spatial variability in glucose release from plant roots. Plant Physiology 178, 1002–1010. doi:10.1104/pp.18.00614

Wang, X.C., Lu, Q., 2006. Beta-glucosidase activity in paddy soils of the Taihu Lake region, China. Pedosphere 16, 118–124.

York, L.M., Carminati, A., Mooney, S.J., Ritz, K., Bennett, M.J., 2016. The holistic rhizosphere: integrating zones, processes, and semantics in the soil influenced by roots. Journal of Experimental Botany 67, 3629–3643. doi:10.1093/jxb/erw108

Zhang, F., Shen, J., Zhang, J., Zuo, Y., Li, L., Chen, X., 2010. Rhizosphere Processes and Management for Improving Nutrient Use Efficiency and Crop Productivity. Implications for China, 1st ed, Advances in Agronomy. Elsevier Inc.

Zhang, X., Kuzyakov, Y., Zang, H., Dippold, M.A., Shi, L., Spielvogel, S., Razavi, B.S., 2020. Rhizosphere hotspots: Root hairs and warming control microbial efficiency, carbon utilization and energy production. Soil Biology and Biochemistry 107872. doi:10.1016/j.soilbio.2020.107872

Zhao, Y., Fu, W., Hu, C., Chen, G., Xiao, Z., Chen, Y., Wang, Z., Cheng, H., 2021. Variation of rhizosphere microbial community in continuous mono-maize seed production. Scientific Reports 11, 1–13. doi:10.1038/s41598-021-81228-1

Zheng, Z., Parent, L.E., Macleod, J.A., 2003. Influence of soil texture on fertilizer and soil phosphorus transformations in Gleysolic soils. Canadian Journal of Soil Science 83, 395–403.

1.10 Contribution to the included manuscripts

The Ph.D. thesis is a cumulative study, which comprises five published, one submitted and one in preparation manuscripts elaborated in cooperation with various co-authors. The extent of the doctoral candidate's contribution to the manuscripts is assessed on the following scale:

A. Has contributed to the work (0-33%)
B. Has made a substantial contribution (34-66%)
C. Did the majority of the work independently (67-100%)

Study 1. Razavi, B.S., Zhang, X., **Bilyera, N.**, Guber, A., Zarebanadkouki, M., 2019. Soil zymography: Simple and reliable? Review of current knowledge and optimization of the method. *Rhizosphere* 11, 100161.

Conceptual design	A
Planning	A
Implementation:	A
Preparation of the manuscript	A

Study 2. Bilyera, N., Kuzyakova, I., Guber, A., Razavi, B.S., Kuzyakov, Y., 2020. How "hot" are hotspots: Statistically localizing the high-activity areas on soil and rhizosphere images. *Rhizosphere* 16, 100259.

Conceptual design	B
Planning	C
Implementation:	C
Preparation of the manuscript	C

Study 3. Bilyera, N., Zhang, X., Duddek, P., Fan, L., Banfield, C.C., Schlüter, S., Carminati, A., Kaestner, A., Ahmed, M. A., Kuzyakov, Y., Dippold, M.A., Spielvogel, S., Razavi, B.S. 2021. Maize genotype-specific exudation strategies: an adaptive mechanism to increase microbial activity in the rhizosphere, *Soil Biology and Biochemistry, 162, 108426*

Conceptual design	B
Planning	C
Implementation:	C
Preparation of the manuscript	C

Study 4. Greenfield, L.M., Razavi, B.S., **Bilyera, N.**, Zhang, X., Jones, D.L., 2021. Rhizosphere Root hairs and protein addition to soil promote leucine aminopeptidase activity of *Hordeum vulgare* L., Rhizosphere, 18, 100329

Conceptual design	A
Planning	A
Implementation:	B
Preparation of the manuscript	A

Study 5. Bilyera, N.*, Hummel, C.*, Daudin, G., Santangeli, M., Zhang, X., Santner, J., Lippold, E., Schlüter, S., Bertrand, I., Wenzel, W., Spielvogel, S., Vetterlein, D., Razavi, B.S., Oburger, E. 2022. Co-localised phosphorus mobilization processes in the rhizosphere of field-grown maize jointly contribute to plant nutrition, Soil Biology and Biochemistry, 165, 108497.

*- equal contribution

Conceptual design	A
Planning	B
Implementation:	B
Preparation of the manuscript	C

Study 6. Zhang, X., **Bilyera, N.**, Fan, L., Duddek, P., Ahmed, M. A., Carminati, A., Kaestner, A., Dippold, M.A., Spielvogel, S., Razavi, B.S. Water availability is more important than exudation for the spatial distribution of microbial activities under drought (*Under review in New Phytologist)*

Conceptual design	A
Planning	B
Implementation:	B
Preparation of the manuscript	A

Study 7. Bilyera, N., Waelchli, J., Shi, L., Caggia, V., Zhang X., Shlaeppi, K., Dippold, M.A., Razavi, B.S., Spielvogel, S. Effect of root hairs and benzoxazinoids on maize microbiome and its enzymatic activity in the rhizosphere hot-and coldspots *(in Preparation)*

Conceptual design	B
Planning	C
Implementation:	C
Preparation of the manuscript	C

2 Publications and manuscripts

2.1 Study 1. Soil zymography: Simple and reliable? Review of current knowledge and optimization of the method

Bahar S. Razavi[a,b], Xuechen Zhang[c,d], Nataliya Bilyera[a,b], Andrey Guber[e], Mohsen Zarebanadkouki[f]*

[a] Institute of Phytopathology, University of Kiel, Kiel, Germany
[b] Institute of Plant Nutrition and Soil Science, University of Kiel, Kiel, Germany
[c] Department of Biogeochemistry of Agroecosystem, University of Göttingen, Göttingen, Germany
[d] Department of Agricultural Soil Science, University of Göttingen, Göttingen, Germany
[e] Department of Plant, Soil, and Microbial Sciences, Michigan State University, USA
[f] Chair of Soil Physics, University of Bayreuth, Bayreuth, Germany

*Corresponding author Bahar S. Razavi, Email: brazavi@phytomed.uni-kiel.de

Status: *published in Rhizosphere, 2019, Vol. 11., 100161, doi: 10.1016/j.rhisph.2019.100161*

2.1.1 Abstract

Within just a few years, soil zymography has become accepted as an attractive and unique approach for 2D mapping of enzyme activities in intact soil samples. With zymography, enzymatic conversion of the substrate into a hydrolysis reaction product can literally be visualized. Soil zymography is, however, fraught with methodical difficulties due to: (i) membrane or gel attachment to the soil surface; (ii) diffusion of substrates through the membrane or gel and of reaction products back to the membrane; (iii) strong effect of imaging (photography) and image analysis on the results. In this review, we describe important procedural details of soil zymography and define the steps necessary to properly visualize enzyme activities in environmental samples. We make the following recommendations to improve zymography results 1) run soil background imaging prior to any soil zymography; 2) confirm that roots are in the soil and not on top of the soil surface; 3) perform soil zymography under the initial environmental conditions of the samples (temperature, water content, light intensity, etc); 4) examine whether membrane/gel attachment during the incubation is appropriate to properly measure enzyme activity; 5) find the right balance

between saturating substrate concentration of soil and selected substrate concentration for zymography; 6) run proper standards to ensure that enzyme activity values can be accurately calculated; 7) fix camera settings and photography conditions; 8) ensure that images are properly analyzed. These steps should help to develop a unified visualization of enzyme activities in soil and ecosystem ecology. Finally, coupling of soil zymography with other imaging techniques and advanced analytical approaches will give insight into the net effect of multiple processes, such as root respiration, rhizodeposition, nutrient and metal(loid) dynamics, plant-mediated oxygen release, microbial respiration and reoxidation of reduced compounds in relation to the activities of enzymes released by plants or microbes.

Keywords*: spatial pattern, enzyme distribution, imaging, microbial activity, hotspots*

2.1.2 Introduction

2.1.2.1 Current knowledge and relevance

The term ‘zymography’ denotes the visualization of enzymatic activity by substrate conversion (essentially enzyme photography). The general biochemical reaction can be detected for either the appearance of the reaction product or the disappearance of the substrate (Vandooren et al., 2013; Spohn et al., 2013; Spohn and Kuzyakov, 2013). Zymography was first introduced in 1962, for detecting collagen degradation in tadpole tissue and described a matrix metalloproteinase (MMP) (Gross and Lapière, 1962; Vandooren et al., 2013). Development of zymography over five decades was mostly focused on the analysis of proteases and their inhibitors in various matrices and media besides soil (Hughes and Herr, 2010; Pan et al., 2011; Choi et al., 2009), for example, to gain insights into tumor formation (Kleiner and Stetlerstevenson, 1994; Nemori and Tachikawa, 1999; Wilkesman and Kurz, 2009).

Kurzbaum et al. (2010), proposed a novel approach to visualize dehydrogenase activity of plant roots by use of tetrazolium violet dye without destructive steps, allowing repeated observations of growing plants and the impact of inhibitors such as sodium azide and cycloheximide. However, this approach was not tested in soil specimens. Visualization of enzyme activities developed rapidly once fluorescently labeled substrates became widely applied in environmental samples. During the first attempt at visualization of enzyme activity in the soil matrix, the fluorescently labeled substrate was dissolved in agarose solution that was then directly poured onto the sample (Baldrian and Větrovský, 2012). The approach was successful in

visualizing the spatial distribution of enzyme activity in soils and in biological specimens such as fungal cell colonies. However, due to the diffusion of the substrate in agar gel, the resolution of this enzyme mapping method was low. The same limitation was visible following the standard zymography assays for the detection of protease and amylase activity in electrophoresis gels (Spohn et al., 2013). The revolutionary optimization of the method started by integrating dissolved fluorescently labeled substrates in membrane filters instead of gels (Spohn and Kuzyakov, 2013; Sanaullah et al., 2016; Razavi et al., 2016).

Soil zymography techniques can be utilized for hydrolases or oxidases acting on any biological substrate such as proteins and peptides, oligosaccharides and polysaccharides, lipids and sugars (Kurzbaum et al., 2010; Spohn et al., 2013; Voothuluru et al., 2018).

To date soil zymography has been adapted for various applications such as studying the impact of plant species (Razavi et al., 2016), root morphology (Ma et al., 2018), pathogens (Razavi et al., 2017a), abiotic controls like temperature (Ge et al., 2017), drought (Guhr et al., 2015; Ahmadi et al., 2018), nutrient availability (Wei et al., 2018; Giles et al., 2018; Heitkötter and Marschner, 2018) and heavy metal pollution (Duan et al., 2018) on the activity of different enzymes in various spheres such as the rhizosphere (Spohn and Kuzyakov, 2013; Sanaullah et al., 2016), detritusphere (Spohn and Kuzyakov, 2014; Liu et al., 2017; Ma et al., 2017; Wei et al., 2019), and biopores (Hoang et al., 2016; Razavi et al., 2017b), in both lab and field studies (Razavi et al., 2017b). Benefiting from all of these developments, we can now test a larger array of hypotheses related to enzyme-based processes and their roles in biogeochemical cycling. Besides its potential application, the simple sample preparation procedure and relatively worldwide accessibility of all necessary chemicals and equipment have made soil zymography one of the most influential imaging techniques in soil.

Despite the widespread adoption of soil zymography, a comprehensive discussion of the details and pitfalls of the method is not available in the literature. In fact, a major motivation for writing this contribution is that the authors (and our colleagues) receive dozens of inquiries each year on the execution and interpretation of soil zymography. The prevalent use of high-throughput soil zymography methods has created the need for a comprehensive review of the current state of the art in ecosystem studies. The potential knowledge gap affects the quality and utility of contemporary soil zymography data; distort results or often resulting in relative activity levels that are incomparable among different studies, even though the same enzymes are studied. Methodological optimization will enable the soil and ecological community to perform larger scale meta-analyses, aiming to improve understanding of how plant and microbial enzymes drive

ecosystem processes. For specific methodological studies regarding the preparation of calibration lines for soil zymography, and the sensitivity of enzyme activity measurements to exposure time during photography we refer readers to the recent works by Guber et al. (2018a) and Giles et al. (2018).

2.1.2.2 Soil zymography and its expected outcomes

Briefly, soil zymography involves visualizing fluorescent compounds produced when a substrate reacts with a substrate-specific enzyme. A membrane filter is soaked in a solution containing a known concentration of fluorescently labeled substrate. The uniformly saturated membrane will be placed in contact with the soil surface either directly (Razavi et al., 2016) or protected by a thin layer of gel (Spohn and Kuzyakov, 2013). The membrane will be incubated on the soil surface for a given period of time (see 6.4.2) and then will be removed and the imprint of the enzyme on the membrane will be imaged under UV light in dark (Fig. 1).

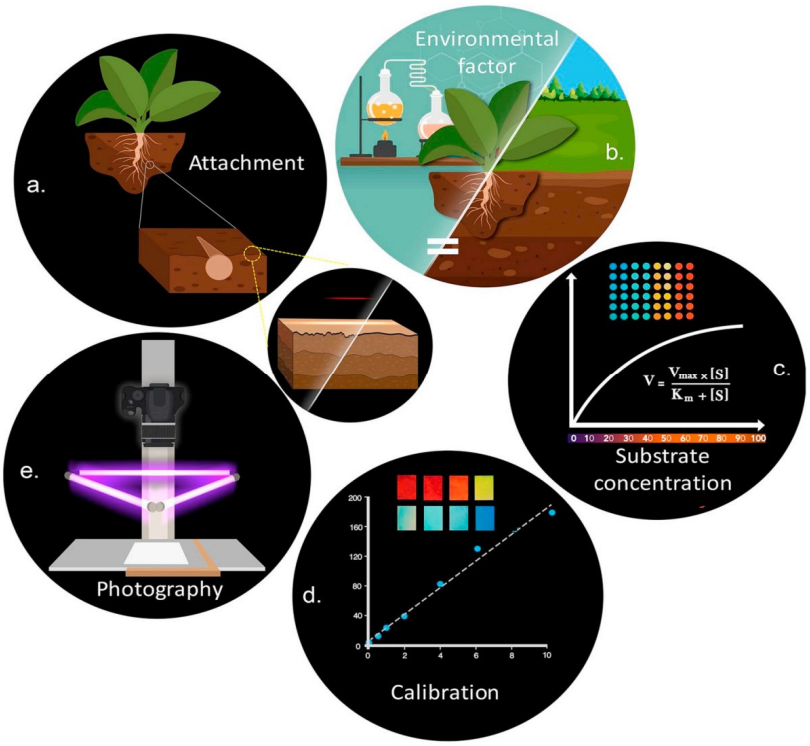

Figure 1. Schematic illustration of soil zymography setup and its main steps: **a.** shows root position and membrane attachment. The inset shows laser scanning for soil surface topography; **b.** Performance of soil zymography under the initial environmental conditions of the samples; **c.** Balance between saturating substrate concentration of soil and selected substrate concentration; **d.** Proper calibration standards; **e.** Fixed camera settings and photography conditions. *Art work: Tahoora Emam.*

The result of zymography is a 2-D image obtained by a normal camera and is called a zymogram. The captured zymogram can be further quantified and related to the probability that a given enzyme reacts with the substrate and activates its fluorescent agent per unit of area and time. The fluorescent substrate is initially on the membrane and gets activated when it meets a specific enzyme located on the soil surface.

Theoretically, this activation process may occur by two contrasting diffusion-driven processes: i) once a membrane saturated by substrate is placed at the soil surface the substrate may diffuse (by Brownian motion) towards the soil surface. As the substrate meets a specific enzyme at the soil surface it gets activated. By the nature of diffusion, the now-fluorescent substrate may move back to the membrane, where its imprint will be visualized, ii) another alternative would be that the enzyme at the soil surface diffuses towards the membrane and activates the fluorescent agent of the substrate. Similarly, this process is also Brownian motion driven and may occur in both directions (i.e. the enzyme may return to the soil). After enough time, both processes will reach a steady state and the detected enzyme activity on the membrane will be constant. Although both processes are theoretically possible, the diffusion rates for substrate towards the soil and fluorescent product return is higher. The diffusion rate of a substance is inversely proportional to the square root of its molecular mass. Typically, enzymes have average molecular weights ranging from 10 kD to 2,000 kD (Ogston, 1962; Wright, 1962), while the substrate used in zymography has a molecular weight of 176 D. This simple consideration would suggest that the probability that substrate diffuses towards the soil is surly more than 7.5 times higher than the enzyme towards the membrane ($D \propto \sqrt{1/M}$, where D is the diffusion rate and M is the molecular weight). Thus, in soil zymography, while the membrane is placed on the soil surface it is very probable that the substrate diffuses from the membrane to the soil. This diffusion depends strongly on soil water content at the soil-membrane interface and the contact between soil and the membrane. A partially dried soil surface may adversely affect the results of enzyme activity (consider the case that only the first soil pore at the interface between membrane and soil are dry while the rest of the soil is wetter). In such cases, if the goal is to estimate potential enzyme activity -besides qualitative visualization- soil zymography could be coupled with classical enzyme assays (Hoang et al., 2016; Ma et al., 2017; Zhang et al., 2019).

One of the most important points to consider when performing soil zymography is that it is not a replacement for classical enzyme assays. Classical enzyme assays measure “maximum potential” enzymatic activity (Burns, 1978; Tabatabai and Dick, 2002; Wallenstein and Weintraub, 2008) in soil or litter. By its nature, soil zymography reflects enzyme activity associated with

surfaces of a given sample rather than its entire volume (Baldrian and Větrovský, 2012). Based on experimental data and simulation it was shown that detected enzyme activity is only a small proportion, around 20-30%, of the actual reactions that take place within the total soil volume (Ma et al., 2017; Guber et al., 2018b).

To ensure that estimations are accurate, several factors must be considered and procedures carried out before starting soil zymography in environmental samples: chemicals and materials, incubation conditions and duration, imaging conditions, sample preparation and image analysis. We will address each of these in turn with some examples of adaptations for specific conditions; however, for detail methodological descriptions of each hotsphere, in the lab and field, we refer the reader to original experimental studies (Hoang et al., 2016; Razavi et al., 2017b, Liu et al., 2017; Ge et al., 2017).

2.1.3 Chemicals and materials

2.1.3.1 Substrate

Current soil zymography has benefitted greatly from fluorescent dye-conjugated substrates [e.g., 4-methylumbelliferone (MUF), 7-amino-4-methylcoumarin (AMC); Marx et al., 2001; Saiya-Cork et al., 2002] for the detection of many hydrolytic enzymes. These fluorescence agents allow rapid and specific determination of the spatial distribution of enzyme activities involved in C, N, P and S cycling and, thus, provide the opportunity to answer questions related to the enzymatic hotspots on broader scales. Besides MUF- or AMC- conjugated substrates, 1-(3,7-dihydroxyphenoxazin-10-yl) ethanone, (OxiRed) and tetrazolium-dye substrates are also suitable for visualization of enzyme activities. OxiRed ($C_{14}H_{11}NO_4$), is a fluorogenic substrate that can be used to detect peroxidase activity (Table 1). The method is based on determination of a fluorescent signal developed from enzymatic oxidation of the substrate in the presence of peroxidase in the soil. In the presence of horseradish peroxidase (HRP), the OxiRed probe reacts in 1:1 stoichiometry with H_2O_2 to produce highly fluorescent resorufin. The substrates can be dissolved in 300µl dimethyl sulfoxide (DMSO) and later diluted with universal buffer to the desired concentration. OxiRed is sensitive to light and oxygen, which makes its application more limited than the other substrates. Tetrazolium violet-based dyes are qualitative redox indicators that enable visualization of dehydrogenase activity (Steponkus and Lanphear, 1967; Kurzbaum et al., 2010).

The substrate concentration normally suggested are 10 mM (Spohn et al., 2014) or 10µM (Razavi et al., 2017b). However, these concentrations are not necessarily an optimum

concentration for all soil types and, for many soils, concentrations much less than 10 mM would be sufficient to reach saturating conditions for each hydrolytic enzyme. The saturated concentration can be inferred from Michaelis-Menten kinetics (Michaelis and Menten, 1913).

Table 1. Enzymes commonly imaged in environmental samples, and their organic matter constituents and substrates.

Enzyme	Synthetic substrate	Organic matter constituent
β-glucosidase	4-MUF- β-D-glucopyranoside	Cellulose degradation products
β-cellobiosidase	4-MUF-β-D-cellobioside	Cellulose degradation products
α-glucosidase	4- MUF- β-D-glucopyranoside	Starch degradation products
Xylanase	4-MUF-b-D-xylopyranoside	Hemicellulose degradation products
Phosphatase	4-MUF-Phosphate	Phytate & Phosphodiester bond degrading
Leucine-aminopeptidase	L-Leucine-7-amino-4-methylcoumarin	leucine and amino acids
Tyrosine-aminopeptidase	L-Tyrosine-7-amido-4methylcoumarin	Tyrosine and amino acids
Chitinase	4-MUF- N-Acetyl-β-D-glucosaminide	Chitin degradation products
Chitotriosidase	4-Nitrophenyl beta-D-N,Nprime, triacetylchitotriose	Chitin degradation products
Peroxidase	1-(3,7-Dihydroxyphenoxazin-10-yl)ethanone	Lignin polymerizing products

(Modified after German et al., 2011)

Therefore, pre-testing is necessary to determine the appropriate substrate concentration for the soil prior to zymography. Application of inappropriate concentrations will complicate the interpretation of images, because obtained signals become insensitive to increments of concentration. This results in gray values that are out of the linear part of the calibration curve (over-saturating signals), (Razavi et al., 2016a; Guber et al., 2018a), (Fig. 2), (for more detail see section 6.6.1).

2.1.3.2 pH

Enzymes are sensitive to pH and display specific pH optima (Tabatabai, 1994; Turner, 2010). However, enzymes in soil may not be at their pH optimum (Burns, 1978). Unlike animal digestive tracts, for example, most microbes cannot control the environmental pH for their enzyme activity. Thus, in order to visualize enzyme activities in environmental samples, soil zymography should be run at the same pH as sample. Based on studies of soil enzymology it is known that

some of the buffers may interfere with enzyme activity (Burns, 1978; Tabatabai, 1994; German et al., 2011; Sinsabaugh, 2010). For instance, phosphate buffer may interfere with the measurement of phosphatase activities, and is an inhibitor of glucosidase (Dahlqvist, 1968), while citrate can chelate iron (Essington et al., 2005), thereby inhibiting enzymes with iron-heme prosthetic groups (Sinsabaugh, 2010). Besides, MUF- or AMC-conjugated substrates fluoresce best at alkaline pH values (>9; Mead et al., 1955).

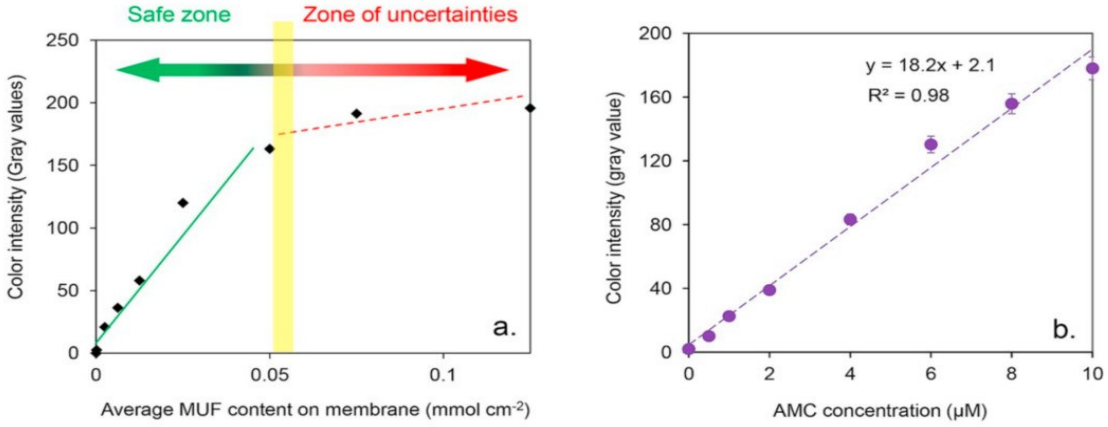

Figure. 2. Examples of calibration line: a) when the correlation of gray values and concentrations are linear; b) when the correlation is not linear. When the calibration line shows non-linear behavior, the safe zone of the curve according to the concentration and gray values should be identified and only the linear range of the calibration should be used. -

Since assays are typically conducted at a pH lower than 9, NaOH is often added to raise the pH immediately before reading the samples in a fluorometer (German et al., 2011). Extreme alkalization compromised assay sensitivity because of variation (increase and decrease) in the fluorescence of the product/standard (German et al., 2011). Another issue regarding alkalization is that the fluorescence of MUF and AMC vary with time following the addition of NaOH (Fig. 3). MUF fluorescence increases until ~20 min after NaOH addition, whereas AMC shows a decrease in fluorescence with time following the alkalization. In soil zymography, this would lead to exaggerated/elimination signals, which would be incorrectly, interpreted as high/low enzyme activities on the soil surface or a high/low percentage of hotspots (Fig. 3). It has even been suggested to omit any buffer for enzyme assays (German et al., 2011); however, pH fluctuation has been observed in assays performed in the absence of buffer (Fig. 3), (Burn, 1978), while, AMC fluorescence with TRIZMA buffer [$C_4H_{11}NO_3$•HCl, $C_4H_{11}NO_3$; pH:7.2] without NaOH addition

showed temporal stationary pattern. Therefore, the substrates can be dissolved in any universal buffer that shows a static trend over time and no inhibitory effect on enzymes (Fig. 3).

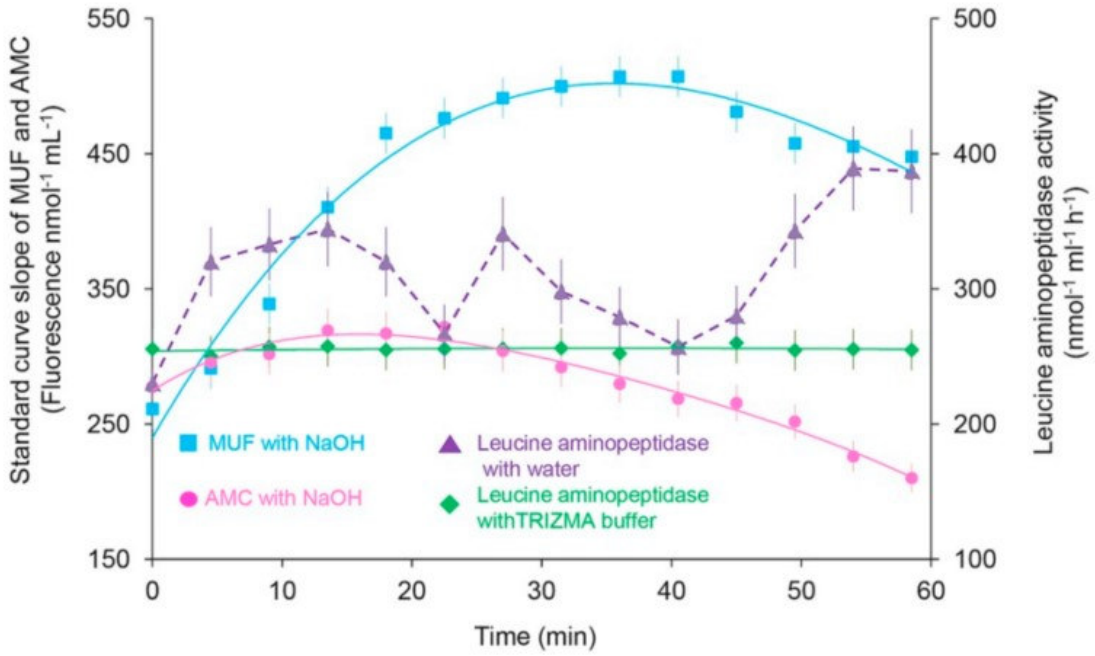

Figure 3. Intensity of MUF and AMC standard curves with and without NaOH, as well as trend of leucine aminopeptidase activity with and without buffer.

2.1.3.3 Membranes

Ideally, the thickness of the membrane filter should be reduced as much as possible to provide uniform vertical distribution of substrate in the membrane. However, thin membranes do not eliminate horizontal diffusion within the membrane, which creates an illusion of a growing area of enzyme activity over time. More specifically, by placing small drops of MUF/AMC with different concentrations in the middle of a membrane saturated with a buffer, followed by monitoring the area of the signal development under UV-light provides sufficient information for estimating the diffusion coefficients. The calculated diffusion coefficient of MUF on a dry membrane filter (Tao Yuan, China) was 5×10^{-5} mm min^{-1}. Estimated diffusion coefficients can be used in calculations of expansion of enzyme activity (for example in the rhizosphere).

2.1.4 Sample preparation

2.1.4.1 Root position and membrane attachment

Proper contact between the soil surface and the membrane is crucial for achieving interpretable results. The interpretation of the fluorescent pattern on zymograms is based on the assumption that locations with high fluorescence reflect locations with high enzyme activities on the soil surface, while locations with no fluorescence correspond to locations on the soil surface without activity. However, the contact between the soil surface and membrane depends on the roughness and topology of the soil surface, which varies depending on soil particle size distribution and the positions of roots.

A lack of proper contact between soil surface and membrane may result in the absence of fluorescence signals on the zymograms and thus are interpreted as regions with no activity. To reduce the risk of misinterpretation, an initial evaluation of soil heterogeneity by taking and analyzing a photograph of the soil surface and, when possible, performing laser scanning to assess the roughness of the soil surface, is recommended. Laser scanning of the soil surface (e.g. using NextEngine, Inc., Santa Monica, California) prior to zymography could be reasonable for soil surface characterization and micro-topography (e.g. the areas of large and medium-sized soil pores at the surface as well as root distribution) (Guber et al., 2018b). The scanner uses a set of laser beams to hit the soil surface from different angles. Each point from the soil surface is automatically positioned by a laser-light sensor in a 3-D coordinate system at a nominal resolution of 1.7 µm (Uteau et al., 2013). While laser scanning provides a detailed soil surface map, it will not yield direct information on which portions of the surface will be in contact with the membrane after its placement on the surface. The general considerations are that the contact will take place at the areas which have the greatest height (peaks) in comparison with another regions of the soil surface, (Guber et al., 2018b).

The positions of roots on the soil surface is another critical factor that should be considered in performing soil zymography. Generally, there are 4 possible positions for root growth in a rhizobox or in field rhizotrons (root windows) (Fig. 4): Roots may be positioned: i) completely on top of the soil surface, ii) partly buried in soil and partly outside of the soil surface, iii) partly buried in soil and positioned at the same level as the soil surface, iv) completely buried in the soil.

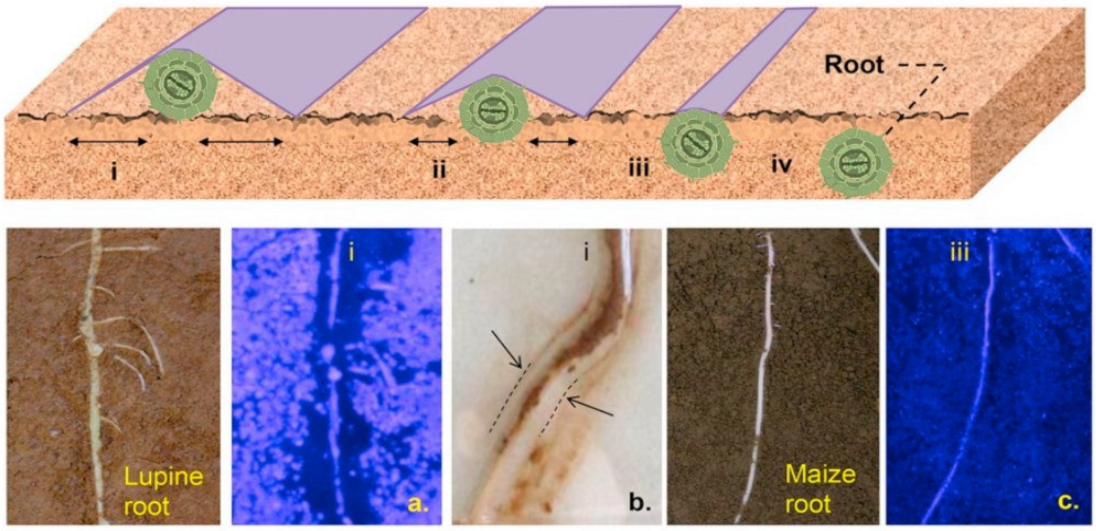

Figure 4. Four possible positions of root in soil: i) completely out of the soil surface, ii) partly buried in soil and positioned partly outside of the soil surface, iii) partly buried in soil and positioned at the same level as the soil surface, iv) completely buried in the soil. The eliminated zones around the lupine root (a) corresponding to the similar root position as position (i). (b), shows eliminated zones around the maize root covered by 1 mm gel plate when the root is at a similar position as (i). A clear imprint of enzyme activity on the root and surrounding soil (c) corresponding to the similar root position as (iii). All images are in true color without image processing.

In the case that a root is in position (i), its footprint will be detected on the zymograms, but it should be kept in mind that the contact between the membrane and the surrounding soil will deteriorate depending on the thickness of the root: i.e. a thick root will prevent membrane contact across a larger region in its surroundings. For the case (ii), the imprint of the root will be detected on the zymograms, but the trail in the surrounding soil will be affected by the thickness of the root standing above the soil surface. Case (iii) is ideal for zymography (Fig. 4). The imprint of both roots and the surrounding soil will be detected safely on the zymograms. For the case that the root is in position (iii), its thickness will not have any effect on the contact between membrane and soil surface and its footprint on the zymogram will reflect its enzymatic activity. If roots are completely buried in the soil, (iv), the imprints may not be detected on the zymograms. In this case, the intensity of the detected signal mostly depends on the thickness of the soil layer between the root and membrane (Fig. 4). It should be noted that, if the root is located in position (i) or (ii), or the soil surface is not uniform, application of any intervening material e.g. filter paper, gel plate, would not improve the attachment and there will be a "blind spot" around the roots (Fig. 4, b). The same is valid for direct application of membrane, as we cannot fold the membrane (Fig. 4. a).

Thus, confirmation of an appropriate root position is a critical step prior to any soil zymography analysis.

2.1.4.2 Incubation conditions and duration

In general, the incubation time depends on the temperature, soil texture, the activity of the tested enzyme in the soil and the soil water content. Soil water content (gravimetric or volumetric water content) and soil texture has a great impact on diffusion of enzyme (Burns et al., 2013). The drier is the soil the longer is the distance that any substrate should diffuse to/from the membrane (the overall chance of enzyme and substrate to diffuse decreases). However, theoretically, diffusion rate will increase at high water content and the probability that substrate would bind to enzyme (form enzyme-substrate complex) will be enhanced (Allison et al., 2011; Manzoni et al., 2012). Hence, the water content of samples should be constant. As the VW refers to the percentage of pores that are filled with water, it would represents the higher portion of enzymes if we assume that enzymes and microorganisms are active in the liquid phase (water-film or biofilms–biosynthesized polymeric substances exude by soil microbiome) (Or et al., 2007), or if we assume soil pores serve as conduits for water flow and chemical transport, as well as habitats for microorganisms, and thus play a key role in determining rates and magnitudes of most of soil chemical and biological processes (Kravchenko et al., 2015). Thus, soil water content has strong effect on results interpretation and accordingly, the incubation time should be long enough for diffusion to take place across the soil surface and the membrane. During this time, it is important to prevent evaporation from the membrane and ensure contact between the membrane and soil surface. To ensure such attachment one may put additional weight onto the membrane. However, different weights will greatly change the obtained signal on the zymograms (Fig. 5). If the load is necessary (for example in case of mapping enzymes around soil columns), then equal weight should be applied to all the samples.

The incubation time should not be too long, as this will cause oversaturation of the membrane. For a coarser soil with lower water content, a longer incubation time would be required than for a wet soil. One hour of incubation is normally selected based on preliminary experiments and previous studies (Dong et al., 2007). The criterion for appropriate incubation time is based on color intensity and diffusion rate: i) reaching the maximum intensity, ii) no detectable horizontal diffusion on the membrane (Fig. 5). After incubation, the membranes should be carefully lifted off the soil surface and any attached soil particles should be gently removed using tweezers. Another option is taking multiple images during the incubation on the soil surface at regular time intervals (2 to 5 minutes) and use the whole image sequence in calculations of enzyme activity.

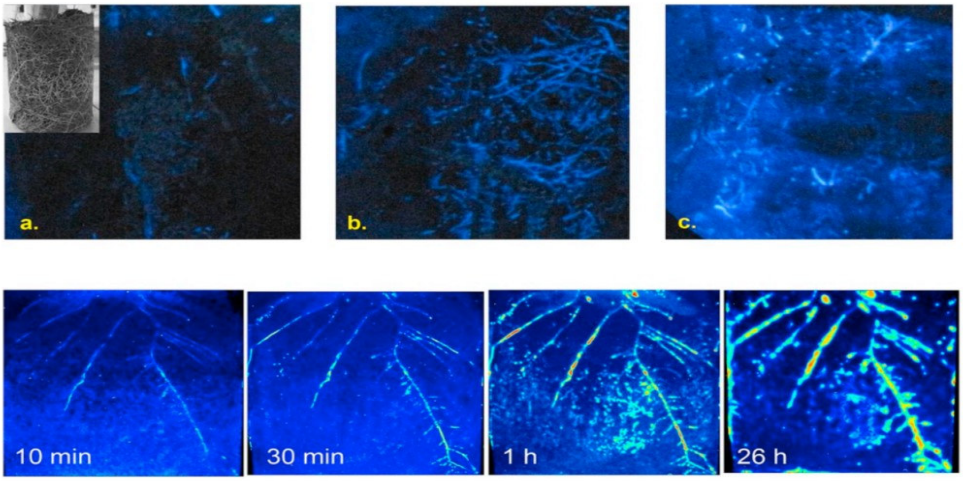

Figure 5. Top: a, b and c presenting three different load levels around a soil column. The sub figure of a, shows real soil column. All images are in true color without image processing. Bottom: four incubation durations. The radial diffusion on the membrane after 26 h is clearly detectable.

2.1.5 Imaging procedure

2.1.5.1 Camera setting

The motivation behind this section is to highlight how strongly the imaging step, camera, and the lens models affect the quality of images as well as interpretation of results.

Analyses of over 95 different full-frame models on the Canon EOS 6D – a randomly selected camera – showed the focal length ranged between 12 mm to 600 mm. These tests revealed that, on average, about 45% of the resolution is lost due to lens defects. The data from DxOMark Image Labs shows that the EOS 6D camera is able to exceed maximum sharpness when paired with the right lens. It should be also taken into account that most digital cameras have internal settings to adjust their capturing properties depending on the intensity of the light received through the lens. In such cases, these settings should be disabled prior to any imaging.

Due to signal variation under different exposure times, the same camera settings should be used for zymograms and calibration standards. For more detailed methodological studies involving the sensitivity of measured enzyme activity to exposure time during photography we refer readers to (Waters, 2009; Guber et al., 2018a; Giles et al., 2018).

2.1.5.2 Photography

To obtain reliable results it is very important to perform zymography under the same conditions, such as temperature and selected incubation time. After/during incubation, the membranes will be placed under ultraviolet (UV) illumination with an excitation wavelength of 355 nm and an emission wavelength of 460 nm, in a light-proof room or chamber. The UV light can be a single circular lamp, a rectangle or a square consisting of 3 or 4 similar lamps, with a wattage range of 18 - 22 W. Important is that the sample will receive equal light intensity from all sides (Fig. 1).

The distance between the UV light sources, the camera and the samples (zymograms) should be fixed. This includes not only a fixed distance between zymogram, camera and UV light but also camera position, orientation, angle, image capture time and all camera settings. Any light or reflection will have a direct effect on the images and cause overestimation of color intensity. Zymograms should be corrected for the empty membrane (I_{em}, zymograms taken without any substrate) and the dark current (I_{dc}, the signal recorded by the camera when there is no zymogram) according to (Eq. 1):

$$I_{norm} = \frac{I - I_{dc}}{I_{em} - I_{dc}} \quad (1)$$

where I_{norm} is the corrected image and I is the original image. Thus, to correct for variations of the light intensity over the image area, background images from the uncoated membrane as well as background images without any membrane are needed (Eq. 1), (Menon et al., 2007). The scaled black flat field similar in all images should be considered as a reference object during whole image processing (Fig. S1). In addition, we strongly recommend a background test for each individual soil. This includes incubation of a water- or buffer-saturated membrane on the soil and imaging under UV light. This step is indispensable as many soil organic compounds can diffuse into the membrane, as can elements that can be detected as fluorescence under UV light: humic and a reduced quinone-like compounds (quinone compounds can be reduced by cellular reductases), (Watanabe et al., 2004) as well as some heavy metals can produce interfering signals (Fig. 6).

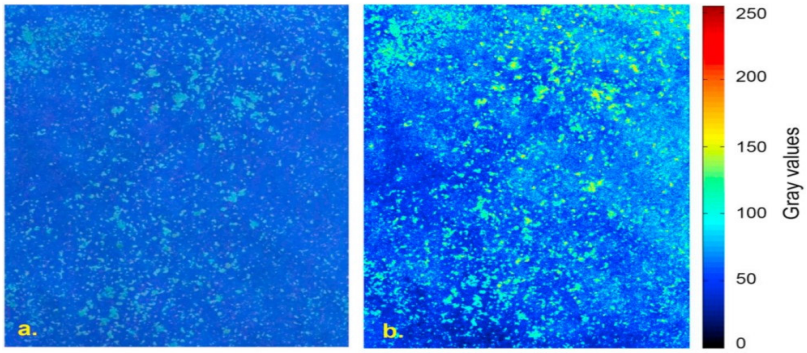

Figure 6. Detected false signals on membrane saturated by sterile water under UV light. Not a single pixel refers to spot with enzyme activity. (a) Shows the original zymogram in true color and (b) shows the same zymogram after image processing.

2.1.6 Image processing, quantification and analysis

2.1.6.1 Calibration line

The amount of MUF, AMC or any other fluorogenic conjugate on an area basis can be calculated from the concentration and volume of the solution taken up by the membrane and its size. The membranes used for calibration should be imaged under UV light and analyzed in the same way as the samples (e.g. imaging and light conditions, the same incubation time and same camera settings).

There are two general approaches for calibration of soil zymograms. The simplest consists of saturating the membrane filters with standard MUF/AMC solutions and taking photographs of these filters using the same settings as for the zymography (Spohn and Kuzyakov, 2013, 2014). The image obtained with zero concentration of the fluorophore is subtracted from the images with known concentrations (background correction). The concentration of MUF/AMC per unit of area can be calculated for each membrane based on the applied concentration and volume of adsorbed solution. A linear regression with zero intercept is fitted to the obtained values of MUF/AMC (Fig. 2b). Normally, the correlation of fluorophore concentration and gray values results in an equation as (Eq. (2)) and is used to calculate enzyme activity per unit of area on zymograms:

$$y=ax+b \qquad (2)$$

where y is enzyme activity, x is the gray value of the zymogram, and a is the slope of the fitted curve. The disadvantage of this approach lies in the deviation of the calibration curves from

linearity due to membrane oversaturation at MUF/AMC content of approximately 12 mM. Using the calibration beyond this concentration is therefore not reliable (Fig. 2, a).

The second approach applies a known volume of the standard MUF/ AMC solution to the membrane surface with continuous imaging. The disadvantage of this approach is the need for many different concentrations and volumes of the standard solutions and a relatively complicated algorithm of pixel-based calibration (Eq. (3)). The algorithm comprises two sections of linear regression:

$$\begin{cases} \overline{M}_{\mathrm{MUF/AMC}} = b_1 \times \overline{G}; & 0 < \overline{G} < G^* \\ \overline{M}_{\mathrm{MUF/AMC}} = a_2 + b_2 \times \overline{G}; & G^* < \overline{G} \\ b_2 = b_1 - a_2 / G^* \end{cases} \quad (3)$$

where $M_{\mathrm{MUF/AMC}}$ is an average MUF/AMC concentration in the membrane, a_2, b_1 and b_2 are parameters of the linear regression, G^* is the grey value at the breakpoint (Fig. 2. yellow line), and G is the grey value averaged across the membrane. The advantage of the second approach is the possibility to extend the calibration curve to larger concentrations of MUF/AMC and overall more accurate calibration due to accounting for non-uniformity in MUF/AMC contents across the membrane (Guber et al., 2018a).

2.1.6.2 Image processing

Processing zymography images includes 5 steps: 1) transformation of signal (fluorescence) from the images to grayscale values, 2) background correction, 3) root segmentation, 4) root skeletonization, and 5) conversion of grayscale values to enzyme activity.

The intensity of fluorescence is proportional to the activity of the enzyme. To obtain quantitative information, it is possible to process the zymograms using the image processing toolbox in Matlab (MATLAB, The MathWorks). Zymograms first should be transformed to grayscale images (8, 16 or 32-bit) as matrices and corrected for light variations and camera noise (Eq. (1)) (Soille, 2003; Menon et al., 2007; Zarebanadkouki et al., 2012). Then, the zymograms will be referenced based on the grayscale value received from a reference object embedded in all the zymograms (or scaled black flat field). After referencing the gray values obtained from the zymograms of calibration lines at the concentration of zero can be calculated and then this value

will be subtracted from all the zymograms. Note that the same membrane filters should be applied to all of the images, including both zymograms of the samples and the calibration line.

For further analysis, the roots can be easily segmented [cut off from the image by one or more points or lines], due to the strong contrast between the soil and roots. To detect the boundaries of the roots, threshold methods provided by Matlab can be used (Chaudhuri et al., 1989; Hoover et al., 2000). It should be noted that image segmentation is a crucial step in image processing, as it affects all subsequent image analyses (Schlüter et al., 2014). Locally adaptive segmentation methods (e.g. watershed algorithm; Beucher and Lantuejoul, 1979) calculate neighborhood statistics for a class assignment in order to smooth object boundaries, avoid noise objects, or compensate for local intensity changes. Due to the added flexibility, local segmentation methods often result in improved segmentation results (Iassonov et al., 2009; Wang et al., 2011). In addition, roots can be segmented and masked by multiplying the zymogram to the mask obtained from root segmentation using the Root-tracker 2D program (Fig. 7, an example Roottracker image). As the program segments the whole root system, the regions with high enzyme activity can be identified and the noise can be excluded from the analysis (Fig. 7).

To calculate enzyme activity as a function of distance along the root, the roots that are not overlapping and are entirely visible at the soil surface should be selected (Fig. 7). The images are then skeletonized with a thinning algorithm (Lam et al., 1992). The segmented roots, their lengths, and radii can be calculated using the Euclidean distance map function in Matlab (Menon et al., 2007; Moradi et al., 2011). For the processing of images using ImageJ, we refer readers to (Schlüter et al., 2014).

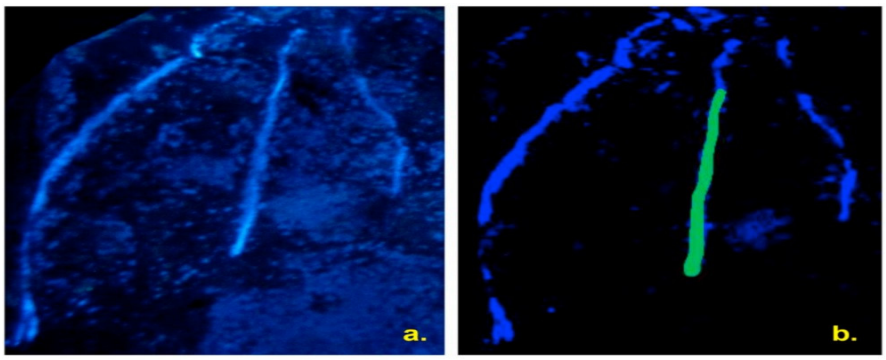

Figure 7. (a) Example of zymogram (true color), and (b) shows segmented root in green, while blue is root and noise which should be excluded from the analysis (when the whole root is not visible or the contrast between root and background is not sufficient).

2.1.7 Identification, quantification and localization of hotspots

Main relevant biogeochemical processes are take place in the microsites, so called hotspots, (Kuzyakov and Blagodatskaya, 2015). Hotspots were defined as the small soil volumes with high process rates and very intensive interactions between pools and organisms (Kuzyakov and Blagodatskaya, 2015). Hotspots are often defined as a qualitative indicator. Precise definitions vary, with typically the highest 10–30% of gray values across the entire image considered as hotspots (Hoang et al., 2016; Liu et al., 2017; Ma et al., 2017; Zhang et al., 2019). Thus, hotspot percentage is an arbitrary value. However, it is valid for the comparison of treatments within one study, provided that the same threshold is applied to all analyses. In order to unify the calculation of hotspot percentage we recommend the following approach (Kuzyakov and Razavi, 2019): First, the mean gray value in the bulk soil and the standard deviation (SD) is calculated. This mean value in the bulk soil is taken as a reference = 1.0 ± SD (Helliwell et al., 2017). Then, moving from the bulk soil to the hotspot, the enzyme activity will increase. The hotspot boundary is accepted as the point at which enzyme activity exceeds +3 SD. The boundary of +3 SD is accepted because 99.7% of all bulk soil values are located within ± 3 SD. This approach may provide the most accurate estimation of hotspots according to its original definition (Kuzyakov and Blagodatskaya, 2015).

In addition to hotspot identification, it is possible to classify different levels of activity (e.g. very low activity, low activity, moderate activity, and hotspots), (Fig. 8). The boundaries of each category can be confirmed by one way analysis of variance (ANOVA). ANOVA can assess the significant differences between independent variables (e.g. mean values of a specific number of adjacent pixels, for example equal to 0.1 mm), (Fig. 8a).

Besides, spatial pattern analysis quadrat methods (Diggle, 1983; Arnold et al., 1997) and calculation of dispersion index can illustrate whether the distribution of hotspots in space are aggregated or dispersed (Fig. 8b), (Hoang et al., 2016). Spatial point pattern analysis is a statistical method applied to obtain information about the spatial structure of the individual points (hotspots) within a study area (zymogram).

There are a number of indices that could be used with the quadrat count method to detect a significant deviation from a Poisson distribution (Fisher et al., 1922). The most common one is dispersion index (I) and is defined as:

$$I = \frac{V}{\bar{X}} \qquad (4)$$

where V and X are the sample variance and the sample mean of the quadrat counts respectively. The method is based on fact that for randomly dispersed points, the variance of the number of points (hotspots) per quadrat is approximately the same as the average number of points per quadrat. Thus, the expected value of the index is I > 1 for clustered distribution patterns and I < 1 for dispersed spatial distributions (Fig. 8b).

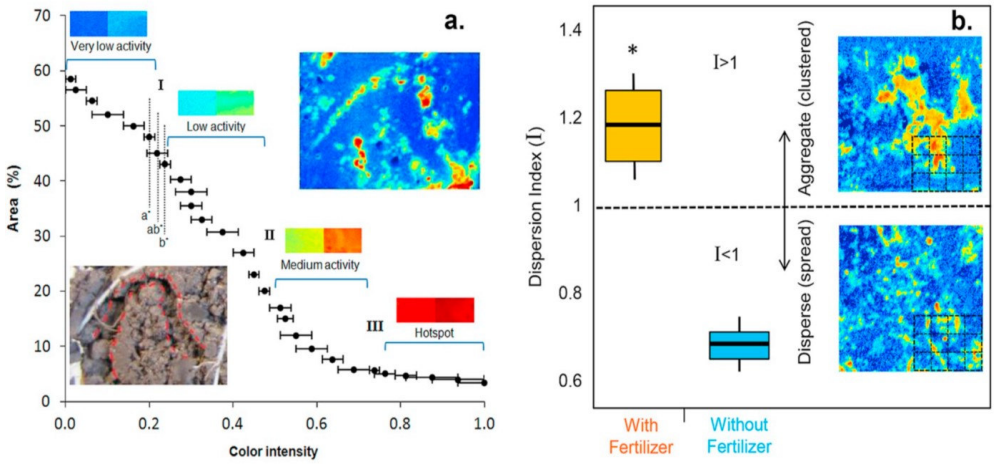

Figure 8. a) Example of detecting the boundaries of different categories of enzyme activities in the specific gradient (biopores). Percentage of the area of MUF/AMC concentration in the total image is considered as a function of color intensity. Asterisks indicate significant differences between the mean values (modified from Hoang et al., 2016). b) Example of spatial distribution of hotspots in soil treated with and without fertilizer. Long-term N fertilization leads to formation of aggregate hotspots while no fertilization caused dispersed distribution of hotspots. The dotted quadrates represent symbolic applied quadrat counts method on images.

Application of spatial point pattern analysis quadrat methods can draw critical conclusions on spatial distribution of hotspots through whole soil profiles with different origins in response to various factors (temperature, time, light intensity, etc.) and promoters (C input, earthworm activities, etc.).

2.1.8 Coupling zymography with other approaches

Soil zymography provides information on the spatial distribution of enzyme activities, an important parameter that cannot be obtained with the classical enzyme assay. Soil zymography can be used to answer broader questions by coupling with classical enzyme assays (Hoang et al., 2016; Ma et al., 2017; Zhang et al., 2019) as well as other imaging approaches such as radioisotope imaging (e.g. ^{14}C, ^{33}P, ^{35}S), (Fig. 9), (Spohn and Kuzyakov, 2013; Hoang et al., 2017), planar optodes (e.g. O_2, CO_2, pH), (Fig. 9), FISH (Spohn et al., 2015), neutron radiography,

gel-based approaches (e.g. diffusive gradients in thin films (DGT), diffusive equilibration in thin films (DET)), and also with μCT to illuminate spatial distributions of enzyme activities in three dimensions (Kravchenko et al*.,* 2019). The relevance of soil zymography for soil and ecological sciences is highlighted by the observation that microorganisms use secreted or cell-membrane-bound digestive enzymes to degrade polymeric substances (e.g., cellulose, chitin) and rely on diffusion to access the degradation products (Burns, 1982; Sinsabaugh et al., 1991; Sinsabaugh, 1994). The products of enzymatic degradation (e.g., glucose, amino acids, phosphate) are then used by microorganisms for metabolism and growth. Soil zymography coupled with other imaging techniques as well as molecular approaches (e.g., qPCR) enables in situ mapping of all these processes in microsites (hotspots) and hotspheres.

2.1.9 Summary and moving forward

Clearly, there are many challenges associated with the visualization of enzyme activities in soil and litter. Therefore, we summarized potential abiotic and biotic factors which may distort results (Table 2). In addition, we would like to conclude with a set of recommendations to improve soil zymography quality and facilitate the sharing of optimization procedures across laboratories:

1) By incubation of water/buffer-saturated membrane on the soil and its photography under UV light (a background test of the soil) prior to any soil zymography, ensure that you are detecting enzyme activity not any other fluorescent compounds.

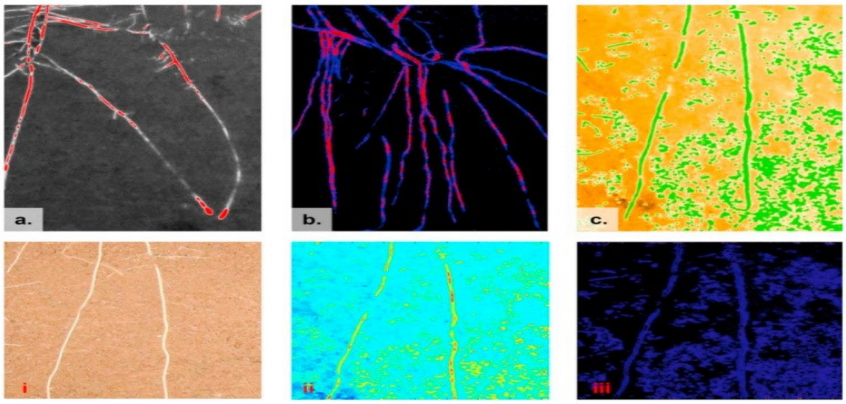

Figure 9. a: an example of overlapped ^{14}C image and zymography. The red color corresponds to β-glucosidase activity and white represents ^{14}C release (root exudate). b: An illustrative example of phosphatase activity (blue) and changes of pH (red) along the maize root. In (a) and (b) background (soil) is converted to black to improve the visibility. c: an example of three overlapped images: real root, zymogram, and CO_2 changes. The green color represents the area where leucine-aminopeptidase activity and CO_2 release overlapped. Sub-figures shows: i. roots, ii. leucine-aminopeptidase imprint, and iii. CO_2 release. There are areas where microbial respiration is visible while imprint of enzyme activity is not detectable (or the activity is low).

2) Identify the four possible positions for root growth in the rhizobox or in field rhizotrons and confirm that the roots are in the soil and not on top of the soil, prior to soil zymography.

3) Perform soil zymography under the initial environmental conditions of samples (e.g. keep exactly the same growth temperature, light intensity, water content, etc., while incubating the membrane).

4) Find the balance between saturating substrate concentrations of your soil and substrate concentration for soil zymography.

5) Examine whether attachment during the incubation is appropriate to properly map enzyme activity, and run laser scanning for soil surface topography in advance.

6) Run proper calibration standards to ensure that enzyme activity values are properly calculated.

7) Ensure that camera settings and photography conditions are the same for all samples as well as the measurement of calibration line.

8) Ensure that images are properly analyzed.

If all of these steps are followed, then researchers can be more certain that their images are indeed reflective of the spatial distribution of enzymatic activity in their samples.

Although great efforts have been made toward developing, quantifying and adapting soil zymography, we still have a long way to go. Standardized, user-friendly and correctly interpretable soil zymography tools for non-experts need to be developed and commercialized. The combination of mass spectrometry techniques and soil zymography will ultimately allow the exact trimming pattern of individual substrates by the enzyme (especially proteases) to be determined in situ and in vivo. Considering how the abiotic environment of the rhizosphere is controlled through a system of feedback loops between roots, microbes, and soil chemistry, in which the dynamics of the microbial community, root exudates, nutrient and elements, enzymes, O_2, pH, and CO_2 play an essential role, it is clear that coupling soil zymography with other novel approaches will be beneficial. Soil zymography can be used as a mapping tool for localization of microbial hotspots and be coupled further with molecular and microbial analysis to identify the microbial community, or microbial growth and efficiency.

Scaling down the soil zymography on a micro-resolution scale or combining soil zymography and other approaches with different scales (for instance nanoSIM) is another untouched side of science that remains as the dark side of the moon to be discovered.

Table 2. Summary of abiotic and biotic factors which may distort results

	Factor	Fictitious effect on result interpretation
Abiotic	High/Low water content	High/Low enzyme activity
	Extra weight on membrane	High enzyme activity
	Photography exposure time	High/low enzyme activity
	Not uniform topography	Disperse hotspot distribution
	Root position at soil surface	Localized hotspots around the root
	Inappropriate attachment	Aggregate hotspots distribution
	Incubation time	Expansion of rhizosphere or hotspots
	High/low temperature	High/low overall enzyme activity
	High substrate concentration	Outlier enzyme activity
	Alkalization	High overall activity for AMC substrates; Low overall activity MUF substrates
Biotic	Pathogen infection	Expansion of rhizosphere; High total hotspots%
	Fungus contamination	High total hotspots%
	Algae contamination	High overall enzyme activity; High total hotspots%

All of these steps will encourage better collaboration among researchers investigating the links between enzyme activities and decomposition. Furthermore, properly estimated enzyme activities may have even more meaning when used in conjunction with functional gene analysis, or emerging proteomic and genomic tools that are expanding our ability to understand microbial decomposers and the significant roles they play in ecosystems (Nannipieri, 2006; Wallenstein and Weintraub, 2008).

2.1.10 Conflict of interest

No conflict of interest.

2.1.11 Acknowledgments

BR thanks Prof. Xingliang Xu for the invitation to write this review. We gratefully acknowledge the German Research Foundation (DFG) for supporting the project: RA3062/3-1 within priority program 2089 and the highlighted importance of imaging approaches to overcome current knowledge gaps between soil, microbiome, and plant scientists. We would like to thank Prof. Yakov Kuzyakov for his valuable comments on the primarily version of the manuscript and Kyle Mason-Jones for the improvement of language and writing style. AG was supported by the National Science Foundation's Long-Term Ecological Research Program (DEB 1027253), by the National Science Foundation's Geobiology and Low-Temperature Geochemistry Program (Award no 1630399), by the Department of Energy Great Lakes Bioenergy Research Center (DOE O_ce of Science BER DE-FC02-07ER64494).

2.1.12 Appendix A, Supplementary data

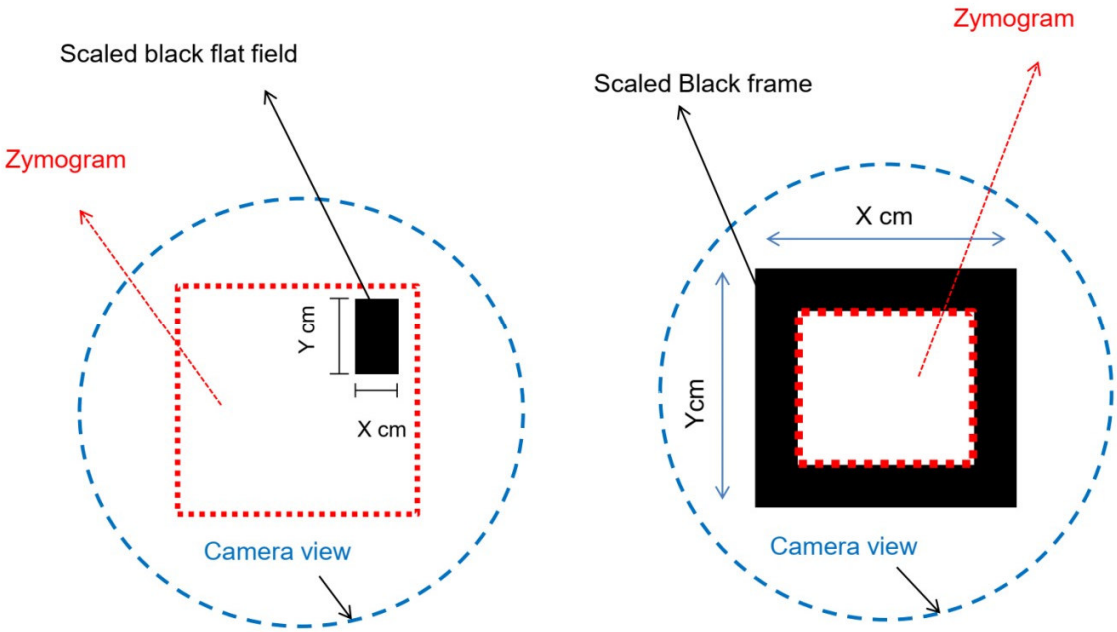

2.1.13 References

Ahmadi, K., Razavi, B.S., Maharjan, M., Kuzyakov, Y., Kostka, S.J., Carminati, A., Zarebanadkouki, M., 2018. Effects of rhizosphere wettability on microbial biomass, enzyme activities and localization. Rhizosphere 7, 35–42.

Allison, S.D., Weintraub, M.N., Gartner, T.B., Waldrop, M.P., 2011. Evolutionary economic principles as regulators of soil enzyme production and ecosystem function. Soil Enzymol. 229–243.

Arnold, S.E., Ruscheinsky, D.D., Han, L.Y., 1997. Further evidence of abnormal cytoarchitecture of the entorhinal cortex in schizophrenia using spatial point pattern analyses. Biol. Psychiatry 42, 639–647.

Baldrian, P., Větrovský, T., 2012. Scaling down the analysis of environmental processes: Monitoring enzyme activity in natural substrates on a millimeter resolution scale. Appl. Environ. Microbiol. https://doi.org/10.1128/AEM.07953-11.

Beucher, S., Lantuejoul, C., 1979. Use of watersheds. In: Contour Detection. International Workshop on Image Processing (Real-Time Edge and Motion Detection/Estimation), Rennes, France.

Burns, R.G., 1978. Enzyme activity in soil: Some theoretical and practical considerations. In: Burns, R.G. (Ed.), Soil Enzymes. Academic Press, London, pp. 295–340.

Burns, R.G., 1982. Enzyme activity in soil: Location and a possible role in microbial ecology. Soil Biol. Biochem. 14, 423–427.

Burns, R.G., Deforest, J.L., Marxsen, J., Sinsabaugh, R.L., Stromberger, M.E., Wallenstein, M.D., Weintraub, M.N., Zoppini, A., 2013. Soil enzymes in a changing environment: Current knowledge and future directions. Soil Biol. Biochem. 58, 216–234.

Chaudhuri, S., Chatterjee, S., Katz, N., Nelson, N., Goldbaum, M., 1989. Detection of blood vessels in retinal images using two dimensional matched filters. IEEE Trans. Med. Imaging 8, 263–269.

Choi, N.S., Kim, B.H., Park, C.S., Han, Y.J., Lee, H.W., Choi, J.H., Lee, S.G., Song, J.J., 2009. Multiple-layer substrate zymography for detection of several enzymes in a single sodium dodecyl sulfate gel. Anal. Chem. 386, 121–122.

Dahlqvist, A., 1968. Assay of intestinal disaccharidases. Anal. Biochem. 22, 99–107.

Diggle, P.J., 1983. Statistical Analysis of Spatial Point Patterns. Academic Press, London.

Dong, S., Brooks, D., Jones, M.D., Grayston, S.J., 2007. A method for linking in situ activities of hydrolytic enzymes to associated organisms in forest soils. Soil Biol. Biochem. 39, 2414– 2419.

Duan, C., Fang, L., Yang, C., Chen, W., Cui, Y., Li, S., 2018. Reveal the response of enzyme activities to heavy metals through in situ zymography. Ecotoxicol. Environ. Saf. 156, 106– 115.

Essington, M.E., Nelson, J.B., Holden, W.L., 2005. Gibbsite and goethite solubility: The influence of 2-ketogluconate and citrate. Soil Sci. Soc. Am. J. 69, 996–1008.

Fisher, R.A., Thornton, H.G., Mackenzie, W.A., 1922. The accuracy of the plating method of estimating the density of bacterial populations, with particular reference to the use of Thornton's agar medium with soil samples. Ann. Appl. Biol. 9, 325–359.

Ge, T.D., Wei, X.M., Razavi, B.S., Zhu, Z.K., Hu, Y.J., Kuzyakov, Y., Jones, D.L., Wu, J.S., 2017. Stability and dynamics of enzyme activity patterns in the rice rhizosphere: Effects of plant growth and temperature. Soil Biol. Biochem. 113, 108–115.

German, D.P., Weintraub, M.N., Grandy, A.S., Lauber, C.L., Rinkes, Z.L., Allison, S.D., 2011. Optimization of hydrolytic and oxidative enzyme methods for ecosystem studies. Soil Biol. Biochem. 43, 1387–1397.

Giles, C.D., Dupuy, L., Boitt, G., Brown, L.K., Condron, L.M., Darch, T., Blackwell, M.S.A., Menezes-Blackburn, D., Shand, C.A., Stutter, M.I., Lumsdon, D.G., Wendler, R., Cooper, P., Wearing, C., Zhang, H., Haygarth, P.M., George, T.S., 2018. Root development impacts on the distribution of phosphatase activity: Improvements in quantification using soil zymography. Soil Biol. Biochem. 116, 158–166.

Gross, J., Lapiere, C.M., 1962. Proc. Natl. Acad. Sci. U. S. A 48, 1014.

Guber, A.K., Kravchenko, A.N., Razavi, B.S., Blagodatskaya, E., Kuzyakov, Y., 2018a. Calibration of 2-D soil zymography for correct analysis of enzyme distribution: Calibration of 2-D soil zymography. Eur. J. Soil Sci. https://doi.org/10.1111/ejss. 12744.

Guber, A., Kravchenko, A., Razavi, B.S., Uteau, D., Peth, S., Blagodatskaya, E., Kuzyakov, Y., 2018b. Quantitative soil zymography: Mechanisms, processes of substrate and enzyme diffusion in porous media. Soil Biol. Biochem. 127, 156–167.

Guhr, A., Borken, W., Spohn, M., Matzner, E., 2015. Redistribution of soil water by a saprotrophic fungus enhances carbon mineralization. Proc. Natl. Acad. Sci. Unit. States Am. 112, 14647–14651.

Heitkötter, J., Marschner, B., 2018. Soil zymography as a powerful tool for exploring hotspots and substrate limitation in undisturbed subsoil. Soil Biol. Biochem. 124, 210–217.

Helliwell, J.R., Sturrock, C.J., Mairhofer, S., Craigon, J., Ashton, R.W., Miller, A.J., Whalley, W.R., Mooney, S.J., 2017. The emergent rhizosphere: Imaging the development of the porous architecture at the root-soil interface. Sci. Rep. 7 14875, 1–10.

Hoang, D.T.T., Pausch, J., Razavi, B.S., Kuzyakova, I., Banfield, C.C., Kuzyakov, Y., 2016. Hotspots of microbial activity induced by earthworm burrows, old root channels, and their combination in subsoil. Biol. Fertil. Soils 52, 1105–1119.

Hoang, D.T.T., Razavi, B.S., Kuzyakov, Y., 2017. Revealing hidden effect of earthworm on C distribution and enzyme activity. Geophys. Res. Abstr. 19 EGU2017-EGU13182-1.

Hoover, A., Kouznetsova, V., Goldbaum, M., 2000. Locating blood vessels in retinal images by piecewise threshold probing of a matched filter response. IEEE Trans. Med. Imaging 19, 203–210.

Hughes, A.J., Herr, A.E., 2010. Quantitative enzyme activity determination with zeptomole sensitivity by microfluidic gradient-gel zymography. Anal. Chem. 82, 3803–3811.

Iassonov, P., Gebrenegus, T., Tuller, M., 2009. Segmentation of X-ray computed tomography images of porous materials: A crucial step for characterization and quantitative analysis of pore structures. Water Resour. Res. 45. https://doi.org/10.1029/ 2009WR008087.

Kleiner, D.E., Stetlerstevenson, W.G., 1994. Quantitative zymography: Detection of picogram quantities of gelatinases. Anal. Biochem. 218, 325–329.

Kravchenko, A.N., Guber, A.K., Razavi, B.S., Koestel, J., Blagodatskaya, E.V., Dippold, M., Kuzyakov, Y., 2019. Spatial patterns of extracellular enzymes: combining X-ray computed micro-tomography and 2D zymography. Soil Biol. Biochem.

Kravchenko, A.N., Negassa, W.C., Guber, A.K., Rivers, M.L., 2015. Protection of soil carbon within macro-aggregates depends on intra-aggregate pore characteristics. Sci. Rep. 5.

Kurzbaum, E., Kirzhner, F., Armon, R., 2010. A simple method for dehydrogenase activity visualization of intact plant roots grown in soilless culture using tetrazolium violet. Plant Root 4, 12–16.

Kuzyakov, Y., Blagodatskaya, E., 2015. Microbial hotspots and hot moments in soil: Concept and review. Soil Biol. Biochem. 83, 184–199.

Kuzyakov, Y., Razavi, B.S., 2019. Rhizosphere size and shape: Temporal dynamics and spatial stationarity. Soil Biol. Biochem. 13, 343-360

Lam, L., Lee, S.-W., Suen, C.Y., 1992. Thinning methodologies-A comprehensive survey. IEEE Trans. Pattern Anal. Mach. Intell. 14, 855–869.

Liu, S., Razavi, B.S., Su, X., Maharjan, M., Zarebanadkouki, M., Blagodatskaya, E., Kuzyakov, Y., 2017. Spatio-temporal patterns of enzyme activities after manure application reflect mechanisms of niche differentiation between plants and microorganisms. Soil Biol. Biochem.

112, 100–109.

Ma, X., Razavi, B.S., Holz, M., Blagodatskaya, E., Kuzyakov, Y., 2017. Warming increases hotspot areas of enzyme activity and shortens the duration of hot moments in the rootdetritusphere. Soil Biol. Biochem. 107, 226–233.

Ma, X., Zarebanadkouki, M., Kuzyakov, Y., Blagodatskaya, E., Pausch, J., Razavi, B.S., 2018. Spatial patterns of enzyme activities in the rhizosphere: Effects of root hairs and root radius.

Soil Biol. Biochem. 118, 69–78.

Manzoni, S., Schimel, J.P., Porporato, A., 2012. Responses of soil microbial communities to water stress: results from a meta-analysis. Ecology 93, 930–938.

Marx, M.-C., Wood, M., Jarvis, S.C., 2001. A microplate fluorimetric assay for the study of enzyme diversity in soils. Soil Biol. Biochem. 33, 1633–1640.

Mead, J.A.R., Smith, J.N., Williams, R.T., 1955. Studies in detoxification. 67. Biosynthesis of the glucuronides of umbelliferone and 4-methylumbelliferone and their use in fluorimetric determination of b-glucuronidase. Biochem. J. 61, 569–574.

Menon, M., Robinson, B., Oswald, S.E., Kaestner, A., Abbaspour, K.C., Lehmann, E., Schulin, R., 2007. Visualization of root growth in heterogeneously contaminated soil using neutron radiography. Eur. J. Soil Sci. 58, 802–810

Michaelis, L., Menten, M.L., 1913. Biorhem 2 (49), 333–369.

Moradi, A.B., Carminati, A., Vetterlein, D., Vontobel, P., Lehmann, E., Weller, U., Hopmans, J.W., Vogel, H.J., Oswald, S.E., 2011. Three-dimensional visualization and quantification of water content in the rhizosphere. New Phytol. 192, 653–663.

Nannipieri, P., 2006. Role of stabilised enzymes in microbial ecology and enzyme extraction from soil with potential applications in soil proteomics. In: Nannipieri, P., Smalla, K. (Eds.), Nucleic Acids and Proteins in Soil. Springer, Berlin, pp. 75–94.

Nemori, R., Tachikawa, T.A., 1999. Review of in situ zymography: Method for localization of protease activities in a tissue. Tissue Cult Eng 25, 29–32.

Ogston, A.G., 1962. Molecular Weights of Enzymes. Nature 196, 171–172.

Or, D., Phutane, S., Dechesne, A., Ection, S.P.S., 2007. Extracellular polymeric substances affecting pore-scale hydrologic conditions for bacterial activity in unsaturated soils. Vadose Zone 6.

Pan, D., Hill, A.P., Kashou, A., Wilson, K.A., Tan-Wilson, A., 2011. Electrophoretic transfer protein zymography. Anal. Chem. 411, 277–283.

Razavi, B.S., Zarebanadkouki, M., Blagodatskaya, E., Kuzyakov, Y., 2016. Rhizosphere shape of lentil and maize: Spatial distribution of enzyme activities. Soil Biol. Biochem. 96, 229– 237.

Razavi, B.S., Hoang, D.T.T., Blagodatskaya, E., Kuzyakov, Y., 2017a. Mapping the footprint of nematodes in the rhizosphere: Cluster root formation and spatial distribution of enzyme activities. Soil Biol. Biochem. 115, 213–220.

Razavi, B.S., Hoang, D., Kuzyakov, Y., 2017b. Visualization of enzyme activities in earthworm biopores by in situ soil zymography. In: Wilkesman, J., Kurz, L. (Eds.), Zymography Methods and Protocols. Humana Press, New York, NY, USA, pp. 229–238.

Saiya-Cork, K.R., Sinsabaugh, R.L., Zak, D.R., 2002. The effects of long term nitrogen deposition on extracellular enzyme activity in an Acer saccharum forest soil. Soil Biol.

Biochem. 34, 1309–1315.

Sanaullah, M., Razavi, B.S., Blagodatskaya, E., Kuzyakov, Y., 2016. Spatial distribution and catalytic mechanisms of b-glucosidase activity at the root-soil interface. Biol. Fertil. Soils 52, 505–514.

Schlüter, S., Sheppard, A., Brown, K., Wildenschild, D., 2014. Image processing of multiphase images obtained via X-ray microtomography: A review. Water Resour. Res. 50, 3615–3639.

Sinsabaugh, R.L., 1994. Enzymatic analysis of microbial pattern and process. Biol. Fertil. Soils 17, 69–74.

Sinsabaugh, R.L., 2010. Phenol oxidase, peroxidase and organic matter dynamics of soil. Soil Biol. Biochem. 42, 391–404.

Sinsabaugh, R.L., Antibus, R.K., Linkins, A.E., 1991. An enzymic approach to the analysis of microbial activity during plant litter decomposition. Agric. Ecosyst. Environ. 34, 43–54.

Soille, P., 2003. Morphological Image Analysis: Principles and Applications, 2nd ed. Springer Verlag, Berlin, Germany, pp. 391.

Spohn, M., Kuzyakov, Y., 2013. Distribution of microbial-and root-derived phosphatase activities in the rhizosphere depending on P availability and C allocation–Coupling soil zymography with 14 C imaging. Soil Biol. Biochem. 67, 106–113.

Spohn, M., Kuzyakov, Y., 2014. Spatial and temporal dynamics of hotspots of enzyme activity as affected by living and dead roots – a soil zymography analysis. Plant Soil 79, 67–77.

Spohn, M., Carminati, A., Kuzyakov, Y., 2013. Soil zymography a novel in situ method for mapping distribution of enzyme activity in soil. Soil Biol. Biochem. 58, 275–280.

Spohn, M., Treichel, N.S., Cormann, M., Schloter, M., Fischer, D., 2015. Distribution of phosphatase activity and various bacterial phyla in the rhizosphere of Hordeum vulgare L. depending on P availability. Soil Biol. Biochem. 89, 44–51.

Steponkus, P.L., Lanphear, F.O., 1967. Refinement of the triphenyl tetrazolium chloride method of determining cold injury. Plant Physiol. 42, 1423–1426.

Tabatabai, M., 1994. Soil enzymes. In: Weaver, R.W., Angle, S., Bottomley, P. (Eds.), Methods of Soil Analysis Part 2: Microbiological and Biochemical Properties. Soil Science Society of America, Madison, pp. 775–833.

Tabatabai, M., Dick, W., 2002. Enzymes in soil: Research and developments in measuring activities. In: Burns, R.G., Dick, R.P. (Eds.), Enzymes in the Environment. Activity, Ecology and Applications. Marcel Dekker, NewYork, pp. 567–596.

Turner, B.L., 2010. Variation in pH optima of hydrolytic enzyme activities in tropical rain forest soils. Appl. Environ. Microbiol. 76, 6485–6493.

Uteau, D., Pagenkemper, S.K., Peth, S., Horn, R., 2013. Aggregate and soil clod volume measurement: A method comparison. Soil Sci. Soc. Am. J. 77, 60–63.

Vandooren, J., Geurts, N., Martens, E., Van den Steen, P.E., Opdenakker, G., 2013. Zymography methods for visualizing hydrolytic enzymes. Nat. Methods 10, 211–220.

Voothuluru, P., Braun, D.M., Boyer, J.S., 2018. An in vivo imaging assay detects spatial variability in glucose release from plant roots. Plant Physiol. 78, 1002–1010.

Wallenstein, M.D., Weintraub, M.N., 2008. Emerging tools for measuring and modeling the in situ activity of soil extracellular enzymes. Soil Biol. Biochem. 40, 2098–2106.

Wang, L., Shi, F., Lin, W., Gilmore, J.H., Shen, D., 2011. Automatic segmentation of neonatal images using convex optimization and coupled level sets. Neuroimage 58, 805–817.

Watanabe, N., Dickinson, D.A., Liu, R.M., Forman, H.J., 2004. Quinones and glutathione metabolism. Methods Enzymol. 378, 319–340.

Waters, J.C., 2009. Accuracy and precision in quantitative fluorescence microscopy. J. Cell Biol.

185, 1135–1148.

Wei, X., Ge, T., Zhu, Z., Hu, Y., Liu, S., Li, Y., Wu, J., Razavi, B.S., 2018. Expansion of rice enzymatic rhizosphere: Temporal dynamics in response to phosphorus and cellulose application. Plant Soil. https://doi.org/10.1007/s11104-018-03902-0.

Wei, X., Razavi, B.S., Yajun Hu, Y., Shen, J., Wu, J., Ge, T., 2019. C/P stoichiometry of dying rice root defines the spatial distribution and dynamics of enzyme activities in root-detritusphere. Biol. Fertil. Soils 55, 251–263.

Wilkesman, J., Kurz, L., 2009. Protease analysis by zymography: A review on techniques and patents. Recent Pat. Biotechnol. 2009, 175–184.

Wright, S.T.C., 1962. An observation suggesting that the molecular weights of enzymes can be arranged in three geometric series. Nature 193, 334–337.

Zarebanadkouki, M., Kim, Y.X., Moradi, A.B., Vogel, H.-J., Kaestner, A., Carminati, A., 2012. Quantification and modeling of local root water uptake using neutron radiography and deuterated water. Vadose Zone J. https://doi.org/10.2136/vzj2011. 0196.

Zhang, X., Dippold, M.A., Kuzyakov, Y., Razavi, B.S., 2019. Spatial pattern of enzyme activities depends on root exudate composition. Soil Biol. Biochem. 133, 83–93.

2.2 Study 2: How “hot” are hotspots: Statistically localizing the high-activity areas on soil and rhizosphere images

Nataliya Bilyera[a,b,], Irina Kuzyakova[c], Andrey Guber[d], Bahar S. Razavi[a], Yakov Kuzyakov[e,f]*

a – Dept. Soil and Plant Microbiome, Institute of Phytopathology, Christian-Albrechts-University of Kiel, 24118 Kiel, Germany
b – Dept. of Soil Science, Institute of Soil Science and Plant Nutrition, Christian-Albrechts-University of Kiel, 24118 Kiel, Germany
c – Dept. Ecoinformatics, Biometrics and Forest Growth, University of Göttingen, 37077, Göttingen, Germany
d – Soil, Plant and Microbial Sciences, Michigan State University, East Lansing, MI 48824, USA
e – Dept. of Agricultural Soil Science, Dept. of Soil Science of Temperate Ecosystems, University of Göttingen, 37077, Göttingen, Germany
f – Institute of Physicochemical and Biological Problems in Soil Science, Russian Academy of Sciences, 142290 Pushchino, Russia

* corresponding author Nataliya Bilyera, E-mail address: nbilyera@yahoo.com

Status: *published in Rhizosphere, 2020, Vol. 16, 100259, doi: 10.1016/j.rhisph.2020.100259*

2.2.1 Abstract

The topic of microbial hotspots in soil requires not only visualizing their spatial distribution and biochemical analyses, but also statistical approaches to identify these hotspots and separate them from the surrounding activities (background). We hypothesized that each hotspot type (e.g. enzyme activities in the rhizosphere, root exudation, localization of herbicide accumulation) is a result of local processes driven by biotic and/or abiotic factors, and the processes rates in the hotspots are much faster than those in the soil background. We further hypothesized that the background and hotspot activities in soil belong to different statistical distributions. Consequently, hotspot determination should be based on statistical separation of activities significantly higher than the background. We analyzed for the statistical distributions of grey values on three groups of published images: 1) ^{14}C images of carbon input by roots into the rhizosphere, 2) ^{14}C glyphosate accumulation in the plant, and 3) zymogram of leucine aminopeptidase activity in rooted soil. The two Gaussian distributions were fit (the first representing the background, the second the hotspots) to the distribution of grey values in the images, the parameters (means and standard

deviations, SD) of the fitted distributions were calculated, and the background was removed. Thus, we identified hotspots as areas outside of the Mean+2SD image intensity (corresponding to the upper ~ 2.5% of activity, being over 97.5% of background values) and finally, visualized images of solely hotspot locations. Finally, we compared these results with previously used decisions on hotspot intensity thresholding (i.e. Top-25% and 17 standard thresholding approaches in ImageJ) and discussed the advantages of the Mean+2SD as well as Mean+3SD approaches. These advantages include: i) simple unification of the thresholding approach for several imaging methods with various principles of activity distribution, ii) identification of hotspots with various activity levels, iii) analysis of "time-specific" hotspots in temporal sequences of images. Compared with 17 standard thresholding methods, we concluded that objectively elucidating and separating the hotspots should be based on statistical distribution analysis, e.g. using the Mean+2SD or Mean+3SD approaches, should be based on statistical tools of distribution analysis. This simple Mean+2SD approach delivered suitable results for three groups of images and so, helps to understand the processes responsible for the highest activities.

Keywords: Rhizosphere, Microbial hotspots quantification, Statistical analyses, Visualization approaches.

2.2.2 Introduction

Soil imaging methods have developed rapidly in last few decades with the advent of advanced techniques (Kuzyakov and Razavi, 2019; Oburger and Schmidt, 2016; Protz et al., 1987; Schlüter et al., 2019). Various non-destructive methods enable visualizing and quantifying parameters reflecting root-soil-microbial interactions (Oburger and Schmidt, 2016), as well as pollutant accumulation in soil and plant (Nandula and Vencill, 2015), soil water distribution (Zarebanadkouki et al., 2012), etc. The non-destructive methods yield soil images at a broad range of scales starting from a few nm (10^{-9} m) up to meters (>1 m) (Schlüter et al., 2019). These methods reliably identify the location and spatial distribution of hidden soil life. They are based on a very broad range of approaches: 1) soil zymography: visualization of enzymatic activity in soil (Spohn et al., 2013), rhizosphere (Razavi et al., 2019), detritusphere (Liu et al., 2017) and earthworm burrows (Hoang et al., 2016); 2) autoradiography and radioisotope imaging: localization of root exudation patterns (Holz et al., 2018) or pesticide accumulations (Alcántara-de la Cruz et al., 2016; Nandula and Vencill, 2015; Pereira et al., 2019) in plants and soil; 3) neutron imaging of water distribution (Carminati et al., 2010); 4) hyperspectral imaging for

quantitative soil classification (Steffens and Buddenbaum, 2013); 5) spatial distribution of SOM fractions by reflectance (Steffens et al., 2014); 6) nano-scale secondary ion mass spectroscopy (nanoSIMS) for nano-scale element heterogeneity and speciation (Werner et al., 2017). Other *in situ* imaging approaches are described in detail in Oburger and Schmidt (2016).

Visualization of spatial patterns is essential for characterizing and further quantifying hotspot processes. Such quantification includes (but is not limited to) the following directions: 1) the principles of hotspot localization: frequency, distribution, common distances and size – the spatial pattern; 2) thresholding by process intensities; 3) connection between microbial hotspots and the physicochemical conditions: co-localization of images for various parameters; and 4) thresholding and clear separation of the hotspots from the background.

The ***first direction*** was successfully developed based on the geostatistical analysis and spatial point pattern analysis of microbial distributions in soil in 2-D (Nunan et al., 2002, 2001; Schmidt et al., 2018) and 3-D space (Juyal et al., 2019; Kravchenko et al., 2013; Nunan et al., 2003).

Various approaches related to the ***second direction*** have been recently developed for the hotspots identified using soil zymography. These include thresholding of the Top-25% grey value intensities (Ma et al., 2017), over 20% (Zhang et al., 2019), 50% (Heitkötter and Marschner, 2018) or 70% (Liu et al., 2017) of mean grey value, and the percentage of segmented areas with the highest enzyme activity that were calculated after determining them as hotspots (Spohn and Kuzyakov, 2014). In some studies, (Hoang et al., 2016; Razavi et al., 2017) first and second directions are combined and thresholding is already included to define hotspot distribution and extent.

The development of correlative imaging (Handschuh et al., 2013; Polzer et al., 2019) successfully advanced the ***third direction***. Combining 3-D (X-ray) with 2-D light and fluorescent microscopy, SIMs and NanoSIMs methods revealed that about ¾ of microorganisms preferably occupy soil micropores <10 µm (Schlüter et al., 2014) or pores < 100 µm (Kravchenko et al., 2019b). The 3-D pore size distributions and particulate organic matter determined by X-ray µCT was correlated with enzyme-active locations identified on multiple 2-D soil cross-sections to identify the locations of soil carbon stabilization (Kravchenko et al., 2019b).

The present methodological study belongs to the ***4th direction*** and is designed to threshold and localize the hotspots based on contrasting image intensities with the background.

In a recent review, Roose et al. (2016) strongly supported the statistical tools for objective image interpretation. Such tools, including variation indexes (Lv et al., 2019), multiple-linear regression (Qiu et al., 2003), and linear and non-linear models (Zhu et al., 2017), were successfully applied for hotspot detection (Table 1). Imaging protocols in neuroscience were developed by using statistical approaches (Dinov, 2011) based on parametric (e.g., paired *t*-test, Two-way ANOVA) and nonparametric (e.g. Kruskal-Wallis, Fliegner-Killeen) statistical tests (Chu et al., 2009) or spatial mixture models (Logan et al., 2008). *K*-means cluster statistical analysis was applied to define phosphorus-rich regions imaged using NanoSIMs (Werner et al., 2017) and SIMs (Bertrand et al., 2001) in soil (Table 1). One-way analysis of variance (ANOVA) was applied to find the boundaries between low and medium activities and the borders of hotspots visualized by soil zymography (Ge et al., 2017; Hoang et al., 2016). ANOVA approach was based on comparing mean values for 4 adjacent pixels and applicable to contrast zones (i.e. rhizosphere, detritusphere, biopores). Unfortunately, the approach was unreliable in low-contrast areas of images. Applying ANOVA is not entirely suitable for imaging methods when the activity at two adjacent pixels is interdependent, or when the prerequisites (independent observations, normal distribution, variance homogeneity) for ANOVA are not fulfilled.

Microbial hotspots have been defined as small soil patches with considerably higher process rates than those within the bulk (or non-rhizosphere) soil (Kuzyakov and Blagodatskaya, 2015). No standardized statistical approaches are currently available for thresholding hotspots in soil imaging applications. This study picks up the challenge and develops and tests a simple approach to identify rhizosphere hotspots in the bulk soil.

We hypothesize that a sharp gradient is present between hotspots and background activity (e.g., enzyme activity in the rhizosphere and soil volume without hotspots). Thus, if the background activity in the soil volume without hotspots follows the normal distribution, then activities above the Mean + 2 standard deviations (SD) (Mean+2SD) are hotspot related.

To separate the distribution of the probability of hotspot locations from the background and to set a threshold, we suggest the Mean+2SD approach. This approach enables obtaining an error probability of < 2.28% (half of all values outside of the ± 2 SD covering 95.44% of all values within the normal distribution). Consequently, if the hotspot area exceeds 2.28% (which corresponds to the normal distribution), then there are specific reasons and processes for the origin of the area with the highest image intensities – the hotspots. According to these prerequisites, the statistical definition of hotspots would be: Hotspots are the soil and rhizosphere

volumes in which the activities of the studied process exceed 2 SD of the mean in the rest of the soil.

Table 1 Approaches to hotspot determination of selected soil parameters in 2-D images

Parameter/ method	Approach	Reference
Enzyme activity/ Soil zymography	Top-25% of grey values	Ma et al., 2017
	>50% of mean values	Heitkötter and Marschner, 2018
	>20% of mean grey values	Zhang et al., 2019
	Above of average grey value (>70%)	Liu et al., 2017
	ANOVA to confirm the boundaries by 5 adjusted pixels	Hoang et al., 2016, Ge et al., 2017
	Percentage of segmented areas (thresholded by enzyme activity levels)	Spohn and Kuzyakov, 2014
Soil moisture content/ mapping	Variation indexes	Lv et al., 2019
	Multiple-linear regression	Qiu et al., 2003
	Linear and non-liner models	Zhu et al., 2017
NanoSIMS	Thresholding by size	Xiao et al., 2016
Light and fluorescent microscopy, SIMs and NanoSIMs	Correlative imaging	Handschuh et al., 2013; Polzer et al., 2019

2.2.3 Materials and methods

2.2.3.1 Images for statistical analysis of hotspots

Three groups of images representing hotspots of different origin were taken from literature: 1) spatial distribution of leucine aminopeptidase activity on soil zymogram (Razavi et al., 2017); 2) spatial distribution of ^{14}C labeled glyphosate in plants (Pereira et al., 2019), and 3) ^{14}C allocation in living roots and exudates (Holz et al., 2018).

All images were processed using the open source software ImageJ (Schindelin et al., 2012). To avoid detailed descriptions of all the underlying experiments elsewhere and to help restrict the data solely to own studies, we have chosen the digital images presented in already published papers (see below). Only the original images (untreated and uncorrected) – monochrome (^{14}C autoradiograms) or taken under UV light (zymograms) – were used; none of these images was transformed by the authors of original papers to color images. The color images (Red-Green-Blue, RGB) usually used in papers for better visualization were excluded because the blue and red colors corresponding to low and high values of a particular parameter are commonly adjusted by the authors and may not be proportional to the grey intensities in the original image. Thus, although color pictures are better for visualization and presentation in publications, they are not suitable for statistical analysis and can cause incorrect data interpretation. The monochrome digital images were converted to 8-bit greyscale images and inversed, if necessary, to obtain lowest value for 0 and the highest greyscale value for 255.

2.2.3.2 Mean + 2SD methodology for hotspot thresholding

Determining hotspots in each image involved 3 steps: 1) splitting the greyscale histogram of the image to two histograms with normal distribution of greyscale values; 2) identifying the greyscale range corresponding to the hotspots; and 3) hotspot mapping on the original image.

1st step: Splitting the greyscale histogram. The intensity of grey values and the corresponding number of pixel counts on images (histograms) were calculated using Histogram toolbox of ImageJ. Statistical analyses were conducted in R, version 3.5.1 (R Developement Core Team, 2014). The package "mixtools" (Benaglia et al., 2009) was used for distribution fitting. The parameters of normal distribution were fitted to the original frequencies of grey values (0…255). Then, the modeled distributions were built and plotted as a histogram (Fig. S1 a-c). The *normalmixEM* function in the “mixtools” package based on the expectation–maximization (EM) algorithm was used to fit two Gaussian component densities to the histogram of grey value intensities. Both Gaussian components fitting are automatically recognized by the package to avoid subjective split of data. The following characteristics of the two normal distributions were identified and calculated (Figs. 1 and S1a): **lambda** (λ) corresponds to the share of each distribution component in the total area occupied by grey values of all activities in the whole histogram, **mu** (μ) corresponds to the mean value, and **sigma** (σ) corresponds to the standard deviation (SD) of each histogram (Fig. S1a).

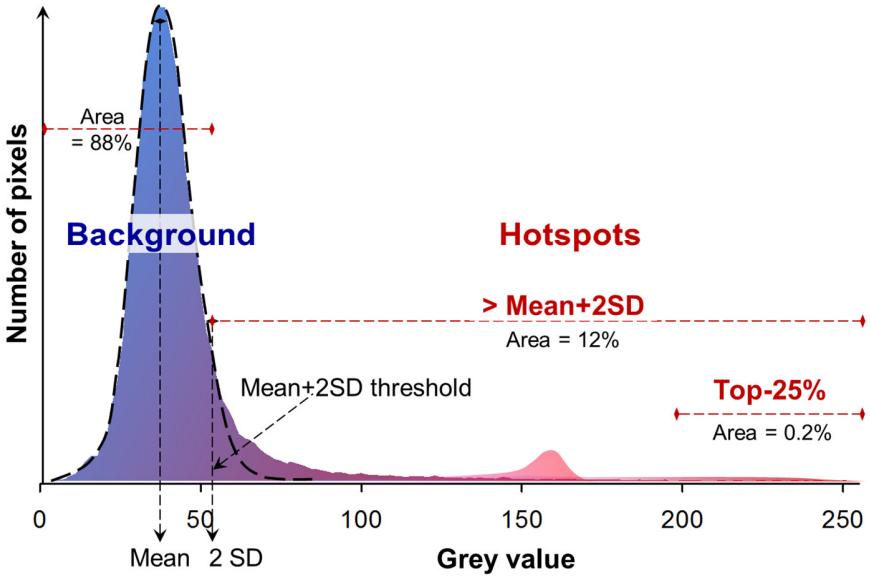

Figure 1. An example of the grey value distribution (from 0 to 255) for leucine aminopeptidase activity in soil (data extracted from the 8-bit image in Fig. 6b in Razavi et al., 2017). The dashed curve reflects the normal distribution of the grey values of the soil background for enzyme activity with its mean + 2 standard deviations (presented as vertical dashed lines). The hotspot area (S) thresholded by the Mean+2SD approach corresponds to 12% of the whole image. Because the Top-25% approach is strongly biased by the highest grey value (here 255), only 0.2% of the total area are highlighted as hotspots.

2^{d} step: Identifying the greyscale range corresponding to the hotspots. The component with the lower mean value was chosen as a background distribution, representing the soil volume without hotspots, while the component with the higher mean value represented the hotspots. Because of considerable overlapping of the two components of the original greyscale histogram (Fig. S1), any single-value thresholding method attributes part of the overlapped area either to the background or to the hotspots. In our approach, we consider hotspots to be represented by pixels with grey values greater than Mean+2SD of the background component of the greyscale histogram. Therefore, to remove 97.5% of the background, the sum of the Mean+2SD was used as a threshold for the original image histogram.

3^{d} step: Hotspot mapping on the original image. Hotspot percentage was calculated, and solely hotspots were mapped in red on the original images by setting a threshold value using the open source software ImageJ, clearly visualizing these locations.

Tested images had two background origins: i) enzyme activity of soil volume without hotspots on the zymogram (Fig. 2) and ^{14}C image of labeled roots and exudates (Fig. 3); and ii) background activity (noise) on the plate – in the ^{14}C image for glyphosate content in plants (Fig. 4). Therefore, we applied the parameters (mean and SD) of the component 1 (representing the background) (Fig. S1) to threshold hotspots in soil (Figs. 2 and 3). Three components were present on the plant image labeled with ^{14}C glyphosate. Specifically, the background around the plant (component 1), plant without glyphosate (component 2) and plant with glyphosate (component 3, i.e. hotspot). To identify the hotspots in the plant, we used the parameters of component 2 to threshold hotspots in the scanned plant (Fig. 4).

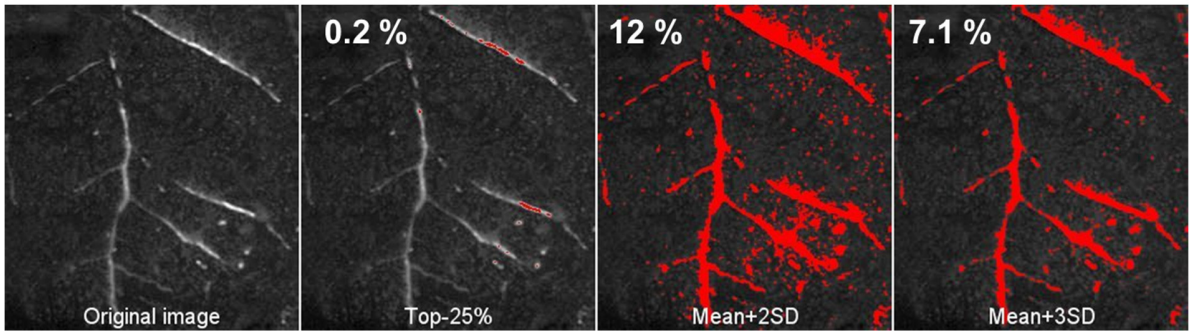

Figure 2. Original soil zymograms of leucine aminopeptidase (Razavi et al., 2017) and hotspots (red) identified using Top-25%, Mean+2SD and Mean+3SD approaches (compare Fig. 1). Numbers on top left show the percentage of the total image area belonged to the hotspots.

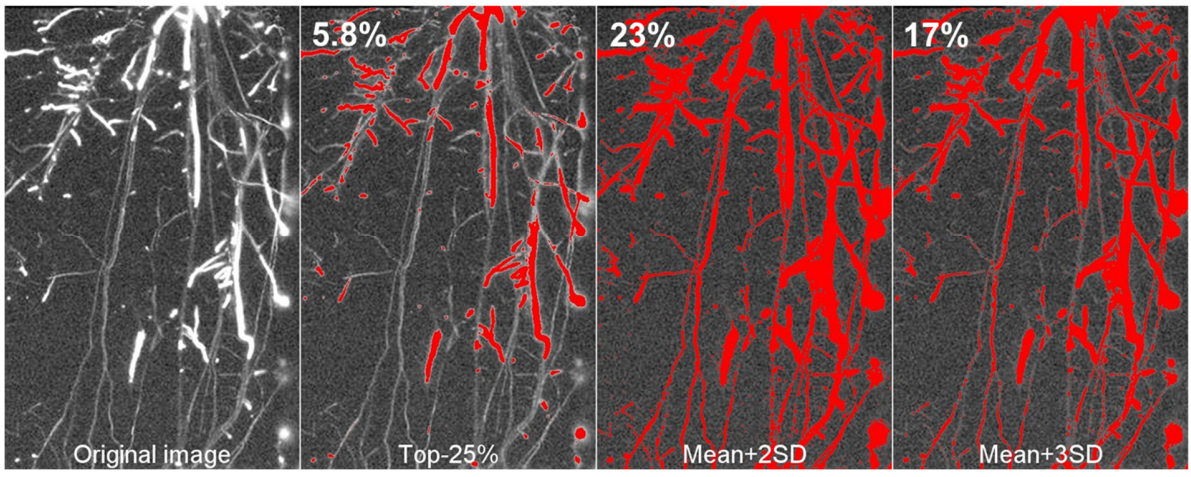

Figure 3. Original and binarized images of roots and exudates in soil after labeling the plants with $^{14}CO_2$ (Holz et al., 2018). The hotspots (red) were identified using Top-25%, Mean+2SD and Mean+3SD approaches. Numbers on top left show the percentage of the total image area belonged to the hotspots.

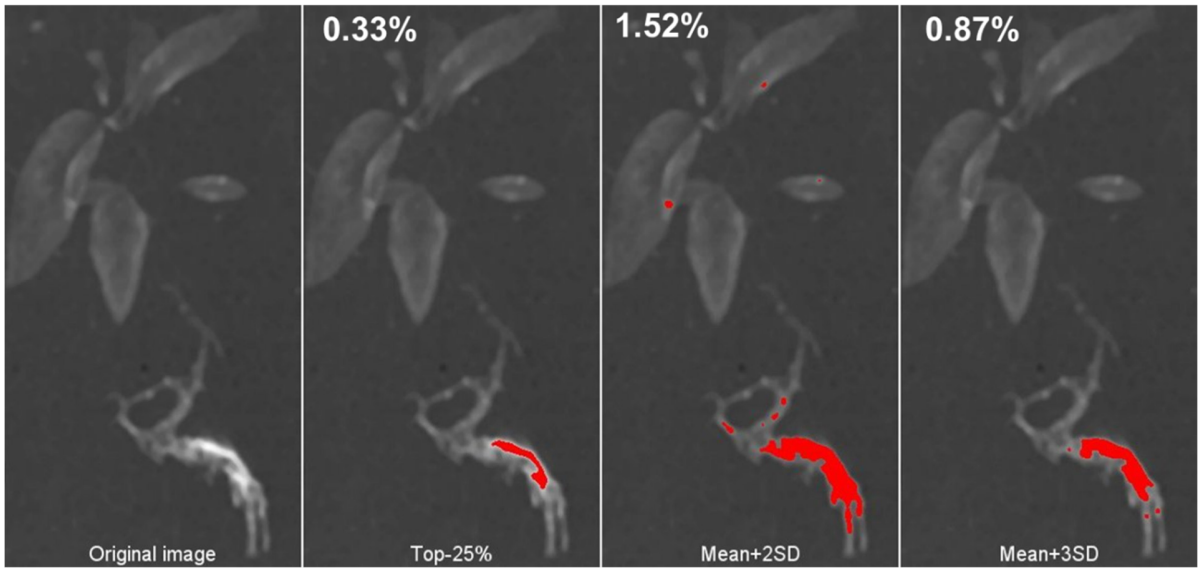

Figure 4. Original and binarized images of ^{14}C-labeled glyphosate in plants (Fig 5 D, Pereira et al., 2019). The hotspots (red) were identified using Top-25%, Mean+2SD and Mean+3SD approaches. Numbers on top left show the percentage of the total image area belonged to the hotspots.

The hotspot area and hotspot localization for the presented Mean+2SD and Mean+3SD statistical approaches were compared with the results obtained by the frequently used Top-25% approach (Ma et al., 2017). The Top-25% hotspot approach is based on the thresholding grey values (i.e. enzyme activity in soil zymography) in the upper quartile (Top 25%) (Ma et al., 2017). The Mean+3SD approach is similar to Mean+2SD, but enables separating the hottest spots (0.15%) by thresholding 99.85% of the background values.

2.2.3.3 Comparison with standard thresholding methods

To compare hotspots defined by the proposed Mean+2SD approach with those defined by traditionally used thresholding methods, we applied 17 thresholding methods built-in in ImageJ software: Default, Otsu, Huang, Triangle, Lee, Mean, MinEntropy, Minimum, Percentile, MinError, Shanbhag, IsoData, IJ_IsoData, Moments, Intermodes, RenyiEntropy, Yen (see details in Landini, 2017, ImageJ, ver. 1. 16. 5). Since the original images were published in 8-bit format (i.e. greyscale values ranged from 0 to 254), the activities in hotspots were compared in relative units (0-1). The thresholding of the ^{14}C image of glyphosate distribution in the plant was applied to the solely plant area (was cut from the whole image prior to thresholding) to exclude the effect of the background around the plant on the hotspot detection. The thresholding of the soil zymogram and

^{14}C-labeled roots was applied to the whole images. The normalized activities and relative area of the hotspots calculated using the standard thresholding methods and Top-25% approach were compared with the results of Mean+2SD and Mean+3SD thresholding (Table S1).

2.2.4 Results

2.2.4.1 Mean+2SD and Mean+ 3SD vs. Top-25% thresholding

Application of the Mean+2SD and Mean+3SD approaches enabled identifying the hotspots of enzyme activity on the leucine aminopeptidase zymogram as being 12% and 7.1% of the image area, respectively (Fig. 2). The hotspots were identified by these statistical approaches mainly along the roots (rhizosphere hotspots) and in the root-free zones (microbial hotspots). Mean+2SD yielded 5% more hotspot area than Mean+3SD because of extended rhizosphere size and due to more micro-hotspots located in the bulk soil (Fig. 2). In contrast, the Top-25% approach thresholded only 0.2 % as a hotspot located in the most active regions of roots. Thus, Mean+2SD and Mean+3SD approaches thresholded 60 and 36 times larger hotspot area for leucine aminopeptidase activity (Fig. 2, Table 2) than the Top-25% approach.

The difference between hotspot areas for the newly tested statistical approaches and Top-25% for the ^{14}C content in soil and exudates (Fig. 3) was much lower that for soil zymography (Fig. 2). The total hotspot areas for ^{14}C in root exudates and roots (Table 2, Fig. 2) were about 4 and 3 times larger for the Mean+2SD and Mean+3SD approaches, respectively, than Top-25%.

The hotspot areas thresholded by the Mean+2SD and Mean+3SD approaches for image of ^{14}C glyphosate content in plant were 4.6 and 2.6 times larger than Top-25% (Table 2). Furthermore, hotspots thresholded by Top-25% and Mean+3SD were located in roots close to seed, from which they grew, but not in the leaves, whereas Mean+2SD detected hotspots in both plant components (Fig. 4).

Thus, mapping hotspots thresholded by three approaches – Mean+2SD, Mean+3SD and Top-25% – revealed significant visual and quantitative differences in hotspot features (Figs. 2-4). These differences include: i) the total area covered by the hotspots and ii) the localization pattern.

Table 2. Comparison of hotspot areas on three images of activity distribution in soils or plants calculated by Mean+2SD, Mean+3SD and Top-25% approaches.

Method	Parameter	Hotspots area, %			Hotspot area increase compared to Top-25%, times	
		Top-25%	Mean +2SD	Mean +3SD	Mean +2SD	Mean +3SD
Soil zymography (Fig. 2)	leucine aminopeptidase activity	0.2	12	7.1	60	36
^{14}C imaging (Fig. 3 and 4)	^{14}C in root exudates and roots	5.8	23.2	17.1	4	3
	Glyphosate (^{14}C) in plant	0.33	1.52	0.87	4.6	2.6

2.2.4.2 Comparison of suggested approach with standard thresholding methods

The performance of the standard ImageJ thresholding methods differed for three tested images. The smallest hotspot area was obtained for the soil zymogram using Minimum method, while the largest was obtained using Percentile method. The difference between the smallest and largest areas estimated by the standard methods was 500 times (Fig. 5a). The ranks of the standard methods changed, though the difference between Minimum and Percentile methods was still 12-fold when thresholding was applied to the $^{14}CO_2$-labeled root image (Fig. 5b).

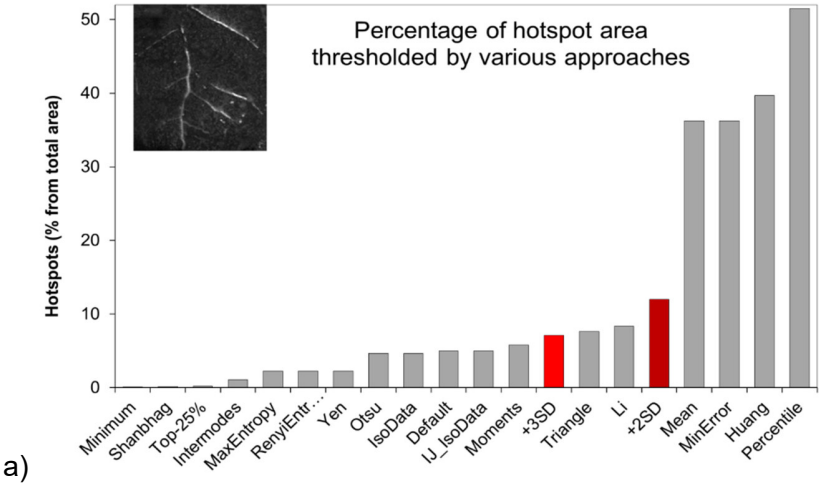

a)

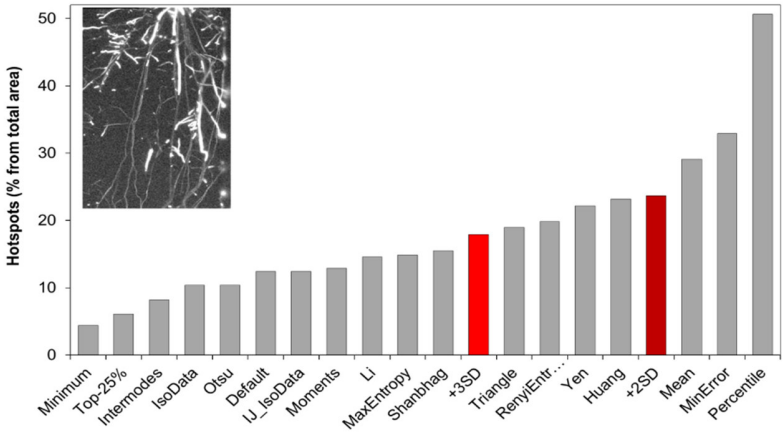

b)

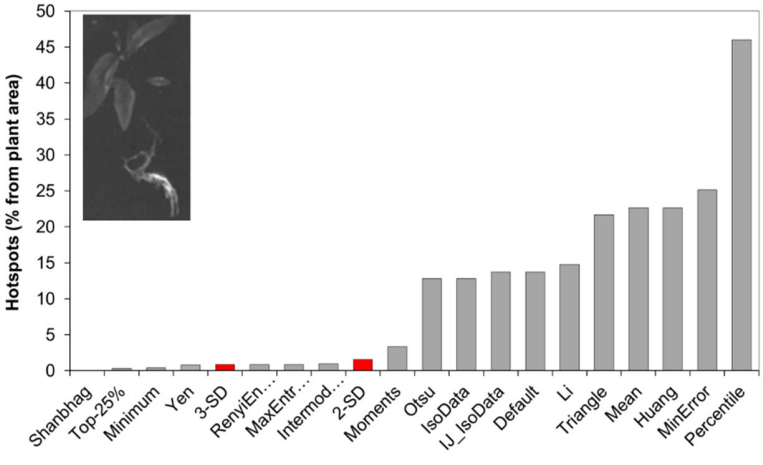

c)

Figure 5. Hotspots in % of the total area thresholded by 17 thresholding built-in methods in ImageJ and Mean+2SD, Mean+3SD or Top-25% for three test images: a) soil zymogram for leucine aminopeptidase (Razavi et al., 2017); b) ^{14}C image for $^{14}CO_2$-labeled root and exudates in soil and c) ^{14}C image of ^{14}C-labeled glyphosate in plants (Pereira et al., 2019).

The differences between standard methods were even more pronounced for the ^{14}C-labeled glyphosate image (Fig. 5c), reaching about 1600 times between Shanghang and Percentile. Changing ranks of the standard methods indicated overall inconsistency in their performance for detecting hotspots. Persistently intermediate values of the hotspot area were obtained using the Mean+2SD and Mean+3SD approaches for the first two tested images and close to mean for the cluster of 7 standard methods for the third image, indicating robustness of the developed approach. As expected, normalized mean hotspot activities (from 0 to 1) computed by different standard method but for the same images demonstrated a trend opposite to that for hotspot areas. Smaller average activities were observed for those segmentation methods that produced larger hotspot areas (Fig. 6). Similar to the hotspots, the Mean+2SD and Mean+3SD approaches generated intermediate estimates of the mean hotspot activity (except for ^{14}C-labeled glyphosate in plants, which showed intermediate estimates only for the cluster of 7 standard methods) among the tested methods.

2.2.5 Discussion

2.2.5.1 Why statistical methods are necessary for hotspot thresholding

We suggest using a simple and freely available statistical approach to detect and localize microbial hotspots. The approach based solely on separating statistical distributions for the background and hotspots is important for quantitatively assessing hotspot areas and localizing them. Separation based on intensity level (but ignoring the density of each pixel (Fig. S1 a-c)) may either under- or overestimate hotspot areas, leading to misinterpretation of *in situ* soil processes and activities. All three examples (Figs. 2-4, Table 2) showed underestimation of hotspot areas by the frequently used Top-25% compared to the suggested Mean+2SD approach.

We conclude that the main reason for this underestimation by Top-25% is inherent in the nature of the approach: the Top-25% is defined by few “hottest” points (Fig. 1) and, in an extreme case, by only one point with maximal activity, thus making it always strongly biased to the right on the activity distribution (Fig. 1). As the whole range of pixel intensities will be divided into four quartiles (25% in each), any points below Top-25% will be automatically disregarded as hotspots, even if they differ significantly from the normal distribution of the background. On the example of the distribution of the pixel grey scale (corresponding to intensities, Figs. 1, S1) on the 8-bit image, all points below grey intensity 192 will be disregarded as hotspots using the Top-25% approach. In contrast, the Mean+2SD approach will definitely highlight these hotspots, including those that are much closer to the background (Figs. 1 and S1).

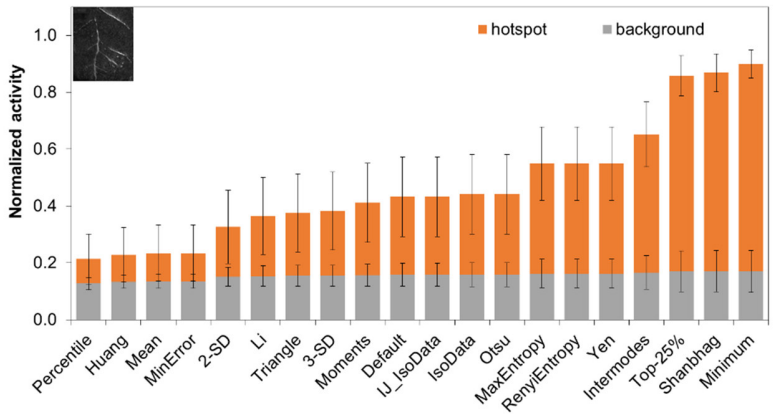

a)

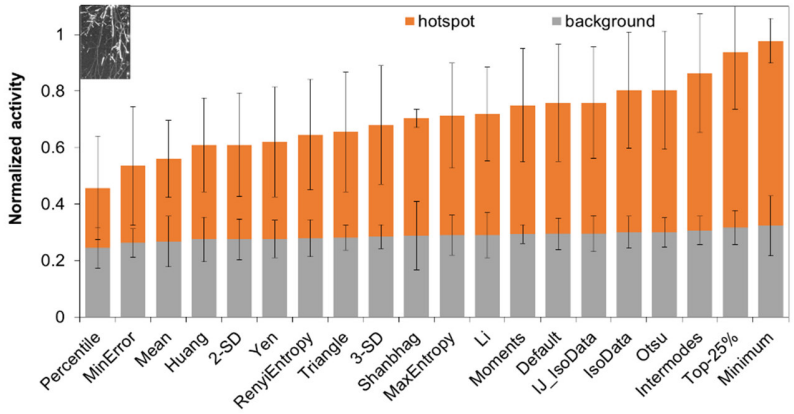

b)

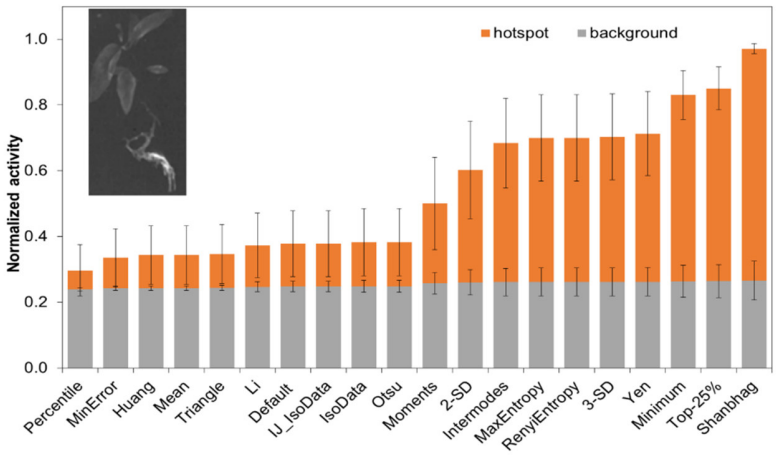

c)

Figure 6. Normalized grey value activities for mean and standard deviation values for background and hotspots separated by 17 thresholding built-in methods in ImageJ and Mean+2SD, Mean+3SD or Top-25% for three test images: a) soil zymogram for leucine aminopeptidase (Razavi et al., 2017); b) ^{14}C image for $^{14}CO_2$-labeled root and exudates in soil (Holz et al., 2018) and c) ^{14}C image of ^{14}C-labeled glyphosate in plants (Pereira et al., 2019).

The distributions of pixel intensities on 2-D soil images are generally bimodal (Schlüter et al., 2019; Schmidt et al., 2018), i.e. two-class pictures consisting of background and hotspots. The main task of thresholding is to determine the objective reasons and threshold value to separate the pixels with high and low intensities (light from dark on the images). Various statistical approaches have already been suggested in soil hydrology (Lv et al., 2019; Qiu et al., 2003; Zhu et al., 2017), but being technique-specific, they cannot be applied directly to all image types (Aslantas et al., 2017).

In a pioneering study on image processing, the mean and standard deviations for peaks of grey-value classes were applied for cell types separation corresponding to various grey-value classes (Prewitt and Mendelsohn, 1966). Mean and standard deviations are the parameters of the well-established Otsu (1979) thresholding approach, which has been used widely for 40 years in medicine and biology based on its clarity and simplicity. That approach is being used as a basic technique for distinguishing between cell compartments on various images. Since that time, various other thresholding approaches (mostly used in diagnostic imaging in medicine) have been developed (Aslantas et al., 2017; Lee et al., 1990; Matsuyama et al., 2016) and became available in imaging software. Triangle (Zack et al., 1977) has a good potential for separating rhizosphere hotspots because it was successfully applied for root thresholding (Tajima and Kato, 2013, 2011). The thresholded hotspot areas by triangle method were similar to Mean+3SD approach showing highest p-value (Table S1) for an image of leucine aminopeptidase distribution along the roots (Fig. 5 a). The Huang method (Huang and Wang, 1995) produced the exact same hotspot area and mean value (*p=1*, Table S1) as the Mean+2SD approach on the ^{14}C image for root and exudates in soil. None of the 17 auto thresholding methods (Figs. S3, Table S1) yielded results very close to Mean+2SD (Fig. 5 a-c) on the ^{14}C image of ^{14}C-labeled glyphosate in plant. Moreover, Yen, ReniyEntropy and MaxEntropy were not statistically different from Mean+3SD (Table S1) and revealed similar results for hotspot areas. Therefore, Yen, Triangle, Huang, ReniyEntropy and MaxEntropy methods in ImageJ have a very good potential to threshold hotspots on soil images, but further studies are needed to test these thresholding methods on a broad dataset of soil images.

This study is focused on the rhizosphere hotspot thresholding, but Mean+2SD approach may be also suitable for detritusphere, drillosphere, biopore and other hotspot types. However, it requires additional study with many zymograms or 14C images, and maybe with some image simulations. Therefore, new testing for different soils, plant roots, and enzymes are interesting avenue for future research.

2.2.5.2 Comparison of the Mean+2SD, Mean+3SD and Top-25% approaches

Applying the Mean+2SD and Mean+3SD approaches for hotspot separation on soil zymograms revealed an up to 36-60 times larger area than the Top-25% approach and helped better localize root and rhizosphere zones on hotspot images (Figs. 2-4, Table 2). Following the statement about the rhizosphere being a microbial hotspot (Kuzyakov and Razavi, 2019), it is evident that hotspots are localized along the whole root system (Fig. 2) and not restricted to the very few root regions revealed by Top-25% thresholding. Clearly, the Mean+3SD approach thresholded fewer roots within hotspots than Mean+2SD and should therefore be applied with caution in rhizosphere studies.

In contrast to the soil zymogram, the difference for hotspot areas on ^{14}C images evaluated by the three approaches (Mean+2SD and Mean+3SD vs. Top 25%) was much lower (but still very high – from 2.4 to 4 times) or negligible (< 0.1 %) (Fig. 4 a-b). We explain this lower difference by the specifics of the ^{14}C imaging method and its processing: i) usually, ^{14}C images have a higher contrast than zymograms (for some uncertainties and constraints of ^{14}C images, see Holz et al. (2019)); this higher contrast reflects the absence of ^{14}C activity in the background soil (the radiocarbon or bomb ^{14}C can be disregarded compared to ^{14}C labeling; the same is valid for cosmogenic or geogenic radioisotopes); ii) ^{14}C images contain many pixels at the maximal grey value of 255, which is not relevant for zymograms. These highest values are definitely thresholded by all three approaches (Mean+2SD, Mean+3SD vs. Top 25%) on ^{14}C images.

In contrast to enzyme activities on soil zymograms, the ^{14}C footprint on images is localized along the roots in soil and in most cases mimics root shape very well (Fig. 4 a-b). Therefore, shape-based methods for segmenting such ^{14}C exudation hotspots (Gao et al., 2019) can be an option for further thresholding improvement. Note, however, that object-based segmentation is inapplicable for soil zymography due to the location of micro-hotspots in micropores (Kravchenko et al., 2019a) and due to the large variation of individual areas from 0.00034 to 2.8 mm^2 (Guber et al., 2018). To avoid any bias, we recommend the pixel-based method for evenly distributed (not object-based) enzyme activity in soil volume without hotspots. For details on the advantages and disadvantages of pixel-based and object-based analysis, see the review of Hussain et al. (2013) .

2.2.5.3 Limitations of statistical approaches to distinguish and localize hotspots

Hotspot thresholding by statistical approaches based on the distribution of pixel intensities has a great advantage because it is person-independent and enables a unified analysis of the obtained images. Nonetheless, certain shortcomings – which are actually independent of the used statistical approach – need to be considered.

1) The quality of the original images plays a significant role in precise hotspot determination. Thus, a **low signal-to-noise ratio** likely results in a wider Gaussian distribution (Weszka and Rosenfeld, 1978) and, consequently, larger SD value. Therefore, poor-quality original images leads to a decrease in some hotspot areas, and some hotspots can even disappear completely. This problem is relevant for any thresholding approach. Solving this issue in image analysis requires: i) improving the quality of the original experimental images, and ii) avoiding the smoothing or de-noising of the original image. This second option may lead to losses of some small hotspots (e.g. in micropores with Ø=60-180 µm (Kravchenko et al., 2019a)) or decreases in hotspot areas.

2) The complexity of soil life and processes can yield a **few (more than two) distributions** of grey values, each reflecting individual process groups or substance concentrations. Each of these distributions reflects specific reasons or mechanisms. We assume that the first distribution (on the left in Fig. 1) always belongs to the background, and further possible distributions represent hotspot groups caused by various factors (e.g. the gradient of labile C, favorable micro-environment for microorganisms, presence of root exudates). Some studies could be focused on the gradients of concentration, then it may be reasonable to subdivide hotspots for subclasses according to changes in gradient. Each hotspot area (peak in the intensity distribution) can be segmented by applying the same procedure further and assuming the next distribution as a background for the remaining hotspots. Thus, evaluating hotspots originating by various processes requires moving toward multi-level thresholding (Mortazavi et al., 2012; Satapathy et al., 2018).

3) It is difficult to **distinguish between** hotspots caused by **^{14}C exudates** released from roots into the soil and ^{14}C activity **of the roots themselves**. In many cases (Holz et al., 2018; Pausch and Kuzyakov, 2011), ^{14}C activity in living or dry roots corresponds to the highest grey value (top values on the 255 gray scale) of 8-bit images and creates a peak on the right border of the 255 scale. Therefore, if the research question involves determining root exudation hotspots,

the activity of roots alone should be separated beforehand by masking. Otherwise, exudate hotspots may be segmented with the background as well.

Importantly, all these (and probably some other) limitations are the same for all approaches (Mean+2SD, Mean+3SD, Top-25%, as well as the 17 approaches implemented in ImageJ) and mainly reflect the nature of the hotspots and the quality of the original images. Further quality improvements of imaging analysis (Baveye et al., 2010) and ongoing development of thresholding approaches (Iassonov et al., 2009; Sezgin and Sankur, 2004) are necessary for more objective conclusions on soil hotspot areas, localization and other characteristics.

2.2.5.4 Relevance and advantages of statistical approaches

1) The suggested Mean+2SD thresholding approach helps to avoid subjective biases in hotspot determination for various parameters such as enzyme activities, rhizodeposition, soil pH and nutrient concentrations. Thresholding based on intensity may result in multi-fold higher average activities for β-glucosidase, chitinase and acid phosphatase hotspots in comparison to non-hotspots (Heitkötter and Marschner, 2018), but much smaller hotspot areas (Top-25%, Figs. 2 and 3). The enzyme activities in hotspots and background differed greatly (up to 7 times) because the hotspot segmentation was done by a non-statistical approach and is biased on a few points with maximal intensity. Moreover, using the Mean+2SD approach yields hotspot images that are visually similar to the originals, but with a distinct and completely black background (Figs. 2-4). In contrast, the very small hotspot areas thresholded using the Top-25% approach yielded subtle (almost “background” covered) hotspot images for enzyme activity (Fig. 2) and lower contrast images for ^{14}C activity (Fig. 3 and 4). Thus, the Mean+2SD thresholding approach enables localizing i) microbial hotspots along the whole root system for enzyme activity (Fig. 2), ii) ^{14}C allocation hotspots in smaller roots (Fig. 3), and iii) glyphosate accumulation hotspots in the seedling and primary root as opposed to only in leaves for the Top-25% approach (Fig. 4).

2) The Mean+2SD and Mean+3SD approaches are much more reliable than Top-25% for microbial (e.g. enzyme activity) hotspot determinations in temporal sequences of images. The thresholding background with contrasting enzyme activity at successive time points can highlight hotspot development, the “time-specific” hotspots and, thus, their lifetime. Accordingly, the set thresholding value for activity may correspond to hotspots at one time point and to the hottest spots at another one (hot moment); the reverse situation is also possible. The challenge to define hotspots at any time, however, is solved by background thresholding, even thought that

background activities themselves may slightly change with time as well. Mean+2SD and Mean+3SD are the universal approaches to overcome such temporal changes of activity and to qualitatively determine hotspot dynamics.

3) The background thresholding approach enables defining the hotspots for various properties with the same statistical approach (enzyme activities, ^{14}C in root exudates, water content, soil pH, soil CO_2 and O_2, nutrient concentrations, etc.). Mean+2SD separates hotspots from the background regardless of their location within a range of low, medium or higher activities. Thereafter, hotspot images can be co-localized and conclusions can be drawn about their spatial co-occurrence.

4) These statistical approaches enable identifying hotspots with various levels of microbial activities or substance concentrations in soil. Both Mean+2SD and Mean+3SD (Razavi et al., 2019) can be used to identify hotspots with high and very high activities. The Mean+3SD approach will highlight the areas with 0.15% highest activities and cut off the “background” with 99.85% lowest activities. Nonetheless, the Mean+3SD approach should be applied with caution, especially for microbial hotspots in the rhizosphere. It might disregard the values along less active rhizosphere parts, and the rhizosphere zones as a microbial hotspot will be incomplete (Figs. 2 and 3). That approach yielded 1.3-2.2 times smaller hotspot areas than Mean+2SD. Hotspots in the rhizosphere were lost along the smaller roots (Figs. 2 and 3) by Mean+3SD. Therefore, that thresholding approach is more appropriate for the highest microbial or ^{14}C activity hotspots and used with discretion for rhizosphere studies.

5) Last but not least, the Mean+1SD/Mean+2SD/ Mean+3SD approaches are very simple and based on a clear principle. The parameters of normal distribution can be fitted easily by free and commonly used imaging software and statistical tools (R, ImageJ, etc.). No special software and tools, nor deep involvement with complex thresholding approaches, are necessary.

2.2.6 Conclusions

Although microbial and rhizosphere hotspots are among the hot topics in soil science, and various imaging techniques help visualize and localize them, statistical approaches to identify the hotspots have not been used. We propose simple statistical approaches to separate hotspots from soil background activities on 2-D images. Our approaches are based on the probability of image areas with intensities higher than mean + 2 standard deviations (Mean+2SD) or + 3

standard deviations (Mean+3SD) of a normal distribution. The Mean+2SD or Mean+3SD approaches include: 1) splitting the greyscale histogram of the image into two histograms with normal distribution of greyscale values; 2) identifying the greyscale range corresponding to the hotspots; and 3) hotspot mapping on the original image. Compared with 17 standard thresholding methods, we concluded that objectively elucidating and separating the hotspots should be based on statistical distribution analysis, e.g. using the Mean+2SD or Mean+3SD approaches. This methodology helps to avoid under- or overestimation and bias in images of lower quality, is applicable to time series experiments, and can couple imaging methods of various parameters.

2.2.7 Acknowledgements

We are very thankful to Sandra Spielvogel for her valuable comments that greatly improved the manuscript. We gratefully acknowledge the Interfaculty Research Cooperation (IRC) “One Health” at University of Bern, Sub-Project 4. Support for this research was provided in part by the USDA NIFA Program (Award # 2019-67019-29361), by the NSF LTER Program (DEB 1027253) at the Kellogg Biological Station, by USDA NC1187 project, by the Great Lakes Bioenergy Research Center, U.S. Department of Energy, Office of Science, Office of Biological and Environmental Research under Award Number DE-SC0018409, and by Michigan State University AgBioResearch. Contribution of Yakov Kuzyakov was supported by the Russian Science Foundation (project No. 18-14-00362). We would like to thank the two anonymous reviewers for their suggestions and comments.

2.2.8 References

Alcántara-de la Cruz, R., Fernández-Moreno, P.T., Ozuna, C. V., Rojano-Delgado, A.M., Cruz-Hipolito, H.E., Domínguez-Valenzuela, J.A., Barro, F., de Prado, R., 2016. Target and non-target site mechanisms developed by glyphosate-resistant hairy beggarticks (Bidens pilosa L.) populations from Mexico. Front. Plant Sci. 7, 1–12. https://doi.org/10.3389/fpls.2016.01492

Aslantas, A., Emre, D., Çakiroğlu, M., 2017. Comparison of segmentation algorithms for detection of hotspots in bone scintigraphy images and effects on CAD systems. Biomed. Res. 28, 676–683.

Baveye, P.C., Laba, M., Otten, W., Bouckaert, L., Dello Sterpaio, P., Goswami, R.R., Grinev, D., Houston, A., Hu, Y., Liu, J., Mooney, S., Pajor, R., Sleutel, S., Tarquis, A., Wang, W., Wei, Q., Sezgin, M., 2010. Observer-dependent variability of the thresholding step in the quantitative analysis of soil images and X-ray microtomography data. Geoderma 157, 51–63. https://doi.org/10.1016/j.geoderma.2010.03.015

Benaglia, T., Chauveau, D., Hunter, D.R., Young, D.S., 2009. Mixtools: An R package for analyzing finite mixture models. J. Stat. Softw. 32, 1–29. https://doi.org/10.18637/jss.v032.i06

Bertrand, I., Grignon, N., Hinsinger, P., Souche, G., Jaillard, B., 2001. The use of secondary ion mass spectrometry coupled with image analysis to identify and locate chemical elements in soil minerals: The example of phosphorus. Scanning 23, 279–291. https://doi.org/10.1002/sca.4950230409

Carminati, A., Moradi, A.B., Vetterlein, D., Vontobel, P., Lehmann, E., Weller, U., Vogel, H.J., Oswald, S.E., 2010. Dynamics of soil water content in the rhizosphere. Plant Soil 332, 163–176. https://doi.org/10.1007/s11104-010-0283-8

Chu, A., Cui, J., Dinov, I.D., 2009. SOCR Analyses: Implementation and Demonstration of a New Graphical Statistics Educational Toolkit . J. Stat. Softw. 30, 1–19. https://doi.org/10.18637/jss.v030.i03

Dinov, I.D., 2011. Neurological imaging: Statistics behind the pictures. Imaging Med. https://doi.org/10.2217/iim.11.37

Gao, W., Schlüter, S., Blaser, S.R.G.A., Shen, J., Vetterlein, D., 2019. A shape-based method for automatic and rapid segmentation of roots in soil from X-ray computed tomography images: Rootine. Plant Soil 441, 643–655. https://doi.org/10.1007/s11104-019-04053-6

Ge, T., Wei, X., Razavi, B.S., Zhu, Z., Hu, Y., Kuzyakov, Y., Jones, D.L., Wu, J., 2017. Stability and dynamics of enzyme activity patterns in the rice rhizosphere: Effects of plant growth and temperature. Soil Biol. Biochem. 113, 108–115. https://doi.org/10.1016/j.soilbio.2017.06.005

Guber, A., Kravchenko, A., Razavi, B.S., Uteau, D., Peth, S., Blagodatskaya, E., Kuzyakov, Y., 2018. Quantitative soil zymography: Mechanisms, processes of substrate and enzyme diffusion in porous media. Soil Biol. Biochem. 127, 156–167. https://doi.org/10.1016/j.soilbio.2018.09.030

Handschuh, S., Baeumler, N., Schwaha, T., Ruthensteiner, B., 2013. A correlative approach for combining microCT, light and transmission electron microscopy in a single 3D scenario. Front. Zool. 10, 1. https://doi.org/10.1186/1742-9994-10-44

Heitkötter, J., Marschner, B., 2018. Soil zymography as a powerful tool for exploring hotspots and substrate limitation in undisturbed subsoil. Soil Biol. Biochem. 124, 210–217. https://doi.org/10.1016/j.soilbio.2018.06.021

Hoang, D.T.T., Razavi, B.S., Kuzyakov, Y., Blagodatskaya, E., 2016. Earthworm burrows: Kinetics and spatial distribution of enzymes of C-, N- and P- cycles. Soil Biol. Biochem. 99, 94–103. https://doi.org/10.1016/J.SOILBIO.2016.04.021

Holz, M., Zarebanadkouki, M., Carminati, A., Kuzyakov, Y., 2019. Visualization and quantification of root exudation using 14C imaging: challenges and uncertainties. Plant Soil 437, 473–485. https://doi.org/10.1007/s11104-019-03956-8

Holz, M., Zarebanadkouki, M., Kuzyakov, Y., Pausch, J., Carminati, A., 2018. Root hairs increase rhizosphere extension and carbon input to soil. Ann. Bot. 121, 61–69. https://doi.org/10.1093/aob/mcx127

Huang, L.K., Wang, M.J.J., 1995. Image thresholding by minimizing the measures of fuzziness. Pattern Recognit. 28, 41–51. https://doi.org/10.1016/0031-3203(94)E0043-K

Hussain, M., Chen, D., Cheng, A., Wei, H., Stanley, D., 2013. Change detection from remotely sensed images: From pixel-based to object-based approaches. ISPRS J. Photogramm. Remote Sens. https://doi.org/10.1016/j.isprsjprs.2013.03.006

Iassonov, P., Gebrenegus, T., Tuller, M., 2009. Segmentation of X-ray computed tomography images of porous materials: A crucial step for characterization and quantitative analysis of pore structures. Water Resour. Res. 45, 1–12. https://doi.org/10.1029/2009WR008087

Juyal, A., Otten, W., Falconer, R., Hapca, S., Schmidt, H., Baveye, P.C., Eickhorst, T., 2019. Combination of techniques to quantify the distribution of bacteria in their soil microhabitats at different spatial scales. Geoderma 334, 165–174. https://doi.org/10.1016/j.geoderma.2018.07.031

Kravchenko, A., Chun, H.C., Mazer, M., Wang, W., Rose, J.B., Smucker, A., Rivers, M., 2013. Relationships between intra-aggregate pore structures and distributions of Escherichia coli within soil macro-aggregates. Appl. Soil Ecol. 63, 134–142. https://doi.org/10.1016/j.apsoil.2012.10.001

Kravchenko, A.N., Guber, A.K., Razavi, B.S., Koestel, J., Blagodatskaya, E. V, Kuzyakov, Y., 2019a. Spatial patterns of extracellular enzymes: Combining X-ray computed micro-tomography and 2D zymography. Soil Biol. Biochem. 135, 411–419. https://doi.org/10.1016/j.soilbio.2019.06.002

Kravchenko, A.N., Guber, A.K., Razavi, B.S., Koestel, J., Quigley, M.Y., Robertson, G.P., Kuzyakov, Y., 2019b. Microbial spatial footprint as a driver of soil carbon stabilization. Nat. Commun. 10, 3121. https://doi.org/10.1038/s41467-019-11057-4

Kuzyakov, Y., Blagodatskaya, E., 2015. Microbial hotspots and hot moments in soil: Concept & review. Soil Biol. Biochem. 83, 184–199. https://doi.org/10.1016/j.soilbio.2015.01.025

Kuzyakov, Y., Razavi, B.S., 2019. Rhizosphere size and shape: Temporal dynamics and spatial stationarity. Soil Biol. Biochem. 135, 343–360. https://doi.org/10.1016/J.SOILBIO.2019.05.011

Landini, G., 2017. ImageJ , 1.16.5 [WWW Document].

Lee, S.U., Yoon Chung, S., Park, R.H., 1990. A comparative performance study of several global thresholding techniques for segmentation. Comput. Vision, Graph. Image Process. 52, 171–190. https://doi.org/10.1016/0734-189X(90)90053-X

Liu, S., Razavi, B.S., Su, X., Maharjan, M., Zarebanadkouki, M., Blagodatskaya, E., Kuzyakov, Y., 2017. Spatio-temporal patterns of enzyme activities after manure application reflect mechanisms of niche differentiation between plants and microorganisms. Soil Biol. Biochem. 112, 100–109. https://doi.org/10.1016/j.soilbio.2017.05.006

Logan, B.R., Geliazkova, M.P., Rowe, D.B., 2008. An evaluation of spatial thresholding techniques in fMRI analysis. Hum. Brain Mapp. 29, 1379–1389. https://doi.org/10.1002/hbm.20471

Lv, L., Liao, K., Zhou, Z., Zhu, Q., Shen, C., 2019. Determining hot moments/spots of hillslope soil moisture variations based on high-resolution spatiotemporal soil moisture data. Catena 173, 150–161. https://doi.org/10.1016/J.CATENA.2018.10.012

Ma, X., Razavi, B.S., Holz, M., Blagodatskaya, E., Kuzyakov, Y., 2017. Warming increases hotspot areas of enzyme activity and shortens the duration of hot moments in the root-detritusphere. Soil Biol. Biochem. 107, 226–233. https://doi.org/10.1016/j.soilbio.2017.01.009

Matsuyama, E., Takahashi, N., Watanabe, H., Tsai, D., 2016. A Method of Using Information Entropy of an Image as an Effective Feature for Com-puter-Aided Diagnostic Applications. J. Biomed. Sci. Eng. 09, 315–322. https://doi.org/10.4236/jbise.2016.96026

Mortazavi, D., Z. Kouzani, A., Zadeh, H.S.-, 2012. A 3S Multi-level Thresholding Technique for Intracranial Segmentation from Brain MRI Images. J. Bioeng. Biomed. Sci. 02. https://doi.org/10.4172/2155-9538.1000109

Nandula, V.K., Vencill, W.K., 2015. Herbicide Absorption and Translocation in Plants using Radioisotopes. Weed Sci. 63, 140–151. https://doi.org/10.1614/ws-d-13-00107.1

Nunan, N., Ritz, K., Crabb, D., Harris, K., Wu, K., Crawford, J.-W., Young, I.-M., 2001. Quantification of the in situ distribution of soil bacteria by large-scale imaging of thin sections of undisturbed soil. FEMS Microbiol. Ecol. 37 (1), 67-77. https://doi.org/10.1111/j.1574-6941.2001.tb00854.x

Nunan, N., Wu, K., Young, I.M., Crawford, J.W., Ritz, K., 2003. Spatial distribution of bacterial communities and their relationships with the micro-architecture of soil. FEMS Microbiol. Ecol. 44, 203–215. https://doi.org/10.1016/S0168-6496(03)00027-8

Nunan, N., Wu, K., Young, I.M., Crawford, J.W., Ritz, K., 2002. In situ spatial patterns of soil bacterial populations, mapped at multiple scales, in an arable soil. Microb. Ecol. 44, 296–305. https://doi.org/10.1007/s00248-002-2021-0

Oburger, E., Schmidt, H., 2016. New Methods To Unravel Rhizosphere Processes. Trends Plant Sci. 21, 243–255. https://doi.org/10.1016/j.tplants.2015.12.005

Otsu, N., 1979. A Threshold Selection Method from Gray-Level Histograms. IEEE Trans. Syst. Man. Cybern. 9, 62–66. https://doi.org/10.1109/TSMC.1979.4310076

Pausch, J., Kuzyakov, Y., 2011. Photoassimilate allocation and dynamics of hotspots in roots visualized by 14C phosphor imaging. J. Plant Nutr. Soil Sci. 174, 12–19. https://doi.org/10.1002/jpln.200900271

Pereira, F.C.M., Tayengwa, R., Alves, P.L.D.C.A., Peer, W.A., 2019. Phosphate Status Affects Phosphate Transporter Expression and Glyphosate Uptake and Transport in Grand Eucalyptus (Eucalyptus grandis). Weed Sci. 67, 29–40. https://doi.org/10.1017/wsc.2018.58

Polzer, C., Ness, S., Mohseni, M., Kellerer, T., Hilleringmann, M., Rädler, J., Hellerer, T., 2019. Correlative two-color two-photon (2C2P) excitation STED microscopy. Biomed. Opt. Express 10, 4516. https://doi.org/10.1364/boe.10.004516

Prewitt, J.M.S., Mendelsohn, M.L., 1966. The analysis of cell images. Ann. N. Y. Acad. Sci. 128, 1035–1053. https://doi.org/10.1111/j.1749-6632.1965.tb11715.x

Protz, R., Shipitalo, M.J., Mermut, A.R., Fox, C.A., 1987. Image analysis of soils - present and future. Geoderma 40, 115–125. https://doi.org/10.1016/0016-7061(87)90017-6

Qiu, Y., Fu, B., Wang, J., Chen, L., 2003. Spatiotemporal prediction of soil moisture content using multiple-linear regression in a small catchment of the Loess Plateau, China. Catena 54, 173–195. https://doi.org/10.1016/S0341-8162(03)00064-X

R Developement Core Team, 2014. R: a language and environment for statistical computing, R Foundation for Statistical Computing.

Razavi, B.S., Hoang, D., Kuzyakov, Y., 2017. Visualization of Enzyme Activities in Earthworm Biopores by In Situ Soil Zymography, in: Wilkesman, J., Kurz, L. (Eds.), Methods in Molecular Biology, Methods in Molecular Biology. Springer New York, New York, NY, pp. 229–238. https://doi.org/10.1007/978-1-4939-7111-4

Razavi, B.S., Zhang, X., Bilyera, N., Guber, A., Zarebanadkouki, M., 2019. Soil zymography: Simple and reliable? Review of current knowledge and optimization of the method. Rhizosphere 11, 100161. https://doi.org/10.1016/J.RHISPH.2019.100161

Roose, T., Keyes, S.D., Daly, K.R., Carminati, A., Otten, W., Vetterlein, D., Peth, S., 2016. Challenges in imaging and predictive modeling of rhizosphere processes. Plant Soil 407, 9–38. https://doi.org/10.1007/s11104-016-2872-7

Satapathy, S.C., Sri Madhava Raja, N., Rajinikanth, V., Ashour, A.S., Dey, N., 2018. Multi-level image thresholding using Otsu and chaotic bat algorithm. Neural Comput. Appl. 29, 1285–1307. https://doi.org/10.1007/s00521-016-2645-5

Schindelin, J., Arganda-Carreras, I., Frise, E., Kaynig, V., Longair, M., Pietzsch, T., Preibisch, S., Rueden, C., Saalfeld, S., Schmid, B., Tinevez, J.-Y., White, D.J., Hartenstein, V., Eliceiri, K., Tomancak, P., Cardona, A., 2012. Fiji: an open-source platform for biological-image analysis. Nat. Methods 9, 676–682. https://doi.org/10.1038/nmeth.2019

Schlüter, S., Eickhorst, T., Mueller, C.W., 2019. Correlative Imaging Reveals Holistic View of Soil Microenvironments. Environ. Sci. Technol. 53, 829–837. https://doi.org/10.1021/acs.est.8b05245

Schlüter, S., Sheppard, A., Brown, K., Wildenschild, D., 2014. Image processing of multiphase images obtained via X-ray microtomography: A review. Water Resour. Res. 50, 3615–3639. https://doi.org/10.1002/2014WR015256

Schmidt, H., Nunan, N., Höck, A., Eickhorst, T., Kaiser, C., Woebken, D., Raynaud, X., 2018. Recognizing Patterns: Spatial Analysis of Observed Microbial Colonization on Root Surfaces. Front. Environ. Sci. 6. https://doi.org/10.3389/fenvs.2018.00061

Sezgin, M., Sankur, B., 2004. Survey over image thresholding techniques and quantitative performance evaluation. J. Electron. Imaging 13, 146–165. https://doi.org/10.1117/1.1631315

Spohn, M., Carminati, A., Kuzyakov, Y., 2013. Soil zymography - A novel in situ method for mapping distribution of enzyme activity in soil. Soil Biol. Biochem. 58, 275–280. https://doi.org/10.1016/j.soilbio.2012.12.004

Spohn, M., Kuzyakov, Y., 2014. Spatial and temporal dynamics of hotspots of enzyme activity in soil as affected by living and dead roots-a soil zymography analysis. Plant Soil 379, 67–77. https://doi.org/10.1007/s11104-014-2041-9

Steffens, M., Buddenbaum, H., 2013. Laboratory imaging spectroscopy of a stagnic Luvisol profile - High resolution soil characterisation, classification and mapping of elemental concentrations. Geoderma 195–196, 122–132. https://doi.org/10.1016/j.geoderma.2012.11.011

Steffens, M., Kohlpaintner, M., Buddenbaum, H., 2014. Fine spatial resolution mapping of soil organic matter quality in a Histosol profile. Eur. J. Soil Sci. 65, 827–839. https://doi.org/10.1111/ejss.12182

Tajima, R., Kato, Y., 2013. A quick method to estimate root length in each diameter class using Freeware Imagej. Plant Prod. Sci. 16, 9–11. https://doi.org/10.1626/pps.16.9

Tajima, R., Kato, Y., 2011. Comparison of threshold algorithms for automatic image processing of rice roots using freeware ImageJ. F. Crop. Res. 121, 460–463. https://doi.org/10.1016/j.fcr.2011.01.015

Werner, F., Mueller, C.W., Thieme, J., Gianoncelli, A., Rivard, C., Höschen, C., Prietzel, J., 2017. Micro-scale heterogeneity of soil phosphorus depends on soil substrate and depth. Sci. Rep. 7, 1–9. https://doi.org/10.1038/s41598-017-03537-8

Weszka, J.S., Rosenfeld, A., 1978. Threshold Evaluation Techniques. IEEE Trans. Syst. Man. Cybern. 8, 622–629. https://doi.org/10.1109/TSMC.1978.4310038

Zack, G.W., Rogers, W.E., Latt, S.A., 1977. Automatic measurement of sister chromatid exchange frequency. J. Histochem. Cytochem. 25, 741–753. https://doi.org/10.1177/25.7.70454

Zarebanadkouki, M., Kim, Y.X., Moradi, A.B., Vogel, H.-J., Kaestner, A., Carminati, A., 2012. Quantification and Modeling of Local Root Water Uptake Using Neutron Radiography and Deuterated Water. Vadose Zo. J. 11, vzj2011.0196. https://doi.org/10.2136/vzj2011.0196

Zhang, X., Dippold, M.A., Kuzyakov, Y., Razavi, B.S., 2019. Spatial pattern of enzyme activities depends on root exudate composition. Soil Biol. Biochem. 133, 83–93. https://doi.org/10.1016/J.SOILBIO.2019.02.010

Zhu, Q., Zhou, Z., Duncan, E.W., Lv, L., Liao, K., Feng, H., 2017. Integrating real-time and manual monitored data to predict hillslope soil moisture dynamics with high spatio-temporal resolution using linear and non-linear models. J. Hydrol. 545, 1–11. https://doi.org/10.1016/J.JHYDROL.2016.12.014

2.2.9 Supplementary Materials

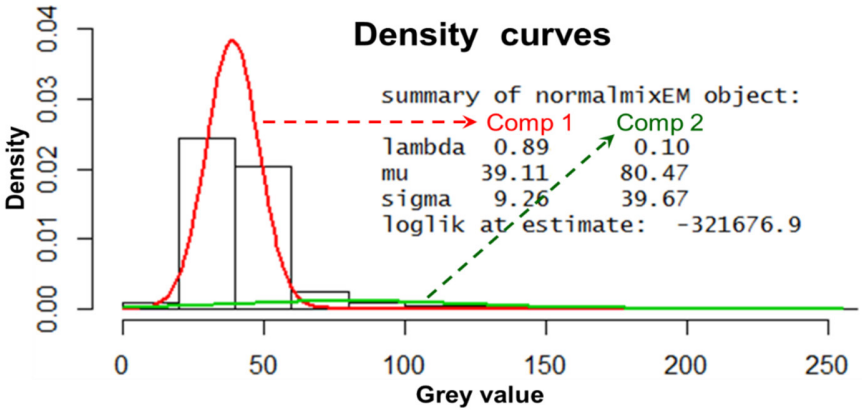

a)

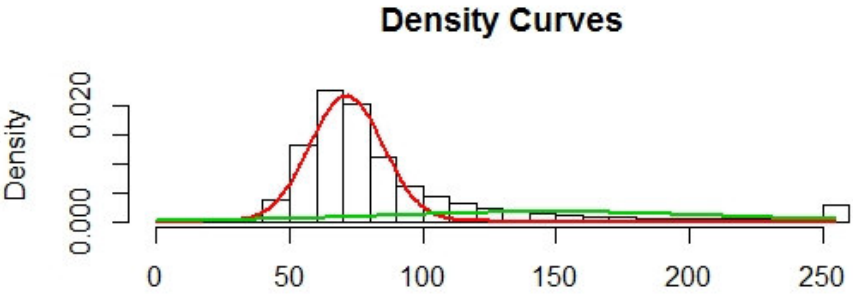

b)

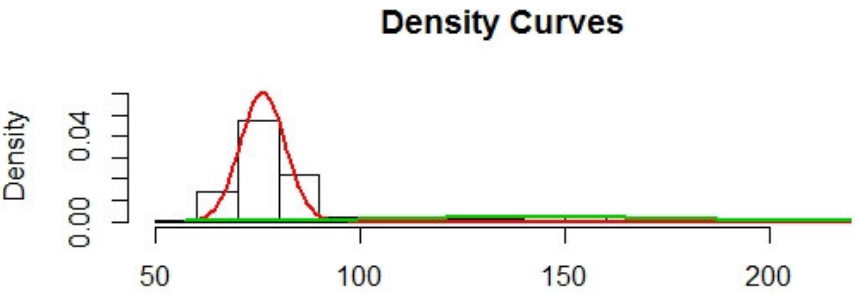

c)

Figure S1. An example of the original grey value distribution (bars) for a) leucine aminopeptidase activity in soil (data extracted from the 8-bit image in Fig. 6b in Razavi et al., 2017); b) ^{14}C image for $^{14}CO_2$-labeled root and exudates in soil (Holz et al., 2018) and c) ^{14}C image of ^{14}C-labeled glyphosate in plants (Pereira et al., 2019) and two fitted normal distributions using the normalmixEM function in R. Red and green lines denote comp 1 and comp 2 distributions in the summary table. As shown at a) red (comp 1) normal distribution covers (lambda (λ)) 89% of the values, while green covers only 11%. Mean values (mu (μ)) and SD (sigma (σ)) were 39 and 81, and 9 and 40 for red and green distribution, respectively.

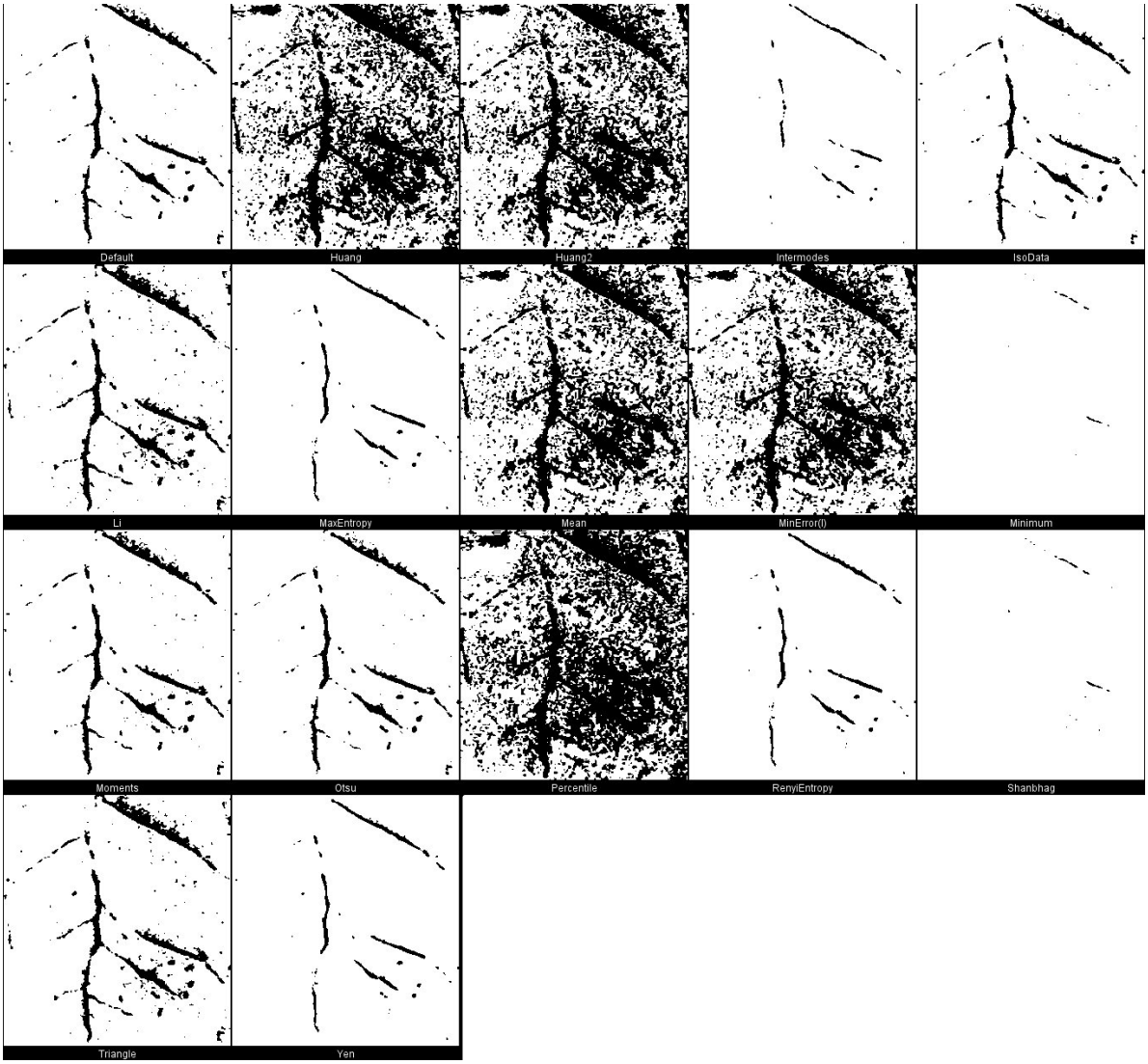

Figure S2. Montage image with results from all built-in thresholding methods in ImageJ (Schindelin et al., 2012) applied to the soil zymogram for leucine aminopeptidase (Razavi et al., 2017).

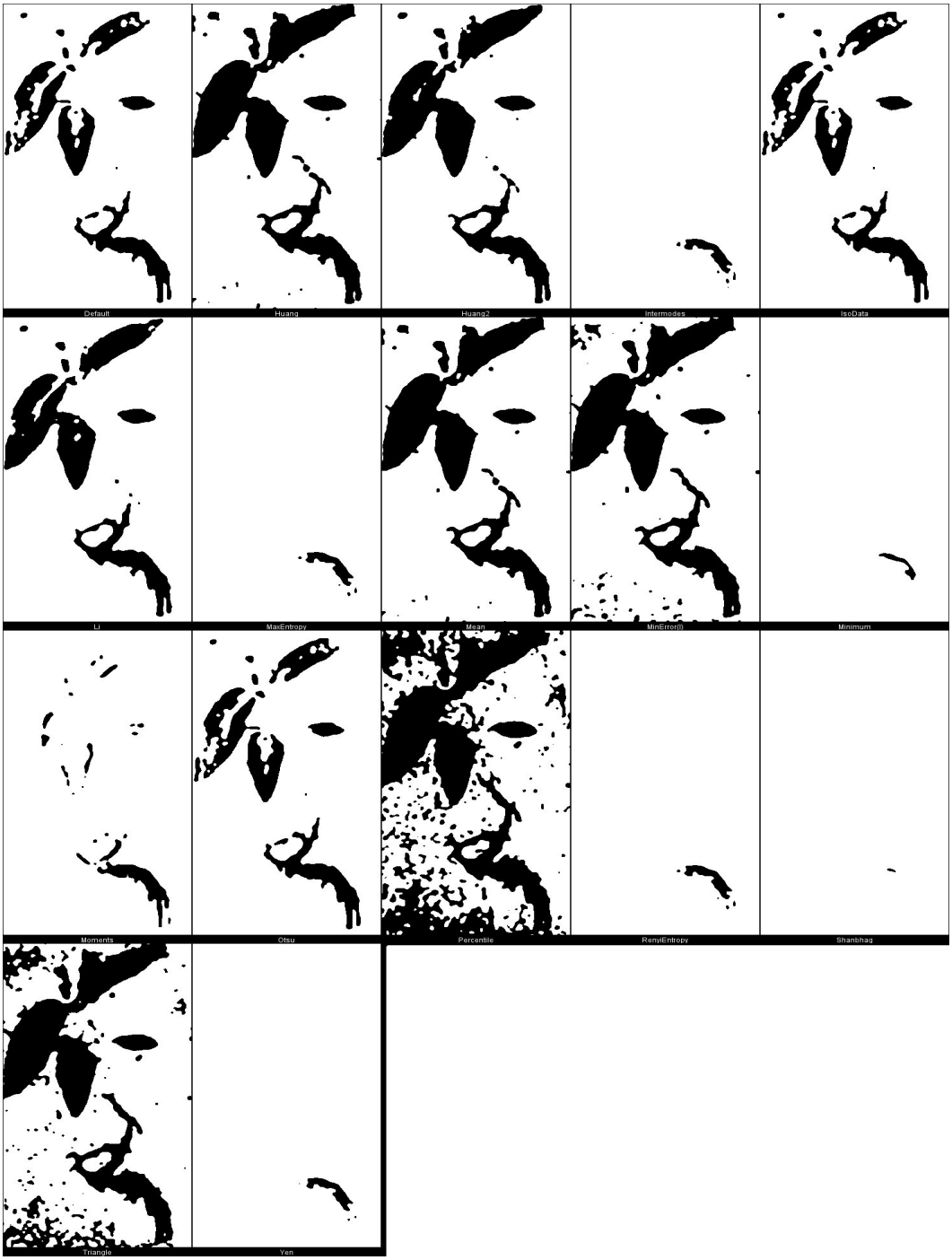

Figure S3. Montage image with results from all built-in thresholding methods in ImageJ (Schindelin et al., 2012) applied to a ^{14}C image of ^{14}C-labeled glyphosate in plants (Pereira et al., 2019).

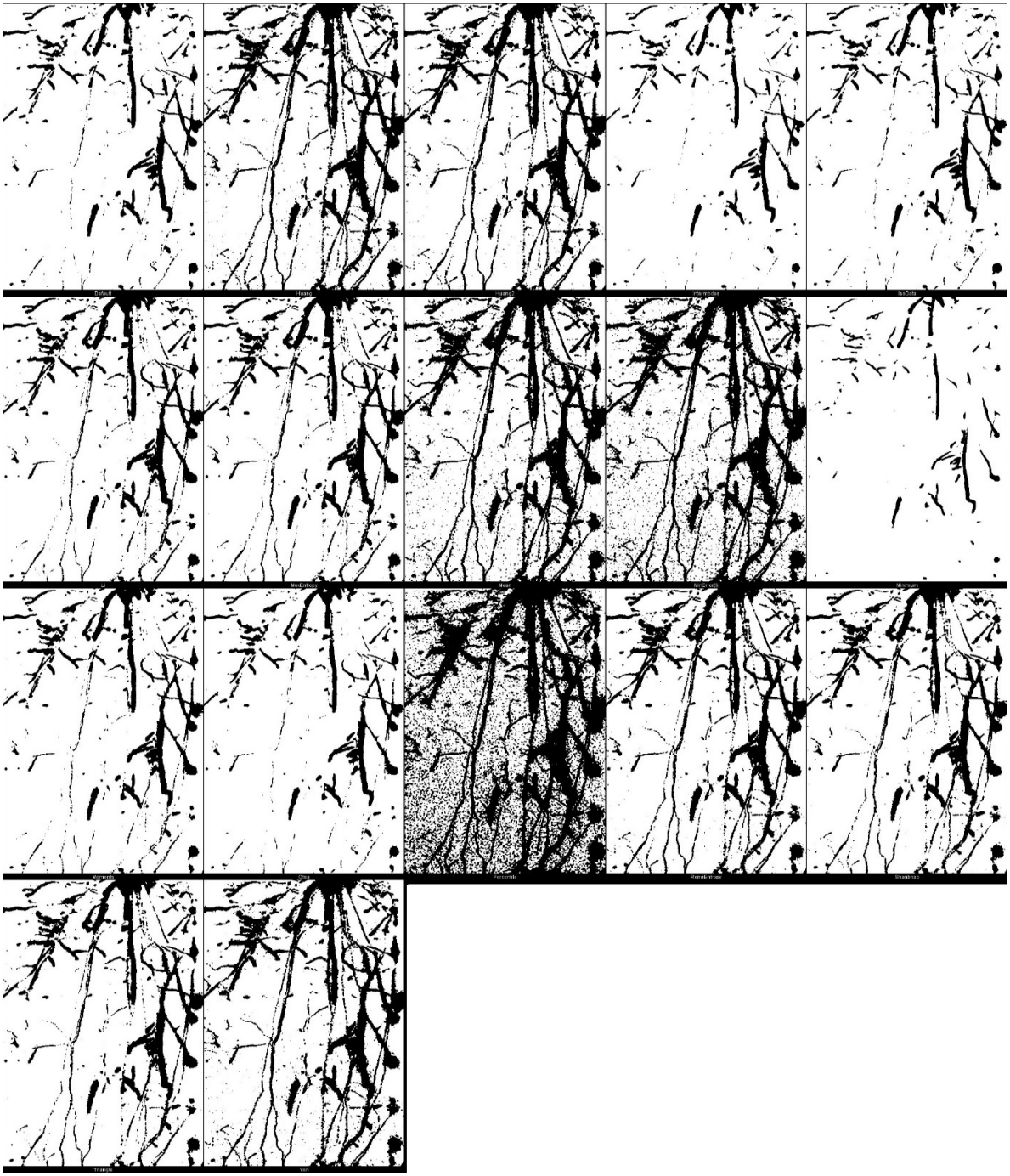

Figure S4. Montage image with results from all built-in thresholding methods in ImageJ (Schindelin et al., 2012) applied to a ^{14}C image for $^{14}CO_2$-labeled roots and exudates in soil (Holz et al., 2018).

Table S1. Results of two-samples t-Test for hotspot mean values between statistical approaches (Mean+2/3SD) and standard methods in ImageJ and Top-25%

Method	^{14}C image for $^{14}CO_2$-labeled root and exudates in soil (Holz et al., 2018)		Soil zymogram for leucine aminopeptidase (Razavi et al., 2017)		^{14}C image of ^{14}C-labeled glyphosate in plants (Pereira et al., 2019)	
	p-values					
	3SD	2SD	3SD	2SD	2SD	3SD
Default	0	0	1.92E-68	0	0	0
Huang	0	**1**	0	0	0	0
Intermodes	0	0	0	0	0	0
IsoData	0	0	1.94E-91	0	0	0
IJ_IsoData	0	0	1.92E-68	0	0	0
Li	8.89E-226	0	1.42E-12	7.83E-74	0	0
MaxEntropy	4.38E-175	0	0	0	0	**0.652**
Mean	0	0	0	0	0	0
MinError	0	0	0	0	0	0
Minimum	0	0	1.7E-279	0	0	0
Moments	0	0	5.56E-27	2.4E-269	0	0
Otsu	0	0	1.94E-91	0	0	0
Percentile	0	0	0	0	0	0
RenyiEntropy	8.87E-196	9.6E-241	0	0	0	**0.652**
Shanbhag	4.52E-91	0	0	0	0	0
Triangle	1.94E-99	0	**0.008838**	2.62E-112	0	0
Yen	0	2.97E-22	0	0	0	**0.148**
Top-25%	0	0	0	0	0	0

2.2.10 Supplementary data – Script in R

Example of script for distribution fitting of distribution parameters in R

```
install.packages("mixtools")

library(mixtools)

setwd("D:/Research/2019/Hot spot approach/Black and white/data for R")

Zymo1<-read.table('Zymo-leu.txt', header=T)

head(Zymo1)

value<-Zymo1$value

Amount<-Zymo1$amount

i<-seq(1,256, by=1)

#test normal distributions

vec<-rep(x=value[i], times = Amount[i])

mod <- normalmixEM(vec)   #test normal distribution

plot(mod,which=2)

summary(mod)
```

2.3 Study 3. Maize genotype-specific exudation strategies: an adaptive mechanism to increase microbial activity in the rhizosphere

Nataliya Bilyera[a,b,], Xuechen Zhang[c], Patrick Duddek[d,e], Lichao Fan[f], Callum C. Banfield[c], Steffen Schlüter[g], Andrea Carminati[d], Anders Kaestner[h], Mutez A. Ahmed[e], Yakov Kuzyakov[f], Michaela A. Dippold[c], Sandra Spielvogel[b], Bahar S. Razavi[a]*

[a] – Department of Soil and Plant Microbiome, Institute of Phytopathology, Christian-Albrechts- University of Kiel, 24118 Kiel, Germany
[b] - Department of Soil Science, Institute for Plant Nutrition and Soil Science, Christian-Albrechts-University Kiel, 24118 Kiel, Germany
[c]- Department of Biogeochemistry of Agroecosystems, University of Göttingen, Göttingen, Germany
[d] - Department of Environmental Systems Science, Physics of Soils and Terrestrial Ecosystems, ETH Zürich, Switzerland
[e] - Chair of Soil Physics, Bayreuth Center of Ecology and Environmental Research (BayCEER), Bayreuth, Germany
[f] - Department of Agricultural Soil Science, Department of Soil Science of Temperate Ecosystems, University of Göttingen, 37077, Göttingen, Germany
[g] - Department Soil System Science, Helmholtz Centre for Environmental Research – UFZ, 06120 Halle, Germany
[h] - Laboratory for Neutron Scattering and Imaging, Paul Scherrer Institute, 5232 Villigen, Switzerland.
[i]- Geo-Biosphere Interactions, University of Tuebingen, 72074 Tuebingen, Germany

Author for correspondence: Nataliya Bilyera (email: n.bilyera@soils.uni-kiel.de)

Status: *published in Soil Biology and Biochemistry, 2021, vol. 162. 108426,*

doi: 10.1016/j.soilbio.2021.108426

2.3.1 Abstract

Plants stimulate microbial enzyme production in the rhizosphere, regulating soil organic matter decomposition and nutrient cycling. The availability of labile organic compounds (i.e. exudates) and water is the main prerequisite for such microbial activity and enzyme production, thus shaping the rhizosphere. Root morphology (i.e., root hairs) and exudate composition define the spatial distribution of properties and functions in the rhizosphere. However, the role of root architecture and exudate composition in this spatial self-organization of the rhizosphere remains unknown.

We coupled three *in situ* imaging approaches: ^{14}C imaging to localize exudates, soil zymography to analyze enzyme activity distribution, and neutron radiography for water fluxes to trace the spatial structure of the rhizosphere of three maize genotypes (wild-type, mutant with defective root-hair prolongation *rth3*, and mutant with reduced benzoxazinoid content in root exudates *bx1*). The co-localization of these three soil images revealed the pivotal role of both optimal water content (neutron radiography) and root exudation (^{14}C imaging) for β-glucosidase production by the rhizosphere microbiome and its hydrolytic activity (zymography). Root hairs increased the exudate release and enlarged the spatial extent of increased β-glucosidase activity around the root axis by 35 %, leading to a two-fold faster decomposition of ^{14}C exudates compared to the mutant with defective root hairs. In contrast, benzoxazinoids suppressed β-glucosidase activity by 30 %, reflecting decreased microbial activity, whereas their absence broadened the rhizosphere. Overall, root hairs in wild type maize increased microbial activity (i.e. β-glucosidase production), whereas the benzoxazinoids in root exudates suppressed microorganisms.

Key words: enzyme activity; primary metabolites; secondary metabolites; soil imaging methods; spatial rhizosphere functioning.

2.3.2 Introduction

The rhizosphere is a microbial hotspot in soil where roots and microorganisms interact (Berg and Smalla, 2009; Pett-Ridge et al., 2021; Philippot et al., 2013; Yang et al., 2017) and accelerate process rates of nutrient mining beyond that in bulk soil (Koranda et al., 2011). To overcome nutrient and water limitations, plants have developed various rhizosphere-related strategies such as root morphological adaptations (Ahmed et al., 2021; Cai et al., 2021; Hinsinger et al., 2009; Vetterlein et al., 2020), beneficial associations with microorganisms (Bucher et al., 2014; Smith et al., 2001), and release of exudates and enzymes (Farrar et al., 2003; Gianfreda, 2015; Jones et al., 2009; Vives-Peris et al., 2020). Despite many efforts to study each of these rhizosphere strategies (Canarini et al., 2019; Downie et al., 2015; Vetterlein et al., 2020; Watt et al., 2020), the spatial organization of the rhizosphere and its functioning remain poorly understood (Vetterlein et al., 2020).

Enzyme activity is crucial for the decomposition of soil organic matter (SOM) and nutrient cycling. The process of SOM decomposition is also responsible for C (i.e., glucose) mining by microorganisms in the rhizosphere. Enzymes are released into the soil by roots and

microorganisms (Sinsabaugh et al., 1992; Waring, 2013). Plants produce β-glucosidase, an enzyme primarily important for the release of the easily available monomer glucose from any oligo- and polysaccharides or glycose is bound via beta-glycosidic linkage. β-glucosidase is released directly from the roots into the soil (Cairns and Esen, 2010; Gómez-Anduro et al., 2011), but plants also facilitate β-glucosidase production in microorganisms by releasing easily available organic substances they can access (Kandeler et al., 2002). Thus, soil microorganisms synthesize β-glucosidase in response to the presence of suitable substrate (i.e., SOM) that must be degraded (Turner et al., 2002; Veres et al., 2015). The extent of β-glucosidase activities is one measure to define the soil volume in which SOM decomposition is altered by root activity (Huo et al., 2017). Beyond substrate (i.e., SOM) availability, optimal abiotic conditions such as soil water content are key prerequisites for microbial activity (Collins et al., 2008; Henry, 2012; Masciandaro et al., 2004). Up to 80% higher β-glucosidase activity was reported in soils with optimal moisture content compared to dry soils (Boeddinghaus et al., 2015; Sardans and Peñuelas, 2005). Soil water is essential for β-glucosidase activity and serves as a medium for diffusion of labile C. Therefore, maintaining a greater enzymatic rhizosphere volume (or extent in 2D images) along with higher β-glucosidase activities and optimal water contents are necessary for plants to acquire nutrients from organic sources (i.e., SOM). The extent to which β-glucosidase activity is controlled by spatial patterns of exudation and soil water content, however, is not fully characterized.

The spatial distribution of released exudates strongly depends on root morphology because organic substances are released along the root axis (mainly at the root tips, elongation zones, and root hairs) (Kaiser et al., 2015; McCully and Canny, 1985; Peterson and Farquhar, 1996). For example, the presence of root hairs increased root ^{14}C exudation up to three-fold (Holz et al., 2018), supposedly due to a larger root surface area (Haling et al., 2013; Silberbush and Barber, 1983). An increased amount of root exudates – forming more readily available C (e.g. sugars, amino acids) – activates microorganisms (Bertin et al., 2003; Liu et al., 2020) and can thus expand the enzymatic rhizosphere extent by up to 1.5 times (Ma et al., 2018a) in root-hair zones.

Along with primary metabolites, plant roots exude secondary metabolites such as benzoxazinoids (Dick et al., 2012) which induce herbivore resistance (Frey et al., 1997; Maag et al., 2016), and have strong fungicidal but less pronounced antibacterial effects (Cotton et al., 2019; Kudjordjie et al., 2019). Apart from plant protective functions (Erb and Kliebenstein, 2020), benzoxazinoids can reduce plant biomass (Hu et al., 2018). Such a negative effect on crop productivity is mainly attributed to the inhibition of beneficial microorganisms belonging to the phylum Glomeromycota or to *Flavobacteriaceae* (Cadot et al., 2020; Hu et al., 2018), which also

release less β-glucosidase (Ahmad et al., 2011; Okamoto et al., 2000; Sørensen et al., 2013). Lower β-glucosidase activity induces less hydrolyzed available C, which is required to maintain higher microbial activity, including microorganisms responsible for nutrient mining. Furthermore, benzoxazinoids decomposition by microorganisms with a high degradation capacity (e.g., *Pseudomonas putida* (Neal et al., 2012)) requires time and energy (Schütz et al., 2019). Accordingly, low or no benzoxazinoids in the exudates may be advantageous for rhizosphere microorganisms but would leave the plant vulnerable to herbivores and fungi. Finally, microorganisms activated at root tips and other root parts with intensive exudation may decompose benzoxazinoids, thus reducing their inhibitory effects. This calls for investigating the influence of root hairs and benzoxazinoids on the spatial distribution of root exudates along and across the roots, and ultimately on the rhizosphere extent and β-glucosidase activity.

Two dimensional imaging methods *per se* provide the advantage of non-destructively visualizing the distribution of compounds or activities in the root-soil continuum. In the case of the rhizosphere, unique relations can be co-localized, such as effects of the water content and the exudation of labile compounds – two prerequisites for high exoenzymatic activity. The spatial distribution of enzyme activity can be detected by soil zymography (Razavi et al., 2019; Spohn et al., 2013), the release of recently assimilated carbon as root exudates visualized with ^{14}C imaging (Holz et al., 2018), and water content localized with neutron radiography (Zarebanadkouki et al., 2012). Soil zymography and neutron radiography (Holz et al., 2019a) have been successfully coupled, similarly to soil zymography and ^{14}C imaging (Spohn and Kuzyakov, 2013). The combination of the three approaches, however, is a novel tool and promises to link two spatially highly variable factors – the newly released photoassimilates and the water content – to elucidate their separate and combined effects on enzyme activity.

In this respect, using genotypes with contrasting rhizosphere morphology (i.e. root-hair defective) (Wen and Schnable, 1994) and exudate profiles (i.e. benzoxazinoids deficit) (Hu et al., 2018) will induce varying interactions in the rhizosphere. We investigated how the spatial distribution of β-glucosidase activity in the rhizosphere of maize depends on the localization of the newly released organic substances by the roots and on the soil water content at the same time point. For this purpose, we compared two maize mutants with the corresponding wild-type. We hypothesized that: (i) the gradients of β-glucosidase activity in the rhizosphere depend on both labile C and soil water availability (H1); (ii) the presence of root hairs expands the rhizosphere extent as well as the maximal activity of β-glucosidase (H2); (iii) the presence of benzoxazinoids in root exudates suppresses microbial activity, reducing β-glucosidase activity (H3). To test these hypotheses, we applied three imaging methods (soil zymography, ^{14}C imaging, neutron

radiography) to three maize genotypes (wild-type, mutant with defective root-hair prolongation (*rth3*), mutant with reduced benzoxazinoids content in root exudates (*bx1*)). Triple method application was needed to ensure the minimum time interval between the imaged parameters (β-glucosidase activity, ^{14}C exudates and soil water content) to be able to co-localize them pairwise quantitatively.

2.3.3 Materials and methods

2.3.3.1 Experimental setup

We used a Haplic Phaeozem soil substrate with a loam texture consisting of sand – 33%, silt – 48%, and clay – 19% (Vetterlein et al., 2021). The soil pH ($CaCl_2$) was 6.21, total C and N were 8.5 and 0.8 g kg^{-1}, respectively; available P and K were 32.7 and 28.5 mg kg^{-1}, respectively (Vetterlein et al., 2021). The following nutrients were added to the soil before filling the rhizoboxes (10×21.2×0.6 cm): 50 mg kg^{-1} N as NH_4NO_3, 50 mg kg^{-1} K as K_2SO_4, 25 mg kg^{-1} Mg as $MgCl_26H_2O$, and 40 mg kg^{-1} P as $CaHPO_4$. The 1 mm sieved soil was homogeneously filled into rhizoboxes, avoiding the formation of layers. The mass of soil was 161-162 g per rhizobox, assuring a homogeneous bulk density of 1.27 g cm^{-3}.

Three maize (*Zea mays* L.) genotypes – wild-type (WT, B73), root-hair defective (>90% less root hairs) mutant (*rth3)* (Hochholdinger et al., 2018, 2008; Wen and Schnable, 1994) and benzoxazinoids (BX) deficit (>90% less benzoxazinoids) mutant (*bx1)* (Frey et al., 1997) – were grown in the rhizoboxes. After 3 days of germination, the pre-germinated seedlings of each genotype were planted in four replicates into separate rhizoboxes and all plants were cultivated for 21 days. The rhizoboxes were placed at an angle of approximately 45° to ensure roots growing towards the wall of the rhizoboxes. About 20-22% of volumetric water content (VWC) was maintained by watering the soil regularly from the top. The spatial distribution of water was visualized by neutron radiography (details below). Plants were grown in a climate chamber with a controlled temperature of 22 °C during the day and 18 °C during the night, a photoperiod of 12 h, relative air humidity of 65%, and a light intensity of 350 µmol m^{-2} s^{-1} of photosynthetically active radiation at the top of the rhizobox (LED Grow Light, GrowLED, France).

2.3.3.2 Imaging methods

2.3.3.2.1 Plant labeling and ^{14}C imaging

After 21 days of growth, each plant was labeled with about 0.5 MBq $^{14}CO_2$ at a target CO_2 concentration of 500 ppm, following the procedure described by Kuzyakov et al. (2006). Briefly, six plants (two replicates of each of three genotypes) were put in an airtight chamber (120 L volume) for two consecutive days. Before labeling, the CO_2 inside the labeling chamber was reduced by cycling the air through 1 M NaOH for 8 h with the grow light off. For the labeling, Na_2CO_3 solution containing 3 MBq of $Na_2{}^{14}CO_3$ was dissolved in 10 ml phosphoric acid (100%). During the labeling, all plants were kept under a grow light (350 µmol m^{-2} s^{-1}) to enable maximum photosynthetic activity. After 6 h, not assimilated $^{14}CO_2$ in the chamber was trapped by pumping the air through 1 M NaOH for 2 h. To check the effectiveness of CO_2 assimilation by plants, the remaining ^{14}C activities in the solutions with trapped $^{14}CO_2$ were determined by liquid scintillation counting using a Hidex 300SL Automatic Liquid Scintillation Counter (Hidex, Turku, Finland) (Banfield et al., 2017). Briefly, 0.5 ml of NaOH with trapped $^{14}CO_2$ were added to the 8 ml scintillation cocktail Rotiszint Eco plus (Carl Roth, Karlsruhe, Germany) and kept in the dark for 24 h for chemiluminescence to cease, and measured for the ^{14}C activities by liquid scintillation counting thereafter. The ^{14}C imaging was done as described in Holz et al. (2018). Briefly, directly after labeling, the rhizoboxes were transferred to a dark room. The rooted soil surfaces were exposed to storage phosphor screens (BAS-IP MS 2040 E, GE Healthcare, U.S.A.). All screens were erased for 10 min under a strong bright light before use, and were protected from moisture by transparent plastic bags (polypropylene, 40 µm thickness, density 0.95 g cm^{-3}, MDF Verpackungen GmbH, Bergisch Gladbach, Germany). After 20 h exposure in the dark, the screens were removed from the soil-root surface and scanned by a laser scanner for phosphorimaging (650 nm excitation, FLA-7000, GE Healthcare, U.S.A.) with a spatial resolution of 25 µm. The duration of 20 h was recommended by previous studies (Holz et al., 2018; Thu Hoang et al., 2020) to best visualize the ^{14}C signal.

Although we did not calculate the ^{14}C activity for the volume of soil in this experiment, the gradient of activities on 2D images was necessary to potentially access the amount of C released along the root. Therefore, the ^{14}C images were calibrated by preparing a series of smooth soils with activities ranging from 0 to 1.55 MBq at cm^{-2}. The same procedure of ^{14}C imaging and image processing procedure was applied. The details are described in Thu Hoang et al. (2020).

Due to the short time (20 h) between labeling and imaging, almost all of the ^{14}C detected can be attributed to exudates and secretion – and a negligible proportion to root cell/tissue turnover, which requires longer observation times (> 5 days).

2.3.3.2.2 Soil zymography

Direct soil zymography (Razavi et al., 2016) was used to study the spatial distribution of enzyme activities immediately after removing the ^{14}C imaging plates. Enzyme activity was visualized using polyamide membranes (0.45 µm mesh size, Tao Yuan, China) saturated with 4-methylumbelliferone (MUF)-labeled substrates. The β-glucosidase activity was detected with 4-methylumbelliferyl-β-D-glucoside (Sigma-Aldrich, Germany). The substrate was completely dissolved in MES buffer ($C_6H_{13}NO_4SNa_{0.5}$) (pH: 6.5) (Sigma-Aldrich, Germany) by shaking to reach the concentration of 1 g L^{-1} (Sanaullah et al., 2016), which corresponds to 3.5 mM. Polyamide membrane filters (20×20 cm) and a pore size of 0.45 µm were cut to 10×20 cm to fit the size of the rhizobox. Each membrane was saturated with 5 ml of the substrate solution by covering it completely with the solution in a flat box for 10 s. The rhizoboxes were opened from the rooted side, and the saturated membranes were applied directly to the soil surface (Razavi et al., 2016). After 1 h incubation at the root-soil interface, the membranes were carefully lifted off, and the few attached soil particles were gently removed using tweezers and a soft-thin paintbrush.

The membranes were placed in a dark room under ultraviolet (UV) light with an excitation wavelength of 355 nm. Photos were taken with a digital camera Canon EOS 6D with a Canon lens EF 94 mm 1: 4L IS. The aperture and shutter speed were set to f/5.6 and 1/30 s, respectively.

A standard calibration that relates the enzyme activities to the gray values of zymogram fluorescence (i.e. of the membrane) was performed. The calibration function (Fig. S1) was obtained by zymography of 4 cm^2 membranes soaked in a solution of MUF with concentrations of 0, 0.01, 0.2, 0.5, 1, 2, 4, 6 and 10 mM. The amount of MUF on an area basis was preliminarily determined to ensure complete membrane saturation but no excess liquid that may drip. The membranes used for calibration were imaged under UV light and analyzed with identical light conditions and camera settings as the samples.

2.3.3.2.3 Neutron radiography

Neutron radiography was used to create images of the water content in the sample and to identify differences in the water content of rhizosphere and bulk soil. Neutron radiographs were

taken straight forward after zymography, which allows to relate spatial distribution of water content with enzyme activity.

Neutron radiography is highly sensitive to hydrous materials and therefore visualizes the water distribution along the roots in the soil (Ahmed et al., 2016; Moradi et al., 2009). A parallel neutron beam propagates through the sample, and the transmitted neutrons behind the sample are detected using a scintillator. The scintillator converts the neutrons into visible light captured by a CCD camera. The exposed image carries information on sample thickness and composition according to the Beer–Lambert's law (Zarebanadkouki et al., 2012):

$$\frac{I-dc}{ff-dc} = exp\left[-\sum_{i=1}^{i=n}(\mu_i d_i)\right] \quad \text{(Eq. 1)}$$

where I is the transmitted neutron beam intensity [cm^{-2} s^{-1}], ff is the flat field (i.e. the transmitted beam without sample) [cm^{-2} s^{-1}], *dc* is the dark current (i.e. transmitted beam when the beam is off) [cm^{-2} s^{-1}], n represents the number of observation, μ_i is the neutron attenuation coefficient [cm^{-1}], and d_i is the thickness [cm] of material i. The materials composing our samples were: aluminum, dry soil, root, and water. The attenuation contribution of aluminum and dry soil were obtained from radiographs of empty and dry samples, respectively. The attenuation coefficient of water was derived from images of step wedge samples of known thickness filled with water. The measurements were performed within 0.5-1 h after zymography at the ICON beamline at the Paul Scherrer Institute (PSI), Villigen, Switzerland (Kaestner et al., 2011). We used a sCMOS camera detector (Andor NEO, Andor Technologies) with an array of 1260 by 1260 pixels, a field of view of 15.75 by 15.75 cm, and an effective spatial resolution of 0.2 mm (or 2160 × 2560 pixels, yielding a field of view of 13.3 × 16 cm and pixel size of 0.062 mm). With this field of view, a 2x2 matrix radiography scan with overlapping marginally was needed to fully cover the rhizobox sample.

2.3.3.3 Image processing and co-localization

2.3.3.3.1 Image processing

All images were processed in ImageJ (version 1.52p) (Abràmoff et al., 2004). Zymograms, neutron radiographs, and ^{14}C images were transformed into 8-bit grayscale images. The backgrounds were calculated and subtracted based on the calibration line at concentration of zero added MUF for zymogram, no ^{14}C activity added for ^{14}C images, and intensity attenuations values of aluminum and dry soil for neutron images.

For each treatment the mean values of β-glucosidase activity were measured from calibrated zymograms (Fig. S2) at three locations (bulk soil, mature root, root tips) using ImageJ. β-glucosidase activity for bulk soil was estimated at 5-7 locations (~2-6 cm^2) away from all adjacent roots. β-glucosidase activity along the mature root and root tip areas was measured at 5-7 root compartments with a good visibility to avoid bias related to attachment issues, as described in Razavi et al. (2019). Rhizosphere hotspots for *β*-glucosidase activity, ^{14}C exudates, and water content were thresholded by a previously developed statistical approach of Mean+2SD (or $\mu+2\sigma$) (Bilyera et al., 2020).

2.3.3.3.2 Rhizosphere thresholding procedure

The rhizosphere extent was determined for root segments of mature root (>3 cm from the tip) and root tip (0-2 cm) (Yu et al., 2016), irrespective of root type and order, for the following parameters: 1) ^{14}C in exudates (^{14}C images); and 2) β-glucosidase activity (soil zymograms). To measure the rhizosphere extent, five horizontal transects (angle to the root ~ 90^0) were randomly drawn across five randomly selected roots for each ^{14}C image and zymogram using ImageJ. In total, this yielded 25 lines per image as pseudo-replicates, and their mean was used for each rhizobox (as a true replicate).

The pixelwise gray values along each section were plotted against their distance from the starting point at the root-soil interface. A minimum of five locations (~2-6 cm^2) of the background activities (bulk soil) per image were manually selected, and their mean pixel intensities were determined (Fig. S2) (Hummel et al., 2021). The threshold value (here lower limit of the rhizosphere activities) for the rhizosphere was taken from the $\mu+2\sigma$ of the pixel intensity distribution, as was mentioned above. Then, in the cross sections, the distance between the points where the threshold was first / last exceeded from both sides of each root was calculated and used as the rhizosphere bidirectional extent (Fig. S2). Root diameters at the same segments of the root system were manually measured in individual photos. Based on the assumption that the rhizosphere is symmetrically distributed around the root (Hinsinger et al., 2005), the rhizosphere extent was calculated as the difference between rhizosphere bidirectional extent and root diameter divided by two.

2.3.3.3.3 Co-localization analysis

We conducted co-localization analysis for paired combination of images for three parameters (^{14}C intensity, β-glucosidase activity, soil water content distributions). The co-

localization of three parameters enables to detect if the imaged parameters spatially overlap / coincide and to which extend β-glucosidase activity depend on the presence of ^{14}C and the distribution of soil water. Prior to co-localization analysis, all three images from each replicate were cropped to the same dimensions and manually registered by spatial alignment with the TrackEM2 plugin (Cardona et al., 2012; Saalfeld et al., 2012) in ImageJ. The co-localization was analyzed using JACoP (Just another co-localization plug-in) (Bolte and Cordelières, 2006) in ImageJ. We did not correct images for root growth during the imaging processes because soil zymography was conducted maximally 10-15 min after the ^{14}C image plate was removed; thus, following 1 h of exposure time for zymography, the samples in rhizoboxes were measured for water content by neutron radiography 1.5-2 h after ^{14}C imaging. The co-localization analysis was conducted for two sets: (1) normalized images of ^{14}C intensity, β-glucosidase activity, and soil water content distributions; and (2) thresholded hotspot areas of β-glucosidase activity, ^{14}C exudates, and water content (binary images of rhizosphere).

We calculated the following co-localization coefficients: (1) Pearson correlation coefficient (PC) – to characterize the correlations of the pixel intensity distribution between two images; (2) overlap coefficient (Fig. S3) (r) – to distinguish if the pixel intensity distribution of two signals overlap with positive values between two images; (3) Mander's or co-occurrence coefficients (Fig. S3): M1 – the co-localization of parameter A with parameter B; M2 – the co-localization of parameter B with parameter A. This image analysis produced two coefficients that represent the fraction of co-localizing objects in each component of a dual-channel image (Manders et al., 1993). The co-localization coefficients were calculated for non-thresholded images in the whole rhizobox area (bulk and rhizosphere soil). Binary images of thresholded rhizosphere were applied for calculation coefficients r, M1 and M2 of the rhizosphere.

Pearson correlation coefficient: $PC = \frac{\sum_i (A_i - a) \cdot (B_i - b)}{\sqrt{\sum_i (A_i - a)^2 \ \sum_i (B_i - b)^2}}$ (Eq. 2)

Overlap coefficient: $r = \frac{\sum_i A_i \cdot B_i}{\sqrt{\sum_i A_i^2 \cdot \sum_i B_i^2}}$ (Eq. 3)

Manders' coefficients:

$M1 = \frac{\sum_i A_{i,coloc}}{\sum_i A_i}$ *with* $A_{i,\ coloc} = A_i$ *if* $B_i > 0$ (Eq. 4)

$M2 = \frac{\sum_i B_{i,coloc}}{\sum_i B_i}$ with $B_{i,\ coloc} = B_i$ *if* $A_i > 0$ (Eq. 5)

where A_i is the intensity at each pixel of image A, B_i is the intensity at each pixel of image B, and a and b are the mean intensities of images A and B, respectively.

The qualitative interpretation of the quantitative co-localization results is provided according to Zinchuk et al. (2013) in five linguistic variables – *very weak, weak, moderate, strong, very strong* (Table S1).

2.3.3.4 Statistical analysis

All data are presented as mean ± standard deviation of four replicate rhizoboxes. The Nalimov outlier test was performed to check the reliability of data sets. The Shapiro-Wilk test was performed for residues of means to check for normality, and the Bartlett test was applied to check the homogeneity of variances. If data met normality and homogeneity, one-way ANOVA and Tukey's HSD post hoc test were performed; if homogeneity was not proved, the Welch test and Games-Howell post-hoc test were performed; if normality was not met, the Kruskal-Wallis test was applied. The experimental factor was a genotype. All analyses were performed using R software, Version 3.6.1 (R Development Core Team, 2011) at a significance level of $\alpha = 0.05$.

2.3.4 Results

2.3.4.1 Spatial distribution of ^{14}C from root exudation, β-glucosidase activity, and soil water content

Visual analysis of the ^{14}C images showed contrasting exudation patterns for the three maize genotypes: 1) stronger exudation at root tip regions in wild-type (WT) (Fig. 1d); 2) rather homogeneous exudation along the whole root system of mutants' *rth3 (*Fig. 1e) *and bx1 (*Fig. 1f). Overall, exudation was higher for *bx1* than for *rth3.* β-glucosidase activities on zymograms were higher at root tips and young roots in WT (Fig. 1g) but mainly on young roots in *rth3* (Fig. 1h) and rather homogeneous along the root axis in *bx1* (Fig. 1i). Neutron images clearly showed the roots themselves due to their high tissue water content (~0.2%) and a very variable water content in close proximity to the root (0-1 mm) (Fig. 1j-l).

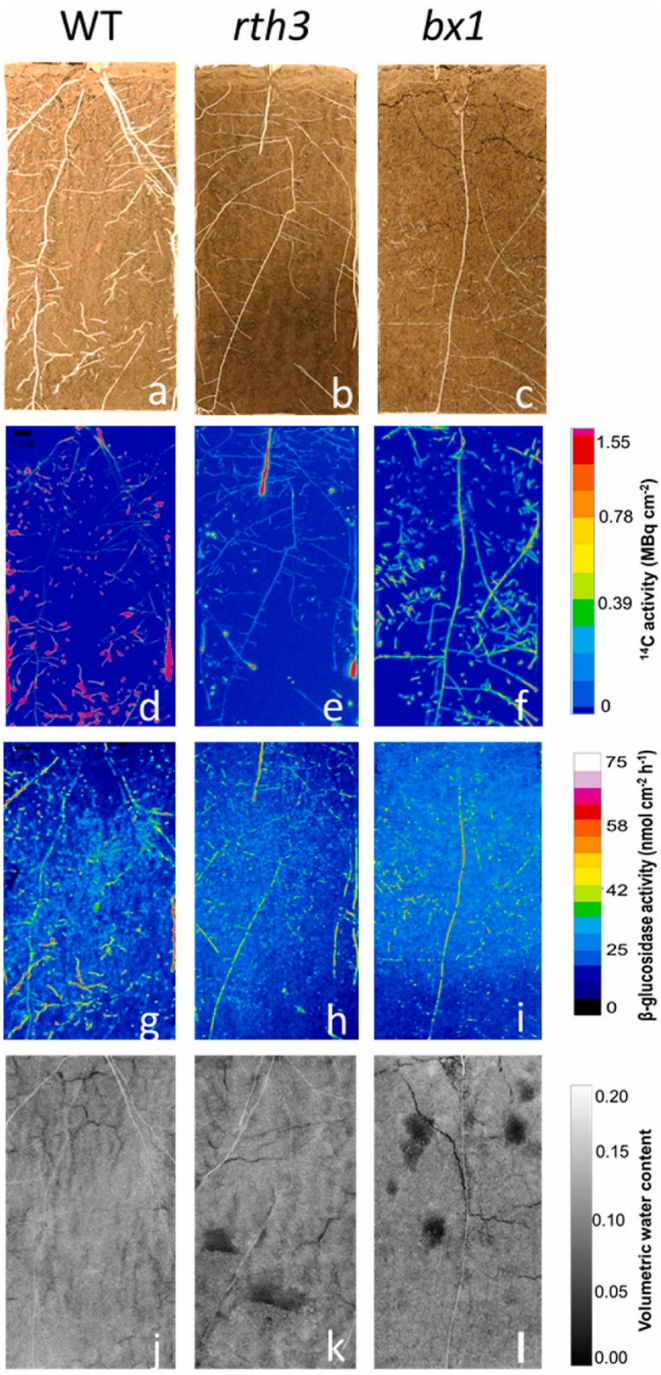

Figure 1. Root images (real light photos) (a,b,c), zymograms of β-glucosidase activity (d,e,f), ^{14}C phosphor images (g,h,i), and neutron radiographs (j,k,l) of three maize genotypes (WT, *rth3* and *bx1*). Side color or gray scales are proportional to β-glucosidase activity (pmol cm^{-2} h^{-1}), ^{14}C activity (MBq) and to volumetric water content. Always one representative replicate out of four was chosen. WT: wild-type maize, *rth3:* root-hair defective mutant*; bx1:* mutant with reduced benzoxazinoids in root exudates.

2.3.4.2 *Rhizosphere extent*

The rhizosphere extent of β-glucosidase activity of *rth3* was 30-35% smaller for the mature root (*P<0.05*) and root tip region (*P*<0.001) than for the corresponding regions of WT, but there was no difference between *bx1* and WT (Fig. 2a). The mean rhizosphere extent with respect to β-glucosidase activity was ~50% greater (*P*<0.001) at the root tip region than along mature roots over all genotypes (Fig. 2a).

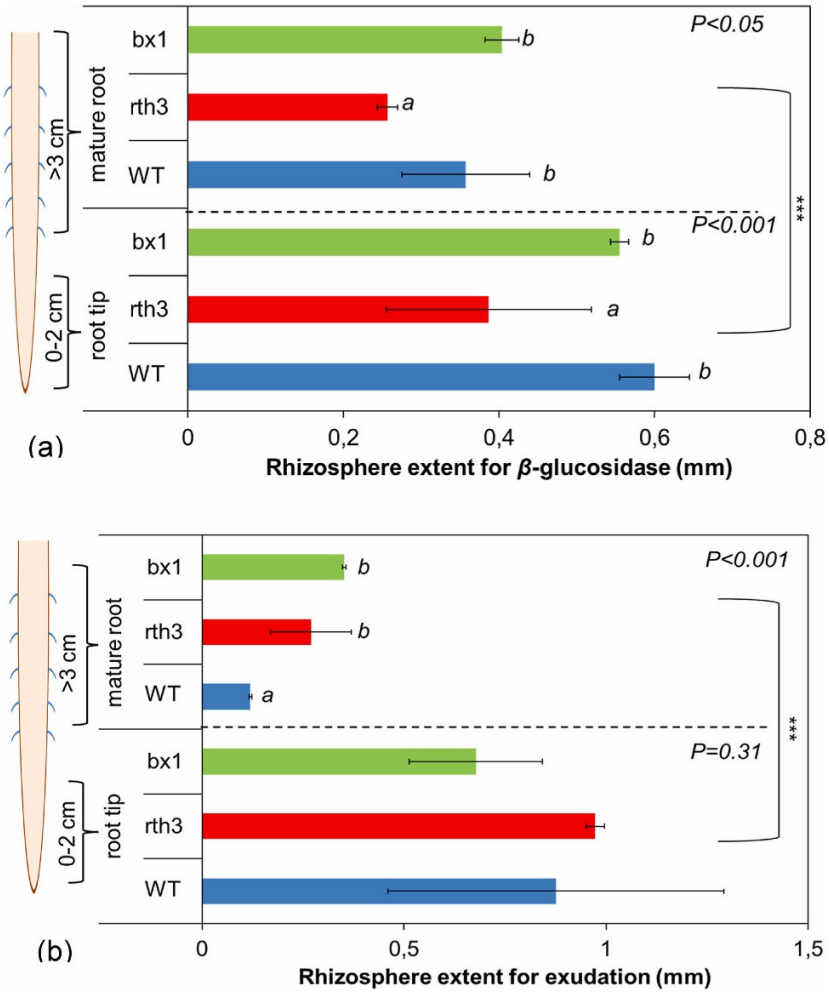

Figure 2. The rhizosphere extent for β-glucosidase activity (a) and ^{14}C-labeled root exudates (b). Data are means for each genotype (WT, *rth3* and *bx1*) (n = 4), error bars indicate standard deviations. Letters within one root type mark significant differences among the genotypes at $P < 0.05$. Asterisks on the bracket at the right side indicate significant differences between root sections ('***' $P < 0.001$; '**' $P < 0.01$; '*' $P < 0.05$).

The rhizosphere extent of exudation along mature roots was about 2.5 times smaller (*P< 0.001*) in the WT versus both mutants (Fig. 2b). In contrast, there was no genotype effect (*P=0.31*)

on the spatial ^{14}C extent around the root tips (Fig. 2b). Generally, the exudation distance increased 2-6 fold at the root tip versus mature root for all genotypes (*P < 0.001*).

2.3.4.3 Mean β-glucosidase activity

Mean β-glucosidase activity in the bulk soil was ~20% (*P<0.001*) higher for *rth3* than *bx1* and WT (Fig. 3). The mean values along mature roots (Fig. 3) increased to 554 pmol cm^{-2} h^{-1} (*P*<0.01) in *bx1* compared to 436 pmol cm^{-2} h^{-1} in WT, whereas they were within the same range (550-571 pmol cm^{-2} h^{-1}, *P=0.34*) for all genotypes at the root tip region (Fig. 3).

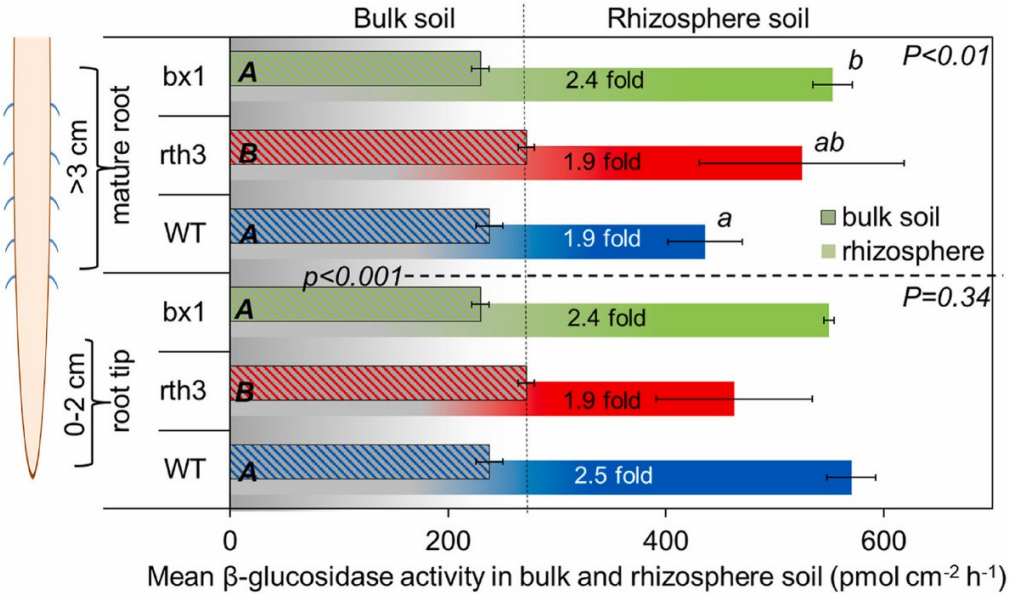

Figure 3. Mean of *β*-glucosidase activity in bulk soil (shaded) and in the rhizosphere along the mature root and root tips. Data are means for each genotype (WT, *rth3* and *bx1*) (n = 4), error bars indicate standard deviations. Letters within one root section mark significant differences among the genotypes at *P* < 0.05. Capital letters refer to bulk soil, while lower case letters refer to rhizosphere soil. Relative increase (fold, times) in β-glucosidase activity along mature root and at root tip compared to bulk soil is marked over arrow at each column. The vertical thin dashed line separates the bars for bulk and rhizosphere activities.

2.3.4.4 Hotspot areas

The percentage of hotspot areas for β-glucosidase activity did not differ (*P=0.24*) among the genotypes (Fig. S4). Mutant *bx1* had the highest percentage (27% of the total rhizobox area) of the hotspot area for exudation (Fig. S4), which was 3.5-fold greater (*P<0.05*) than for WT or *rth3*.

2.3.4.5 Co-localization

The co-localization analysis of the whole image revealed a moderate Pearson coefficient (PC) (in the order *rth3* < WT < *bx1*) for the dependence of β-glucosidase activity gradients on the intensity of the newly released ^{14}C exudates (Table S2). The presence of ^{14}C root exudates strongly induced β-glucosidase activity in *rth3* (r=0.85, Table S2), but much less pronounced in WT and *bx1* (r=0.26-0.31). Note that in contrast to PC, overlap coefficient (r) accesses only spatial co-localization, but does not take into account the gradients of two parameters. The area of enhanced β-glucosidase activity, which co-occurred with ^{14}C exudates (represented here by Mander's coefficient (M1)), increased ($P < 0.001$) from 0.26 in WT and 0.39 in *bx1* to 0.99 in *rth3* (Table S2). β-glucosidase activity co-localized strongly (r=0.89-0.96, Table S2) with soil water content for all three genotypes. In contrast, PC for the water*enzyme interaction was dependent on genotype ($P < 0.01$), from very weak in *rth3* to moderate in both WT and *bx1* (Table S2).

Restricting the co-localization analysis to the rhizosphere hotspot area defined by highest β-glucosidase activity resulted in similar overlap coefficients within genotypes for ^{14}C exudate hotspots (0.37-0.50) and rhizosphere water hotspots (0.39-0.43) (Fig. 4b). The area of the β-glucosidase activity hotspot co-occurring with ^{14}C exudates in hotspots (M2) was about two times larger in mutant *bx1* than WT (Fig. 4a). The area of β-glucosidase activity co-occurring with the rhizosphere water hotspot (or wet rhizosphere) (M1) was similar for all genotypes (0.30-0.39).

2.3.5 Discussion

2.3.5.1 Role of root exudation and water distribution in β-glucosidase activity

The WT released exudates primarily from root tips (Fig. 1), as already previously identified by ^{14}C labeling (McCully and Canny, 1985; Pausch and Kuzyakov, 2011; Rovira, 1973). In contrast, the *rth3* and *bx1* mutants released ^{14}C exudates along the whole roots (Fig. 1d-f), i.e. not restricted to root tips. The change in spatial distribution of exudates in *rth3* and *bx1* is presumably a plant strategy to maintain high microbial activity and thus enzyme activity (including β-glucosidase) by releasing easily available C into the entire rhizosphere (Cotton et al., 2019; McDougall and Rovira, 1970; Voothuluru et al., 2018). The *rth3* mutant could compensate for its up to 70 % smaller root surface area (Raghothama and Karthikeyan, 2005; Segal et al., 2008; Tachibana and Ohta, 1983) by increasing the total amount of exudates distributed longitudinally along the roots (Lagos et al., 2015). Similarly, the deficit of benzoxazinoids in *bx1* induces not

only an altered exudate composition (Hu et al., 2018), with a higher labile C content, but also distributed the exudates along longer segments of its root system (Fig. 1).

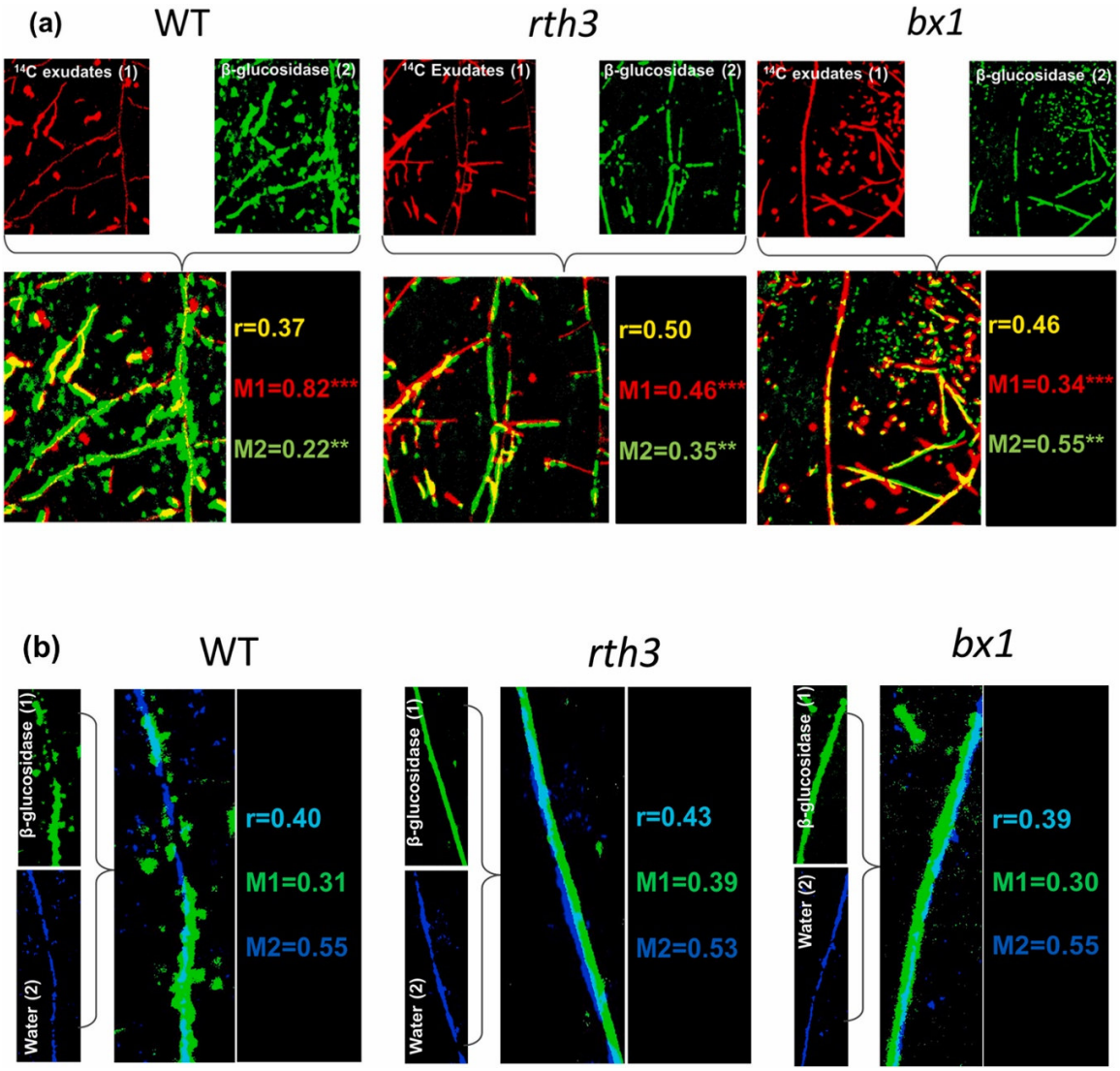

Figure 4. Region of interest (ROIs) images of hotspots for (a) exudates and β-glucosidase activity; and (b) β-glucosidase activity and water content, and their overlap image for three maize genotypes (WT, *rth3, bx1*). The results of co-localization analysis are given as means of four replicates and presented by overlap coefficient (r) and two Manders coefficients (M1 and M2, see detailed explanation in Fig. S3). Asterisks on the values indicate significant difference between genotypes ('*' $P < 0.05$; '**' $P < 0.01$; '***' $P < 0.001$).

Water is crucial not only for microbial functions, but especially for substance diffusion. Microorganisms in bulk soil, being at least 12-14 mm away from ^{14}C exudation hotspots, rely

mainly on SOM as a C source (Vedere et al., 2020). SOM is sparsely and patchily distributed a few mm away from roots, and the long diffusion pathways between non-diffusible enzymes and substrate require closed water films (Benard et al., 2019a; Hobley et al., 2018; Vedere et al., 2020). Low water content reduces the continuity of such substrate diffusion paths and increases the probability of enzyme sorption and inactivation (Allison, 2006; Guber et al., 2019; Kandeler, 1990; Vedere et al., 2020). Accordingly, the dependence of enzyme activity on soil moisture is supported by the high correlation (r=0.89-0.96) between β-glucosidase activity and water content (Table S2).

Because enzyme diffusion in soil in nearly absent (Guber et al., 2018; Kandeler, 1990; Vedere et al., 2020), the high co-localization of β-glucosidase activities (zymography) with exudate distribution (^{14}C) outside the root surface clearly shows that rhizosphere microorganisms use root exudates to produce enzymes. In contrast, the co-localization of root derived ^{14}C with enzyme activity may indicate that primary metabolites and enzymes jointly exude from the root. Thus, based on the results of co-localization analysis we may assume that much (65-78 %) of the β-glucosidase activity in the rhizosphere is produced by microorganisms, not by roots (only 22-35%, M2 for WT and *rth3,* Fig. 4a).

Enzyme activity in the rhizosphere is controlled by environmental conditions favorable for microorganisms. Such conditions are present in a biofilm-like environment, which stabilizes abiotic conditions and provides a buffer of C availability (Flemming et al., 2016). Consequently, root exudates (visible by ^{14}C imaging) with high C availability, which are close to the root surface (0-2 mm), create ideal conditions for maximum microbial activity (Paterson et al., 2008).

^{14}C shows the spatial distribution of exudates, and mucilage distribution determines the rhizosphere water content (Carminati et al., 2010). Mucilage in the rhizosphere increases microbial activity by providing favorable conditions for C diffusion and enzyme production (Ahmed et al., 2018; Holz et al., 2019a). The higher β-glucosidase activities and enhanced rhizosphere extension of the WT are attributable to mucilage production at the root tips rather than along older root sections (Guinel and McCully, 1986; Horst *et al.*, 1982, this study – Figs. 2 and 3). Generally, the distinct rhizosphere extent for enzyme activity and exudation, along with the increased β-glucosidase activities at root tips compared to mature roots, support a bimodal distribution of rhizosphere properties (Carminati and Vetterlein, 2013). This concept reflects different age-based properties at the root tip and mature root zone (root tips lack fully developed functional tissues). This determines their respective functions and hence their ability to acquire water and nutrients.

Our findings clearly support the bimodal nature of the rhizosphere in WT, but this was less pronounced in *bx1* and *rth3* (Figs. 2, 3).

Overall, unlike in a bulk soil, enzyme activity (here β-glucosidase) in the rhizosphere was equally co-localized with optimal water content (r=0.39-0.43) and ^{14}C exudates (r=0.37-0.50) (Fig. 4). This supports our hypothesis (H1) on the important role of soil water and C availability in enzyme activity gradients.

2.3.5.2 Role of root hairs for the spatial distribution of exudates and β-glucosidase activity

Root hairs are usually abundant only 1-5 cm above the root tip (Jungk, 2001), but the rhizodeposits formed when such hairs break and lyse promote microbial activity in the rhizosphere of the root region above 5-6 cm from the root tip, as the root continues growing. These root-hair rhizodeposits, along with the released exudates, increase the active portion of microbial biomass in the rhizosphere (Zhang et al., 2020) and therefore stimulate β-glucosidase production (Wang and Lu, 2006). Generally, the presence of root hairs enlarged the enzymatic rhizosphere by up to 50% (Greenfield et al., 2021; Ma et al., 2018b), which our study also confirmed for β-glucosidase activity (+35% of rhizosphere extent) (Fig. 2). The rhizosphere radius (~0.36 mm) of maize with root hairs is equivalent to the average length of root hairs alone (~0.4 mm) (Ma et al., 2018b). The root hair regions (Gilroy and Jones, 2000; Haling et al., 2013) could belong to nutrient-depletion zones (Hummel et al., 2021; Kreuzeder et al., 2018). When experiencing nutrient limitation, active microorganisms induce higher enzyme activity generally and β-glucosidase activity in particular. This expands the rhizosphere radius of maize at least within the length of root hairs. Thus, the expanded rhizosphere enzymatic zone along the root axis in WT maize (Fig. 1g-l) proves that gradients of β-glucosidase activity strongly depend on root hair presence (H2).

In contrast, the absence of root hairs (*rth3*) induces an increased exudation of primary metabolites and β-glucosidase (Gramss et al., 1999) from the mature root zone in *rth3.* This might reflect the higher membrane permeability in the absence of root hairs. The substrate limitation for microorganisms can stimulate exudation by roots (Williams and Vries, 2020) and increase the spatial extent of the ^{14}C exudation patterns along the mature root section (Fig. 2). Nonetheless, we cannot exclude methodological issues of ^{14}C imaging (i.e. detection limits) due to root hair presence: such hairs may result in a more fuzzy distributions of ^{14}C images (Holz et al., 2019b). Assuming the same amount of released root exudates from WT and *rth3*, then the much smaller root surface area in *rth3* due to the deficient root hairs (Segal et al., 2008; Tachibana and Ohta,

1983) will probably yield a larger and/or faster exudation rate per root area. Some exudates are decomposed by microorganisms within 24 h of ^{14}C imaging (Holz et al., 2019b), and this portion is expected to be larger along the root hairs colonized by bacteria (Mercado-blanco and Prieto, 2012). Higher decomposition in WT was confirmed by the almost two-fold larger overlap coefficient for ^{14}C exudates (82 % vs. 46 % in the *bx1* and *rth3* mutants) and by the formed β-glucosidase hotspot due to the presence of root hairs (Fig. 4). Nonetheless, we cannot reject the effect of patchiness along the root axis (active and inactive segments/patterns) in the rhizosphere, which may contribute to the co-localization results.

2.3.5.3 Role of benzoxazinoids for the spatial distribution of exudates and β-glucosidase activity

The *bx1* maize plant did not need to invest high energy into synthesizing benzoxazinoids and therefore probably produced more primary metabolites (Pott et al., 2019). Consequently, microbes very close to the root are less inhibited by defensive secondary metabolites (10-40 % lower amount, Fig. 2) but instead have 20-30 % more primary (soluble protein, amino acids, sugars) metabolites (Hu et al., 2018). The larger ^{14}C accumulation area in the soil in *bx*1 is because the ^{14}C is localized along the whole root, not only at the root tip as in WT. Due to the 25% stronger concentration gradients of sugars (Hu et al., 2018), ^{14}C exudates from *bx1* diffused faster than from WT. Favorable (~15-20 %) soil water contents facilitate the diffusion of primary and secondary metabolites from the rhizosphere into the bulk soil, especially if this diffusion is induced by the presence of mucilage, ensuring continuous water films (Benard et al., 2019b, 2018). Nevertheless, due to their short (< 24 h) half-life in the soil (Macías et al., 2005) benzoxazinoids can diffuse no more than 1 cm from the root surface (Rice et al., 2012). This means they will not directly affect microbial activity in the bulk soil of WT. In contrast, primary exudation metabolites diffuse over larger distances from the whole root surface, but not from root tips as in WT. (Fig. 2). More available C further from the root surface presumably enlarges the rhizosphere extent for β-glucosidase activity in *bx1,* but this was not demonstrated in our results. Instead, excluding benzoxazinoids from exudates resulted in a sharp gradient of β-glucosidase activity (2.4-fold) between the rhizosphere and bulk soil (Fig. 3). Moreover, the two-times larger area of non-rhizosphere β-glucosidase hotspots away from the root surface in *bx1* supports the indirect influence of the inhibitory effect of benzoxazinoids (Hu et al., 2018) or other secondary metabolites (Banerjee et al., 2018). Some β-glucosidase hotspots may belong to the rhizosphere of roots covered by soil particles and not visible on Fig. 1a-c, but detected by neutron images (Fig. 1j-l). Even if the influence on bulk soil remains speculative, the lower benzoxazinoids content

increases microbial functionality in the rhizosphere (Das and Varma, 2010; Igalavithana et al., 2017) and induces higher microbial activation. Thus, the 30% higher β-glucosidase activity in the rhizosphere along the root axis of *bx1* (Fig. 3) reflects the absence of the fungicidal effect of benzoxazinoids (Kudjordjie et al., 2019). In contrast, the presence of benzoxazinoids in exudates of WT probably reduces the production rate of β-glucosidase by microorganisms (Turner et al., 2002). These findings support our hypothesis (H3) that microbial activity in the rhizosphere is inhibited by the presence of benzoxazinoids in root exudates.

2.3.6 Conclusions

Coupling three *in situ* imaging approaches – ^{14}C imaging for root exudate localization, soil zymography for analysis of enzyme activity distribution, and neutron radiography for tracing water fluxes – yielded insights into the spatial structure of biochemical gradients and functioning in the rhizosphere. This is the first study to provide evidence of maize genotype-specific exudation strategies, including their implications for microbial functions. Beyond the previously confirmed preferable exudation via the root tip regions in wild-type maize, maize mutants with defective root hairs (*rth3)* and secondary metabolism (*bx1)* released considerable amounts of exudates including enzymes from the entire root. The co-localization analysis of zymograms, ^{14}C exudates, and neutron radiography images revealed an equal dependence of β-glucosidase activity on water and ^{14}C exudate availability in the rhizosphere. The greater role of water over ^{14}C exudate availability in the bulk soil underlines the pivotal role of water availability for the functioning of the soil microbiome and its hydrolytic activity.

We conclude that the shape and extent of the rhizosphere for β-glucosidase activity are genotype-specific and depend on the released rhizodeposits. This study shows that gene knock-out often substantially alters the process-network in the rhizosphere, including its spatial localization along and across the roots. Intensive exudation by root hairs and the resulting microbial activity increased the utilization of ^{14}C exudates up to two-fold. This, in turn, induced a broader rhizosphere extent for β-glucosidase activity.

Altered exudation of defensive compounds (i.e., reduced benzoxazinoids), along with a strong additional influence of abiotic factors such as water content, lead to a spatial reorganization of rhizomicrobial activities in mutants compared to wild-type maize. The release of benzoxazinoids by roots suppressed the activities of rhizosphere microorganisms, which led to 30% lower β-glucosidase activity on root surface and in the rhizosphere but did not change the rhizosphere extent. The absence of benzoxazinoids induced increased root exudation along the

whole root, but not at the root tip as in the wild type. The result was 2.5-fold larger ^{14}C exudate hotspot areas.

Overall, our findings confirm the contrasting exudation strategies of maize (Fig. 5) to ensure beneficial (i.e. producing β-glucosidase) microbial activity in the rhizosphere 1) to overcome energy and nutrient limitations due to the absence of root hairs, and 2) to compensate for the altered exudation composition and a shift from secondary to primary exudates in the profile.

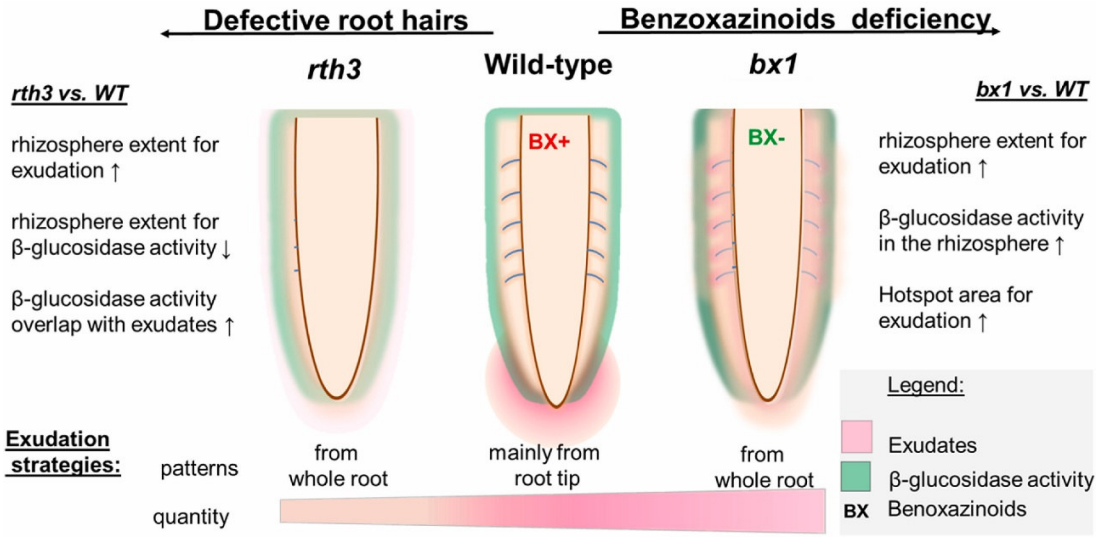

Figure 5. General pattern of the effects of maize mutations (root-hair defective *rth3* and benzoxazinoids (BX) deficient *bx1* as compared to wild-type (WT) on the rhizosphere extent, hotspots, enzyme activity gradient and overlap of β-glucosidase with exudates. Significant increase and decrease indicated by ↑ and ↓, respectively.

2.3.7 Declaration of competing interest

The authors declare that they have no known competing financial interests or personal relationships that could have appeared to influence the work reported in this paper.

2.3.8 Acknowledgments

We deeply grateful Doris Vetterlein for her valuable comments and helpful suggestions on the earlier draft of this manuscript. We gratefully acknowledge Jan Hovind from the ICON imaging station of the Paul Scherrer Institute (PSI), Villigen, Switzerland for their facilities and excellent technical support during the measurements with neutron radiography and providing us an imager

(FLA-7000), and facilities for zymography installations. We greatly acknowledge Mohsen Zarebanadkouki for providing us his code to calculate water contents in the neutron images. We acknowledge Caroline Marcon and Frank Hochholdinger (University of Bonn) for kindly providing seeds of maize mutant *rth3*. We sincerely acknowledge two anonymous reviewers for very valuable comments and suggestions, which improved the manuscript. This project was carried out in the framework of the priority programme 2089 “Rhizosphere spatiotemporal organization – a key to rhizosphere functions’ funded by the Deutsche Forschungsgemeinschaft (DFG, German Research Fundation) – Project numbers: 403670038 (BSR &SPP), 403670197 (MAA). The work was funded by the Interfaculty Research Cooperation (IRC) “One Health” at University of Bern, Sub-Project 4. We gratefully acknowledge the China Scholarship Council (CSC) for the financial support of Xuechen Zhang and Lichao Fan, and the Robert Bosch Foundation for supporting Michaela Dippold and this study via the Robert Bosch Junior Professorship 2017.

2.3.9 Appendix A. Supplementary data

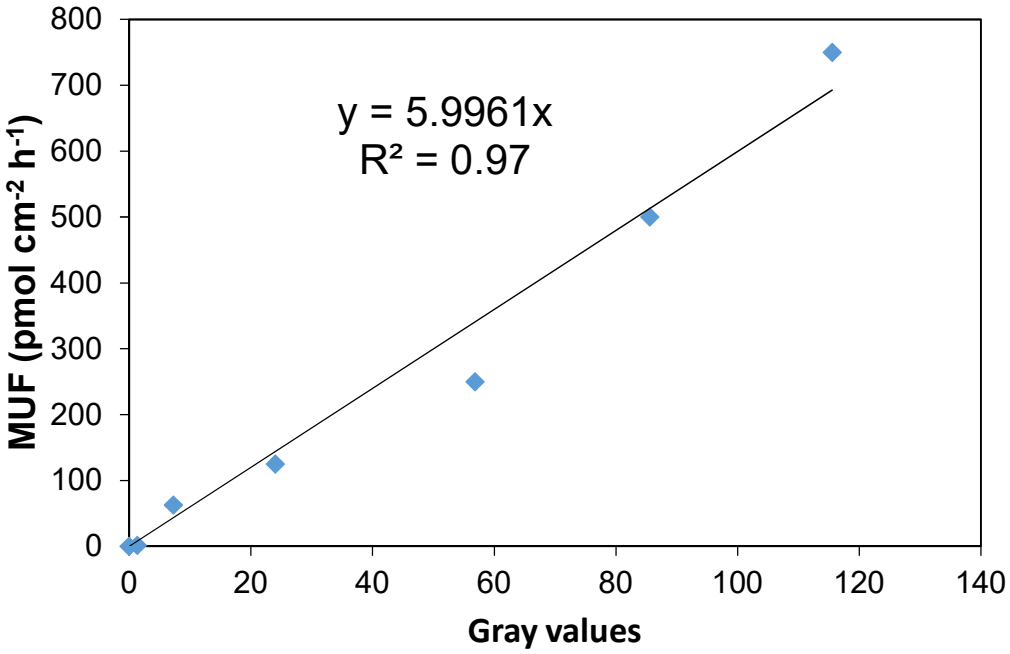

Figure S1. Linear correlation between the gray values of the calibration membranes incubated for one hour and methylumbelliferone (MUF) concentrations.

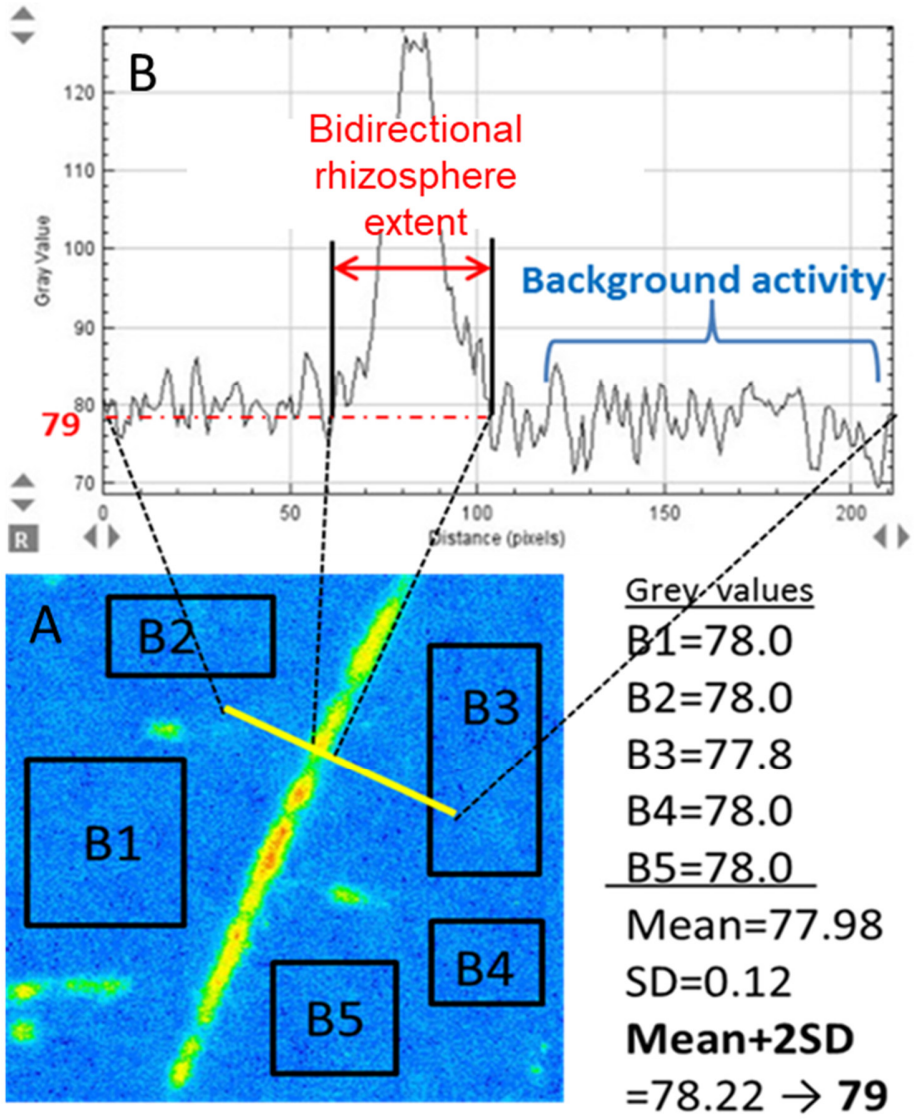

Figure S2. Sketch of rhizosphere thresholding methodology: a) an example of zymogram with five rectangles (B1-B5) which represent the areas of background β-glucosidase activity; b) gray values plotted against the distance.

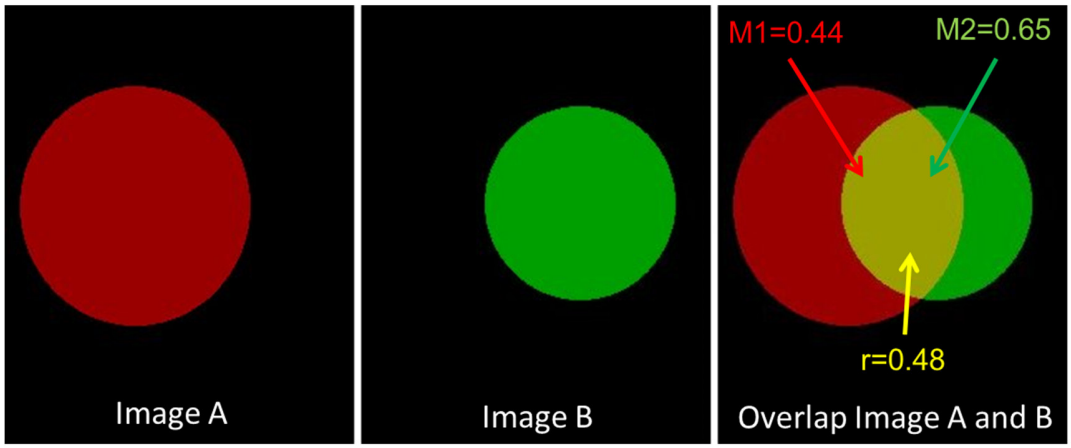

Figure S3. Schematic illustration of quantitative co-localization of activities/hotspots on two images A (Hotspot 1 – red) and B (Hotspot 2 – green) hotspots. Yellow part indicates 48% of overlap between two hotspot images (r=0.48); Manders coefficient 1 indicates that 44% of Hotspot 1 (yellow fraction of red hotspot) is considered as co-localized with Hotspot 2 (M1=0.44); Manders coefficient 2 indicates that 65 % of Hotspot 2 (yellow fraction of green hotspot) is considered as co-localized with Hotspot 1 (red hotspot) (M2=0.65).

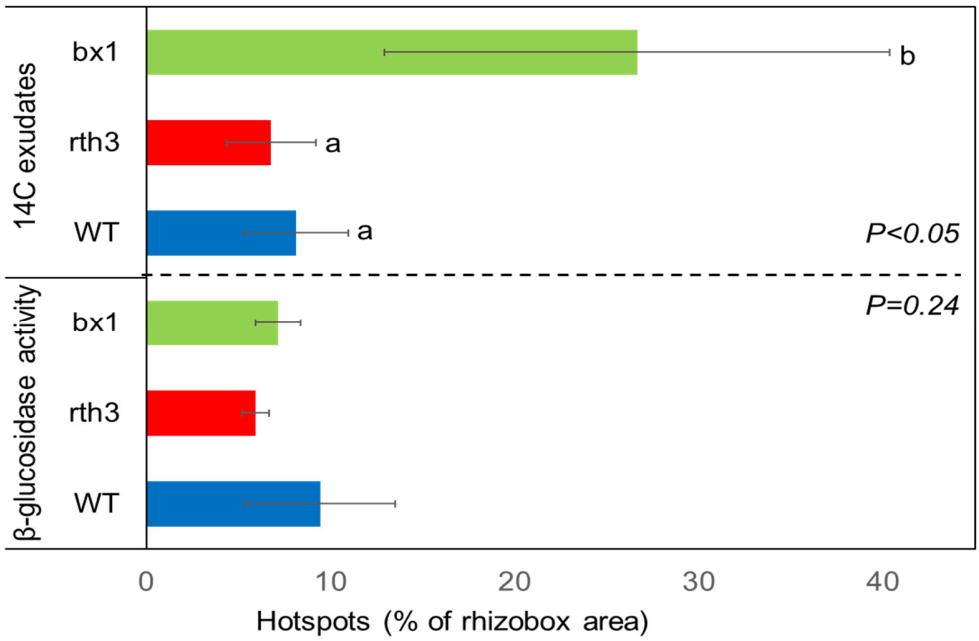

Figure S4. Hotspots for *β*-glucosidase activity and ^{14}C exudation. Data are means for each genotype (WT, *rth3* and *bx1*) (n=4), error bars indicate standard deviations. Letters within one hotspot type marks significant differences among the genotypes at $P<0.05$.

Table S1. Degrees of co-localization as fuzzy linguistic variables and the respective ranges of values of popular coefficients used to estimate co-localization, such as PC, r, and M1(M2), (Zinchuk *et al.*, 2013).

Degree of colocalization (Fuzzy linguistic variables)	Pearson coefficient (PC)	Overlap coefficient (r)	Manders coefficients M1or M2
Very weak	(-1) -(-0.27)	0-0.49	0-0.54
Weak	(-0.26) -0.09	0.50-0.70	0.55-0.77
Moderate	0.1-0.48	0.71-0.88	0.78-0.94
Strong	0.49-0.84	0.89-0.97	0.96-0.98
Very strong	0.85-1	0.98-1.0	0.99-1.0

Table S2. Result of co-localization analysis for the whole image of water content at neutron image (Water), ^{14}C exudates (Exudates) and *β*-glucosidase activity (Enzyme). The co-localization parameters are overlay coefficient (r), Mander's coefficient 1 (M1) and 2 (M2). Data are means for each genotype and parameter (n=4) ± standard deviations. Capital letters mark significant differences among the genotypes at *P<0.1.* Asterisks on the p-values indicate significant differences between root type ('(*)'*P<0.1;* '*' *P<0.05*; '**' *P<0.01;* '***' *P<0.001*).

Genotype	Co-localization coefficients											
	Water (1)*Exudates(2)				Water (1)*Enzyme(2)				Enzyme (1)*Exudates(2)			
	PC	r	M1	M2	PC	r	M1	M2	PC	r	M1	M2
WT	0.03AB	0.22A	0.24A	1.0	0.19B	0.89	0.99B	0.99	0.18	0.26A	0.26A	0.992
	±0.01	±0.06	±0.11	±0.001	±0.10	±0.09	±0.007	±0.001	±0.08	±0.04	±0.17	±0.009
rth3	0.07B	0.89B	0.99C	0.99	-0.02A	0.96	0.99B	0.99	0.14	0.85B	0.999B	0.995
	±0.06	±0.05	±0.001	±0.001	±0.01	±0.01	±0.009	±0.001	±0.007	±0.09	±0.001	±0.008
bx1	0.002A	0.26A	0.38B	0.99	0.23B	0.93	0.972A	0.99	0.24	0.31A	0.39A	0.977
	±0.006	±0.11	±0.14	±0.01	±0.01	±0.04	±0.031	±0.002	±0.04	±0.08	±0.12	±0.026
P value	*<0.01*	*<0.001*	*<0.001*	*0.41*	*<0.01*	*0.15*	*<0.001*	*0.19*	*0.14*	*<0.001*	*<0.001*	*0.30*

2.3.10 References

Abràmoff, M.D., Magalhães, P.J., Ram, S.J., 2004. Image processing with imageJ. Biophotonics International 11, 36–41. doi:10.1201/9781420005615.ax4

Ahmad, S., Veyrat, N., Gordon-Weeks, R., Zhang, Y., Martin, J., Smart, L., Glauser, G., Erb, M., Flors, V., Frey, M., Ton, J., 2011. Benzoxazinoid Metabolites Regulate Innate Immunity against Aphids and Fungi in Maize. Plant Physiology 157, 317–327. doi:10.1104/pp.111.180224

Ahmed, M.A., Sanaullah, M., Blagodatskaya, E., Mason-Jones, K., Jawad, H., Kuzyakov, Y., Dippold, M.A., 2018. Soil microorganisms exhibit enzymatic and priming response to root mucilage under drought. Soil Biology and Biochemistry 116, 410–418. doi:10.1016/j.soilbio.2017.10.041

Ahmed, M.A., Vetterlein, D., Carminati, A., 2021. Advances in understanding plant root water uptake. pp. 373–392. doi:10.19103/AS.2020.0075.17

Ahmed, M.A., Zarebanadkouki, M., Kaestner, A., Carminati, A., 2016. Measurements of water uptake of maize roots: the key function of lateral roots. Plant and Soil 398, 59–77. doi:10.1007/s11104-015-2639-6

Allison, S.D., 2006. Soil minerals and humic acids alter enzyme stability: implications for ecosystem processes. Biogeochemistry 81, 361–373. doi:10.1007/s10533-006-9046-2

Banerjee, S., Schlaeppi, K., van der Heijden, M., 2018. Keystone taxa as drivers of microbiome structure and functioning. Nature Reviews Microbiology 16, 567–576. doi:10.1038/s41579-018-0024-1

Banfield, C.C., Zarebanadkouki, M., Kopka, B., Kuzyakov, Y., 2017. Labelling plants in the Chernobyl way: A new 137Cs and 14C foliar application approach to investigate rhizodeposition and biopore reuse. Plant and Soil 417, 301–315. doi:10.1007/s11104-017-3260-7

Benard, P., Zarebanadkouki, M., Brax, M., Kaltenbach, R., Jerjen, I., Marone, F., Couradeau, E., Felde, V.J.M.N.L., Kaestner, A., Carminati, A., 2019a. Microhydrological Niches in Soils: How Mucilage and EPS Alter the Biophysical Properties of the Rhizosphere and Other Biological Hotspots. Vadose Zone Journal 18, 1–10. doi:10.2136/vzj2018.12.0211

Benard, P., Zarebanadkouki, M., Carminati, A., 2019b. Physics and hydraulics of the rhizosphere network. Journal of Plant Nutrition and Soil Science 182, 5–8. doi:10.1002/jpln.201800042

Benard, P., Zarebanadkouki, M., Hedwig, C., Holz, M., Ahmed, M.A., Carminati, A., 2018. Pore-Scale Distribution of Mucilage Affecting Water Repellency in the Rhizosphere. Vadose Zone Journal 17, 170013. doi:10.2136/vzj2017.01.0013

Berg, G., Smalla, K., 2009. Plant species and soil type cooperatively shape the structure and function of microbial communities in the rhizosphere. FEMS Microbiology Ecology 68, 1–13. doi:10.1111/j.1574-6941.2009.00654.x

Bertin, C., Yang, X., Weston, L.A., 2003. The role of root exudates and allelochemicals in the rhizosphere. Plant and Soil 256, 67–83. doi:10.1023/A:1026290508166

Bilyera, N., Kuzyakova, I., Guber, A., Razavi, B.S., Kuzyakov, Y., 2020. How “hot” are hotspots: Statistically localizing the high-activity areas on soil and rhizosphere images. Rhizosphere 16, 100259. doi:doi.org/10.1016/j.rhisph.2020.100259

Boeddinghaus, R.S., Nunan, N., Berner, D., Marhan, S., Kandeler, E., 2015. Do general spatial relationships for microbial biomass and soil enzyme activities exist in temperate grassland soils? Soil Biology and Biochemistry 88, 430–440. doi:10.1016/j.soilbio.2015.05.026

Bolte, S., Cordelières, F.P., 2006. A guided tour into subcellular colocalization analysis in light microscopy. Journal of Microscopy. doi:10.1111/j.1365-2818.2006.01706.x

Bucher, M., Hause, B., Krajinski, F., Küster, H., 2014. Through the doors of perception to function in arbuscular mycorrhizal symbioses. New Phytologist 204, 833–840. doi:10.1111/nph.12862

Cadot, S., Guan, H., Bigalke, M., Walser, J.C., Jander, G., Erb, M., van der Heijden, M., Schlaeppi, K., 2020. Specific and conserved patterns of microbiota-structuring by maize benzoxazinoids in the field. BioRxiv. doi:10.1101/2020.05.03.075135

Cai, G., Carminati, A., Abdalla, M., Ahmed, M.A., 2021. Soil textures rather than root hairs dominate water uptake and soil-plant hydraulics under drought. Plant Physiology. doi:10.1093/plphys/kiab271

Cairns, J.R.K., Esen, A., 2010. β-Glucosidases. Cellular and Molecular Life Sciences 67, 3389–3405. 10.1007/s00018-010-0399-2

Canarini, A., Kaiser, C., Merchant, A., Richter, A., Wanek, W., 2019. Root exudation of primary metabolites: Mechanisms and their roles in plant responses to environmental stimuli. Frontiers in Plant Science 10. doi:10.3389/fpls.2019.00157

Cardona, A., Saalfeld, S., Schindelin, J., Arganda-Carreras, I., Preibisch, S., Longair, M., Tomancak, P., Hartenstein, V., Douglas, R.J., 2012. TrakEM2 software for neural circuit reconstruction. PLoS ONE 7. doi:10.1371/journal.pone.0038011

Carminati, A., Moradi, A.B., Vetterlein, D., Vontobel, P., Lehmann, E., Weller, U., Vogel, H.J., Oswald, S.E., 2010. Dynamics of soil water content in the rhizosphere. Plant and Soil 332, 163–176. doi:10.1007/s11104-010-0283-8

Carminati, A., Vetterlein, D., 2013. Plasticity of rhizosphere hydraulic properties as a key for efficient utilization of scarce resources.

Annals of Botany 112, 277–290. doi:10.1093/aob/mcs262

Collins, S.L., Sinsabaugh, R.L., Crenshaw, C., Green, L., Porras-Alfaro, A., Stursova, M., Zeglin, L.H., 2008. Pulse dynamics and microbial processes in aridland ecosystems. Journal of Ecology 96, 413–420. doi:10.1111/j.1365-2745.2008.01362.x

Cotton, T.E.A., Pétriacq, P., Cameron, D.D., Meselmani, M. Al, Schwarzenbacher, R., Rolfe, S.A., Ton, J., 2019. Metabolic regulation of the maize rhizobiome by benzoxazinoids. The ISME Journal 13, 1647–1658. doi:10.1038/s41396-019-0375-2

Das, S.K., Varma, A., 2010. Soil enzymology. Soil Enzymology 22, 275–285. doi:10.1007/978-3-642-14225-3

Dick, R., Rattei, T., Haslbeck, M., Schwab, W., Gierl, A., Frey, M., 2012. Comparative analysis of benzoxazinoid biosynthesis in monocots and dicots: Independent recruitment of Stabilization and activation functions. Plant Cell 24, 915–928. doi:10.1105/tpc.112.096461

Downie, H.F., Adu, M.O., Schmidt, S., Otten, W., Dupuy, L.X., White, P.J., Valentine, T.A., 2015. Challenges and opportunities for quantifying roots and rhizosphere interactions through imaging and image analysis. Plant, Cell and Environment 38, 1213–1232. doi:10.1111/pce.12448

Erb, M., Kliebenstein, D.J., 2020. Plant Secondary Metabolites as Defenses, Regulators, and Primary Metabolites: The Blurred Functional Trichotomy. Plant Physiology 184, 39–52. doi:10.1104/pp.20.00433

Farrar, J., Hawes, M., Jones, D., Lindow, S., 2003. How roots control the flux of carbon to the rhizosphere. Ecology 84, 827–837. doi:10.1890/0012-9658(2003)084[0827:HRCTFO]2.0.CO;2

Flemming, H.C., Wingender, J., Szewzyk, U., Steinberg, P., Rice, S.A., Kjelleberg, S., 2016. Biofilms: An emergent form of bacterial life. Nature Reviews Microbiology 14, 563–575. doi:10.1038/nrmicro.2016.94

Frey, M., Chomet, P., Glawischnig, E., Stettner, C., Grün, S., Winklmair, A., Eisenreich, W., Bacher, A., Meeley, R.B., Briggs, S.P., Simcox, K., Gierl, A., 1997. Analysis of a chemical plant defense mechanism in grasses. Science 277, 696–699. doi:10.1126/science.277.5326.696

Gianfreda, L., 2015. Enzymes of importance to rhizosphere processes. Journal of Soil Science and Plant Nutrition 0–0. doi:10.4067/S0718-95162015005000022

Gilroy, S., Jones, D.L., 2000. Through form to function: root hair development and nutrient uptake. Trends in Plant Science 5, 56–60. doi:10.1016/S1360-1385(99)01551-4

Gómez-Anduro, G., Ceniceros-Ojeda, E.A., Casados-Vázquez, L.E., Bencivenni, C., Sierra-Beltrán, A., Murillo-Amador, B., Tiessen, A., 2011. Genome-wide analysis of the beta-glucosidase gene family in maize (Zea mays L. var B73). Plant Molecular Biology 77, 159–183. doi:10.1007/s11103-011-9800-2

Gramss, G., Voigt, K.-D., Kirsche, B., 1999. Oxidoreductase enzymes liberated by plant roots and their effects on soil humic material. Chemosphere 38, 1481–1494. doi:10.1016/S0045-6535(98)00369-5

Greenfield, L.M., Razavi, B.S., Bilyera, N., Zhang, X., Jones, D.L., 2021. Rhizosphere Root hairs and protein addition to soil promote leucine aminopeptidase activity of Hordeum vulgare L 18.

Guber, A., Kravchenko, A., Razavi, B.S., Uteau, D., Peth, S., Blagodatskaya, E., Kuzyakov, Y., 2018. Quantitative soil zymography: Mechanisms, processes of substrate and enzyme diffusion in porous media. Soil Biology and Biochemistry 127, 156–167. doi:10.1016/j.soilbio.2018.09.030

Guber, A.K., Kravchenko, A.N., Razavi, B.S., Blagodatskaya, E., Kuzyakov, Y., 2019. Calibration of 2-D soil zymography for correct analysis of enzyme distribution. European Journal of Soil Science 70, 715–726. doi:10.1111/ejss.12744

Haling, R.E., Brown, L.K., Bengough, A.G., Young, I.M., Hallett, P.D., White, P.J., George, T.S., 2013. Root hairs improve root penetration, root–soil contact, and phosphorus acquisition in soils of different strength. Journal of Experimental Botany 64, 3711–3721. doi:10.1093/jxb/ert200

Henry, H.A.L., 2012. Soil extracellular enzyme dynamics in a changing climate. Soil Biology and Biochemistry 47, 53–59. doi:10.1016/j.soilbio.2011.12.026

Hinsinger, P., Bengough, A.G., Vetterlein, D., Young, I.M., 2009. Rhizosphere: Biophysics, biogeochemistry and ecological relevance. Plant and Soil 321, 117–152. doi:10.1007/s11104-008-9885-9

Hinsinger, P., Gobran, G.R., Gregory, P.J., Wenzel, W.W., 2005. Rhizosphere geometry and heterogeneity arising from root-mediated physical and chemical processes. New Phytologist 168, 293–303. doi:10.1111/j.1469-8137.2005.01512.x

Hobley, E., Steffens, M., Bauke, S.L., Kögel-Knabner, I., 2018. Hotspots of soil organic carbon storage revealed by laboratory hyperspectral imaging. Scientific Reports 8, 13900. doi:10.1038/s41598-018-31776-w

Hochholdinger, F., Wen, T.-J., Zimmermann, R., Chimot-Marolle, P., da Costa e Silva, O., Bruce, W., Lamkey, K.R., Wienand, U., Schnable, P.S., 2008. The maize (Zea mays L.) roothairless3 gene encodes a putative GPI-anchored, monocot-specific, COBRA-like protein that significantly affects grain yield. The Plant Journal 54, 888–898. doi:10.1111/j.1365-313X.2008.03459.x

Hochholdinger, F., Yu, P., Marcon, C., 2018. Genetic Control of Root System Development in Maize. Trends in Plant Science 23, 79–88. doi:10.1016/j.tplants.2017.10.004

Holz, M., Zarebanadkouki, M., Carminati, A., Hovind, J., Kaestner, A., Spohn, M., 2019a. Increased water retention in the rhizosphere

allows for high phosphatase activity in drying soil. Plant and Soil 443, 259–271. doi:10.1007/s11104-019-04234-3

Holz, M., Zarebanadkouki, M., Carminati, A., Kuzyakov, Y., 2019b. Visualization and quantification of root exudation using 14C imaging: challenges and uncertainties. Plant and Soil 437, 473–485. doi:10.1007/s11104-019-03956-8

Holz, M., Zarebanadkouki, M., Kuzyakov, Y., Pausch, J., Carminati, A., 2018. Root hairs increase rhizosphere extension and carbon input to soil. Annals of Botany 121, 61–69. doi:10.1093/aob/mcx127

Hu, L., Robert, C.A.M., Cadot, S., Zhang, X., Ye, M., Li, B., Manzo, D., Chervet, N., Steinger, T., Van Der Heijden, M.G.A., Schlaeppi, K., Erb, M., 2018. Root exudate metabolites drive plant-soil feedbacks on growth and defense by shaping the rhizosphere microbiota. Nature Communications 9, 1–13. doi:10.1038/s41467-018-05122-7

Hummel, C., Boitt, G., Santner, J., Lehto, N.J., Condron, L., Wenzel, W.W., 2021. Co-occurring increased phosphatase activity and labile P depletion in the rhizosphere of Lupinus angustifolius assessed with a novel, combined 2D-imaging approach. Soil Biology and Biochemistry 153. doi:10.1016/j.soilbio.2020.107963

Huo, C., Luo, Y., Cheng, W., 2017. Rhizosphere priming effect: A meta-analysis. Soil Biology and Biochemistry 111, 78–84. doi:10.1016/j.soilbio.2017.04.003

Igalavithana, A.D., Lee, S.S., Niazi, N.K., Lee, Y.H., Kim, K.H., Park, J.H., Moon, D.H., Ok, Y.S., 2017. Assessment of soil health in urban agriculture: Soil enzymes and microbial properties. Sustainability (Switzerland) 9. doi:10.3390/su9020310

Jones, D.L., Nguyen, C., Finlay, R.D., 2009. Carbon flow in the rhizosphere: carbon trading at the soil–root interface. Plant and Soil 321, 5–33. doi:10.1007/s11104-009-9925-0

Jungk, A., 2001. Root hairs and the acquisition of plant nutrients from soil. Journal of Plant Nutrition and Soil Science 164, 121–129. doi:10.1002/1522-2624(200104)164:2<121::AID-JPLN121>3.0.CO;2-6

Kaestner, A.P., Hartmann, S., Kühne, G., Frei, G., Grünzweig, C., Josic, L., Schmid, F., Lehmann, E.H., 2011. The ICON beamline A facility for cold neutron imaging at SINQ. Nuclear Instruments and Methods in Physics Research, Section A: Accelerators, Spectrometers, Detectors and Associated Equipment 659, 387–393. doi:10.1016/j.nima.2011.08.022

Kaiser, C., Kilburn, M.R., Clode, P.L., Fuchslueger, L., Koranda, M., Cliff, J.B., Solaiman, Z.M., Murphy, D. V., 2015. Exploring the transfer of recent plant photosynthates to soil microbes: Mycorrhizal pathway vs direct root exudation. New Phytologist 205, 1537–1551. doi:10.1111/nph.13138

Kandeler, E., 1990. Characterization of free and adsorbed phosphatases in soils. Biology and Fertility of Soils 9, 199–202.

Kandeler, E., Marschner, P., Tscherko, D., Singh Gahoonia, T., Nielsen, N.E., 2002. Microbial community composition and functional diversity in the rhizosphere of maize. Plant and Soil 238, 301–312. doi:10.1023/A:1014479220689

Koranda, M., Schnecker, J., Kaiser, C., Fuchslueger, L., Kitzler, B., Stange, C.F., Sessitsch, A., Zechmeister-Boltenstern, S., Richter, A., 2011. Microbial processes and community composition in the rhizosphere of European beech – The influence of plant C exudates. Soil Biology and Biochemistry 43, 551–558. doi:10.1016/j.soilbio.2010.11.022

Kreuzeder, A., Santner, J., Scharsching, V., Oburger, E., Hoefer, C., Hann, S., Wenzel, W.W., 2018. In situ observation of localized, sub-mm scale changes of phosphorus biogeochemistry in the rhizosphere. Plant and Soil 424, 573–589. doi:10.1007/s11104-017-3542-0

Kudjordjie, E.N., Sapkota, R., Steffensen, S.K., Fomsgaard, I.S., Nicolaisen, M., 2019. Maize synthesized benzoxazinoids affect the host associated microbiome. Microbiome 7, 1–17. doi:10.1186/s40168-019-0677-7

Kuzyakov, Y., Shevtzova, E., Pustovoytov, K., 2006. Carbonate re-crystallization in soil revealed by 14C labeling: Experiment, model and significance for paleo-environmental reconstructions. Geoderma 131, 45–58. doi:10.1016/j.geoderma.2005.03.002

Lagos, M.L., Maruyama, F., Nannipieri, P., Mora, M.L., Ogram, A., Jorquera, M.A., 2015. Current overview on the study of bacteria in the rhizosphere by modern molecular techniques: A mini-review. Journal of Soil Science and Plant Nutrition 15, 504–523. doi:10.4067/s0718-95162015005000042

Liu, Y., Shahbaz, M., Ge, T., Zhu, Z., Liu, S., Chen, L., Wu, X., Deng, Y., Lu, S., Wu, J., 2020. European Journal of Soil Biology Effects of root exudate stoichiometry on CO 2 emission from paddy soil. European Journal of Soil Biology 101, 103247. doi:10.1016/j.ejsobi.2020.103247

Ma, X., Liu, Y., Zarebanadkouki, M., Razavi, B.S., Blagodatskaya, E., Kuzyakov, Y., 2018a. Spatiotemporal patterns of enzyme activities in the rhizosphere: effects of plant growth and root morphology. Biology and Fertility of Soils 54, 819–828. doi:10.1007/s00374-018-1305-6

Ma, X., Zarebanadkouki, M., Kuzyakov, Y., Blagodatskaya, E., Pausch, J., Razavi, B.S., 2018b. Spatial patterns of enzyme activities in the rhizosphere: Effects of root hairs and root radius. Soil Biology and Biochemistry 118, 69–78. doi:10.1016/j.soilbio.2017.12.009

Maag, D., Köhler, A., Robert, C.A.M., Frey, M., Wolfender, J.L., Turlings, T.C.J., Glauser, G., Erb, M., 2016. Highly localized and persistent induction of Bx1-dependent herbivore resistance factors in maize. Plant Journal 88, 976–991. doi:10.1111/tpj.13308

Macías, F.A., Oliveros-Bastidas, A., Marín, D., Castellano, D., Simonet, A.M., Molinillo, J.M.G., 2005. Degradation studies on benzoxazinoids. Soil degradation dynamics of (2R)-2-O-β-D-glucopyranosyl-4-hydroxy-(2H)-1,4-benzoxazin-3(4H)-one (DIBOA-Glc) and its degradation products, phytotoxic allelochemicals from gramineae. Journal of Agricultural and Food Chemistry 53, 554–561. doi:10.1021/jf048702l

Manders, E.M.M., Verbeek, F. J., Aten, J.A., 1993. Measurement of co-localization of objects in dual-colour confocal images. Journal of Microscopy 169, 375–382. doi:10.1111/j.1365-2818.1993.tb03313.x

Masciandaro, G., Ceccanti, B., Benedicto, S., Lee, H.C., Cook, H.F., 2004. Enzyme activity and C and N pools in soil following application of mulches. Canadian Journal of Soil Science 84, 19–30. doi:10.4141/S03-045

McCully, M.E., Canny, M.J., 1985. Localisation of translocated 14C in roots and root exudates of field-grown maize. Physiologia Plantarum 65, 380–392. doi:10.1111/j.1399-3054.1985.tb08661.x

McDougall, B.M., Rovira, A.D., 1970. Sites of exudation of 14C-labelled compounds from wheat roots. New Phytologist 69, 999–1003.

Mercado-blanco, J., Prieto, P., 2012. Bacterial endophytes and root hairs. Plant and Soil 301–306. doi:10.1007/s11104-012-1212-9

Moradi, A.B., Conesa, H.M., Robinson, B., Lehmann, E., Kuehne, G., Kaestner, A., Oswald, S., Schulin, R., 2009. Neutron radiography as a tool for revealing root development in soil: capabilities and limitations. Plant and Soil 318, 243–255. doi:10.1007/s11104-008-9834-7

Neal, A.L., Ahmad, S., Gordon-Weeks, R., Ton, J., 2012. Benzoxazinoids in root exudates of maize attract pseudomonas putida to the rhizosphere. PLoS ONE 7. doi:10.1371/journal.pone.0035498

Okamoto, K., Nakano, H., Yatake, T., Kiso, T., Kitahata, S., 2000. Purification and Some Properties of a β-Glucosidase from Flavobacterium johnsonae. Bioscience, Biotechnology, and Biochemistry 64, 333–340. doi:10.1271/bbb.64.333

Paterson, E., Osler, G., Dawson, L.A., Gebbing, T., Sim, A., Ord, B., 2008. Labile and recalcitrant plant fractions are utilised by distinct microbial communities in soil : Independent of the presence of roots and mycorrhizal fungi. Soil Biology and Biochemistry 40, 1103–1113. doi:10.1016/j.soilbio.2007.12.003

Pausch, J., Kuzyakov, Y., 2011. Photoassimilate allocation and dynamics of hotspots in roots visualized by 14C phosphor imaging. Journal of Plant Nutrition and Soil Science 174, 12–19. doi:10.1002/jpln.200900271

Peterson, R.L., Farquhar, M.L., 1996. Root hairs: Specialized tubular cells extending root surfaces. The Botanical Review 62, 1–40. doi:10.1007/BF02868919

Pett-Ridge, J., Shi, S., Estera-Molina, K., Nuccio, E., Yuan, M., Rijkers, R., Swenson, T., Zhalnina, K., Northen, T., Zhou, J., Firestone, M.K., 2021. Rhizosphere Carbon Turnover from Cradle to Grave: The Role of Microbe–Plant Interactions. pp. 51–73. doi:10.1007/978-981-15-6125-2_2

Philippot, L., Raaijmakers, J.M., Lemanceau, P., van der Putten, W.H., 2013. Going back to the roots: the microbial ecology of the rhizosphere. Nature Reviews Microbiology 11, 789–799. doi:10.1038/nrmicro3109

Pott, D.M., Osorio, S., Vallarino, J.G., 2019. From Central to Specialized Metabolism: An Overview of Some Secondary Compounds Derived From the Primary Metabolism for Their Role in Conferring Nutritional and Organoleptic Characteristics to Fruit. Frontiers in Plant Science 10. doi:10.3389/fpls.2019.00835

R Development Core Team, R., 2011. R: A Language and Environment for Statistical Computing. R Foundation for Statistical Computing, R Foundation for Statistical Computing. doi:10.1007/978-3-540-74686-7

Raghothama, K.G., Karthikeyan, A.S., 2005. Phosphate Acquisition. Plant and Soil 274, 37–49. doi:10.1007/s11104-004-2005-6

Razavi, B.S., Zarebanadkouki, M., Blagodatskaya, E., Kuzyakov, Y., 2016. Rhizosphere shape of lentil and maize: Spatial distribution of enzyme activities. Soil Biology and Biochemistry 79, 229–237. doi:10.1016/j.soilbio.2016.02.020

Razavi, B.S., Zhang, X., Bilyera, N., Guber, A., Zarebanadkouki, M., 2019. Soil zymography: Simple and reliable? Review of current knowledge and optimization of the method. Rhizosphere. doi:10.1016/j.rhisph.2019.100161

Rice, C.P., Cai, G., Teasdale, J.R., 2012. Concentrations and allelopathic effects of benzoxazinoid compounds in soil treated with rye (secale cereale) cover crop. Journal of Agricultural and Food Chemistry 60, 4471–4479. doi:10.1021/jf300431r

Rovira, A.D., 1973. Zones of exudation along plant roots and spatial distribution of micro-organisms in the rhizosphere. Pesticide Science 4, 361–366. doi:10.1002/ps.2780040313

Saalfeld, S., Fetter, R., Cardona, A., Tomancak, P., 2012. Elastic volume reconstruction from series of ultra-thin microscopy sections. Nature Methods 9, 717–720. doi:10.1038/nmeth.2072

Sanaullah, M., Razavi, B.S., Blagodatskaya, E., Kuzyakov, Y., 2016. Spatial distribution and catalytic mechanisms of β-glucosidase activity at the root-soil interface. Biology and Fertility of Soils 52, 505–514. doi:10.1007/s00374-016-1094-8

Sardans, J., Peñuelas, J., 2005. Drought decreases soil enzyme activity in a Mediterranean Quercus ilex L. forest. Soil Biology and Biochemistry 37, 455–461. doi:10.1016/j.soilbio.2004.08.004

Schütz, V., Bigler, L., Girel, S., Laschke, L., Sicker, D., Schulz, M., 2019. Conversions of Benzoxazinoids and Downstream Metabolites by Soil Microorganisms. Frontiers in Ecology and Evolution 7. doi:10.3389/fevo.2019.00238

Segal, E., Kushnir, T., Mualem, Y., Shani, U., 2008. Water Uptake and Hydraulics of the Root Hair Rhizosphere. Vadose Zone Journal 7, 1027–1034. doi:10.2136/vzj2007.0122

Silberbush, M., Barber, S.A., 1983. Sensitivity of simulated phosphorus uptake to parameters used by a mechanistic-mathematical model. Plant and Soil 74, 93–100. doi:10.1007/BF02178744

Sinsabaugh, R.L., Antibus, R.K., Linkins, A.E., McClaugherty, C.A., Rayburn, L., Repert, D., Weiland, T., 1992. Wood decomposition over a first-order watershed: Mass loss as a function of lignocellulase activity. Soil Biology and Biochemistry 24, 743–749. doi:10.1016/0038-0717(92)90248-V

Smith, S.E., Dickson, S., Smith, F.A., 2001. Nutrient transfer in arbuscular mycorrhizas: how are fungal and plant processes integrated? Functional Plant Biology 28, 685. doi:10.1071/PP01033

Sørensen, A., Lübeck, M., Lübeck, P.S., Ahring, B.K., 2013. Fungal beta-glucosidases: A bottleneck in industrial use of lignocellulosic materials. Biomolecules 3, 612–631. doi:10.3390/biom3030612

Spohn, M., Carminati, A., Kuzyakov, Y., 2013. Soil zymography - A novel in situ method for mapping distribution of enzyme activity in soil. Soil Biology and Biochemistry 58, 275–280. doi:10.1016/j.soilbio.2012.12.004

Spohn, M., Kuzyakov, Y., 2013. Distribution of microbial- and root-derived phosphatase activities in the rhizosphere depending on P availability and C allocation - Coupling soil zymography with 14C imaging. Soil Biology and Biochemistry 67, 106–113. doi:10.1016/j.soilbio.2013.08.015

Tachibana, Y., Ohta, Y., 1983. Root surface area, as a parameter in relation to water and nutrient uptake by cucumber plant. Soil Science and Plant Nutrition 29, 387–392. doi:10.1080/00380768.1983.10434642

Thu Hoang, D.T., Maranguit, D., Kuzyakov, Y., Razavi, B.S., 2020. Accelerated microbial activity, turnover and efficiency in the drilosphere is depth dependent. Soil Biology and Biochemistry 147, 107852. doi:10.1016/j.soilbio.2020.107852

Turner, B.L., Hopkins, D.W., Haygarth, P.M., Ostle, N., 2002. B-Glucosidase Activity in Pasture Soils. Applied Soil Ecology 20, 157–162. doi:10.1016/S0929-1393(02)00020-3

Vedere, C., Harlote, Vieubl, L., Girardin, C., Chenu, C., 2020. Spatial and temporal evolution of detritusphere hotspots at different soil moistures. Soil Biology and Biochemistry 150, 107975. doi:10.1016/j.soilbio.2020.107975

Veres, Z., Kotroczó, Z., Fekete, I., Tóth, J.A., Lajtha, K., Townsend, K., Tóthmérész, B., 2015. Soil extracellular enzyme activities are sensitive indicators of detrital inputs and carbon availability. Applied Soil Ecology 92, 18–23. doi:10.1016/j.apsoil.2015.03.006

Vetterlein, D., Carminati, A., Kögel-Knabner, I., Bienert, G.P., Smalla, K., Oburger, E., Schnepf, A., Banitz, T., Tarkka, M.T., Schlüter, S., 2020. Rhizosphere spatiotemporal organisation - a key to rhizosphere functions. Frontiers in Agronomy 2, 8. doi:10.3389/FAGRO.2020.00008

Vetterlein, D., Lippold, E., Schreiter, S., Phalempin, M., Fahrenkampf, T., Hochholdinger, F., Marcon, C., Tarkka, M., Oburger, E., Ahmed, M., Javaux, M., Schlüter, S., 2021. Experimental platforms for the investigation of spatiotemporal patterns in the rhizosphere—Laboratory and field scale. Journal of Plant Nutrition and Soil Science 184, 35–50. doi:10.1002/jpln.202000079

Vives-Peris, V., de Ollas, C., Gómez-Cadenas, A., Pérez-Clemente, R.M., 2020. Root exudates: from plant to rhizosphere and beyond. Plant Cell Reports 39, 3–17. doi:10.1007/s00299-019-02447-5

Voothuluru, P., Braun, D.M., Boyer, J.S., 2018. An in vivo imaging assay detects spatial variability in glucose release from plant roots. Plant Physiology 178, 1002–1010. doi:10.1104/pp.18.00614

Wang, X.C., Lu, Q., 2006. Beta-glucosidase activity in paddy soils of the Taihu Lake region, China. Pedosphere 16, 118–124.

Waring, B.G., 2013. Exploring relationships between enzyme activities and leaf litter decomposition in a wet tropical forest. Soil Biology and Biochemistry 64, 89–95. doi:10.1016/j.soilbio.2013.04.010

Watt, M., Fiorani, F., Usadel, B., Rascher, U., Muller, O., Schurr, U., 2020. Phenotyping: New Windows into the Plant for Breeders. Annual Review of Plant Biology 71, 689–712. doi:10.1146/annurev-arplant-042916-041124

Wen, T.-J., Schnable, P.S., 1994. Analyses of Mutants of Three Genes that Influence Root Hair Development in Zea mays (Gramineae) Suggest that Root Hairs are Dispensable. American Journal of Botany 81, 833. doi:10.2307/2445764

Williams, A., Vries, F.T., 2020. Plant root exudation under drought: implications for ecosystem functioning. New Phytologist 225, 1899–1905. doi:10.1111/nph.16223

Yang, Y., Wang, N., Guo, X., Zhang, Y., Ye, B., 2017. Comparative analysis of bacterial community structure in the rhizosphere of maize by highthroughput pyrosequencing. PLoS ONE 12, 1–11. doi:10.1371/journal.pone.0178425

Yu, P., Baldauf, J.A., Lithio, A., Marcon, C., Nettleton, D., Li, C., Hochholdinger, F., 2016. Root Type-Specific Reprogramming of Maize Pericycle Transcriptomes by Local High Nitrate Results in Disparate Lateral Root Branching Patterns. Plant Physiology 170, 1783–1798. doi:10.1104/pp.15.01885

Zarebanadkouki, M., Kim, Y.X., Moradi, A.B., Vogel, H.-J., Kaestner, A., Carminati, A., 2012. Quantification and Modeling of Local Root Water Uptake Using Neutron Radiography and Deuterated Water. Vadose Zone Journal 11, vzj2011.0196. doi:10.2136/vzj2011.0196

Zhang, X., Kuzyakov, Y., Zang, H., Dippold, M.A., Shi, L., Spielvogel, S., Razavi, B.S., 2020. Rhizosphere hotspots: Root hairs and warming control microbial efficiency, carbon utilization and energy production. Soil Biology and Biochemistry 107872. doi:10.1016/j.soilbio.2020.107872

Zinchuk, V., Wu, Y., Grossenbacher-Zinchuk, O., 2013. Bridging the gap between qualitative and quantitative colocalization results in fluorescence microscopy studies. Scientific Reports 3, 1–5.

2.4 Study 4. Root hairs and protein addition to soil promote leucine aminopeptidase activity of *Hordeum vulgare L.*

Lucy M. Greenfield[a], Bahar S. Razavi[b], Nataliya Bilyera[b,c], Xuechen Zhang[b], & Davey L. Jones[a,c]*

[a]School of Environment, Natural Resources & Geography, Bangor University, Gwynedd, LL57 2UW, UK
[b]Department of Soil and Plant Microbiome, Christian-Albrechts-University of Kiel, Kiel, Germany
[c] Department od Soil Science, Christian-Albrechts-University of Kiel, Kiel, Germany
[d]School of Agriculture and Environment, University of Western Australia, Crawley, WA 6009, Australia

*Corresponding author: Lucy M. Greenfield, E-mail:lucygreenfield8@gmail.com

Status: *Published in Rhizosphere, 2021, Vol. 18, 100329, doi:10.1016/j.rhisph.2021.100329*

2.4.1 Abstract

Protein typically represents the largest input of organic nitrogen (N) into soil. Proteases subsequently make this protein available for use by both plants and microorganisms, however, the factors that regulate protein breakdown in the rhizosphere remain limited. Root exudation of carbon (C) and N into soil promotes microbial growth and thus enzyme production, which is further enhanced by root morphological traits such as root hairs. However, it is not clear how inputs of protein from external sources (e.g. necromass) affect enzyme activity in the rhizosphere. Insight into the interaction between protein addition and root morphology will enhance our knowledge of plant and microbial strategies for promoting N acquisition. Using soil zymography, we investigated the spatial distribution of leucine aminopeptidase activity in the rhizosphere of *Hordeum vulgare* L. (barley) with and without root hairs subject to localised protein addition. Seedlings of barley were grown for two weeks in rhizoboxes and soluble protein was applied 48 h before analysis of leucine aminopeptidase activity. *In situ* zymography was used to quantitatively

visualise leucine aminopeptidase activity while *ex situ* sampling was used to determine its enzyme kinetics. In the zymograms, we found that mean and maximal leucine aminopeptidase activity was highest in the barley genotype with root hairs and in the presence of soil protein hotspots. This suggests that microorganisms and plant roots in the rhizosphere of genotypes with root hairs have a greater advantage in accessing protein hotspots in the soil. Leucine aminopeptidase activity did not follow the same trends when analysed by *in situ* zymography and *ex situ* sampling methods. Therefore, we recommend the use of *in situ* zymography to detect the spatial distribution of enzymatic hotspots and rhizosphere extent followed by *ex situ* sampling for assessing enzyme kinetics in the hotspot areas detected by *in situ* sampling. However, sampling biases must be considered to ensure enzyme activities are being interpreted as the true rhizosphere.

Key words: Nitrogen mineralisation; Enzyme activity; Soil zymography; Soil organic matter

2.4.2 Introduction

Protein is an important source of carbon (C) and nitrogen (N) for soil microorganisms and N is a key macronutrient for plant growth. Furthermore, protein is estimated to contribute ca. 40% of total soil N and 9–16% of soil organic C (Schulten and Schnitzer, 1997; Stevenson and Cole, 1999). However, soil protein is generally considered a stable fraction of soil organic matter (SOM) due to its ability to form many bonds and complexes with components in the soil matrix e.g. polyphenols and clay mineral surfaces (Rillig et al., 2007). Yet, many soil systems have regular inputs of protein available for degradation and use by microorganisms. These include: plant litter, root biomass and decaying micro- and macrofauna as well as functional proteins released into the soil by plants and microorganisms to carry out specific functions (Rillig et al., 2007). Based on estimates of below-ground turnover in cropping systems, we estimate that the annual input of protein into soil from roots alone is 0.4–0.8 t ha^{-1} y^{-1} (Steingrobe et al., 2001). Considering the age of most agricultural soils and amount of protein held in SOM, this indicates that only a small amount of protein enters the stable SOM pool each year. Extracellular protease enzymes produced by microorganisms and plant roots break down proteins into oligopeptides and amino acids. However, whether plant root-derived proteases have any functional significance in N nutrition remains unclear (Greenfield et al., 2020a).

Microbial activity is typically greater in the rhizosphere (relative to the bulk soil) due to the high rates of root C and N exudation of a variety of compounds (e.g. carbohydrates, amino acids, enzymes, proteins and phenols) (Jones et al., 2009; Koo et al., 2005). Studies have found C and N exudation to enhance enzyme activities in the rhizosphere (Brzostek et al., 2013; Kandeler et al., 1994). Furthermore, protein mineralisation and protease activity have been found to be regulated by supply of substrate rather than limitations in protein turnover (Greenfield et al., 2020b). Thus, the influx of soluble protein into the soil system is likely to stimulate protease activity in the rhizosphere. The rate of protein mineralisation is faster in soil-plant systems compared to bulk soil and particularly in the rhizosphere (Jan et al., 2009; Loeppmann et al., 2016). Due to the short turnover time of proteinaceous N, estimated to range from hours to days (Greenfield et al., 2020b; Hill et al., 2012; Jan et al., 2009), an excess of easily available C and N is likely to be depleted by the microbial community within a few days (Kuzyakov and Xu, 2013). However, few studies have investigated the spatial responses to external protein addition on enzyme activity in the rhizosphere (e.g. necromass hotspots) that can create 'hot moments' (Hill et al., 2019; Kuzyakov and Blagodatskaya, 2015).

Root morphology plays a major role in determining the quality, quantity and distribution of exudates on the surface of the root. One key root morphological trait which is known to increase C substrate availability for microorganisms is the presence of root hairs (Holz et al., 2018; Jones et al., 2009). They are also responsible for the majority of N uptake in roots (Waisel et al., 2002). Root hairs increase the rhizosphere extent of rhizosphere enzyme activity by increasing the surface area and volume of soil exploited by the root (Holz et al., 2020; Ma et al., 2018). Interestingly, it has been found that hairless genotypes compensate for the reduced surface area and volume by increasing enzyme activity close to the root surface in response to phosphorous (P) limitation (Holz et al., 2020). However, plants with root hairs are likely to be able to access N from larger soil volumes due to the larger rhizosphere extent and the greater diffusion rates of N relative to P. Understanding the interaction between protein addition and root morphology will further extend our knowledge of plant and microbial strategies for N acquisition.

The aim of this study was to determine the spatial distribution of leucine aminopeptidase activity in the rhizosphere of *Hordeum vulgare* L. with and without root hairs subject to localised protein addition. We applied soil zymography, a two-dimensional imaging technique, to visualise the spatial distribution of leucine aminopeptidase activity in the rhizosphere and measured leucine aminopeptidase kinetics in destructive soil samples to link *in situ* and *ex situ* techniques for assessing rhizosphere enzyme activity. We hypothesised that 1) protein addition would increase leucine aminopeptidase activity in the rhizosphere due to an increase in substrate availability, 2)

root hairs would accelerate leucine aminopeptidase activity in the rhizosphere by providing a higher surface area and more root exudates, and 3) root hairs would increase the rhizosphere extent of leucine aminopeptidase activity due to the larger surface area of the root.

2.4.3 Materials & methods

2.4.3.1 Soil and plant preparation

The soil was collected from the top 20 cm of a grassland (*Lolium perenne* L.) sandy clay loam, classified as a Eutric Cambisol, located in Abergwyngregyn, Wales (53°13′ N, 4°00’ W). Prior to the experiment, the soil was 2 mm sieved to remove stones and plant residues. General soil properties are presented in Table 1. Soil pH (H_2O) and electrical conductivity (EC) were measured in a 1:5 (w/v) soil:distilled water suspension. Total organic C and total N were determined using a Leco CHN 2000 analyzer (Leco Corp., St Joseph, MI, USA). Dissolved organic C (DOC) and total dissolved N (TDN) were measured using 1:5 (w/v) soil: 0.5 M K_2SO_4 extracts on a Multi-N/C Series NPOC-TN analyser (Analytik Jena, Germany). Dissolved organic nitrogen (DON) was calculated as the difference between TDN and dissolved inorganic N. Ammonium (NH_4^+) and nitrate (NO_3^-) concentrations were both determined colorimetrically according to the salicylic acid procedure of Mulvaney (1996) and VCl_3 procedure of Miranda et al. (2001), respectively. Plant-available P was measured using the 0.5 M acetic acid of Vaz et al. (1994). Rhizoboxes with inner dimensions of 12.5 × 12.5 × 2.5 cm were filled with soil to a final density of 1.2 g cm^{-3}.

Table 1. General properties of the soil used in the experiments. Values are expressed on a dry weight basis and represent mean ± SE (*n = 3*).

Soil property	Units	Value
pH(H_2O)		6.50 ± 0.11
EC	(µS cm^{-1})	34.4 ± 3.54
Organic matter	(g kg^{-1})	55.6 ± 1.50
DOC	(mg kg^{-1})	41.0 ± 5.21
DON	(mg kg^{-1})	7.28 ± 2.41
NH_4^+	(mg kg^{-1})	7.98 ± 4.14
NO_3^-	(mg kg^{-1})	1.98 ± 0.60
Available P	(mg kg^{-1})	3.54 ± 1.67

Two genotypes of barley (*Hordeum vulgare* L.), the wild type and a hairless mutant, were germinated on moist filter paper for 72 h. More detailed information on the two genotypes of barley and microscope images of the roots can be found in Brown et al. (2012). One seedling was

planted at a depth of 5 mm into each rhizobox with 3 biological replications in separate boxes. The rhizoboxes were kept in a climate-controlled chamber at 20 ± 1 °C, 55% relative humidity and 12 h photoperiod with a photosynthetically active radiation intensity of 500 µmol photons m^{-2} s^{-1}. During the growth period, the rhizoboxes were kept inclined at an angle of 45° so that the roots grew along the lower wall of the rhizobox. The rhizoboxes were irrigated with distilled water to maintain a water content at 60% of the water holding capacity (i.e. 60% field capacity). No additional nutrients were added to the soils.

To determine the effect of protein hotspots on the plant-soil interface, bovine serum albumin (BSA) was added to soil in 0.5 cm tall protein horizontal bands (Fig. 1). BSA was chosen as it is a soluble protein and was used by Paungfoo-Lonhienne et al. (2008). Briefly, 100 µl of 6 mg ml^{-1} BSA was added to each 0.5 × 0.5 cm area along a protein band. We found 100 µl to effectively cover a 0.5 cm × 0.5 cm area of the soil surface. The concentration of protein was used to ensure saturation of the soil with protein and was found to be the optimum protein concentration for plant growth by Paungfoo-Lonhienne et al. (2008). Three control bands were also added by pipetting 100 µl of sterile, distilled water into 0.5 × 0.5 cm regions along the band. Rhizoboxes were then incubated for 48 h, to allow sufficient time for microorganisms to respond to the protein addition, under the same conditions as growth before imaging.

Figure 1. Rhizobox set-up showing the position of the protein and control (sterile water) horizontal bands in soil.

2.4.3.2 Soil zymography

After two weeks of growth and 48 h after soluble protein addition, direct zymography was applied to visualise the activity of leucine aminopeptidase (E.C. 3.4.11.1). Leucine aminopeptidase was used as a proxy to measure protease activity. It catalyses the cleavage of N-terminus amino acids from peptide and protein substrates and is involved in fundamental plant rhizosphere processes and plant development e.g. degradation of storage protein (Kania and Gillner, 2015). Thin polyamide membrane filters (Tao Yuan, China) with a size of 10 × 10 cm and a pore size of 0.45 mm were saturated with 10 mM L-leucine-7-amino-4-methyl-coumarin hydrochloride (dissolved in 0.05 M Trizma buffer, pH 7). We chose pH 7 because the pH optimum of leucine aminopeptidase is ca. 7 (Puissant et al., 2019). The rhizoboxes were opened on the lower, rooted side and the saturated membranes were placed directly on to the root-soil surface. After 1 h incubation, the membranes were carefully removed from the rhizobox and any attached soil particles gently removed using a small soft brush. The membranes were placed under ultraviolet (UV) light in a dark room. The distance between the camera (EOS M50, Canon), the sample, and the UV light were fixed, and a photograph of the membrane taken. The camera settings were f/5.6, ISO 800, 40 mm zoom and exposure 1/40 s.

Images were calibrated by saturating 4 cm^2 membranes in 60 µl 7-amino-4-methyl-coumarin hydrochloride (AMC) with the following concentrations: 0, 0.05, 0.1, 0.2, 0.5, 1, 2, 3, 4, 5, 10 mM. The amount of AMC on an area basis was calculated from the volume of solution taken up by the membrane and its size (Spohn and Kuzyakov, 2014). The membranes used for calibration were imaged under UV light in the same way as described for the rhizoboxes. A calibration curve was fitted using a power function equation y=axb, by plotting concentrations (pmol mm^{-2}) versus grey values obtained in Matlab (MATLAB, The MathWorks) using a script published in Razavi et al. (2019).

2.4.3.3 Image processing and analysis

Images were processed and analysed in ImageJ 1.x (Schindelin et al., 2012). Images were transformed to 32-bit grayscale images as matrices and corrected for light variations and camera noise (Razavi et al., 2016). The grey value blank from the 0 mM AMC standard was used as a referencing signal and subtracted from the zymograms. Then a power function (y=axb) of the calibration was used to relate the grey values to leucine aminopeptidase activity.

Root area was measured as the area of root per rhizobox surface using a triangle thresholding algorithm in ImageJ (Tajima and Kato, 2011). Leucine aminopeptidase hotspots

were thresholded with mean + 2 standard deviations approach (Bilyera et al., 2020). An individual thresholding value for each replicate image was used.

Rhizosphere extent was measured as the distance of a region with at least 30% higher enzyme activity than the bulk soil from the point the enzyme activity started increasing to the point it ceased to increase using a threshold by a default algorithm in ImageJ (Tajima and Kato, 2011). Ten locations (lines across the root) in each band were selected and measurements taken. The diameter of the root was measured at the same locations as rhizosphere extent from root masks thresholded by a triangle algorithm in ImageJ (Tajima and Kato, 2011). Root diameter was then subtracted from the rhizosphere distance and divided by two to obtain the rhizosphere extent from the root surface (mm). Leucine aminopeptidase activity in the bulk soil was defined in the region with the absence of elevated activities. The mean and maximum leucine aminopeptidase activity across the rhizosphere extent was measured.

2.4.3.4 Enzyme kinetics

Rhizosphere enzyme kinetics were measured according to Marx et al. (2001) with some modifications. After two weeks of growth, soil was collected from the rhizosphere of each of the three protein and control bands and combined to make a composite sample for each treatment (protein or control) to give 0.2 g soil for each biological replicate (n = 3). Rhizosphere soil was collected carefully with a needle to avoid mixing with bulk soil from as close to the root surface as possible. A soil slurry was created by adding 20 ml of sterile deionised water to the soil. The soil slurry was homogenised by shaking at 250 rev min^{-1} for 30 min 50 µl of soil suspension, 100 µl a range of substrate concentrations from low to high (0, 5, 10, 20, 40, 80, 100, 200 µM) and 50 µl of Trizma buffer (pH 7) was added to a 96-well microplate. Fluorescence was measured in microplates at an excitation wavelength of 355 nm and an emission wavelength of 460 nm, and a slit width of 20 nm, with a Cary Eclipse Fluorescence Spectrophotometer (Agilent Corp., Santa Clara, CA). Enzyme activities were measured 30 min, 1 h and 2 h after adding soil solution, buffer and substrate solution. Microplates were incubated at 20 °C between measurements. The difference between activities at 2 h and 1 h was used to determine AMC release in nmol per g dry soil per hour (nmol g^{-1} dry $soil^{-1}$). The leucine aminopeptidase assays were performed in three analytical replicates. The Michaelis-Menten constant K_m and V_{max} were determined using the Michaelis-Menten equation:

$$v = \frac{Vmax[S]}{Km+[S]} \quad (1)$$

where V is the reaction rate (as a function of substrate concentration), [S] is the substrate concentration, K_m is the substrate concentration at half-maximal rate and V_{max} is the maximum reaction rate.

2.4.3.5 Statistical analysis

All statistical analyses were performed in R 3.5.0 (R Core Team, 2018). Treatments were performed in triplicate (n = 3). Normality of the data was determined by Shapiro-Wilk test ($p > 0.05$) then visually checked using *qqnorm* plots. Data without a normal distribution was square root transformed to achieve normality. Homogeneity of variance of the data was visually determined using residuals vs. fitted plots. Two-way ANOVAs followed by the Duncan Test ($p < 0.05$) were used to determine if there was a significant difference between root morphology and protein addition.

2.4.4 Results

Examples of leucine aminopeptidase zymograms clearly demonstrated the spatiotemporal distribution of enzyme activity in the rhizosphere of the two genotypes of barley (+/− root hairs) (Fig. 2). Faint protein bands can be seen on the zymogram of the barley genotype without root hairs, but no bands are visible on the zymogram with root hairs. Root density was similar for the two barley genotypes (Table 2). Leucine aminopeptidase hotspots were twice the area for barley with root hairs although this was not significantly different (Table 2).

Table 2. Root area and leucine aminopeptidase hotspot of the two barley genotypes per plant. Values represent mean ± S.E (n = 3). Different lowercase letters indicate a significant difference between genotypes ($p < 0.05$).

	+ root hairs	**- root hairs**
Root area (cm^2 $plant^{-1}$)	2.58 ± 0.28[a]	2.66 ± 0.44[a]
Leucine aminopeptidase hotspot (cm^2 $plant^{-1}$)	3.79 ± 1.36[a]	1.88 ± 0.33[a]

The rhizosphere extent of leucine aminopeptidase was significantly greater when soluble protein was added, but did not differ between barley root genotypes with or without root hairs except for the control band (Table 3; Fig. 3). Mean and maximum leucine aminopeptidase activity was 1.5 times higher in the protein-rich areas with root hairs compared to the control (Table 3, Fig. 3). Comparing the barley genotypes, mean and maximal leucine aminopeptidase activity was highest (by over three times) in the protein band of the barley genotype with root hairs (Table

3, Fig. 3). The interaction between root hair and protein treatments was significant for rhizosphere extent only (Table 3).

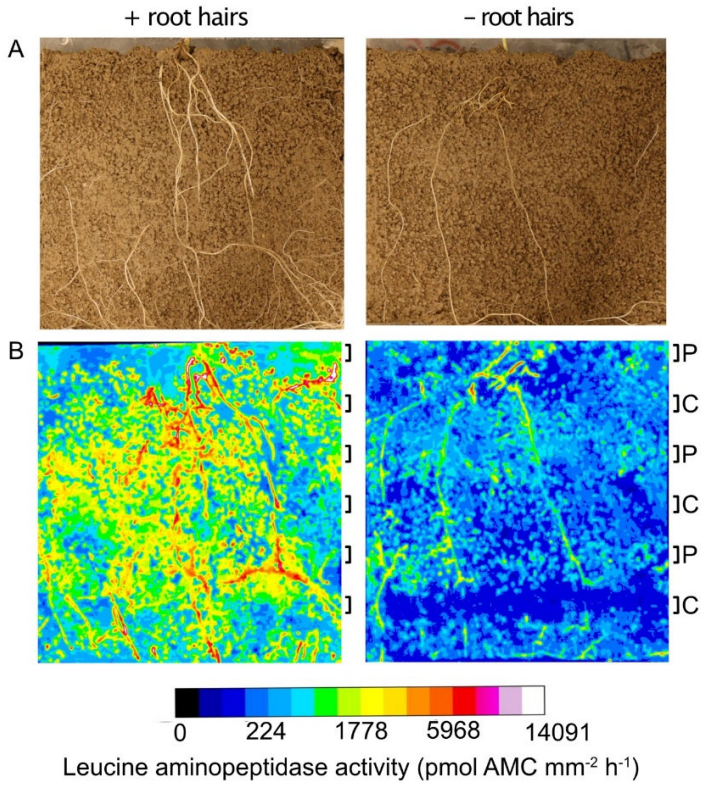

Figure. 2. Examples of barley roots grown in rhizoboxes (A) and the spatial distribution of leucine aminopeptidase activity in the soil and rhizosphere of barley roots (B) with and without root hairs. Side colour bar is proportional to the enzyme activity (pmol mm^{-2} h^{-1}) and protein (P) and control (C) band positions are indicated on the right-hand side of the zymograms.

Table 3. Two-way ANOVA results for each of the measured variables using $p < 0.05$ as the cut-off for statistical significance (as indicated by values in bold).

Variable	**Residuals**	**Root hairs**			**Protein**			**Root hairs x protein**		
		df	*F*	*p*	*df*	*F*	*p*	*df*	*F*	*p*
Rhizosphere extent	356	1	14.7	**<0.001**	1	47.0	**<0.001**	1	5.0	**0.03**
Mean LAP activity	356	1	419	**<0.001**	1	41.5	**<0.001**	1	3.38	0.07
Max LAP activity	356	1	370	**<0.001**	1	45.9	**<0.001**	1	0.73	0.39
V_{max}	8	1	1.26	0.29	1	0.05	0.83	1	0.004	0.95
K_m	8	1	0.50	0.50	1	1.41	0.27	1	3.24	0.11

Note: LAP = leucine aminopeptidase activity, *df* = degrees of freedom, *F* = *F* value and *p* = *p* value.

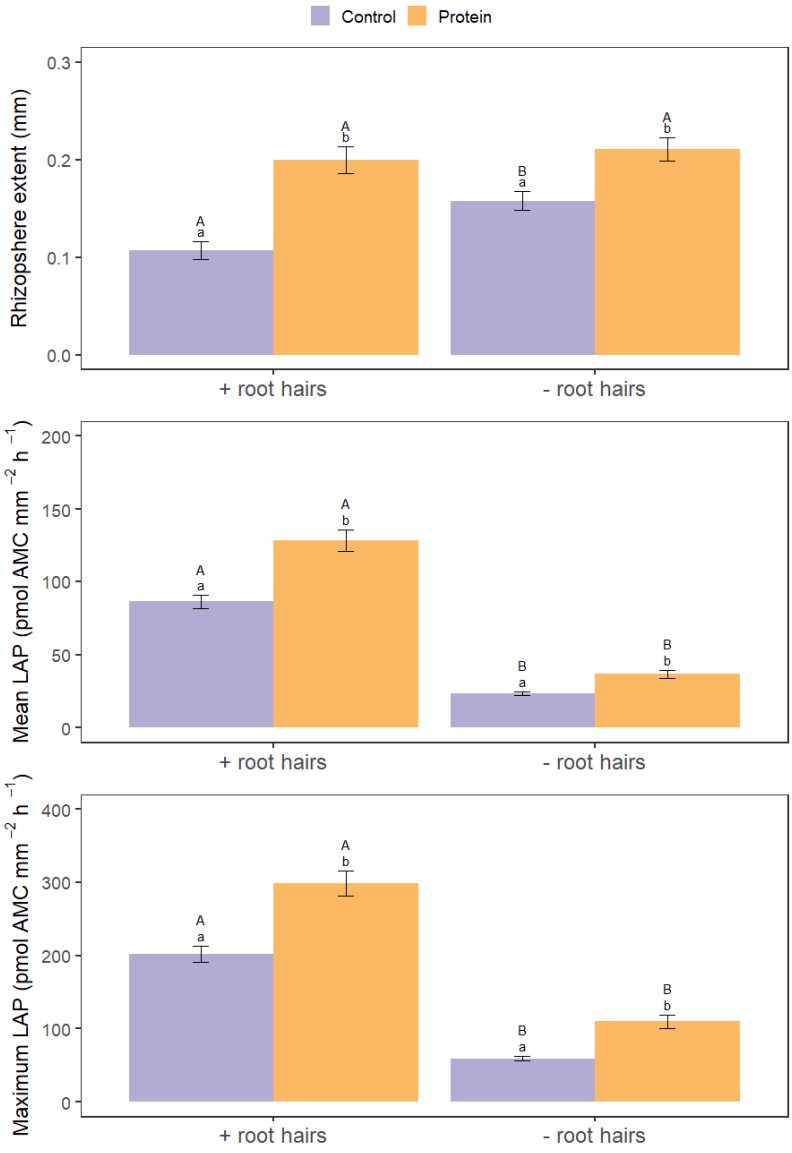

Figure 3. Rhizosphere extent of leucine aminopeptidase activity (distance from the root surface, mm), mean leucine aminopeptidase activity (LAP) across the rhizosphere and maximum leucine aminopeptidase activity of the rhizosphere (pmol AMC mm^{-2} h^{-1}) for barley genotypes with and without roots hairs and with protein or control (sterile water) addition. Values represent mean ± SE (n = 90). Different lowercase letters indicate a significant difference between protein and control treatments and different uppercase letters indicate a significant difference between root hair genotype ($p < 0.05$).

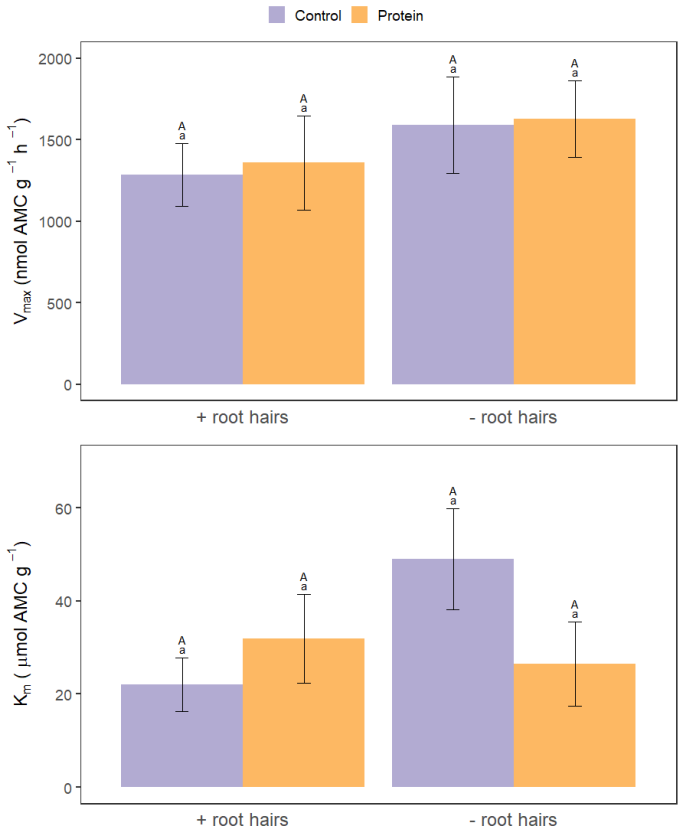

Figure 4. The kinetic parameters V_{max} (nmol AMC g^{-1} h^{-1}) and K_m (µmol AMC g^{-1}) of soil leucine aminopeptidase activity for barley genotypes with and without roots hairs and with protein or control (sterile water) addition. Values represent mean ± SE (n = 3). Different lowercase letters indicate a significant difference between protein and control treatments and different uppercase letters indicate a significant difference between root hair genotype (p < 0.05).

Enzyme kinetics (V_{max} and K_m) showed no significant differences between roots with and without root hairs and protein addition (Table 3; Fig. 4). V_{max} was slightly higher in the barley genotype without root hairs whilst K_m was highest in the control treatment of the barley genotype without root hairs.

2.4.5 Discussion

2.4.5.1 In situ *versus* ex situ *sampling*

Rhizosphere leucine aminopeptidase activity did not follow the same trends when analysed by *in situ* zymography and *ex situ* destructive sampling. This suggests these two methods are not measuring the same part of the rhizosphere or are causing unreliable results

due to the sampling method. The rhizosphere extent of leucine aminopeptidase activity we measured in our experiment by zymography extended <0.2 mm beyond the root surface.

Yet, our *ex situ* destructive sampling method involved collecting soil from distances up to 2 mm from the root surface. Our ability to constrain the sampling to smaller distances from the root surface proved impossible due to (a) logistical difficulties in recovering rhizosphere soil, (b) aggregation of the soil, and (c) the requirement for enough soil to perform the enzymatic assays. This shows that our *ex situ* measurements of leucine aminopeptidase activity included soil from around ten times further away from the root surface than the rhizosphere of the barley plants extended. However, it should be noted that 20% of the enzyme reactions that occur in the volume of the rhizosphere are in direct contact with the zymograph membrane and, thus, 80% of rhizosphere enzyme activity is not measured by *in situ* zymography (Guber et al., 2018). Oburger and Jones (2018) reviewed sampling techniques used to measure root exudation from the rhizosphere and concluded that current techniques have myriad of problems that cause biases when determining exudation dynamics.

These problems include: a) damage to roots and fungal hyphae, b) the sampling area is more likely related to bulk soil than the true rhizosphere area because not all soil adhered to the root surface (Neumann et al., 2009), and c) the removal of plant C inputs may induce changes in microbial metabolism (i.e. less metabolically active) and the types of organisms which remain active (Oburger and Jones, 2009). However, destructive sampling provides a quantitative measure of the rhizosphere effect per unit of soil mass. These measurements can then be linked to process rates (e.g. C and N mineralisation) per unit of soil mass. Therefore, we recommend *in situ* spatial sampling techniques for a more representative measurement of the spatial distribution of rhizosphere enzyme activity combined with *ex situ* assays to determine enzyme kinetics. Together these will provide an insight into the catalytic mechanism of the enzyme. However, caution is needed when interpreting rhizosphere enzyme activity from *ex situ* destructive sampling as it may greatly underestimate enzyme activity at the root surface.

2.4.5.2 Effect of root hairs and protein addition on rhizosphere leucine aminopeptidase activity

As we hypothesized, mean and maximum rhizosphere leucine aminopeptidase activity were highest for the barley genotype with root hairs. This was further demonstrated by a larger area of leucine aminopeptidase hotspots in the barley genotype with root hairs. It is likely that root hairs increase the availability of substrates in the rhizosphere through their high surface area per

unit root length and thus greater rates of passive C exudation (i.e. which in turn increases microbial enzyme activity) (Holz et al., 2018; Jones et al., 2009). Thus, it appears that the increase in leucine aminopeptidase activity due to root hairs induces greater rhizosphere priming thereby enhancing the release of N from soil organic matter required to fuel microbial growth (Brzostek et al., 2013; Dijkstra et al., 2013; Zhu et al., 2014). The rhizosphere extent of leucine aminopeptidase activity in the rhizosphere was largest when soluble protein was applied, and this enhancement was seen for both barley genotypes irrespective of the presence of root hairs. We hypothesized that root hairs would increase the area of high leucine aminopeptidase activity in the rhizosphere compared to roots without hairs via an increased surface area of the root for microbial colonisation (Gilroy and Jones, 2000; Haling et al., 2013). Similarly, an increased rhizosphere extent was observed when measuring phosphatase activity of barley with and without root hairs (Holz et al., 2020) as well as plants with differing length hairs (Ma et al., 2018). As the root areas were similar for both barley genotypes it is unlikely that root density affected specific root response to protein addition. A possible reason for the similar rhizosphere extents of leucine aminopeptidase activity could be a result of soluble protein addition having a more dominant effect on rhizosphere extent than the presence of root hairs. In addition, root hairs had a greater effect on the enzyme activity per root surface area rather than overall rhizosphere extent. Degradation of high-concentrations of organic compounds and substrates is energetically favourable for microbial decomposers (German et al., 2011). Thus, our evidence suggests that the available soluble protein promoted expression of proteases and enlarged the extent of rhizosphere independent of root morphology. Overall, the influence of the root on protease activity seems to be limited to a narrow zone <0.2 mm from the root surface. This is an efficient strategy for plants to compete with microorganisms in the rhizosphere for N (Kuzyakov and Xu, 2013). Enzyme activities are less reported than many other rhizosphere properties (e.g. pH) which extend much further from the root surface. This could be due to slow diffusion of proteases relative to other solutes (e.g. H^+) and that they are primarily produced by the most active microorganisms in the rhizosphere which are likely to be located on the rhizoplane.

As expected, soluble protein addition increased leucine aminopeptidase activity in the rhizosphere of the barley. Many studies have shown organic fertiliser to increase soil protease activity due to the removal of substrate limitation (Liu et al., 2019; Ma et al., 2020; Marinari et al., 2000; Melero et al., 2006; Niemi et al., 2008). Fewer studies have assessed protein amendments specifically, but those that have, have also found protein addition to increase protease activity (e.g. Geisseler and Horwath, 2009). The increase in protease activity has been shown to be faster and larger when amended with soluble protein e.g. casein compared to insoluble protein e.g.

gluten and zein (Geisseler and Horwath, 2009). This is probably due to the greater ability of soluble proteins to diffuse through soil solution and thus come into contact with free exoenzymes and membrane-bound proteases. Protein addition also resulted in the largest rhizosphere extent in both the barley genotypes irrespective of the presence of root hairs by <50%. Our finding is supported by a study on the effect of root exudate compounds on artificial rhizosphere extent which found that alanine substantially increase the rhizosphere extent compared to water (Zhang et al., 2019).

Leucine aminopeptidase activity was higher in the rhizosphere with root hairs and protein addition compared to the other treatment combinations. This suggests that microorganisms and plant roots in the rhizosphere of barley genotype with root hairs have a greater advantage in utilising protein hotspots in the soil. The ability to obtain more N is particularly important in agricultural soils where crops tend to be more N limited (Rütting et al., 2018). It is important to note that this study was carried out with a low number of biological replicates ($n = 3$), one plant species, one soil type, one protease type and one time point. Therefore, further studies are needed in order to determine the effect of protein addition and root morphology on rhizosphere protease activity in different species, soil types and growth stages of plants.

2.4.6 Conclusions

We found the combination of root hairs and protein addition to produce the highest leucine aminopeptidase activity in the rhizosphere creating an advantage for plants with root hairs to access protein hotspots in soil. The ability to obtain more N from organic sources is particularly important in agricultural soils where crops tend to be more N limited and rely on inorganic N fertilizers. In addition, our results have shown clear evidence on the disparity between *in situ* and *ex situ* rhizosphere sampling methods for leucine aminopeptidase activity. Therefore, we recommend the combined use of *in situ* and *ex situ* sampling techniques when assessing rhizosphere enzyme activity, but consideration must be taken to determine biases in both sampling techniques.

2.4.7 Declaration of competing interest

The authors declare that they have no known competing financial interests or personal relationships that could have appeared to influence the work reported in this paper.

2.4.8 Acknowledgements

We would like to thank Tim George and Lawrie Brown at the James Hutton Institute for supplying the wild type and mutant barley seeds. Thanks to John Langley for the soil property data. Thanks to Jonathan Roberts and Sarah Chesworth for their technical support. This work was supported by the UK Biotechnology and Biological Sciences Research Council and the Natural Environment Research Council [Grant number NE/M009106/1], by a Soils Training and Research Studentships (STARS) grant to LMG. STARS is a consortium consisting of Bangor University, British Geological Survey, UK Centre for Ecology and Hydrology, Cranfield University, James Hutton Institute, Lancaster University, Rothamsted Research and the University of Nottingham.

2.4.9 References

Bilyera, N., Kuzyakova, I., Guber, A., Razavi, B.S., Kuzyakov, Y., 2020. How “hot” are hotspots: Statistically localizing the high-activity areas on soil and rhizosphere images. Rhizosphere 16, 100259.

Brown, L.K., George, T.S., Thompson, J.A., Wright, G., Lyon, J., Dupuy, L., Hubbard, S.F., White, P.J., 2012. What are the implications of variation in root hair length on tolerance to phosphorus deficiency in combination with water stress in barley (Hordeum vulgare)? Ann. Bot. 110, 319–328.

Brzostek, E.R., Greco, A., Drake, J.E., Finzi, A.C., 2013. Root carbon inputs to the rhizosphere stimulate extracellular enzyme activity and increase nitrogen availability in temperate forest soils. Biogeochemistry 115, 65–76.

Dijkstra, F.A., Carrillo, Y., Pendall, E., Morgan, J.A., 2013. Rhizosphere priming: a nutrient perspective. Front. Microbiol. 4, 216.

Geisseler, D., Horwath, W.R., 2009. Relationship between carbon and nitrogen availability and extracellular enzyme activities in soil. Pedobiologia. 53, 87–98.

German, D.P., Chacon, S.S., Allison, S.D. 2011 Substrate concentration and enzyme allocation can affect rates of microbial decomposition. Ecology, 92 (2011), 1471-1480.

Gilroy, S., Jones, D.L., 2000. Through form to function: Root hair development and nutrient uptake. Trends Plant Sci. 5, 56–60.

Greenfield, L.M., Hill, P.W., Paterson, E., Baggs, E.M., Jones, D.L., 2020a. Do plants use root-derived proteases to promote the uptake of soil organic nitrogen? Plant Soil.

Greenfield, L.M., Hill, P.W., Seaton, F.M., Paterson, E., Baggs, E.M., Jones, D.L., 2020b. Is soluble protein mineralisation and protease activity in soil regulated by supply or demand? 150, 108007.

Guber, A., Kravchenko, A., Razavi, B.S., Uteau, D., Peth, S., Blagodatskaya, E., Kuzyakov, Y., 2018. Quantitative soil zymography: Mechanisms, processes of substrate and enzyme diffusion in porous media. Soil Biol. Biochem. 127, 156–167.

Haling, R.E., Brown, L.K., Bengough, A.G., Young, I.M., Hallett, P.D., White, P.J., George, T.S., 2013. Root hairs improve root penetration, root-soil contact, and phosphorus acquisition in soils of different strength. J. Exp. Bot. 64, 3711–3721.

Hill, E.J., Jones, D.L., Paterson, E., Hill, P.W., 2019. Hotspots and hot moments of amino acid N in soil: Real-time insights using continuous microdialysis sampling. Soil Biol. Biochem. 131, 40–43.

Hill, P.W., Farrell, M., Jones, D.L., 2012. Bigger may be better in soil N cycling: Does rapid acquisition of small l-peptides by soil microbes dominate fluxes of protein-derived N in soil? Soil Biol. Biochem. 48, 106–112.

Holz, M., Zarebanadkouki, M., Carminati, A., Becker, J.N., Spohn, M., 2020. The effect of root hairs on rhizosphere phosphatase activity. J. Plant Nutr. Soil Sci. 183, 382–388.

Holz, M., Zarebanadkouki, M., Kuzyakov, Y., Pausch, J., Carminati, A., 2018. Root hairs increase rhizosphere extension and carbon input to soil. Ann. Bot. 121, 61–69.

Jan, M.T., Roberts, P., Tonheim, S.K., Jones, D.L., 2009. Protein breakdown represents a major bottleneck in nitrogen cycling in grassland soils. Soil Biol. Biochem. 41, 2272–2282.

Jones, D.L., Nguyen, C., Finlay, R.D., 2009. Carbon flow in the rhizosphere: Carbon trading at the soil-root interface. Plant Soil 321,

5–33.

Kandeler, E., Eder, G., Sobotik, M., 1994. Microbial biomass, N mineralization, and the activities of various enzymes in relation to nitrate leaching and root distribution in a slurry-amended grassland. Biol. Fertil. Soils 18, 7–12.

Kania, J., Gillner, D., 2015. Aminopeptidases isolated from plants of great economic value - role and characteristics. Chemik 69, 466–468.

Koo, B.-. J., Adriano, D.C., Bolan, N.S., Barton, C.D., 2005. Root exudates and microorganisms, in: Encyclopedia of Soils in the Environment. Elsevier, pp. 421–428.

Kuzyakov, Y., Blagodatskaya, E., 2015. Microbial hotspots and hot moments in soil: Concept & review 83, 184–199.

Kuzyakov, Y., Xu, X., 2013. Competition between roots and microorganisms for nitrogen: mechanisms and ecological relevance. New Phytol. 198, 656–669.

Liu, Y., Hou, H., Ji, J., Lv, Z., Liu, X., Liu, G., Li, Z., 2019. Long-term fertiliser (organic and inorganic) input effects on soil microbiological characteristics in hydromorphic paddy soils in China. Soil Res. 57, 459.

Loeppmann, S., Semenov, M., Blagodatskaya, E., Kuzyakov, Y., 2016. Substrate quality affects microbial- and enzyme activities in rooted soil. J. Plant Nutr. Soil Sci. 179, 39–47.

Ma, Q., Wen, Y., Wang, D., Sun, X., Hill, P.W., Macdonald, A., Chadwick, D.R., Wu, L., Jones, D.L., 2020. Farmyard manure applications stimulate soil carbon and nitrogen cycling by boosting microbial biomass rather than changing its community composition. Soil Biol. Biochem. 144, 107760.

Ma, X., Zarebanadkouki, M., Kuzyakov, Y., Blagodatskaya, E., Pausch, J., Razavi, B.S., 2018. Spatial patterns of enzyme activities in the rhizosphere: Effects of root hairs and root radius. Soil Biol. Biochem. 118, 69–78.

Marinari, S., Masciandaro, G., Ceccanti, B., Grego, S., 2000. Influence of organic and mineral fertilisers on soil biological and physical properties. Bioresour. Technol. 72, 9–17.

Marx, M.-C., Wood, M., Jarvis, S.., 2001. A microplate fluorimetric assay for the study of enzyme diversity in soils. Soil Biol. Biochem. 33, 1633–1640.

Melero, S., Porras, J.C.R., Herencia, J.F., Madejon, E., 2006. Chemical and biochemical properties in a silty loam soil under conventional and organic management. Soil Tillage Res. 90, 162–170.

Miranda, K.M., Espey, M.G., Wink, D.A., 2001. A Rapid, Simple Spectrophotometric Method for Simultaneous Detection of Nitrate and Nitrite. Biol. Chem. 5, 62–71.

Mulvaney, R.L., 1996. Nitrogen - Inorganic Forms, in: Methods of Soil Analysis. Part 3 - Chemical Methods. Soil Science Society of America, Madison, WI, USA, pp. 1123–1200.

Neumann, G., George, T.S., Plassard, C., 2009. Strategies and methods for studying the rhizosphere-the plant science toolbox. Plant Soil 321, 431–456.

Niemi, R., Vepsäläinen, M., Wallenius, K., Erkomaa, K., Kukkonen, S., Palojärvi, A., Vestberg, M., 2008. Conventional versus organic cropping and peat amendment: Impacts on soil microbiota and their activities. Eur. J. Soil Biol. 44, 419–428.

Oburger, E., Jones, D.L., 2018. Sampling root exudates – Mission impossible? Rhizosphere 6, 116–133.

Oburger, E., Jones, D.L., 2009. Substrate mineralization studies in the laboratory show different microbial C partitioning dynamics than in the field. Soil Biol. Biochem. 41, 1951–1956.

Paungfoo-Lonhienne, C., Lonhienne, T.G.A., Rentsch, D., Robinson, N., Christie, M., Webb, R.I., Gamage, H.K., Carroll, B.J., Schenk, M., Schmidt, S., 2008. Plants can use protein as a nitrogen source without assistance from other organisms. PNAS 105, 4524–4529.

Puissant, J., Jones, B., Goodall, T., Mang, D., Blaud, A., Gweon, H.S., Malik, A., Jones, D.L., Clark, I.M., Hirsch, P.R., Griffiths, R., 2019. The pH optimum of soil exoenzymes adapt to long term changes in soil pH. Soil Biol. Biochem. 138, 1076012.

R Core Team, 2018. R: A language and environment for statistical computing.

Razavi, B.S., Zarebanadkouki, M., Blagodatskaya, E., Kuzyakov, Y., 2016. Rhizosphere shape of lentil and maize: Spatial distribution of enzyme activities. Soil Biol. Biochem. 96, 229–237.

Razavi, B.S., Zhang, X., Bilyera, N., Guber, A., Zarebanadkouki, M., 2019. Soil zymography: Simple and reliable? Review of current knowledge and optimization of the method. Rhizosphere 11, 100161.

Rillig, M.C., Caldwell, B.A., Wösten, H.A.B.B., Sollins, P., 2007. Role of proteins in soil carbon and nitrogen storage: Controls on persistence. Biogeochemistry 85, 25–44.

Rütting, T., Aronsson, H., Delin, S., 2018. Efficient use of nitrogen in agriculture. Nutr. Cycl. Agroecosystems 110, 1–5.

Schindelin, J., Arganda-Carreras, I., Frise, E., Kaynig, V., Longair, M., Pietzsch, T., Preibisch, S., Rueden, C., Saalfeld, S., Schmid, B., Tinevez, J.Y., White, D.J., Hartenstein, V., Eliceiri, K., Tomancak, P., Cardona, A., 2012. Fiji: An open-source platform for biological-image analysis. Nat. Methods 9, 676–682.

Schulten, H.-R., Schnitzer, M., 1997. The chemistry of soil organic nitrogen: a review. Biol. Fertil. Soils 26, 1–15.

Spohn, M., Kuzyakov, Y., 2014. Spatial and temporal dynamics of hotspots of enzyme activity in soil as affected by living and dead roots—a soil zymography analysis. Plant Soil, 379, 67-77

Steingrobe, B., Schmid, H., Gutser, R., Claassen, N., 2001. Root production and root mortality of winter wheat grown on sandy and loamy soils in different farming systems. Biol. Fertil. Soils 33, 331–339.

Stevenson, F.J., Cole, M.A., 1999. The Carbon Cycle, in: Stevenson, F.J., Cole, M.A. (Eds.), Cycles of Soil : Carbon, Nitrogen, Phosphorus, Sulfur, Micronutrients. Wiley, IL, USA, pp. 1–78.

Tajima, R., Kato, Y., 2011. Comparison of threshold algorithms for automatic image processing of rice roots using freeware ImageJ. F. Crop. Res. 121, 460–463.

Vaz, M.D.., Edwards, A.C., Shan, C.A., Cresser, M.S., 1994. Changes in the chemistry of soil solution and acetic-acid extractable P following different types of freeze/thaw episodes. Eur. J. Soil Sci. 45, 353–359.

Waisel, Y., Eshel, A., Kafkafi, U., 2002. Plant roots – the hidden half (3rd), Annals of Botany, New York, USA

Zhang, X., Dippold, M.A., Kuzyakov, Y., Razavi, B.S., 2019. Spatial pattern of enzyme activities depends on root exudate composition. Soil Biol. Biochem. 133, 83–93.

Zhu, B., Gutknecht, J.L.M., Herman, D.J., Keck, D.C., Firestone, M.K., Cheng, W., 2014. Rhizosphere priming effects on soil carbon and nitrogen mineralization. Soil Biol. Biochem. 76, 183–192.

2.5 Study 5. Co-localised phosphorus mobilization processes in the rhizosphere of field-grown maize jointly contribute to plant nutrition

Nataliya Bilyera[a,b,1], Christina Hummel[c,1], Gabrielle Daudin[d], Michael Santangeli[c], Xuechen Zhang[e], Jakob Santner[f], Eva Lippold[g], Steffen Schlüter[g], Isabelle Bertrand[d], Walter Wenzel[c], Sandra Spielvogel[b,] Doris Vetterlein[g,h], Bahar S. Razavi[a,] and Eva Oburger[c,*]*

a. Department of Soil and Plant Microbiome, Institute of Phytopathology, Christian-Albrechts-University of Kiel, 24118 Kiel, Germany
b. Department of Soil Science, Institute for Plant Nutrition and Soil Science, Christian-Albrechts-University of Kiel, 24118 Kiel, Germany
c. Department of Forest and Soil Science, Institute of Soil Research, University of Natural Resources and Life Sciences, Tulln, Austria
d. Eco&Sols, Univ Montpellier, CIRAD, INRAE, IRD, Montpellier SupAgro, Montpellier, France
e. Department of Biogeochemistry of Agroecosystems, University of Göttingen, 37077 Göttingen, Germany
f. Institute of Agronomy, University of Natural Resources and Life Sciences, Tulln, Austria
g. Department of Soil System Science, Helmholtz Centre for Environmental Research - UFZ, Theodor-Lieser-Strasse. 4, 06120 Halle/Saale, Germany
h. Institute of Agricultural and Nutritional Sciences, Martin Luther University Halle-Wittenberg, Von-Seckendorff-Platz 3, 06120 Halle/Saale, Germany

[1] *These authors contributed equally to this work.*

* *Corresponding authors: Eva Oburger (eva.oburger@boku.ac.at) and Bahar S. Razavi (brazavi@phytomed.uni-kiel.de)*

Status: *published in Soil Biology and Biochemistry, 165, 108497,*
doi: 10.1016/j.soilbio.2021.108497

2.5.1 Abstract

Understanding phosphorus (P) dynamics in the rhizosphere is crucial for sustainable crop production. P mobilization processes in the rhizosphere include the release of plant and microbially-derived protons and extracellular phosphatases. We investigated the effect of root hairs and soil texture on the spatial distribution and intensity of P mobilizing processes in the rhizosphere of *Zea mays* L. root-hair defective mutant (*rth3*) and wild-type (WT) grown in two substrates (loam, sand). We applied 2D-chemical imaging methods in custom-designed root windows installed in the field to visualize soil pH (optodes), acid phosphatase activity (zymography), and labile P and Mn fluxes (diffusive gradients in thin films, DGT).

The average rhizosphere extent for phosphatase activity and pH was greater in sand than in loam, while the presence of root-hairs had no impact. Acidification was significantly stronger at young root tissue (<2 cm from root cap) than at older root segments (>4 cm from root cap) and stronger in WT than *rth3.* Accompanied with stronger acidification, higher P flux was observed mainly around young, actively growing root tissues for both genotypes. Our results indicate that acidification was linked to root growth and created a pH optimum for acid phosphatase activity, *i.e*., mineralization of organic P, especially at young root tissues which are major sites of P uptake. Both genotypes grew better in loam than in sand; however, the presence of root hairs generally resulted in higher shoot P concentrations and greater shoot biomass of WT compared to *rth3*. We conclude that soil substrate had a larger impact on the extent and intensity of P solubilization processes in the rhizosphere of maize than the presence of root hairs. For the first time, we combined 2D-imaging of soil pH, phosphatase activity, and nutrient gradients in the field and demonstrated a novel approach of stepwise data integration revealing the interplay of various P solubilizing processes *in situ*.

KEYWORDS: diffusive gradients in thin films (DGT); planar pH optodes; root hairs; root window; soil texture; soil zymography.

2.5.2 Introduction

Phosphorus (P) is extremely immobile in soil and therefore often the growth-limiting nutrient. Understanding P mobilization mechanisms of roots and related dynamics in the rhizosphere is a prerequisite for exploiting poorly available, recalcitrant soil P, *i.e.*, P sorbed, precipitated or immobilized in organic forms (Pierzynski et al., 2005; Stutter et al., 2012). Plants can only take up soluble inorganic P (P_i, *i.e.* HPO_4^{2-} or $H_2PO_4^-$), which is present in soil solution in low concentrations due to its high reactivity and strong retention by the soil matrix (Pierzynski et al., 2005). Organic P (P_o) can only be used by plants after enzyme-mediated conversion to phosphate via mineralization into soluble compounds (Jones and Oburger, 2011). Soil mineralogy and soil texture strongly influence P availability as P is precipitated as Ca, Fe, Al phosphates, or sorbed on Fe and Al (hydr)oxides, organic matter and clay minerals (Baldovinos and Thomas, 1967).

To overcome P deficiency, morphological root traits like higher root density and formation of root hairs increase the root surface to expand the area that is in contact with the exploitable

soil and contribute to an up to 50% higher P uptake (Daly et al., 2016; Itoh and Barber, 1983; Ruiz et al., 2020).

If soil solution concentrations are too low, morphological adaptations might not be sufficient to meet the plants P demand (Gerke, 2015) and roots (bio)chemically modify their rhizosphere to render P more plant available and increase P_i uptake (George et al., 2018). Plant and microbially derived phosphatases, organic acids, and protons directly increase P availability due to mineralization of organic P to orthophosphate (Jones and Oburger, 2011; Sims and Pierzynski, 2005; Turner et al., 2002), ligand exchange (Bertrand et al., 1999; Jones, 1998), and mineral dissolution (Barrow, 2017; Barrow et al., 2020). In addition, root hairs were found to enlarge the rhizosphere extent for acid phosphatase activity (Holz et al., 2020; Ma et al., 2018) and cause P depletion (Gahoonia et al., 2001). Moreover, carbon from rhizo-deposits also indirectly increases P availability by stimulation of P solubilizing microorganisms to release phosphatases (Manzoor et al., 2017; Merbach et al., 2010; Whipps, 2001; Yang et al., 2017), thus facilitating rapid turnover of P immobilized in microbial biomass (Raymond et al., 2020; Turner et al., 2003). P solubilization processes such as acidification and carboxylate exudation can co-solubilize other nutrients such as manganese (Mn) (Lambers et al., 2015) resulting in co-localized, increased labile P and Mn concentrations in the rhizosphere (Kreuzeder et al., 2018).

Individual P solubilization processes in the rhizosphere might interact but are difficult to measure in intact soil. Non-destructive 2D imaging techniques enable to semi-quantitatively assess the spatiotemporal distribution of rhizosphere parameters at µm to mm scales (Oburger and Schmidt, 2016). For instance, planar optodes visualize pH patterns (Blossfeld and Gansert, 2007), zymography and colorimetric imaging assess the distribution of phosphatase activity (Dinkelaker and Marschner, 1992; Grierson and Comerford, 2000; Razavi et al., 2019; Spohn et al., 2013), and diffusive gradients in thin films (DGT) maps the distribution of the labile fraction of nutrients such as P (Kreuzeder et al., 2013). Particularly when combined, these imaging techniques allow unique insights into interactions of individual P solubilisation processes (Hummel et al., 2021; Kreuzeder et al., 2018; Ma et al., 2021, 2018). Rhizoboxes provide easy access to roots and rhizosphere soil and facilitate the application of imaging techniques in the laboratory (Kuzyakov and Razavi, 2019; Neumann et al., 2009; Oburger and Schmidt, 2016), however such laboratory-based studies are often limited to early-plant developmental stages and consequently spatiotemporal information on rhizosphere parameters of mature plants is scarce. Permanently installed flat root windows enable non-destructive sampling across plant development *in situ* under field conditions (Dong et al., 2007; Hahn and Marschner, 1998; Marschner et al., 1991; Stober et al., 2000), but, to the best of our knowledge, (bio)chemical imaging techniques for pH,

phosphatase activity and labile nutrients have not yet been performed and combined under field-conditions in croplands.

Here we investigated the interplay of two P solubilization processes (e.g., acidification and mineralization of organic P to phosphate) by combining planar optodes, zymography and DGT imaging under field conditions using custom-made root windows, which enable non-destructive and repeated sampling *in situ*. Two *Zea mays* L. genotypes, *i.e.*, a root-hair forming wild-type and root-hair defective mutant *rth3*, were grown on two substrates with contrasting textures (sand and loam) (Vetterlein et al., 2021). Due to lower total P and fewer sorption sites in sand than in loam, we hypothesized that the lower P and pH buffer capacity in sand will induce stronger rhizosphere acidification and higher phosphatase activity consequently resulting in a larger rhizosphere extent of both parameters combined with stronger P depletion gradients in sand compared to loam. Furthermore, we expected that root hairs not only enlarge the absorption surface for nutrients (Jungk, 2001) but also enhance the rhizosphere extent for acidification, phosphatase activity, and P depletion compared to root-hair defective *rth3* irrespective of soil texture. We applied different strategies of data integration to derive quantitative information from the high-resolution images and investigate the effect of soil substrate (i.e., loam vs. sand) and the presence of root hairs on pH, phosphatase and labile P and Mn patterns. We started with radial parameter distribution extending from the root surface (rhizosphere gradients). Then, we defined spatial domains, *i.e.*, root surface, rhizosphere, and bulk soil, based on thresholds and calculated the average concentration/activity within these spatial domains. Furthermore, we investigated to which extent hotspots were associated with the rhizosphere and root surface, and to which extent the observed parameter hotspots were co-localized. To capture differences occurring along the roots, we compared young root tissues to older root regions.

2.5.3 Material and methods

2.5.3.1 Site description and experimental setup

All chemical imaging procedures were conducted at the experimental field site of the DFG priority program 2089 “Rhizosphere Spatiotemporal Organisation – A Key to Rhizosphere Functions” in Bad Lauchstädt, Germany (N 51.390424, E 11.875933). A detailed description of the experimental field site can be found in Vetterlein et al. (2021). Briefly, two maize genotypes (*Zea mays* L. wild-type (B73) (WT) and root hair defective mutant (*rth3*)) (Hochholdinger et al., 2018, 2008; Wen and Schnable, 1994) were grown on two substrates of different texture (loam L;

and sand S; Table 1) in 6 replicate plots (each 3.1 x 11.0 m) in a randomized block design (Vetterlein et al., 2021).

Table 1. General substrate characteristics before fertilization. Data are represent mean ± standard error (*n*=12) (from Vetterlein et al. (2021).

Soil substrate	Loam	Sand	Method
Sand (%)	32.5±0.36	91.8±0.51	ISO 11277, 1998; ISO 11277, 2002
Silt (%)	47.9±0.17	5.6±0.35	
Clay (%)	19.5±0.26	2.6±0.17	
Bulk density (g cm^3)	1.39±0.01	1.50±0.01	
CEC ($mmol_c$ kg^{-1})	98.6±4.7	33.1±2.6	Ammonium acetate, pH 7 (Carter and Gregorich, 2007)
Soil pH ($CaCl_2$)	6.37	6.29	0.01 M $CaCl_2$ solution (soil:solution ratio of 1:2.5)
Organic C (g kg^{-1})	8.5±0.1	1.5±0.1	CNS analyzer
Total N (g kg^{-1})	0.83±0.01	0.17±0.01	CNS analyzer
Total P (mg kg^{-1})	416±4.35	52.9±4.68	Aqua regia (ISO 11466)
Iron oxides (g kg^{-1})	1.32±0.01	0.25±0.01	Oxalate + dithionate (Mehra and Jackson, 1960; Schwertmann, 1964)
P_{CAL} (mg kg^{-1})	32.7±0.4	8.29±0.37	Calcium acetate lactate (Schüller, 1969)
K_{CAL} (mg kg^{-1})	28.5±0.72	7.84±0.61	Calcium acetate lactate (Schüller, 1969)

The treatments were L-WT, L-*rth3*, S-WT and S-*rth3.*The substrate ‘loam’ originated from the 0-50 cm depth of a Haplic Phaeozem near Schladebach, Germany (51°18′31.41″ N; 12°6′16.31″ E) which had been under agricultural use before excavation. The substrate ‘sand’ was obtained by sieving and mixing 16.7% of the beforementioned loam with 83.3% quartz sand (WF 33, Quarzwerke Weferlingen, Germany). Both substrates were sieved < 4mm and filled into the plots. General substrate characteristics before fertilization are shown in Table 1 and were already reported by Vetterlein et al. (2021). Both substrates were carbonate-free.

The amount of fertilizer applied to the field plots was experimentally pre-determined by Vetterlein et al. (2021) aiming at comparable nutrient availability for both substrates under homogenized (thorough mixing of substrate and fertilizer) and well-watered conditions. In the field, fertilizers were only surface applied and the substrates generally differ in water and nutrient transport, particularly under non-saturated conditions. To provide sufficient nutrients for maize growth while avoiding luxurious supply, soil plots were fertilized with nutrients at the rates (kg ha^{-1}) 50 N, 12 P, 50 K, 18 Mg, 27 Ca on loam, and 100 N, 24 P, 100 K, 33 Mg, 52 Ca + 100 Excello

331 Special (Jost GmbH, Micronutrients (%): 1 B; 3 Mn, 3 Zn, 0.3 Cu ,) on sand. The fertilizers included calcium ammonium nitrate, triple superphosphate, 60s corn potash and Epsom salt (Vetterlein et al., 2021). Fertilizers were surface applied in two rates: 50% prior to seeding and 50 % at growth stage BBCH14 which corresponded to 14 and 6 weeks before the imaging campaign at growth stage BBCH 59, respectively. Planting density in the plots was 9.5 plants m^2 (Vetterlein et al., 2021), ensuring 2-5 plants per root window. Plant growth was characterized by cold spring, followed by a heat period with minimal precipitation that peaked during the imaging campaign. During the heat periods, prior to sampling, the soil area close to the root window was irrigated in the evening.

2.5.3.2 Root windows

Custom designed root windows were installed in 3 individual replicate plots per substrate and maize genotype combination, resulting in a total number of 12 root windows. Root windows were constructed on site in April 2019, prior to the first planting of the experimental plots. For root window installation, a pit (1 × 1 × 1.6 m) was excavated at the short end of each plot and three pit walls were stabilized by an open-end wooden crate inserted into the pit (Fig. 1a), which facilitates repeated access to the root windows during the entire duration of the SPP2089 program (6 years). Root windows were positioned at the open, top end of the crate. The wooden walls were stabilised with an aluminium bar (5 × 5 cm, Fig. 1b). The root windows were made from a grey polyvinyl chloride (PVC) frame into which a transparent removable 5 mm thick acrylic glass plate with an observation area of 60 × 60 cm was inserted (Fig. 1c). The PVC window frame was inserted vertically (orthogonal to the soil surface) and fixed by a wooden stake construction, with the window frame reaching about 30 cm into the soil plots (Fig. 1a). Prior to the insertion of the removable observation plate, the entire observation area was covered by a transparent PVC plastic sheet (fixed onto the frame via tape) to protect the roots from damage when removing the observation plate. The PVC plastic sheet was renewed after every sampling event. The observation acrylic glass plate was then placed onto the soil and covered with two 30 × 60 cm grey PVC boards that were pressed against the soil block by two removable aluminium bars (3 × 3 cm) to provide stability and protection against light (Fig. 1b). The pressure of the PVC boards against the soil plot could be individually adjusted by wing bolts (Fig. 1b). In between the sampling events, the root window pits were covered with wooden boards (Fig. 1d). Figure 1c shows a root window of one of the L-WT plots at BBCH 59.

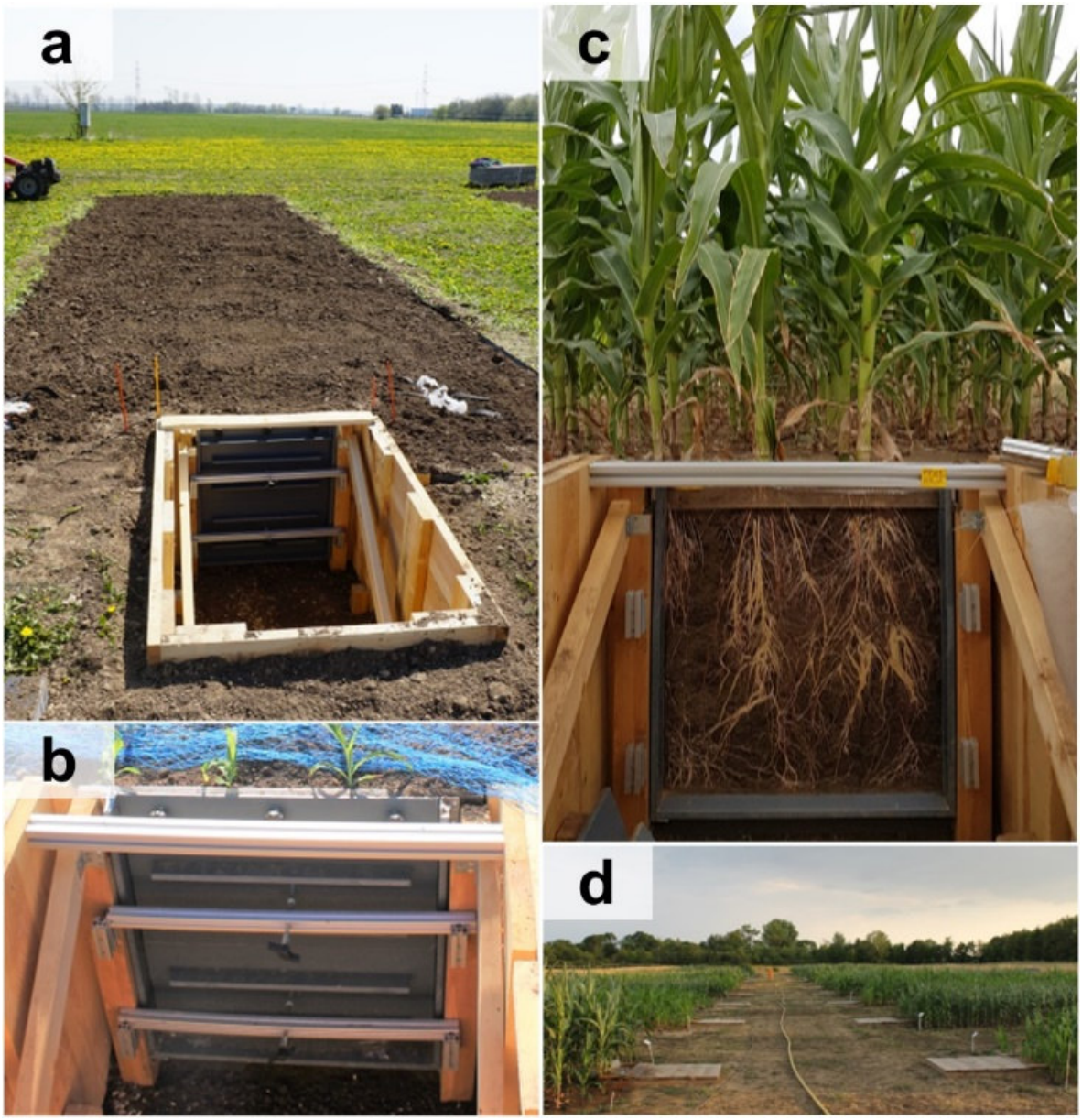

Figure 1. Custom designed root window construction at the experimental field site of the DFG priority program 2089 “Rhizosphere Spatiotemporal Organisation – A Key to Rhizosphere Functions”. (a) Experimental plot (loam) with newly installed root window construction and observation pit at the short end of the plot. (b) Close-up of the root window construction, with observation window being covered by two removable PVC boards that are pressed against the soil plot with aluminium bars and wing bolts for stability and protection against light. (c) Root window observation area (60 x 60 cm) of a loam plot planted with *Zea mays* L. wild-type (B73) at growth stage BBCH 59. (d) Root window pits covered by wooden boards in between sampling campaigns.

2.5.3.3 Bio-chemical imaging

The imaging was conducted at the start of flowering (BBCH 59) (Bleiholder et al., 2001). Acid phosphatase activity was imaged with direct soil zymography, soil pH was visualized with

planar optodes, and labile P and Mn-fluxes were imaged using diffusive gradients in thin films (DGT).

The three imaging techniques were consecutively applied within 2-3 days to all 12 root windows (3 replicates × 4 treatments, Table 2). Zymograms covered 10 × 20 cm (n_{total}=19); pH optodes (2 x× 3 cm, n_{total}=60) and DGT gels (1.5 × 2.5 cm, n_{total}=41) were applied within the zymogram area at depth 10-50 cm with the focus on root tips and good soil-sensor/soil-gel contact while avoiding cavities. All sampling areas were sprayed with water before membrane/sensor/gel application to ensure good contact and diffusion while avoiding drying of sensors/gels and thus shrinkage. To avoid bias associated with diurnal plant processes, zymography membranes were always applied at the photosynthetic activity peak (10 am to 2 pm) for 1h. For pH optodes, we used an optimized deployment time of ~12h overnight to ensure a reliable pH signal under field moist conditions. DGT gels were deployed for 24h to allow accumulation of labile nutrients over a complete day. The effect of changing weather and temperature conditions was randomized by sampling replicate windows over different days. The sequence of applied techniques within each window and the depth of application is presented in Table 2.

Acid phosphatase activity was detected by direct soil zymography as described in Razavi et al. (2019) with polyamide membranes soaked in 3.3 mM L^{-1} 4-methylumbelliferyl-phosphate disodium salt dissolved in MES buffer (pH 6.5) directly applied to the soil surface and covered with aluminum foil. A soft foam rubber was placed between the aluminum foil and acrylic glass plate to ensure optimal soil contact. After 1 h, the membranes were carefully lifted off and photographed in a dark room under ultraviolet light (excitation wavelength 355 nm). Calibration was performed as described in Razavi et al. (2019). Zymograms were transformed to 8-bit grayscale images in ImageJ (Schindelin et al., 2012) and calibrated to acid phosphatase activity (Section S1, Eq. S1).

Planar optodes (sensor foils SF-HP5R) combined with the VisiSens TD imaging system from PreSens GmbH (Regensburg, Germany) were used to visualize pH (Blossfeld and Gansert, 2007). The self-adhesive sensor foils were cut and pasted on a transparent polyester foil (125 µm thick, Melinex®506, DuPont Teijin Films, USA), pre-equilibrated in phosphate-NaCl buffer (pH 6.5, ionic strength 100 mM) and then fixed on the inner side of the root window observation plate with tape. Sensor foils were applied overnight (~12 h), and images were recorded in the morning in dark conditions using black cloth to cover the observation pits. The camera was placed directly on the observation plate to keep a constant distance between camera and optode resulting in a field of view of 5cm × 3.7cm. The ionic strength of the soil solution was estimated from the electrical conductivity as described in SI (Section S2). Sensor foils were calibrated using

phosphate buffers (pH 5.0 to pH 8.5) with the ionic strength adjusted with NaCl to 40 and 16mM for loam and sand, respectively. The details are described in Section S2 in SI.

DGT solute binding gels were applied to map labile nutrient fluxes. By exposing an infinite solute sink to soil, DGT continuously accumulates the targeted solute species, here P and Mn. The accumulated solute mass is often reported as time-averaged solute flux (pg cm^{-2} s^{-1}) from the soil to the gel, which provides a measure of the local solute resupply capacity of the soil. In the DGT imaging setup, this allows for a relative comparison between different locations. The DGT gels were prepared as described by Kreuzeder et al. (2013) (for details see also Supplementary Information – Section S3). Gels were covered by a Nuclepore membrane (Nuclepore Track-Etched Membrane 0.2 µm, Whatman, UK) and fixed to acid washed Melinex foil and mounted to the inner side of the root window observation plate. Two layers of sponge cloth pieces were fixed between the observation plate and the grey PVC stabilization boards at the position of each DGT gel to improve the soil-gel contact when closing the window. After 24 h, the gels were retrieved, rinsed with deionised water, and dried. Spatial distribution of elements captured by the DGT was analysed by laser-ablation inductively coupled mass spectrometry (LA-ICPMS). LA-ICPMS was performed in line scanning mode (interline distance 400 µm, spot size 150 µm, laser speed 150 µm s^{-1}) with a UP 193-FX (ESI, NWR Division, Portland, USA) laser ablation system coupled to a quadrupole ICPMS (Elan 9000 DRCe, Perkin Elmer, USA). The resulting pixel size in the images was 99.4 µm × 400 µm. Details regarding gel analysis and calibration are described in the supporting information (Section S3) and in Wagner et al. (2020a). Depending on the DGT-soil-root-interface contact, two to three DGT replicate images per treatment were analyzed (Table 2).

2.5.3.4 Image analysis

Image analysis of pH and acid phosphatase activity was based on 5-6 regions of interest (ROI) per treatment (Table 2), not necessarily representing 3 biological replicates as the quality of some ROI was not optimal due to poor contact or large cavities. For DGT less ROI were available (3 in L-WT, 3 in L-*rth3*, 2 in S-WT and 2 in S-*rth3*) due to the challenging field conditions (cavities, contact issues) and generally lower number of DGT-gels (n_{total}=41).

Root photographs and DGT images were scaled to the size of pH maps and zymograms (resolution 0.038 mm per pixel) without interpolation in ImageJ Fiji (Schindelin et al., 2012). The images were aligned in Photoshop (CS5, V12.0) with the help of photographs during the application. It must be noted that the angle of some root photographs was not perfectly orthogonal resulting in small image distortions and slight inaccuracies in scaling and rectification. Templates

Table 2. Application sequence of imaging techniques including number of zymograms, optodes and DGT gels applied, number of regions of interest (ROI) used for image analysis with corresponding position (distance from the soil surface) within the root window**.** Biological replicates are represented by the root system grown in individual root window from different field plots Note that analysed DGT replicates were limited due to application challanges in the field (cavities, poor contact).

Fieldplot (biological replicate)	**Substrate**	**Genotype**	**Method sequence**	**Days between first and last assay**	**Number of zymograms applied**	**Number of optodes applied**	**Number of DGT gels applied**	**ROI for analysis** pH & zymo.	**ROI for analysis** DGT	**Position in window** (distance from soil surface)
FP01	Loam	Wildtype	DGT-zymo-optode	1	1	5	3	1		40-50 cm
FP02	Loam	Wildtype	DGT-zymo-optode	1	1	4	2	2	1	10-20 cm
FP03	Loam	Wildtype	DGT-zymo-optode	1	1	6	3	3	2	20-40 cm
FP07	Loam	*rth3*	DGT-zymo-optode	1	3	7	5	2	1	20-30 cm
FP08	Loam	*rth3*	DGT-zymo-optode	1	2	3	3	1	1	20-30 cm
FP09	Loam	*rth3*	DGT-zymo-optode	1	2	6	4	2	1	30-40 cm
FP13	Sand	Wildtype	Optode-zymo-DGT	2	2	4	4	1		40-50 cm
FP14	Sand	Wildtype	Zymo-DGT-optode	3	1	5	3	1		10-20 cm
FP15	Sand	Wildtype	Zymo-DGT-optode	2	1	7	3	3	2	30-40 cm
FP19	Sand	*rth3*	Optode-zymo-DGT	2	2	3	5	1		30-40 cm
FP20	Sand	*rth3*	Zymo-DGT-optode	3	1	7	3	2	1	30-40 cm
FP21	Sand	*rth3*	Optode-zymo-DGT	2	2	3	3	2	1	30-40 cm
Total					19	60	41	21	10	

(*e.g.,* angle for rotation and coordinates for alignment) prepared in Photoshop were used for extracting the ROI for analysis in ImageJ.

Root masks were prepared from the root photographs in ImageJ by drawing lines along the roots and adjusting the line thickness to each individual root. Rhizosphere extent was determined with plots of average concentration in soil as a function of root distance, *i.e.*, concentration-distance plots (Fig. S1, step 2). These were computed according to Lucas et al., (2019) with adaptations for 2D images. Briefly, a "Euclidian Distance Transform" (EDT) function was applied on the binary root mask image with the "Exact Euclidian Distance Transform (3D)" method in ImageJ resulting in a distance map, where a grey value corresponding to the distance to the closest root was assigned to each pixel.

The distance map was then combined with the analyte image (phosphatase, pH images, or DGT flux; further transformed to 8-bit grayscale, according to minimum and maximum value) into a composite image. Every pixel in the composite image contained the concentration in one channel and the distance to the closest root information in another channel. A loop in the x and y dimensions was then initiated on the composite image to retrieve the information of both channels simultaneously. The average analyte concentration for each distance class (class width 0.038 mm) from the root, was saved as text file. More information and the ImageJ script can be found in Lucas et al. (2019). In addition to distance classes, we defined 3 spatial domains in each analyte image: bulk, rhizosphere, and root surface (Fig. S1). Bulk soil concentrations were measured in the image area remaining after subtraction of the root mask enlarged by 2.5 mm. Root surface concentration was measured on the area of the root mask. Note that the spatial domain 'root surface' refers to root surface exposed, *i.e.*, in direct contact with the measurement device (membrane, optode, DGT gel) without soil in between and hence reflects activity of the root.

The gradual rhizosphere extent in the concentration-distance plots was compartmentalized with activity/concentration thresholds to define an artificial boundary between rhizosphere and bulk soil and hence to calculate 'the average rhizosphere extent' (individual rhizosphere for each investigated parameter): for each ROI image, an individual threshold was calculated by adding two times the respective standard deviation (+2 × SD; or -2 × SD in the case of pH) to the determined average bulk soil concentrations/activities (Fig. S1). Note that an individual threshold for each ROI was also required to cope with variations in bulk concentrations/activities due to differences in moisture content during sampling campaign (sunshine vs. rain). These thresholds were also used to (i) define hotspots (*i.e.*, all activities/concentrations greater (or lower in case of pH) than the determined threshold) (ii) determine the relative spatial hotspot coverage (% of total area) of each spatial domain and (iii)

to create binary hotspot images for co-localisation analysis. Analysis of spatial co-localization/coincidence of hotspots for four parameters (acid phosphatase activity, pH (acidification), Mn and P-fluxes) was performed using 'Just another co-localization plug-in' (JACoP) (Bolte and Cordelières, 2006) in ImageJ. The thresholded binary images of hotspot activities for each parameter were created for two spatial domains (root surface defined by root masks and standardized rhizosphere of 2.5 mm to ensure the same co-localization areas) separately and corresponding co-localization analysis was done, *i.e.*, how much area of one parameter co-localizes with the area of another parameter. The calculated overlap coefficient (r, Eq. 1) represents the percentage of the overlapping hotspot areas from two parameters (A, B) and shows the share of common hotspot area of the two parameters within the cumulative hotspot area of the same two parameters:

$$\text{Overlap coefficient (\%): } r = \frac{\sum_i A_i \cdot B_i}{\sqrt{\sum_i A_i^2 \cdot \sum_i B_i^2}} * 100 \qquad \textit{Eq .1}$$

where A_i – is the value at each pixel of image A, B_i – is the value at each pixel of image B.
Spatial changes along the root axis were assessed by measuring root surface pH, acid phosphatase activity, P and Mn-flux for young root tissues (<2 cm from root cap) and older root sections (>4 cm from root cap).

2.5.3.5 Statistics

All data are presented as mean ± standard error (SE) of 5-6 replicate ROIs for zymograms and optodes deriving from 3 root windows and 2-3 replicates for DGT ROIs deriving from 2, 3, 1, and 2 root windows for L-WT, L-*rth3*, S-WT and S-*rth3*, respectively (Table 2). The Shapiro-Wilk test was performed for residues of means to check for normality, and the Bartlett test was applied to check the homogeneity of variances. All data were log transformed for statistical analysis. T-test, one- or two-way ANOVA and Tukey's HSD post-hoc test were performed in RStudio (version 1.3.1093) at a significance level of α = 0.05. Figures were prepared in Sigma Plot (V.12.0, Systat Software Inc.) and Microsoft Publisher for Microsoft 365 (V2010).

2.5.4 Results

Generally, both maize genotypes grew better on loam (L) than on sand (S), and the wildtype (WT) developed a higher shoot biomass than the root-hair defective mutant (*rth3*) irrespective of substrate (see also Vetterlein et al., 2021). At BBCH 59, P contents (mg plant^{-1})

were highest in L-WT (180±25) followed by L-*rth3* (105±6), S-WT (71±5) and S-*rth3* (58±6) (Vetterlein et al., in preparation).

2.5.4.1 Direct observations on high resolution images

Acidification features were observed mainly on/around root tips and actively growing roots (Fig. 2 and S2). Elevated acid phosphatase activity was relatively homogenously distributed along the roots in all treatments (Fig. 2, S3 and b). P depletion zones were not clearly pronounced, patchy and only inconsistently observed around some older root sections (Fig. 2, white arrows). Increased P and Mn fluxes occurred mainly on the root surface at the root tips (Fig. 2, red arrows, and Fig. S4).

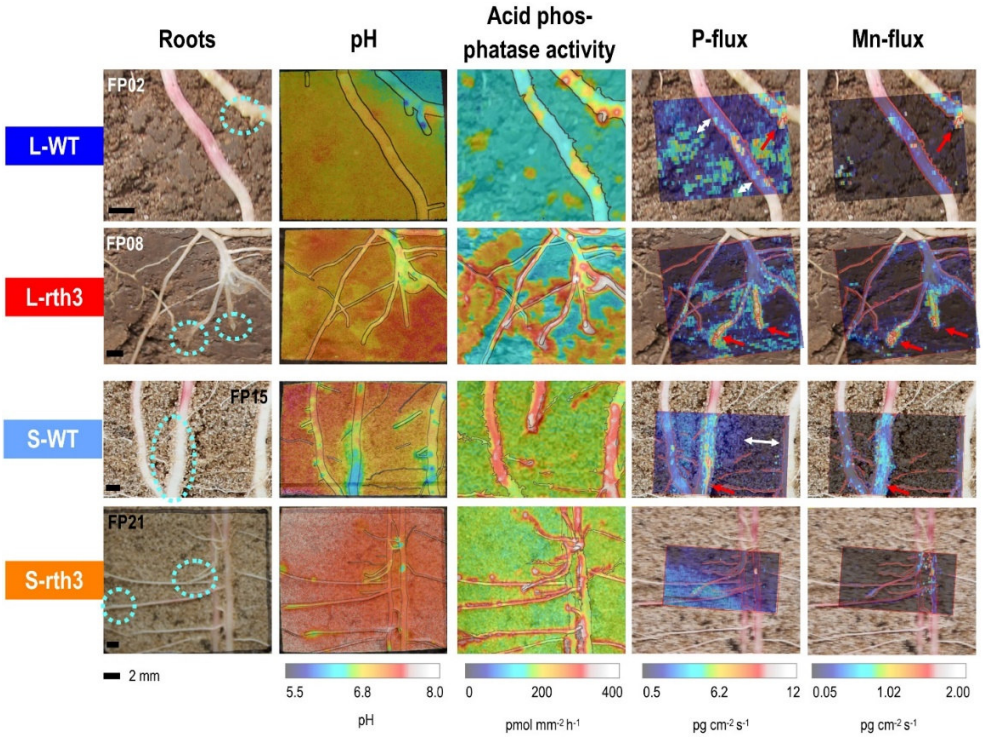

Figure 2. Exemplary root images, pH, acid phosphatase activity (pmol mm^{-2} h^{-1}), P flux and Mn flux (pg cm^{-2} s^{-1}) images (overlaid on the corresponding root image with 50% transparency) of two maize genotypes (wild-type (WT) and root hair defective mutant (*rth3*)) grown in root windows on loam (L) and sand (S) in the field. The identification number of each field plot (FP) is indicated in the top part of root images. Dotted circles highlight actively growing roots during method application. Red arrows highlight P hotspots at actively growing root tips and white arrows indicate possible P depletion zones around older roots.

2.5.4.2 Rhizosphere gradients and boundaries between spatial domains (i.e., average rhizosphere extents).

Generally, rhizosphere gradients were either comparable or steeper in sand than in loam. Average rhizosphere extents were greater in sand when compared to loam (Fig. 3). However due

to the large image heterogeneity, most of the observed differences in rhizosphere extents were not statistically significant, except for phosphatase activity, where we found a significant effect of substrate (Fig. 3 & Table S1). The rhizosphere extent for acidification tended to increase in the order L-WT (mean±SE: 0.79±0.42 mm) < L-*rth3* (0.98±0.48 mm) < S-WT (1.25±0.34 mm) < S-*rth3* (1.45±0.40 mm) (Fig. 3). Acid phosphatase activity rhizosphere extents were significantly larger in sand (S-WT: 1.59±0.36 mm; S-*rth3*: 1.26±0.24 mm) than in loam (L-*rth3*: 0.62±0.45 mm; L-WT 0.29±0.16 mm; *p=0.005*, Table S1), with no significant difference between genotypes. The average rhizosphere gradients of P fluxes showed no clear trend, and no rhizosphere extents could be defined from the concentration-distance plots (Fig. 3). The rhizosphere gradients of Mn flux showed a slightly steeper decrease in *rth3* than in WT in both substrates combined with less pronounced rhizosphere extents for *rth3* (0.27±0.14 and 0.75±0.21 mm in L and S, respectively) than for WT (0.88±0.47 and 1.12±0.04 mm in L and S, respectively) (*p=0.160*, Table S1, Fig. 3).

2.5.4.3 Average pH, acid phosphatase activity, P and Mn fluxes in individual spatial domains (bulk soil, rhizosphere and on root surface)

Despite the patchiness of visualized parameter values (Fig. 2), averaging activities/concentration/fluxes within each spatially defined domain (root surface, rhizosphere, bulk soil) showed distinct trends (Fig. 3, Fig. 4). Acidification was found on the young root tissue surface of both maize genotypes that extended into the adjacent rhizosphere (Fig. 4a). For *rth3* the decrease in averaged pH from the bulk soil > rhizosphere > root surface was statistically significant irrespective of growth substrate (Fig. 4a). The same trend was observed for WT; however, the differences were not statistically significant. Bulk pH was 7.06±0.06 and 7.30±0.06 in loam and sand, respectively. As expected, rhizosphere acidification was on average more pronounced in sand (by 0.21±0.03 pH units) than in loam (by 0.12±0.02 pH units). Average root surface pH was 6.80±0.13, 7.01±0.12, 6.89±0.30 and 6.94±0.23 in L-WT, L-*rth3*, S-WT and S-*rth3*, respectively and did not differ between the treatments.

Average acid phosphatase activity tended to increase across spatial domains in the order bulk - rhizosphere – root surface with more distinct differences in sand than in loam (Fig. 4b). However, neither a statistically significant genotype nor a substrate-specific effect in any of these spatial domains (*p=0.216-0.887*, Table S2) were observed. Irrespective of genotype and substrate, phosphatase activity was 36±0.03 % higher on the root surface and 11±0.10 % higher in the rhizosphere than in the bulk soil.

Average P flux (representing a measure of the local solute resupply capacity of the soil s triggered by biogeochemical conditions) for S-WT showed on average a higher P flux on the root

surface compared to rhizosphere and bulk soil while it remained constant among the spatial domains for other treatments (Fig. 4c). The elevated P flux in S-WT was mainly associated with thick root tips that were actively growing during DGT application and extended slightly into the rhizosphere.

Averaged Mn flux increased in the order bulk – rhizosphere – root surface irrespective of substrate and genotype. Due to the heterogeneity within and between the replicate images (see above), observed differences were mainly non-significant, except for S-WT which displayed a significant higher average Mn flux on the root surface compared to bulk soil (Fig. 4d).

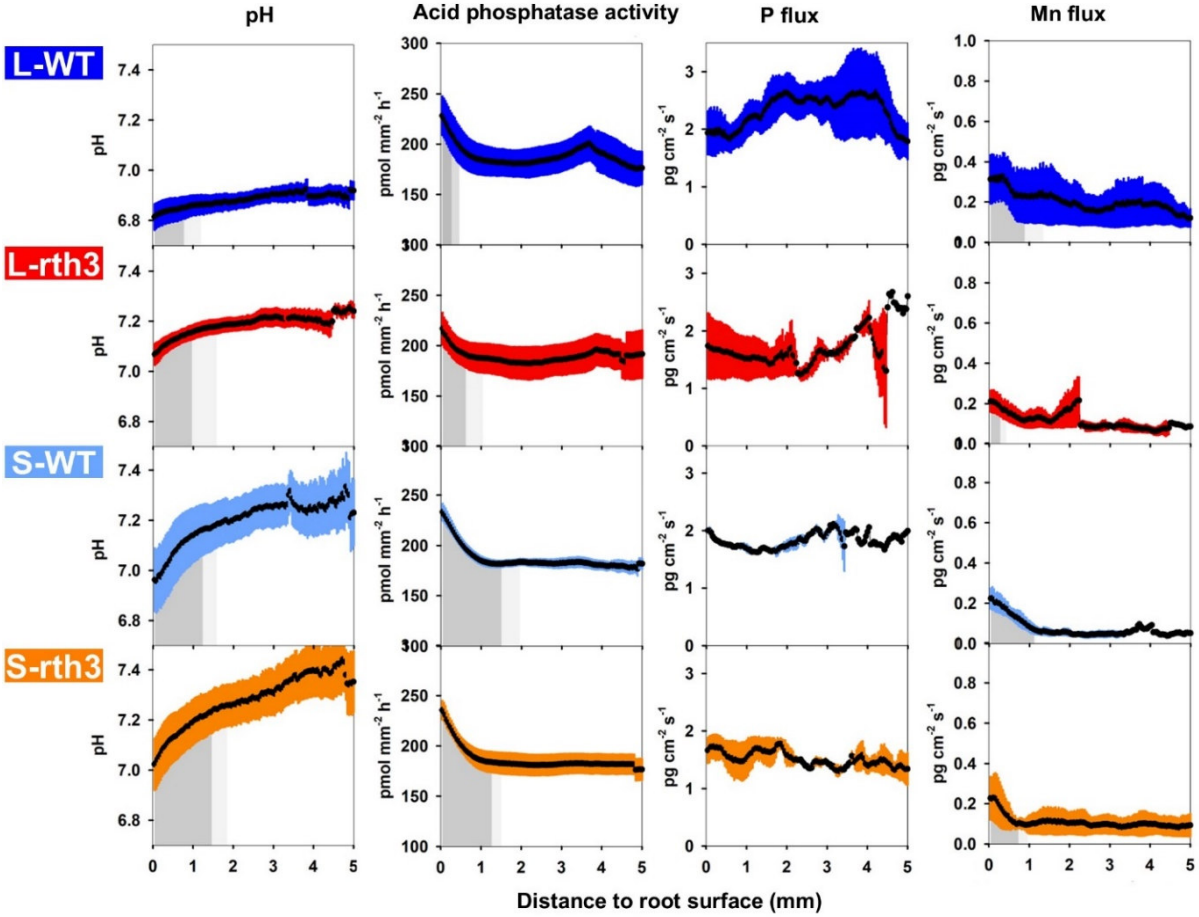

Figure 3. Average pH, acid phosphatase activity, P and Mn flux as a function of distance to the root surface of two maize genotypes (wild-type (WT) and root hair defective mutant (*rth3*)) grown in loam (L) and sand (S). Coloured error bars represent standard error of *n*=6 (L-WT) or *n*=5 (L-*rth3*, S-WT, S-*rth3*) for pH and acid phosphatase activity; *n*=3 (L-WT, L-*rth3*) or *n*=2 (S-WT, S-*rth3*) for P and Mn flux. The average rhizosphere extent is shown as dark grey areas and was determined from individual concentration-distance plots with a threshold value (mean concentration at distance >2.5mm (*i.e.*, bulk soil +/- 2xSD); light grey areas indicate standard error for the average rhizosphere extent. No rhizosphere extent was defined for P flux.

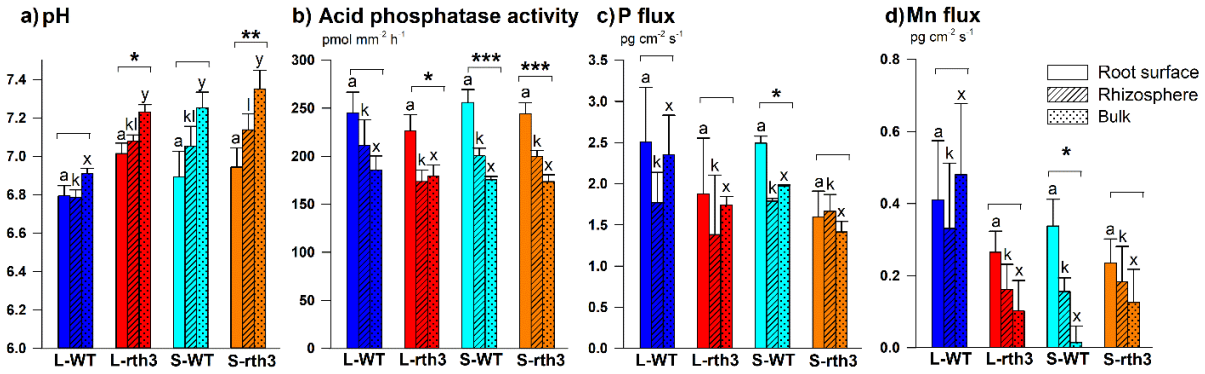

Figure 4. Averaged **(a)** pH, **(b)** acid phosphatase activity, **(c)** P and **(d)** Mn fluxes of bulk soil (area excluding root surface mask enlarged by 2.5 mm), rhizosphere (individual rhizosphere extent) and root surface (area of image covered by root tissue only) of two maize genotypes (wild-type (WT) and root-hair defective mutant (*rth3*)) grown in loam (L) and sand (S). Error bars represent SE of n = 6 (L-WT), or n = 5 (L-*rth3*, S-WT, S-*rth3*) for pH and acid phosphatase; n = 3 (L-WT, L-*rth3*) or n = 2 (S-WT, S-*rth3*) for P and Mn flux. *Note: P rhizosphere flux was measured within the area of Mn rhizosphere extent, as no P rhizosphere extent could be defined.* Letters above the bars indicate significant differences between treatments according to two-way ANOVA for each spatial domain according to Tukey post-hoc test, *i.e.,* root surface (a), rhizosphere (k-m), and bulk (x-y). Asterisks indicate significant differences between the spatial domains (bulk, rhizosphere, root surface) within one treatment (one-way ANOVA, '.' *p<0.10*, '*' *p<0.05*, '**' *p<0.01*, '***' *p<0.001*).

2.5.4.4 Root surface and rhizosphere hotspot distribution.

Calculating the relative coverage of areas identified as activity hotspots (defined as bulk soil activity/concentration + 2 x SD for phosphatase activity, P, Mn flux; - 2 x SD for pH) revealed a rather patchy hotspot distribution that differed for each investigated parameter. Relative hotspot coverage on root surface and in the rhizosphere was greatest for acidification (73±4 and 63±2%) followed by phosphatase activity (70±4 and 49±3%), Mn flux (59±8 and 42±4%) and P flux (24±5 and 22±5 %) of root surface and rhizosphere area, respectively, averaged across all substrates and genotypes, with generally greater hotspot coverage on the root surface than in the rhizosphere and a mostly non-significant trend of greater hotspot coverage in sand than in loam (Fig 5, Table S3). Bulk soil hotspot coverage was 35±2%, 15±2%, 22±3%, and 18±2% for pH, phosphatase activity, P and Mn flux, respectively (Fig. 5). Differences between root surface and rhizosphere were only statistically significant in sand for pH (*rth3* only) and Mn-flux (WT only, Fig. 5, Table S4). The hotspot coverage for root surface pH and acid phosphatase activity was significantly higher in sand than in loam (*p=0.04* and *p=0.03*, respectively, Table S3), but there was no statistically significant effect of genotype for any of the parameters (Table S3).

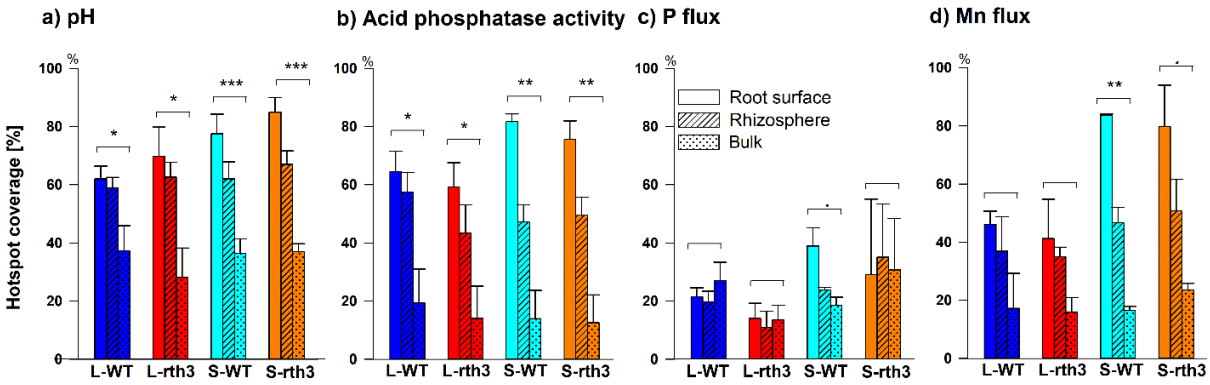

Figure 5. Hotspot coverage of pH (a), acid phosphatase activity (b), P flux (c), and Mn flux (d) on the root surface, in the individual rhizosphere and in the bulk soil expressed as relative percentage based on the total area of respective spatial domain. Bars and error bars represent mean and standard error of L-WT (n = 6), L-*rth3* (n = 5), S-WT (n = 5), S-*rth3* (n = 5) for pH and phosphatase, for P and Mn flux, L-WT and L-*rth3* (n = 3); and S-WT and S-*rth3* (n=2). Note that P rhizosphere flux was measured in the Mn rhizosphere. Asterisks indicate significant differences between root surface, rhizosphere, bulk hotspot coverage according to one way-ANOVA (' ' n.s., '.' p <0.10, '*' $p < 0.05$, '**' $p< 0.01$).

2.5.4.5 Co-localization of hotspots.

Spatial co-occurrence of parameter hotspots indicates possible interactions of P solubilizing processes. Overlap coefficients show the share of the common hotspot area of two parameters within the cumulative hotspot area of the same two parameters. Acidification and acid phosphatase hotspots showed a high co-localization on the root surface as revealed by relatively high overlap coefficients (*i.e.*, L-WT 63±3 %, L-*rth3* 66±9 %, S-WT 79±4 %, S-*rth3* 81±7 %), with a pronounced substrate ($p=0.028$) but no genotype ($p=0.969$) effect (Table 3). Co-localization of Mn-flux hotspots with hotspot phosphatase activity (70±5 %, averaged across all treatments) and acidification (67±6 %) on the root surface was in a similar range as co-localization of hotspot phosphatase activity and acidification (72±3%) (Table 3). In line with the relative area covered by individual parameter hotspots (Fig. 5), overlap coefficients for pH-phosphatase, pH-Mn and phosphatase-Mn were smaller in the rhizosphere compared to the root surface and generally followed a similar though less distinct trend as observed for the root surface (Table 3). Low overlap coefficients of P flux hotspots with acidification or acid phosphatase hotspots (35±4% to 40±5%) on root surface were mainly determined by the much lower occurrence of P flux hotspots in comparison to acidification and phosphatase hotspots (Fig. 5). P-related overlap coefficients (pH-P, phosphatase-P and Mn-P) also only showed minor, mostly non-significant differences between the root surface and the rhizosphere (Table S5).

Table 3. Top: Overlap coefficients for co-localized hotspots of acidification (pH), acid phosphatase, P and Mn flux in two spatial domains (root surface and rhizosphere) across treatments. Data represent means ± SE, following by the number of replicates for pairs of parameters in parentheses (n). **Bottom**: *p-values* from two-way ANOVA comparing the effect of substrate, genotype, and their interaction across treatments within each parameter combination. Significant effects (p<0.05) are marked **in bold.** Different letters in each column indicate significant (p<0.05) difference between treatments within each parameter combination as revealed by the corresponding Tukey post-hoc test.

Treatment	**Overlap coefficient for co-localized hotspots, %**											
	pH-phosphatase (a,b)	**pH-P (c,d)**	**pH-Mn (e,f)**	**Phosphatase -P (g,h)**	**Phosphatase -Mn (k,l)**	**P-Mn (m,n)**	**pH-phosphatase (a,b)**	**pH-P (c,d)**	**pH-Mn (e,f)**	**Phosphatase -P (g,h)**	**Phosphatase -Mn (k,l)**	**P-Mn (m,n)**
	Root surface						**Standardized rhizosphere (2.5 mm)**					
L_WT	64 ± 3^{a} (n=6)	32 ± 4^{c} (n=3)	52 ± 4^{c} (n=3)	44 ± 5^{g} (n=3)	62 ± 6^{k} (n=3)	53 ±4^{m} (n=3)	42 ±6^{a} (n=6)	28 ±7^{c} (n=3)	31 ± 10^{e} (n=3)	36 ± 2^{g} (n=3)	39 ± 11^{k} (n=3)	34 ± 9^{m} (n=3)
L_*rth3*	66 ± 9^{a} (n=5)	34 ± 8^{c} (n=3)	58 ± 11^{e} (n=3)	33 ± 8^{g} (n=3)	57 ±10^{k} (n=3)	44 ±9^{m} (n=3)	41 ± 10^{a} (n=5)	31 ± 4^{c} (n=3)	35 ± 6^{e} (n=3)	33 ± 4^{g} (n=3)	33 ±3^{k} (n=3)	38 ±0^{m} (n=3)
S_WT	79 ± 4^{a} (n=5)	39 ± 1^{c} (n=2)	82 ± 6^{e} (n=2)	40 ± 11^{g} (n=2)	86 ± 3^{k} (n=2)	48 ±5^{m} (n=2)	53 ±2^{a} (n=5)	38 ± 0^{c} (n=2)	59 ±2^{e} (n=2)	31 ± 3^{g} (n=2)	56 ± 2^{k} (n=2)	50 ±4^{m} (n=2)
S_*rth3*	81 ± 7^{a} (n=5)	37 ± 20^{c} (n=2)	82 ±10^{c} (n=2)	42 ±27^{g} (n=2)	87 ±3^{k} (n=2)	40 ±22^{m} (n=2)	52 ±5^{a} (n=5)	36 ± 10^{c} (n=2)	45 ± 2^{e} (n=2)	42 ± 20^{g} (n=2)	46 ± 4^{k} (n=2)	51 ± 3^{m} (n=2)
Overall mean	**72 ± 3 (n=21)**	**35 ±4 (n=10)**	**67 ± 6 (n=10)**	**40 ± 5 (n=10)**	**70 ±5 (n=10)**	**47 ±5 (n=10)**	**47 ±3 (n=21)**	**32 ± 3 (n=10)**	**41 ± 5 (n=10)**	**35 ± 3 (n=10)**	**42 ± 4 (n=10)**	**42 ± 3 (n=10)**
	Two-way ANOVA											
Substrate	***0.0277****	*0.780*	***0.0234****	*0.929*	***0.0386****	*0.584*	***0.0276****	*0.331*	*0.136*	*0.994*	***0.0805***	***0.0586***
Genotype	*0.9686*	*0.809*	*0.6630*	*0.458*	*0.6751*	*0.331*	*0.7926*	*0.851*	*0.883*	*0.950*	*0.4839*	*0.5176*
*Substrate * Genotype*	*0.9129*	*0.722*	*0.8779*	*0.817*	*0.7084*	*0.817*	*0.9851*	*0.636*	*0.420*	*0.574*	*0.8253*	*0.6363*

2.5.4.6 *Spatial dynamics along the root axis*

While average parameters within each spatial domain are useful to report general trends of soil texture and genotypes, the high variability within and between replicates mostly only showed non-significant differences. Thus, we conducted a more spatially resolved analysis to identify differences occurring along the root in axial direction and to unravel potential treatment effects. Younger root tissues (<2 cm from root cap) were 0.35-0.68 pH units more acidic than older root tissues (>4 cm from root cap) with wild-type root tips being generally more acidic than tips of root-hair defective mutant (*rth3*), irrespective of the substrate (Fig. 6, Table S6). pH values on the older root sections were not significantly different from bulk soil pH (Table S6). Acid phosphatase was slightly higher at younger root tissue than at older ones, but no genotype or substrate effect could be observed. For P and Mn flux at young and older root tissue no significant trend was observed due to the large variability between roots.

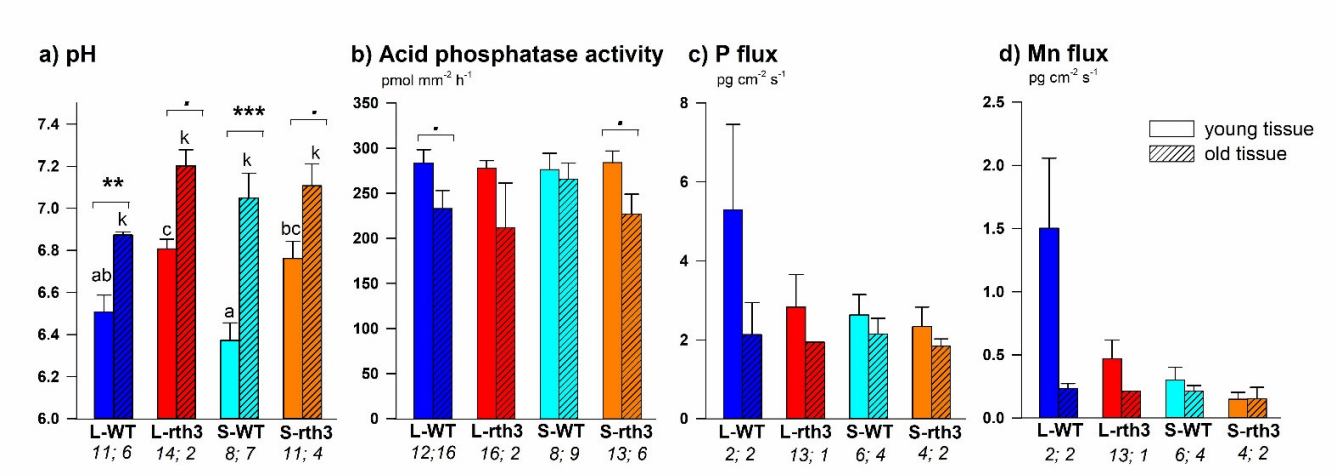

Figure 6. Spatial differences along root axis: Root surface pH (a), and acid phosphatase activity (b), P (c) and Mn flux (d) of young (< 2 cm from root cap) and older root tissue (> 4 cm from root cap). Number below each bar represents replicates (individual root sections on which the parameter was measured). Asterisks indicate significant differences between young and older tissues (*t-test* with '.' $p < 0.10$, '*' $p < 0.05$, '**' $p < 0.01$). Letters indicate significant differences between the treatments for young tissues (a-c) and old tissues (k) (two-way ANOVA $p < 0.05$, Tukey post-hoc test).

2.5.5 Discussion

2.5.5.1 *Methodological challenges*

For the first time, planar optodes, zymography, and DGT were successfully combined under field conditions to visualize pH, acid phosphatase activity and labile P and Mn around roots of older maize plants (growth stage BBCH 59) grown in a real agroecosystem environment with

uncontrolled weather conditions, which would not have been possible in the laboratory. However, working in the field, the following conditions challenged image analysis which need to be considered when interpreting our findings: i) root tips were growing during and between the method applications (total duration for individual root window: 2-3 days), which made image overlay and co-localization analysis more difficult; ii) contact between probes and soil/root was not always perfect and more difficult to control compared to lab conditions; iii) especially in loam, large pores between big aggregates inhibited diffusion and contributed to a high degree of variability; iv) high root density, overlapping rhizospheres combined with generally small regions of interest (especially for DGT) limited the root-free areas on the analysed images and the number of replicates of comparable root types and sections; v) areas obviously affected by artefacts needed to be excluded from analysis reducing the number of actually analysed replicates (for details see Table 2); vi) due to the dense root systems and the presence of 2-5 plants per root window, we were not able to identify different root types, *e.g.* embryonal primary and seminal roots, shoot-borne crown roots, and laterals of several orders, which all possess different functions in terms of nutrient and water acquisition, transport, anchorage (Hochholdinger et al., 2004); vii) aligning of images with different resolution is prone to error due to small inaccuracies in scaling and rectification, if the angle of root photographs was not perfectly orthogonal. Despite these difficulties, we investigated general trends of root surface and rhizosphere pH, phosphatase activity and labile P and Mn drivenby soil substrate and the presence of root hairs by averaging over different root types and positions along the root with different root diameters (*i.e.*, cap, elongation zone, root-hair zone, mature parts) and across as many technical replicates as possible.

In addition to the challenge of actively growing roots during our chemical imaging campaign, the consecutive application of different imaging techniques could potentially introduce a bias in our results as one imaging technique could affect the results of the following one. However, we observed the same general trends in our images from both substrates, even though the image technique application sequence differed between both substrates (Table 2). Consequently, we rule out any significant influence of the previously applied imaging technique to the results of the following one. Furthermore, maximum P input after zymography application can be expected to be around 0.003 ng cm^{-2} (maximum potential mass accumulation on a DGT that can be derived from a soaked membrane after 1h membrane application with a 10x20cm membrane soaked in 5 mL 3.3 mM MUF-P), which is negligible compared to the bulk soil DGT-P accumulation in our soils > 100 ng cm^{-2} (mass accumulation on a DGT sampler after 24h application period, corresponds to a P flux > 1.16 pg cm^{-2} s^{-1}, Figure 3 & 4). Although pH optodes

were pre-equilibrated in 20 mM L^{-1} phosphate buffer, the optode matrix does not chemically interact with P and optodes were carefully rinsed before application (see more details below), consequently rendering it unlikely to affect detected P fluxes.

2.5.5.2 Acidification

We attribute the steeper rhizosphere gradients of pH in sand compared to loam irrespective of genotype (Fig. 3) to the higher pH buffer capacity of loam due to the greater presence of secondary minerals, clay, and organic matter (Table 1). Moreover, the effective diffusion coefficient of protons is larger in sand compared to loam (Olesen et al., 2001) contributing to ~0.45 mm larger rhizosphere extents in sand (on average 1.35 mm) than in loam (on average 0.89 mm, Fig. 3). Similar rhizosphere extents were also found for younger maize crown roots by Rudolph-Mohr et al. (2017), who observed acidification up to 1 pH unit within 0.75-1.5 mm from the root surface in a sandy soil.

Rhizosphere acidification under P limiting conditions has often been associated with the release of organic acids. However, organic acids only marginally contribute (0.2-0.3%) to acidification by maize roots as they are exuded as deprotonated acid anions due to their low p*Ka* and a cytosolic pH of around 7 (Hinsinger, 2001; Jones, 1998; Petersen and Böttger, 1991). Also, the release of protons to maintain the charge balance upon NH_4^+ uptake was often linked to rhizosphere acidification (Hinsinger et al., 2003; Prjanischnikow, 1929; Sorrell and Orr, 1993). In our case, extrusion of protons by maize roots according to the acid growth theory seems more likely, as acidification occurred mainly around root tips and young root tissue which actively grew during optode application (~12h) (Fig. S2). According to the acid growth theory, the extrusion of protons from the cytosol through plasma membrane into the apoplast supports the loosening of the cell wall stimulating cellexpansion (Hager, 2003). At the end of cell growth the calcium ion concentration in the cytosol is increased which inhibits the H+-ATPase activity raising the apoplastic pH consequently halting wall expansion. (Majda and Robert, 2018). The pH measured on the surface of young root tissue of the wild-type was 0.3-0.4 pH units more acidic than that of young root parts of the root-hair defective mutant (*rth3*) also supports that root tissue growth coincides with rhizosphere acidification as our observations can be linked to the growth of root hairs. Furthermore, the observed increased in labile calcium concentration in the DGT images of growing root tissues (Fig. S5) would suggest that some of this Ca is released from the cytosol during this signalling cascade.

2.5.5.3 Root and microbially-derived acid phosphatase activity

Similar to pH, acid phosphatase activity rhizosphere extents were larger in sand than in loam, but neither average root surface nor average rhizosphere acid phosphatase activity differed significantly between the genotypes or substrates (Fig. 4b). As enzyme diffusion in soil is negligible (Guber et al., 2018), we attribute the larger rhizosphere extent to a greater activity of phosphatase-releasing microbes in the rhizosphere of sand-grown maize. Maize derived root exudates (*i.e.*, C-containing primary and secondary metabolites released by roots) (Bilyera et al., 2021, Santageli et al., in prep) can be expected to be more strongly sorbed in loam than in sand hence limiting exudate diffusion and consequently the extent of their microbial stimulation effect in loam. Moreover, sorption of extracellular enzymes to soil minerals can protect them from degradation and change their biochemical properties and thus their activity and persistence in soil. The specific activity of enzymes was found to be higher after sorption to a soil with a low sorption site availability, such as the sand in our study, compared to soils with more abundant sorption sites, *i.e.*, the loam (Olagoke et al., 2020, 2019), which possibly also explains the larger rhizosphere extent in sand.

In contrast to other studies investigating different species, we did not find a significant effect of root hairs on phosphatase activity and its related rhizosphere extent. Root hairs of this maize genotype were with only ~0.24 mm (Lippold et al., 2021) rather short compared to other species such as barley, which could explain why we did not observe a clear genotype effect on the rhizosphere extents. Nevertheless, similar acid phosphatase rhizosphere extents of around 1 mm were found by Kandeler et al. (2002) after soil slicing (resolution 0.2 mm) or by Ma et al. (2018) (1-2 mm measured with zymography from the root centre) and Razavi et al. (2016) for younger maize plants (7-21 days old). Nevertheless, our results are comparable to these zymography studies when adding the root radii (ranging from 0.1-1.0 mm) to the rhizosphere extents.

Efficacy of phosphatases generally depends on P_o availability and P esters might strongly sorb to the soil solid-phase (Huang et al., 2005), which limits hydrolysis by phosphatases (Gerke, 2015). In loam, P_o (estimated from soil organic matter, Section S4) was nearly 6-times higher compared to sand. Hence, in loam similar phosphatase activities in the rhizosphere could have mobilized a larger amount of phosphate from P_o compared to sand.

In contrast to the rather homogenous distribution of phosphatase activity along the entire root for barley (Holz et al., 2020), we found a trend of higher phosphatase activity on young compared to older root sections which was significant ($p<0.01$) for L-WT and S-rth3 (Fig. 6, Table S6). Holz et al. (2020) found that 4-week-old root-hairless barley had higher phosphatase activity

than the wild-type barley which developed larger acid phosphatase rhizosphere extents in the root hair zone than the mutant. Contrastingly, in this study the influence of root hairs on acid phosphatase activity was negligible for 12-week-old maize (Fig. 4b).

2.5.5.4 P flux

DGT images provide a snapshot of labile nutrient patterns on the root and in the rhizosphere that are determined by mobilization and immobilization processes. Despite no clear treatment effect on average P flux in any spatial domain and no clear trends for P flux gradients, the slightly lower average rhizosphere P flux (Fig. 4c) as well as the darker areas in the P flux images around older root tissues (white arrows in Fig. 2) indicate the development of P depletion zones. As already discussed and despite the high sensitivity of DGT-LA-ICPMS (*i.e.,* low limits of detection), poor contact due to the presence of large pores, and a small share of root-free area within the small DGT-ROIs led to bulk soil values with a high variability. Moreover, averaging of old and young root sections and different root types could hamper the detection of P depletion zones. The size of a depletion zone around a root generally depends on the soil texture, P availability, age of the root (Hübel and Beck, 1993) and varies along the root, as P uptake is usually highest within the first cm from the tip (Colmer and Bloom, 1998; Fang et al., 2007; Marschner et al., 2011; Santner et al., 2012) and gradually decreases along the root axis as root hairs decrease (De Bauw et al., 2021; White et al., 2013). If replenishment of depletion zones around older and rather inactive root sections occurred over a longer period, depletion zones cannot be observed any more. This is favoured in soils having a high sorption capacity (Hübel and Beck, 1993) establishing new equilibrium conditions over time, which was likely the case in the loam. However, in sand the lower P binding on Al and Fe oxides, higher diffusion, and faster desorption kinetics (Menezes-Blackburn et al., 2016; Smolders et al., 2020) might also allow fast replenishment. Moreover, phosphate hydrolysed by phosphatases could also cause replenishment of depletion zones of older root sections, especially as phosphatases were homogenously distributed along the roots.

The observed high labile P flux on the root surface of young root tissues could originate either from the growing root itself or from the soil. Possible reasons could be P released from sloughed off cells as proposed by Santner et al. (2012) or P efflux from root tips which depends on P supply and was previously observed even under P deficient conditions (Cogliatti and María, 1990; Elliott et al., 1984). As DGT images visualize the result (i.e. labile P) of several processes occurring simultaneously, it is not possible to distinguish between individual processes.

2.5.5.5 Mn flux

Mn is highly sensitive to changes in pH and redox conditions in the rhizosphere (Husson, 2013; Rengel, 2015). Therefore, solubility of Mn in the rhizosphere might increase due to acidification or the exudation of organic compounds capable of complexing Mn. Even though we did not directly measure the redox potential, Mn solubility could be also increased by oxygen depletion caused by root and microbial respiration (Rengel, 2015; Sparrow and Uren, 1987). Moreover, soil organic matter mineralization in the rhizosphere by microorganisms, *i.e.*, oxidation, is often accompanied by Mn reduction which is optimal at pH 6–7 (Myers and Nealson, 1988), and can explain elevated rhizosphere Mn flux at sites of higher carbon (*e.g.* exudate) turnover and acidification. The often homogenous Mn distribution along the roots and the high degree of co-localisation of phosphatase activity and Mn (70±5%) on the root surface also suggests that we potentially analysed Mn present in acid phosphatases that might have bound to the DGT gel, as these metallo-enzymes consist of Fe^{3+}-Mn^{2+} centres (Carboni and Latour, 2011; Schenk et al., 2013) which are required co-factors for activation (Schmidt and Husted, 2019; Smith and Walker, 1991).

2.5.5.6 Interactions of P solubilisation processes in the rhizosphere

Overlap coefficients for pH-phosphatase, pH-Mn and phosphatase-Mn on the root surface were in a similar range around 70% which suggests interactions of all 3 parameters as root-induced processes. The high co-occurrence of acidification and acid phosphatase hotspots indicates that protons released by roots shifted the pH optimum (*i.e.*, pH < 7) in favour for increased acid phosphatase activity (Dick et al., 2000). Even though average overlap coefficients of P flux hotspots with acidification or acid phosphatase hotspots were generally low on different root segments, root tips showed co-localized hotspots of acidification, phosphatase activity, P flux (Fig. S4), Mn flux (Fig. S4) and Zn flux (Fig. S6). The root tips and elongation zone growing into previously P-undepleted soil are more biochemically active than basal parts of the root and are thus the main contributors to overall P uptake (De Bauw et al., 2020). The co-occurrence of pH < 7 and elevated acid phosphatase activity is hence especially favourable at the major sites of P uptake, *i.e.*, young root tissues. Mn and Zn are often co-mobilized by P-deficiency-induced rhizosphere processes such as acidification and organic acids (Kreuzeder et al., 2018; Lambers et al., 2015; Neumann and Romheld, 2002). Co-localized P, Mn and Zn fluxes hence suggest that elevated P fluxes around root tips are at least partly derived from soil mobilization processes.

In sand, co-localisation coefficients of acidification and acid phosphatase activity were higher than in loam which is in line with the slightly higher hotspot coverage and (slightly) larger rhizosphere extents of both parameters in sand compared to patchier distribution along the roots in loam. The higher hotspot coverage of pH, acid phosphatase activity and Mn on the root surface in sand may indicate more pronounced root processes in response to P-limitation (*i.e.* lower total P and P_{CAL}, Table 1) or may be a result of less sorption or improved detection due to better sensor-soil contact in sand. Due to the higher amount of Ca-phosphates deriving from the fertilization in sand, acidification might be more important in terms of P solubilization because solubility of Ca-phosphates increases with lower pH (Penn and Camberato, 2019). But the effect of fertilization was likely restricted to the upper parts of the plots as the P fertilizer was surface applied and was limited as reflected by the generally lower P contents in maize grown on sand. The higher presence of organic P (Section S4) suggests that, in loam, acid phosphatase activity played a more prominent role in plant P nutrition compared to the sand. Due to the relatively short root hairs (0.24 mm; (Lippold et al., 2021), we did not observe a clear effect of root hairs on average rhizosphere extents of acidification and acid phosphatase activity. However, WT root tips were more acidic than *rth3* tips, potentially contributing to locally increased P solubility and uptake. As we could not observe increased P fluxes in WT (Fig. 2 and S4), the higher P contents in WT compared to *rth3* are most likely related to the higher absorption surface due to the presence of root hairs leading to greater P uptake despite similar extent and intensity of P solubilizing processes in the rhizosphere of both maize genotypes.

2.5.6 Conclusion & perspectives

For the first time, we visualised multiple P mobilization processes, *i.e.*, rhizosphere acidification, acid phosphatase activity as well as labile P and Mn *in situ* on and around field-grown maize roots at the transition of vegetative to reproductive growth (BBCH 59). Images showed a strong patchiness of root and rhizosphere hotspot activities/concentrations and a large variability between replicates, which necessitated elaborate image analysis. To obtain more robust results under field conditions, we suggest increasing particularly the number of applied DGT gels to at least 12-16 per treatment to increase the number of replicates suitable for analysis to 3-4, considering that only ¼ from the total applied DGTs were suitable for analysis in our study. This should be considered in experimental and financial planning of future field studies. Additionally, the area of the ROI should be larger to ensure that tips are not growing out of the ROI during application. Moreover, keeping the time between the individual methods as short as possible should provide more replicates suitable for co-localization analysis. Nevertheless, our

novel strategy to integrate data of average rhizosphere gradients, average concentrations/activities within defined spatial domains (root surface, rhizosphere, bulk soil), hotspot coverage and co-localization within each domain and over different positions along the root axis enabled identification of root hair and substrate effects in the field.

We found average rhizosphere extents up to 1.6 mm for acidification, acid phosphatase activity and Mn flux, but could not define them for P depletion presumably due to the co-occurrence of P mobilizing processes and rapid P uptake. The presence of root-hairs (with a relatively short length of about 0.24 mm) did not significantly increase the average intensity or rhizosphere extent of any parameter, while the soil substrate, *i.e.*, texture and soil organic matter and the associated content of organic P, had a more pronounced impact. In sand average rhizosphere extents for acid phosphatase activity were ~1 mm larger, and average rhizosphere acidification showed steeper gradients and was ~0.1 pH units stronger than loam. We attribute these findings to the lower buffer capacity and more pronounced diffusion of solutes in the sand compared to loam. Furthermore, acidification was observed mainly around young root tissues (<2 cm from root cap) and wild-type tips were more acidic than tips of root-hair defective *rth3.* High P flux co-localized with acidification at root tips. Acidification was likely linked to root growth and created a pH optimum for acid phosphatase activity, (i.e., transformation of P_o to available phosphate) and P uptake especially at the root tips and within the elongation zone which are the major sites of P uptake. Due to the higher P availability, both genotypes grew better in loam than in sand; however, the presence of root hairs resulted in a higher P uptake and greater shoot biomass production of WT compared to *rth3*.

The combined imaging of phosphatase activity, soil pH and nutrient gradients *in situ* revealed that individual P solubilizing processes co-localized and interacted in the rhizosphere. Our results also demonstrate the challenge to find significant and clear trends under field conditions as several processes occur simultaneously, *i.e.*, mobilization, solubilization, desorption, enzymatic conversion of P_o to P_i, microbial mobilization, and immobilization as well as P uptake. P mobilization in the rhizosphere is thus often masked by competitive and rapid P uptake by roots and microbes. Moreover, different root types and changing parameter dynamics along the roots exhibited a large variability affecting average trends, which should be considered for modelling studies. Nevertheless, imaging techniques are non-destructive, can be applied *in situ* in both lab and field studies and can easily be coupled with other methods such as localized sampling for analysis of soil properties, microbes, or exudates to get a better understanding of soil-root-microorganism interactions. Our presented approach of stepwise integration of imaging

data can also further be applied in nutrient cycling models and upscaling scenarios from the single root to (field) plot scale.

2.5.7 Acknowlegments

This work was conducted within the framework of the priority program 2089, funded by the Deutsche Forschungsgemeinschaft (DFG, German Research Foundation) – Project numbers: 403803214 (EO), 403670038 (BSR & SSP), 403801423 (DV), 403640293 (DV & SSL). Seeds of the maize mutant *rth3* were provided by Caroline Marcon and Frank Hochholdinger (University of Bonn). An exchange between the universities of Kiel and Montpellier was funded by a German Academic Exchange Service (DAAD) scholarship (57445354, BSR & IB). GD and IB received funding from the PHC PROCOPE programme (GD, IB). CH was partly funded by Gesellschaft für Forschungsförderung Niederösterreich m.b.H. (SC17-015). JS received funding from the Austrian Science Fund (FWF) and the Federal State of Lower Austria (P27571-BBL). EO was also supported by the ERC StG 801954 PhytoTrace. Authors gratefully acknowledge Gottfried Wieshammer from Technisches Büro für Bodenkultur, Austria (gottfried.wieshammer@aon.at) for his part in designing and constructing the root windows, as well as project coordinator Susanne Schreiter and Sebastian Häusler for their great organizational help during the application of our imaging methods in the field.

2.5.8 References

Baldovinos, F., Thomas, G.W., 1967. The Effect of Soil Clay Content on Phosphorus Uptake. Soil Science Society of America Journal 1, 2–4. doi:https://doi.org/10.2136/sssaj1967.03615995003100050020x

Barrow, N.J., 2017. The effects of pH on phosphate uptake from the soil. Plant and Soil 410, 401–410. doi:10.1007/s11104-016-3008-9

Barrow, N.J., Debnath, A., Sen, A., 2020. Measurement of the effects of pH on phosphate availability. Plant and Soil 454, 217–224. doi:10.1007/s11104-020-04647-5

Bauke, S.L., Landl, M., Koch, M., Hofmann, D., Nagel, K.A., Siebers, N., Schnepf, A., Amelung, W., 2017. Macropore effects on phosphorus acquisition by wheat roots – a rhizotron study. Plant and Soil 416, 67–82. doi:10.1007/s11104-017-3194-0

Bertrand, I., Hinsinger, P., Jaillard, B., Arvieu, J.C., 1999. Dynamics of phosphorus in the rhizosphere of maize and rape grown on synthetic, phosphated calcite and goethite. Plant and Soil 211, 111–119. doi:10.1023/A:1004328815280

Bilyera, N., Zhang, X., Duddek, P., Fan, L., Banfield, C.C., Schlüter, S., Carminati, A., Kaestner, A., Ahmed, M.A., Kuzyakov, Y., Dippold, M.A., Spielvogel, S., Razavi, B.S., 2021. Maize genotype-specific exudation strategies: an adaptive mechanism to increase microbial activity in the rhizosphere. Soil Biology and Biochemistry 162, 108426. doi:10.1016/j.soilbio.2021.108426

Bleiholder, H., Weber, E., Lancashire, P.D., Feller, C., Burh, L., Hess, M., Wicke, H., Hack, H., Meier, U., Klose, R., van den Boom, T., Strauss, R., 2001. Growth stages of mono-and dicotyledonous plants. BBCH Monograph, Second. ed, Federal Biological Research Centre for Agriculture and Forestry.

Blossfeld, S., Gansert, D., 2007. A novel non-invasive optical method for quantitative visualization of pH dynamics in the rhizosphere of plants. Plant, Cell and Environment 30, 176–186. doi:10.1111/j.1365-3040.2006.01616.x

Bolte, S., Cordelières, F.P., 2006. A guided tour into subcellular colocalization analysis in light microscopy. Journal of Microscopy. doi:10.1111/j.1365-2818.2006.01706.x

Carboni, M., Latour, J.M., 2011. Enzymes with an heterodinuclear iron-manganese active site: Curiosity or necessity? Coordination Chemistry Reviews 255, 186–202. doi:10.1016/j.ccr.2010.08.003

Carter, M.R., Gregorich, E.G., 2007. Soil Sampling and Methods of Analysis, 2d ed. CRC Press, Boca Raton, FL, USA. doi:10.1201/9781420005271

Cogliatti, D.H., María, G.E.S., 1990. Influx and efflux of phosphorus in roots of wheat plants in non-growth-limiting concentrations of phosphorus. Journal of Experimental Botany 41, 601–607. doi:10.1093/jxb/41.5.601

Colmer, T.D., Bloom, A.J., 1998. A comparison of NH4+ and NO3- net fluxes along roots of rice and maize. Plant, Cell and Environment 21, 240–246. doi:10.1046/j.1365-3040.1998.00261.x

Daly, K.R., Keyes, S.D., Masum, S., Roose, T., 2016. Image-based modelling of nutrient movement in and around the rhizosphere. Journal of Experimental Botany 67, 1059–1070. doi:10.1093/jxb/erv544

De Bauw, P., Mai, T.H., Schnepf, A., Merckx, R., Smolders, E., Vanderborght, J., 2020. A functional-structural model of upland rice root systems reveals the importance of laterals and growing root tips for phosphate uptake from wet and dry soils. Annals of Botany 126, 789–806. doi:10.1093/aob/mcaa120

De Bauw, P., Smolders, E., Verbeeck, M., Senthilkumar, K., Houben, E., Vandamme, E., 2021. Micro-dose placement of phosphorus induces deep rooting of upland rice. Plant and Soil. doi:10.1007/s11104-021-04914-z

Demidchik, V., Shabala, S., Isayenkov, S., Cuin, T.A., Pottosin, I., 2018. Calcium transport across plant membranes: mechanisms and functions. New Phytologist 220, 49–69. doi:10.1111/nph.15266

Dick, W.A., Cheng, L., Wang, P., 2000. Soil acid and alkaline phosphatase activity as pH adjustment indicators. Soil Biology and Biochemistry 32, 1915–1919. doi:doi.org/10.1016/S0038-0717(00)00166-8

Dinkelaker, B., Marschner, H., 1992. In vivo demonstration of acid phosphatase activity in the rhizosphere of soil-grown plants. Plant and Soil 144, 199–205. doi:10.1007/BF00012876

Dong, S., Brooks, D., Jones, M.D., Grayston, S.J., 2007. A method for linking in situ activities of hydrolytic enzymes to associated organisms in forest soils. Soil Biology and Biochemistry 39, 2414–2419. doi:10.1016/j.soilbio.2007.03.030

Elliott, G.C., Lynch, J., Läuchli, A., 1984. Influx and efflux of P in roots of intact maize plants: Double-labeling with 32P and 33P. Plant Physiology 76, 336–341. doi:10.1104/pp.76.2.336

Fang, Y.Y., Babourina, O., Rengel, Z., Yang, X.E., Pu, P.M., 2007. Spatial distribution of ammonium and nitrate fluxes along roots of wetland plants. Plant Science 173, 240–246. doi:10.1016/j.plantsci.2007.05.006

Gahoonia, T.S., Nielsen, N.E., Joshi, P.A., Jahoor, A., 2001. A root hairless barley mutant for elucidating genetic of root hairs and phosphorus uptake. Plant and Soil 235, 211–219. doi:10.1023/A:1016252614393

George, T.S., Giles, C.D., Menezes-Blackburn, D., Condron, L.M., Gama-Rodrigues, A.C., Jaisi, D., Lang, F., Neal, A.L., Stutter, M.I., Almeida, D.S., Bol, R., Cabugao, K.G., Celi, L., Cotner, J.B., Feng, G., Goll, D.S., Hallama, M., Krueger, J., Plassard, C., Rosling, A., Darch, T., Fraser, T., Giesler, R., Richardson, A.E., Tamburini, F., Shand, C.A., Lumsdon, D.G., Zhang, H., Blackwell, M.S.A., Wearing, C., Mezeli, M.M., Almås, Å.R., Audette, Y., Bertrand, I., Beyhaut, E., Boitt, G., Bradshaw, N., Brearley, C.A., Bruulsema, T.W., Ciais, P., Cozzolino, V., Duran, P.C., Mora, M.L., de Menezes, A.B., Dodd, R.J., Dunfield, K., Engl, C., Frazão, J.J., Garland, G., González Jiménez, J.L., Graca, J., Granger, S.J., Harrison, A.F., Heuck, C., Hou, E.Q., Johnes, P.J., Kaiser, K., Kjær, H.A., Klumpp, E., Lamb, A.L., Macintosh, K.A., Mackay, E.B., McGrath, J., McIntyre, C., McLaren, T., Mészáros, E., Missong, A., Mooshammer, M., Negrón, C.P., Nelson, L.A., Pfahler, V., Poblete-Grant, P., Randall, M., Seguel, A., Seth, K., Smith, A.C., Smits, M.M., Sobarzo, J.A., Spohn, M., Tawaraya, K., Tibbett, M., Voroney, P., Wallander, H., Wang, L., Wasaki, J., Haygarth, P.M., 2018. Organic phosphorus in the terrestrial environment: a perspective on the state of the art and future priorities. Plant and Soil 427, 191–208. doi:10.1007/s11104-017-3391-x

Gerke, J., 2015. The acquisition of phosphate by higher plants: Effect of carboxylate release by the roots. A critical review. Journal of Plant Nutrition and Soil Science 178, 351–364. doi:10.1002/jpln.201400590

Grierson, P.F., Comerford, N.B., 2000. Non-destructive measurement of acid phosphatase activity in the rhizosphere using nitrocellulose membranes and image analysis. Plant and Soil 218, 49–57. doi:10.1023/a:1014985327619

Guber, A., Kravchenko, A., Razavi, B.S., Uteau, D., Peth, S., Blagodatskaya, E., Kuzyakov, Y., 2018. Quantitative soil zymography: Mechanisms, processes of substrate and enzyme diffusion in porous media. Soil Biology and Biochemistry 127, 156–167. doi:10.1016/j.soilbio.2018.09.030

Hager, A., 2003. Role of the plasma membrane H+-ATPase in auxin-induced elongation growth: Historical and new aspects. Journal of Plant Research 116, 483–505. doi:10.1007/s10265-003-0110-x

Hahn, G., Marschner, H., 1998. Effect of acid irrigation and liming on root growth of Norway spruce. Plant and Soil 199, 11–22.

Hinsinger, P., 2001. Bioavailability of soil inorganic P in the rhizosphere as affected by root-induced chemical changes: A review, in: Plant and Soil. pp. 173–195. doi:10.1023/A:1013351617532

Hinsinger, P., Plassard, C., Tang, C., Jaillard, B., 2003. Origins of root-mediated pH changes in the rhizosphere and their responses to environmental constraints: A review. Plant and Soil 248, 43–59. doi:10.1023/A:1022371130939

Hochholdinger, F., Wen, T.-J., Zimmermann, R., Chimot-Marolle, P., da Costa e Silva, O., Bruce, W., Lamkey, K.R., Wienand, U., Schnable, P.S., 2008. The maize (Zea mays L.) roothairless3 gene encodes a putative GPI-anchored, monocot-specific, COBRA-like protein that significantly affects grain yield. The Plant Journal 54, 888–898. doi:10.1111/j.1365-313X.2008.03459.x

Hochholdinger, F., Woll, K., Sauer, M., Dembinsky, D., 2004. Genetic dissection of root formation in maize (Zea mays) reveals root-

type specific developmental programmes. Annals of Botany 93, 359–368. doi:10.1093/aob/mch056

Hochholdinger, F., Yu, P., Marcon, C., 2018. Genetic Control of Root System Development in Maize. Trends in Plant Science 23, 79–88. doi:10.1016/j.tplants.2017.10.004

Holz, M., Zarebanadkouki, M., Carminati, A., Becker, J.N., Spohn, M., 2020. The effect of root hairs on rhizosphere phosphatase activity. Journal of Plant Nutrition and Soil Science 000, 1–7. doi:10.1002/jpln.201900426

Huang, Q., Liang, W., Cai, P., 2005. Adsorption, desorption and activities of acid phosphatase on various colloidal particles from an Ultisol. Colloids and Surfaces B: Biointerfaces 45, 209–214. doi:10.1016/j.colsurfb.2005.08.011

Hübel, F., Beck, E., 1993. In-situ determination of the P-relations around the primary root of maize with respect to inorganic and phytate-P. Plant and Soil 157, 1–9. doi:10.1007/bf00038742

Hummel, C., Boitt, G., Santner, J., Lehto, N.J., Condron, L., Wenzel, W.W., 2021. Co-occurring increased phosphatase activity and labile P depletion in the rhizosphere of Lupinus angustifolius assessed with a novel, combined 2D-imaging approach. Soil Biology and Biochemistry 153. doi:10.1016/j.soilbio.2020.107963

Husson, O., 2013. Redox potential (Eh) and pH as drivers of soil/plant/microorganism systems: A transdisciplinary overview pointing to integrative opportunities for agronomy. Plant and Soil 362, 389–417. doi:10.1007/s11104-012-1429-7

Itoh, S., Barber, S.A., 1983. A numerical solution of whole plant nutrient uptake for soil-root systems with root hairs. Plant and Soil 70, 403–413. doi:10.1007/BF02374895

Jones, D.L., 1998. Organic acids in the rhizosphere – a critical review. Plant and Soil 205, 25–44. doi:10.1023/A:1004356007312

Jones, D.L., Oburger, E., 2011. Solubilization of Phosphorus by Soil Microorganisms, in: Bünemann, E., Oberson, A., Frossard, E. (Eds.), Phosphorus in Action, Soil Biology. Springer Berlin Heidelberg, Berlin, Heidelberg, pp. 215–243. doi:10.1007/978-3-642-15271-9

Jungk, A., 2001. Root hairs and the acquisition of plant nutrients from soil. Journal of Plant Nutrition and Soil Science 164, 121–129. doi:10.1002/1522-2624(200104)164:2<121::AID-JPLN121>3.0.CO;2-6

Kandeler, E., Marschner, P., Tscherko, D., Singh Gahoonia, T., Nielsen, N.E., 2002. Microbial community composition and functional diversity in the rhizosphere of maize. Plant and Soil 238, 301–312. doi:10.1023/A:1014479220689

Kreuzeder, A., Santner, J., Prohaska, T., Wenzel, W.W., 2013. Gel for simultaneous chemical imaging of anionic and cationic solutes using diffusive gradients in thin films. Analytical Chemistry 85, 12028–12036. doi:10.1021/ac403050f

Kreuzeder, A., Santner, J., Scharsching, V., Oburger, E., Hoefer, C., Hann, S., Wenzel, W.W., 2018. In situ observation of localized, sub-mm scale changes of phosphorus biogeochemistry in the rhizosphere. Plant and Soil 424, 573–589. doi:10.1007/s11104-017-3542-0

Kuzyakov, Y., Razavi, B.S., 2019. Rhizosphere size and shape: Temporal dynamics and spatial stationarity. Soil Biology and Biochemistry 135, 343–360. doi:10.1016/J.SOILBIO.2019.05.011

Lambers, H., Hayes, P.E., Oliveira, R.S., Laliberte, E., Turner, B.L., 2015. Leaf manganese accumulation and phosphorus-acquisition efficiency. Trends in Plant Science. doi:10.1016/j.tplants.2014.10.007

Lang, F., Bauhus, J., Frossard, E., George, E., Kaiser, K., Kaupenjohann, M., Krüger, J., Matzner, E., Polle, A., Prietzel, J., Rennenberg, H., Wellbrock, N., 2016. Phosphorus in forest ecosystems: New insights from an ecosystem nutrition perspective. Journal of Plant Nutrition and Soil Science 2015, 129–135. doi:10.1002/jpln.201500541

Lippold, E., Phalempin, M., Schlüter, S., Vetterlein, D., 2021. Does the lack of root hairs alter root system architecture of Zea mays? Plant and Soil. doi:10.1007/s11104-021-05084-8

Lucas, M., Schlüter, S., Vogel, H., Vetterlein, D., 2019. Roots compact the surrounding soil depending on the structures they encounter. Scientific Reports 9, 16236. doi:10.1038/s41598-019-52665-w

Ma, X., Liu, Y., Shen, W., Kuzyakov, Y., 2021. Phosphatase activity and acidification in lupine and maize rhizosphere depend on phosphorus availability and root properties : Coupling zymography with planar optodes. Applied Soil Ecology 167, 104029. doi:10.1016/j.apsoil.2021.104029

Ma, X., Zarebanadkouki, M., Kuzyakov, Y., Blagodatskaya, E., Pausch, J., Razavi, B.S., 2018. Spatial patterns of enzyme activities in the rhizosphere: Effects of root hairs and root radius. Soil Biology and Biochemistry 118, 69–78. doi:10.1016/j.soilbio.2017.12.009

Majda, M., Robert, S., 2018. The role of auxin in cell wall expansion. International Journal of Molecular Sciences 19. doi:10.3390/ijms19040951

Manzoor, M., Abbasi, M.K., Sultan, T., 2017. Isolation of Phosphate Solubilizing Bacteria from Maize Rhizosphere and Their Potential for Rock Phosphate Solubilization–Mineralization and Plant Growth Promotion. Geomicrobiology Journal 34, 81–95. doi:10.1080/01490451.2016.1146373

Marschner, H., Häussling, M., George, E., 1991. Ammonium and nitrate uptake rates and rhizosphere pH in non-mycorrhizal roots of Norway spruce [Picea abies (L.) Karst.]. Trees 5, 14–21. doi:10.1007/BF00225330

Marschner, P., Crowley, D., Rengel, Z., 2011. Rhizosphere interactions between microorganisms and plants govern iron and

phosphorus acquisition along the root axis - model and research methods. Soil Biology and Biochemistry 43, 883–894. doi:10.1016/j.soilbio.2011.01.005

Mehra, O.P., Jackson, M.L., 1960. Iron oxide removal from soils and clays by a dithionite-citrate system buffered with sodium bicarbonate, in: Proc. 7th Nat. Conf. Clays. pp. 317–327.

Menezes-Blackburn, D., Zhang, H., Stutter, M., Giles, C.D., Darch, T., George, T.S., Shand, C., Lumsdon, D., Blackwell, M., Wearing, C., Cooper, P., Wendler, R., Brown, L., Haygarth, P.M., 2016. A Holistic Approach to Understanding the Desorption of Phosphorus in Soils. Environmental Science & Technology 50, 3371–3381. doi:10.1021/acs.est.5b05395

Merbach, W., Deubel, A., Gransee, A., Ruppel, S., Klamroth, A.-K., 2010. Phosphorus solubilization in the rhizosphere and its possible importance to determine phosphate plant availability in soil. A review with main emphasis on German results. Archives of Agronomy and Soil Science 56, 119–138. doi:10.1080/03650340903005640

Myers, C.R., Nealson, K.H., 1988. Bacterial Manganese Reduction and Growth with Manganese Oxide. Science 240, 1319–1321.

Neumann, G., George, T.S., Plassard, C., 2009. Strategies and methods for studying the rhizosphere-the plant science toolbox. Plant and Soil 321, 431–456. doi:10.1007/s11104-009-9953-9

Neumann, G., Romheld, V., 2002. Root-induced changes in the ability of nutrients in the rhizosphere, in: Waisel, Y., Eshel, A., Kafkafi, U. (Eds.), Plant Roots–the Hidden Half. Marcel Dekker, Inc., New York, pp. 617–649.

Oburger, E., Schmidt, H., 2016. New Methods To Unravel Rhizosphere Processes. Trends in Plant Science 21, 243–255. doi:10.1016/j.tplants.2015.12.005

Olagoke, F.K., Kaiser, K., Mikutta, R., Kalbitz, K., Vogel, C., 2020. Persistent activities of extracellular enzymes adsorbed to soil minerals. Microorganisms 8, 1–15. doi:10.3390/microorganisms8111796

Olagoke, F.K., Kalbitz, K., Vogel, C., 2019. Control of soil extracellular enzyme activities by clay minerals—perspectives on microbial responses. Soil Systems 3, 1–16. doi:10.3390/soilsystems3040064

Olesen, T., Moldrup, P., Yamaguchi, T., Rolston, D.E., 2001. Constant slope impedance factor model for predicting the solute diffusion coefficient in unsaturated soil. Soil Science 166, 89–96. doi:10.1097/00010694-200102000-00002

Penn, C.J., Camberato, J.J., 2019. A critical review on soil chemical processes that control how soil ph affects phosphorus availability to plants. Agriculture 9, 1–18. doi:10.3390/agriculture9060120

Petersen, W., Böttger, M., 1991. Contribution of organic acids to the acidification of the rhizosphere of maize seedlings. Plant and Soil 132, 159–163. doi:10.1007/BF00010396

Pierzynski, G.M., McDowell, R.M., Sims, J.T., 2005. Chemistry, cycling, and potential movement of inorganic phosphorus in soils, in: Phosphorus: Agriculture and the Environment. American Society of Agronomy, pp. 53–86.

Prjanischnikow, D., 1929. Zur Frage nach der Ammoniak Ernährung von höheren Pflanzen. Biochimische Zeitschrift 227, 341–349.

Raymond, N.S., Gómez-Muñoz, B., Bom, F.J.T., Nybroe, O., Jensen, L.S., Müller-Stöver, D.S., Oberson, A., Richardson, A.E., 2020. Phosphate-solubilising microorganisms for improved crop productivity: a critical assessment. New Phytologist nph.16924. doi:10.1111/nph.16924

Razavi, B.S., Zarebanadkouki, M., Blagodatskaya, E., Kuzyakov, Y., 2016. Rhizosphere shape of lentil and maize: Spatial distribution of enzyme activities. Soil Biology and Biochemistry 79, 229–237. doi:10.1016/j.soilbio.2016.02.020

Razavi, B.S., Zhang, X., Bilyera, N., Guber, A., Zarebanadkouki, M., 2019. Soil zymography: Simple and reliable? Review of current knowledge and optimization of the method. Rhizosphere. doi:10.1016/j.rhisph.2019.100161

Read, D.B., Bengough, A.G., Gregory, P.J., Crawford, J.W., Robinson, D., Scrimgeour, C.M., Young, I.M., Zhang, K., Zhang, X., 2003. Plant roots release phospholipid surfactants that modify the physical and chemical properties of soil. New Phytologist 157, 315–326. doi:10.1046/j.1469-8137.2003.00665.x

Rengel, Z., 2015. Availability of Mn, Zn and Fe in the rhizosphere. Journal of Soil Science and Plant Nutrition 15, 397–409. doi:10.4067/s0718-95162015005000036

Rudolph-Mohr, N., Tötzke, C., Kardjilov, N., Oswald, S.E., 2017. Mapping water, oxygen, and pH dynamics in the rhizosphere of young maize roots. Journal of Plant Nutrition and Soil Science 180, 336–346. doi:10.1002/jpln.201600120

Ruiz, S., Koebernick, N., Duncan, S., Fletcher, D.M., Scotson, C., Boghi, A., 2020. Significance of root hairs at the field scale – modelling root water and phosphorus uptake under different field conditions 281–304.

Santner, J., Zhang, H., Leitner, D., Schnepf, A., Prohaska, T., Puschenreiter, M., Wenzel, W.W., 2012. High-resolution chemical imaging of labile phosphorus in the rhizosphere of Brassica napus L. cultivars. Environmental and Experimental Botany 77, 219–226. doi:10.1016/j.envexpbot.2011.11.026

Schenk, G., Mitić, N.Š., Hanson, G.R., Comba, P., 2013. Purple acid phosphatase: A journey into the function and mechanism of a colorful enzyme. Coordination Chemistry Reviews 257, 473–482. doi:10.1016/j.ccr.2012.03.020

Schindelin, J., Arganda-Carreras, I., Frise, E., Kaynig, V., Longair, M., Pietzsch, T., Preibisch, S., Rueden, C., Saalfeld, S., Schmid, B., Tinevez, J.-Y., White, D.J., Hartenstein, V., Eliceiri, K., Tomancak, P., Cardona, A., 2012. Fiji: an open-source platform for biological-image analysis. Nature Methods 9, 676–682. doi:10.1038/nmeth.2019

Schmidt, Husted, 2019. The Biochemical Properties of Manganese in Plants. Plants 8, 381. doi:10.3390/plants8100381

Schüller, H., 1969. Die CAL-Methode, eine neue Methode zur Bestimmung des pflanzenverfügbaren Phosphates in Böden. Zeitschrift Für Pflanzenernährung Und Bodenkunde 123, 48–63. doi:10.1002/jpln.19691230106

Schwertmann, U., 1964. Differenzierung der Eisenoxide des Bodens durch Extraktion mit Ammoniumoxalat-Lösung. Zeitschrift Für Pflanzenernährung, Düngung, Bodenkunde 105, 194–202. doi:10.1002/jpln.3591050303

Shahandeh, H., Hossner, L.R., Turner, F.T., 2003. Phosphorus Relationships To Manganese and Iron in Rice Soils. Soil Science 168, 489–500. doi:10.1097/01.ss.0000080334.10341.6a

Sims, J., Pierzynski, G., 2005. Chemistry of phosphorus in soil, in: Tabatabai, A., Sparks, D. (Eds.), Chemical Processes in Soil, SSSA Book Series 8. SSSA, Madison, pp. 151–192.

Smith, R.D., Walker, J.C., 1991. Isolation and expression of a maize type 1 protein phosphatase. Plant Physiology 97, 677–683. doi:10.1104/pp.97.2.677

Smolders, E., Nawara, S., De Cooman, E., Merckx, R., Martens, S., Elsen, A., Odeurs, W., Vandendriessche, H., Santner, J., Amery, F., 2020. The phosphate desorption rate in soil limits phosphorus bioavailability to crops. European Journal of Soil Science. doi:10.1111/ejss.12978

Sorrell, B.K., Orr, P.T., 1993. H + exchange and nutrient uptake by roots of the emergent hydrophytes, Cyperus involucratus Rottb., Eleocharis sphacelata R. Br. and Juncus ingens N. A. Wakef. New Phytologist 125, 85–92. doi:10.1111/j.1469-8137.1993.tb03866.x

Sparrow, L.A., Uren, N.C., 1987. Oxidation and reduction of Mn in acidic soils: Effect of temperature and soil pH. Soil Biology and Biochemistry 19, 143–148. doi:10.1016/0038-0717(87)90073-3

Spohn, M., Carminati, A., Kuzyakov, Y., 2013. Soil zymography - A novel in situ method for mapping distribution of enzyme activity in soil. Soil Biology and Biochemistry 58, 275–280. doi:10.1016/j.soilbio.2012.12.004

Stober, C., George, E., Persson, H., 2000. Root Growth and Response to Nitrogen. pp. 99–121. doi:10.1007/978-3-642-57219-7_5

Ström, L., Owen, A.G., Godbold, D.L., Jones, D.L., 2002. Organic acid mediated P mobilization in the rhizosphere and uptake by maize roots. Soil Biology and Biochemistry 34, 703–710. doi:10.1016/S0038-0717(01)00235-8

Stutter, M.I., Shand, C.A., George, T.S., Blackwell, M.S.A., Bol, R., MacKay, R.L., Richardson, A.E., Condron, L.M., Turner, B.L., Haygarth, P.M., 2012. Recovering Phosphorus from Soil: A Root Solution? Environmental Science & Technology 46, 1977–1978. doi:10.1021/es2044745

Turner, B.L., Driessen, J.P., Haygarth, P.M., Mckelvie, I.D., 2003. Potential contribution of lysed bacterial cells to phosphorus solubilisation in two rewetted Australian pasture soils. Soil Biology and Biochemistry 35, 187–189. doi:10.1016/S0038-0717(02)00244-4

Turner, B.L., Mckelvie, I.D., Haygarth, P.M., 2002. Characterisation of water-extractable soil organic phosphorus by phosphatase hydrolysis. Soil Biology and Biochemistry 34, 27–35.

Vetterlein, D., Lippold, E., Schreiter, S., Phalempin, M., Fahrenkampf, T., Hochholdinger, F., Marcon, C., Tarkka, M., Oburger, E., Ahmed, M., Javaux, M., Schlüter, S., 2021. Experimental platforms for the investigation of spatiotemporal patterns in the rhizosphere—Laboratory and field scale. Journal of Plant Nutrition and Soil Science 184, 35–50. doi:10.1002/jpln.202000079

Wagner, S., Hoefer, C., Prohaska, T., Santner, J., 2020. Two-Dimensional Visualization and Quantification of Labile, Inorganic Plant Nutrients and Contaminants in Soil. Journal of Visualized Experiments. doi:10.3791/61661

Wen, T.-J., Schnable, P.S., 1994. Analyses of Mutants of Three Genes that Influence Root Hair Development in Zea mays (Gramineae) Suggest that Root Hairs are Dispensable. American Journal of Botany 81, 833. doi:10.2307/2445764

Whipps, J.M., 2001. Microbial interactions and biocontrol in the rhizosphere. Journal of Experimental Botany 52, 487–511. doi:10.1093/jxb/52.suppl_1.487

White, P.J., George, T.S., Gregory, P.J., Bengough, A.G., Hallett, P.D., McKenzie, B.M., 2013. Matching roots to their environment. Annals of Botany 112, 207–222. doi:10.1093/aob/mct123

Yang, Y., Wang, N., Guo, X., Zhang, Y., Ye, B., 2017. Comparative analysis of bacterial community structure in the rhizosphere of maize by highthroughput pyrosequencing. PLoS ONE 12, 1–11. doi:10.1371/journal.pone.0178425

2.5.9 Supporting information

2.5.9.1 Detailed bio-chemical imaging methods description

Section S1: Zymography to determine phosphatase activity

Direct soil zymography was applied under field conditions to study the spatial distribution of acid phosphatase activities in the rhizosphere of maize as previously described (Razavi et al., 2016). Measurement of phosphatase activity is based on the emerging fluorescing pattern of a fluorescent product (MUF: 4-methylumbelliferone) which is released upon the contact of phosphatase substrate (4-methylumbelliferyl-phosphate disodium salt) with phosphatase enzymes and detected under UV (Guber et al., 2018; Spohn et al., 2013).

Materials and application details: Acid phosphatase activity was detected with 3.3 mM 4-methylumbelliferyl-phosphate disodium salt (M8168, Sigma-Aldrich, Germany) dissolved in MES buffer (pH 6.5, M8902, Sigma-Aldrich, Germany). Polyamide membrane filters (size of 20×20 cm; pore size of 0.45 µm; Tao Yuan, China) were cut to 10×20 cm or 10×10 cm.

Each membrane was saturated with the 5 ml substrate solution to a final amount of 0.025 ml per cm^2. The root windows were opened and the saturated membranes were applied directly to the soil surface and covered with aluminum foil to avoid evaporation. Prior to closing the root window with the membrane in place, soft materials (i.e. foam rubber) were placed between the aluminum foil and Plexiglas plate to ensure optimal soil contact with minimal compression of the membrane. After incubation for 1 h, the root window was re-opened, membranes were carefully lifted off the soil surface, covered with aluminum foil, placed into a lightproof box and transported to the lab within 5 min. Soil particles attached to membrane were gently removed using tweezers and a soft hair-paint brush.

Photos of the membrane were taken by a digital camera Canon EOS 6D with a Canon lens EF 24–105 mm 1: 4L IS. The aperture and shutter speed were set to f/5.6 and 1/30 s, respectively.

Calibration: A standard calibration that relates the enzyme activities to the gray values of zymogram fluorescence was performed. The linear calibration function was obtained from 4 cm^2 membranes soaked in solutions of fluorescent 4-methylumbelliferone (MUF) with concentrations of 0, 0.01, 0.2, 0.5, 1 and 2 mM. The amount of MUF on an area basis was preliminary determined to ensure complete membrane saturation but no excess liquid that may drip. The membranes

used for calibration were imaged under UV light and analyzed in the same way as the samples. Grey values in the zymograms were transformed to activities with the following linear function (Eq. S1).

$$\text{Phosphatase activity (pmol mm}^{-2}\text{ h}^{-1}\text{)} = 2.19*GV-120.76 \quad \text{Eq. S1,}$$

where GV is the grey value.

Image processing: Zymograms were transformed from JPG-format into 8-bit grayscale images in ImageJ (Schindelin et al., 2012) and calibrated to phosphatase activities, as described above. The calibrated zymograms were further used for image analysis.

Section S2: Planar optodes to determine pH

Visualization and measurement of pH with planar optodes is based on a change of fluorescence emission of a pH-sensitive dye (Blossfeld and Gansert, 2007).

Materials and application details: In this study we used sensor foils from PreSens GmbH, combined with the VisiSens TD imaging system (PreSens GmbH, Regensburg, Germany).

The self-adhesive pH sensor foils were cut in a size from 1 cm^2 to 10 cm^2 and stuck on to an optically transparent polyester foil (Melinex ® 506). As recommended by the supplier, sensor foils were pre-equilibrated for at least 3 hours in 100 mM ionic strength phosphate-NaCl buffer. Then, they were fixed on the inner side of the root window observation plate with tape and the plate was then gently pressed against the rooted soil block.

All measurements were carried out in the morning, after one night of contact with the root-soil interface. Images were taken in dark conditions provided by black cloth covering the observation pits to avoid disturbance by ambient light.

After image recording, root windows were opened, optodes were removed from the observation plate, carefully rinsed with deionised water and stored in the equilibration buffer. To ensure that the sensor foils showed no signs of degradation after soil application, one optode of each plot was put in a buffer solution with known pH and an image was recorded.

Calibration: Calibration was done in a dark room with sensor foils fixed on a 5 mm-thick Plexiglas plates (same thickness as observation window) and subsequently immersed in eight phosphate-NaCl buffer solutions from pH 5.0 to pH 8.5 in Petri dishes. The calibration buffers were prepared by mixing 10 mM NaH_2PO_4/30 mM NaCl and 10 mM Na_2HPO_4/10 mM NaCl stocks, or further 2.5-fold dilution for the Sand, to adjust the ionic strength to the substrates. The ionic

strength of the Loam was previously estimated according to Alva et al. (Alva et al., 1991) after measurement of the electrical conductivity in a deionised water extract (SSR 1:2, 20 h equilibration) and correction for the actual water content. The estimated ionic strength of the Loam and Sand was 40 and 16 mM, respectively.

Image processing: Image processing was done with ImageJ software (FiJi distribution). Images were in RGB format with size of 1292*964 pixels and a pixel size of 38.5µm. The fluorescence of the non-sensitive and the pH-sensitive dye were captured in the red and green channel, respectively. For calibration, the Boltzmann model (Blossfeld and Gansert, 2007) was applied to the ratio (R) between the red and the green channel:

$$pH = pKa' + dpH.\ \ln\left(\frac{R_{min} - R_{max}}{R - R_{max}} - 1\right) \qquad \textit{Eq. S2}$$

Where, *pKa'* is the acid dissociation constant of the pH indicator dye (inflection point of the curve); *dpH* is the slope of the curve and R is the measured ratio-value; R_{min} and R_{max} are the maximum and minimum ratio-values (asymptotes of the curve). Model parameters were determined by R software (version 3.6.1)(R Development Core Team, 2011), and then applied in imageJ Fiji to transform ratio images and create pH maps (32-bit).

Section S3: Diffusive gradients in thin films (DGT) to determine labile phosphorus and manganese

Diffusive gradients in thin-film (DGT) gels are hydrogels containing resins that are capable of irreversible binding of labile cations and anions. The masses of these ions bound at different locations in the gel reflect how much can be resupplied to the DGT probe interface by the soil due to diffusion and desorption from the labile solid phase at a given location. In addition, processes linked to biological activity, such as plant nutrient uptake, dissolution of minerals by root exudates or release of ions from organic pools by enzymes also determine the ion flux into the DGT gel. DGT images hence represent fluxes of readily bio-available anions (e.g. P) and cations such as iron, copper, zinc, and manganese (Kreuzeder et al., 2013).

Materials and application details: DGT gels were prepared as described by (Kreuzeder et al., 2013). SPR-IDA (suspended particulate reagent-iminodiacetate, CETAC Technologies, Nebraska, USA) and zirconium hydroxide precipitate were embedded in a polyurethane-based

hydrogel matrix (HydroMed-D4, AdvanSource biomaterials, Massachusetts, USA) and served as a resin for labile cations and anions, respectively.

In a clean bench, DGT gels covered by a Nuclepore membrane (Nuclepore Track-Etched Membrane 0.2 µm, Whatman, UK) were fixed to acid washed polyester foil (125 µm thick, Melinex® 506, DuPont Teijin Films, USA) using tape. After visual identification of suitable application spots within the area imaged by zymography, the polyester foils with the membrane-gel stacks were then mounted to the inner side of the root window observation plate with tape and the windows were closed. After 24h of soil contact, the gels were retrieved, rinsed with deionised water and dried on a polyether sulfone membrane (140 µm thick, 0.45 µm pore size, Supor®450, Pall Corporation, Washington, US) on top of a blotting paper (GB005, Whatman, Maidstone, UK) covered by a polyethene foil in a gel drier.

Calibration and analysis: Spatial distribution of elements captured by the DGT resins was analysed by laser-ablation inductively coupled mass spectrometry (LA-ICPMS). Calibration standards were prepared by immersing resin-gel disks assembled in conventional DGT samplers in deployment solutions containing Mn or P in quadruplicates. Three loaded gel disks were eluted for 24 h either in 1M HNO_3 or 1M NaOH, for Mn and P standards, respectively. HNO_3 eluates were diluted to 2% HNO_3. NaOH eluates were diluted 1:10, neutralised and acidified to 2% HNO_3/0.1% HF. Eluates were analysed together with matrix matched standards and quality control standards by sector field ICPMS (ELEMENT XR, Thermo Fisher Scientific, Bremen, Germany). Loading was calculated with previously determined elution factors (Hummel et al., in preparation). The fourth standard gel disk was dried as described for the sample gels above and analysed together with sample gels and blank gels by LA-ICPMS.

LA-ICPMS was performed in line scanning mode with a UP 193-FX (ESI, NWR Division, Portland, USA) laser ablation system coupled to an quadrupole ICPMS (Elan 9000 DRCe, Perkin Elmer, Waltham, MA, USA). Helium was used as the carrier gas (flow rate of 900 mL min^{-1}) and mixed with the nebulizer gas stream prior to introduction into the ICPMS. The ICPMS method was set to scan for ^{13}C, ^{31}P and ^{55}Mn. Dwell times were between 30 to 80 ms, depending on signal to gas blank ratio (min 10). Scan cycle time was 0.641 s. The diameter of the laser beam was 150 µm, the scan speed across the gel was 155 µm s^{-1}, line distance was 400 µm. The laser output energy was 45%, repetition rate was 10 Hz and fluence at the sample was 3.16 J cm^{-2}. Between the scans, wash out was 20 s and laser warm up was 7 s. The resulting pixel size in the images

is 99.355 µm times 400 µm. Depending of the quality of obtained DGT-soil-root-interface contact, two to three DGT images per treatment (genotype x substrate) were analysed.

Image processing: The sample counts (intensity) were sorted in MS Excel and corrected for the mean gas blank signal before each laser line and normalized to the ^{13}C signal, which was used as internal standard. Means of 40 corrected readings from sample blank gel and standard gels were plotted against the average loadings of the 3 standard replicates to produce a linear calibration curve in MS Excel. The mass (ng cm^{-2}) accumulated on the DGT sample gels was corrected using the average mass from the sample blank and expressed as average flux over the DGT deployment time (pg cm^{-2} s^{-1}).

The LOD and LOQ were calculated from the signal of the sample gel blank as 3 and 10 times the standard deviation (SD) of the mean signal, respectively. After calibration in MS Excel and the data matrix was saved as text file and imported to ImageJ Fiji, rotated, flipped and scaled (x=1, y=4.026) to obtain square pixels from the initial rectangular pixels (resulting from the laser scan speed and the interline distance). Finally, the images were displayed from LOQ to the maximum calibration standard and the look up table 'royal' was applied.

Section S4: Calculations of soil organic P

Soil organic phosphorus (SOP) for each substrate was calculated from the soil organic carbon (SOC) values based on the SOC:SOP ratio corresponded to 919:1 (Tipping et al., 2016). SOC in Loam was 8.5 g kg^{-1} and in Sand 1.5 g kg^{-1} (Vetterlein et al., 2021).

In Loam: SOP is 8.5/919= 0.0092 g kg^{-1}= 9.2 mg kg^{-1}

In Sand: SOP is 1.5/919= 0.0016 g kg^{-1}=1.6 mg kg^{-1}

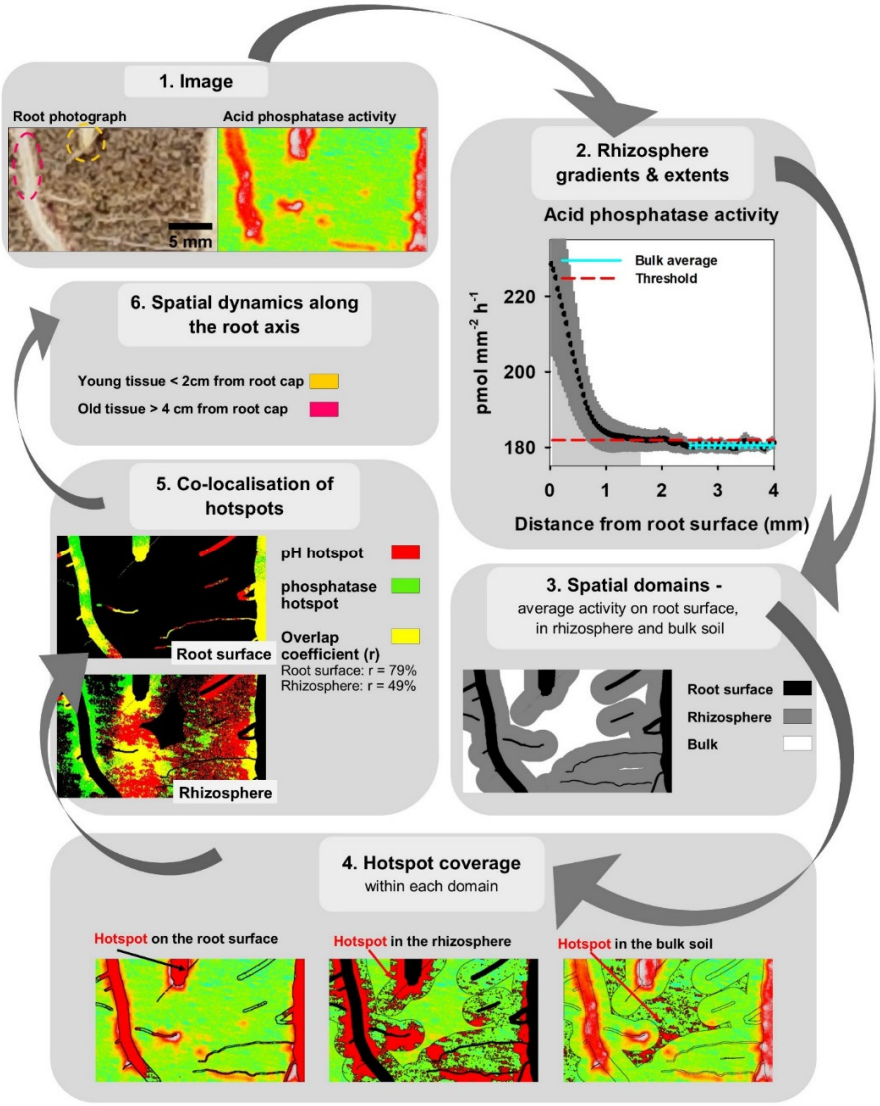

Figure S1. Image analysis workflow on the example of a ROI image of acid phosphatase activity. **Step 1** shows the photograph of ROI in the window of field plot 15 (S-WT) and the corresponding zymogram. **Step 2** depicts the concentration-distance plot of this ROI: the black line represents the average phosphatase activity for each distance class (*i.e.* 1 pixel = 0.038 mm) as a function of distance to the root mask, the light grey error bars show the standard deviation within each distance class. The blue line represents the bulk average phosphatase activity at a distance >2.5mm from the root surface, while the dotted lines represent the standard deviation. The red line represents the threshold (bulk + 2x SD) for determining the rhizosphere extent and hotspots. **Step 3** shows the areas to measure the average activity within each spatial domain, *i.e.,* the root surface in black, the rhizosphere in grey and bulk soil in white. **Step 4** shows how much of each spatial domain is covered by hotspots (*i.e.*, areas of phosphatase activity > threshold, in red colour). **Step 5** shows the hotspot area of two parameters (here pH-only in red, phosphatase-only in green) and the common area of both hotspot areas in yellow for the root surface and the standardized rhizosphere (2.5 mm from the root surface). The overlap coefficient (r) gives the share of common hotspot area within the cumulative area of the pH and phosphatase activity hotspot area. **Step 6** refers to the assessment of spatial changes along the root axis, *i.e.*, measurements at young root tissues (< 2 cm from the root cap) and older root sections (> 4 cm from the root cap).

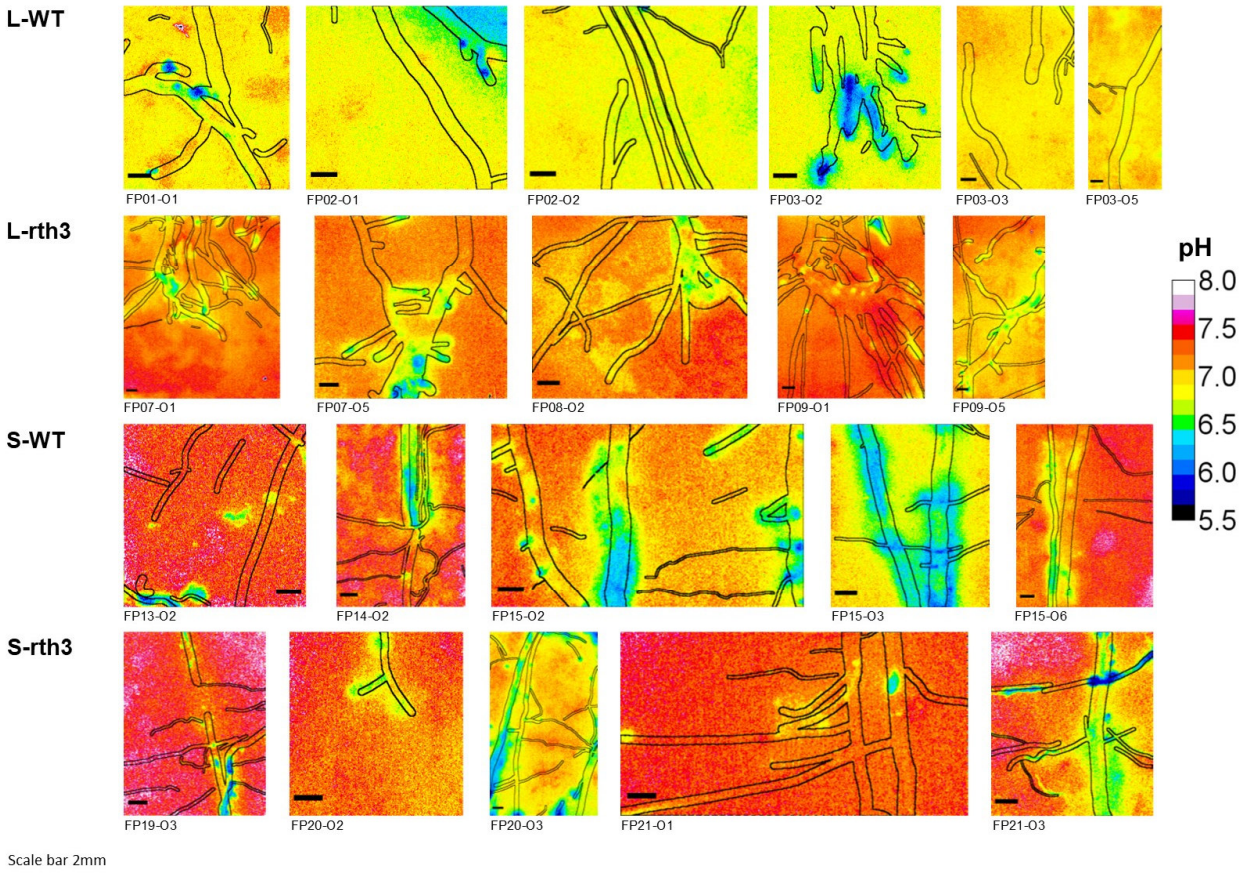

Figure S2. pH replicate regions of interest (ROI) used for image analysis.

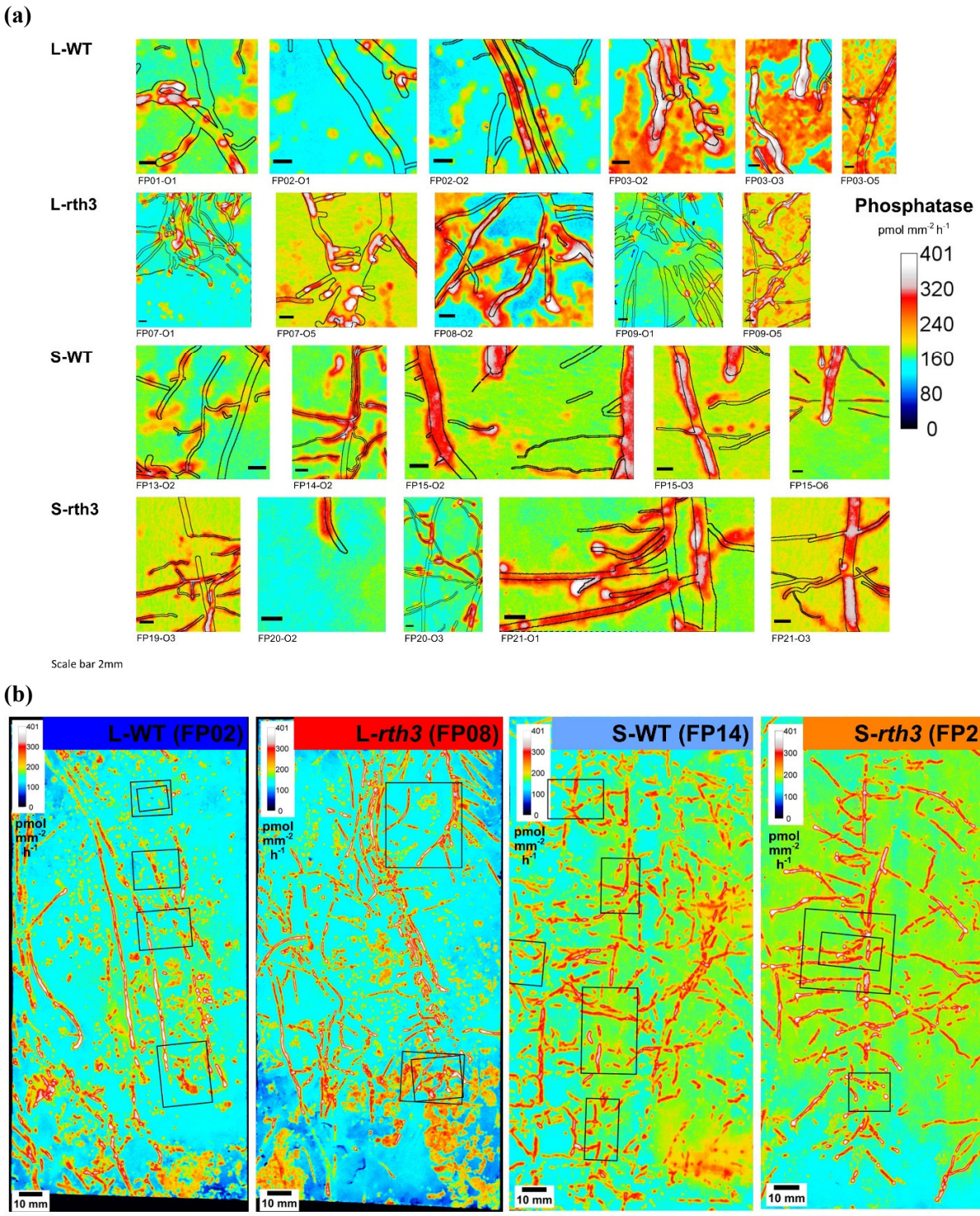

Figure S3. Acid phosphatase activity replicate regions of interest (ROI) used for image analysis (a) and an exemplary of the entire zymograms for each treatment (b).

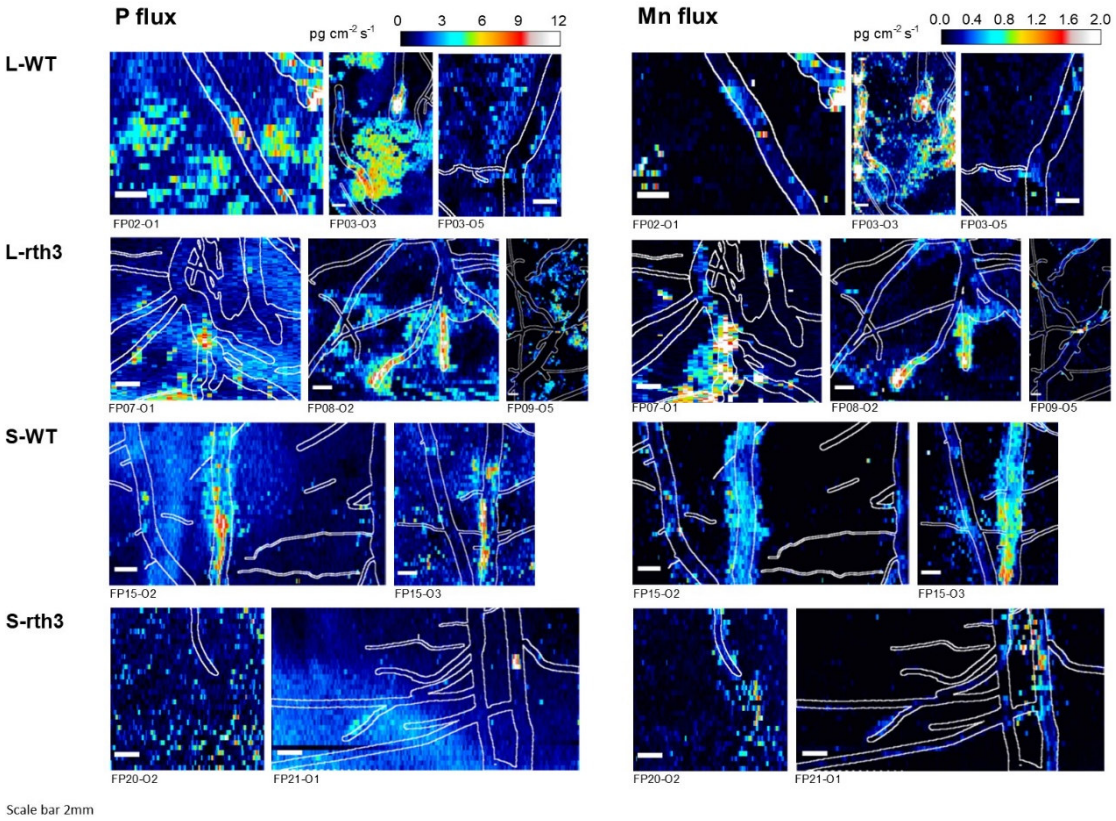

Figure S4. P flux (left side) and Mn flux (right side) replicate regions of interest (ROI) used for image analysis.

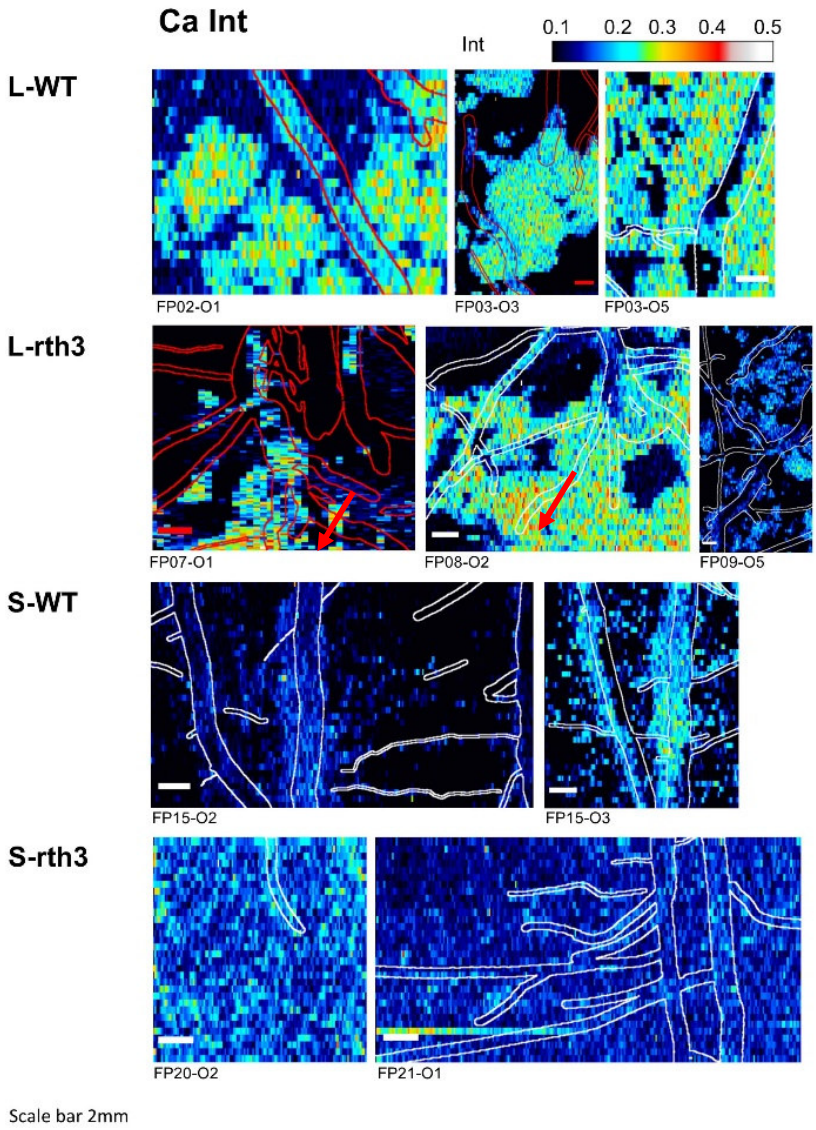

Figure S5. Labile calcium (Ca) net intensity in DGT replicate regions of interest (ROI). Note: high Ca concentration in the elongation zone of roots that grew during method application, i.e., middle root in FP15-O2, and both roots in FP15-O3 (red arrows).

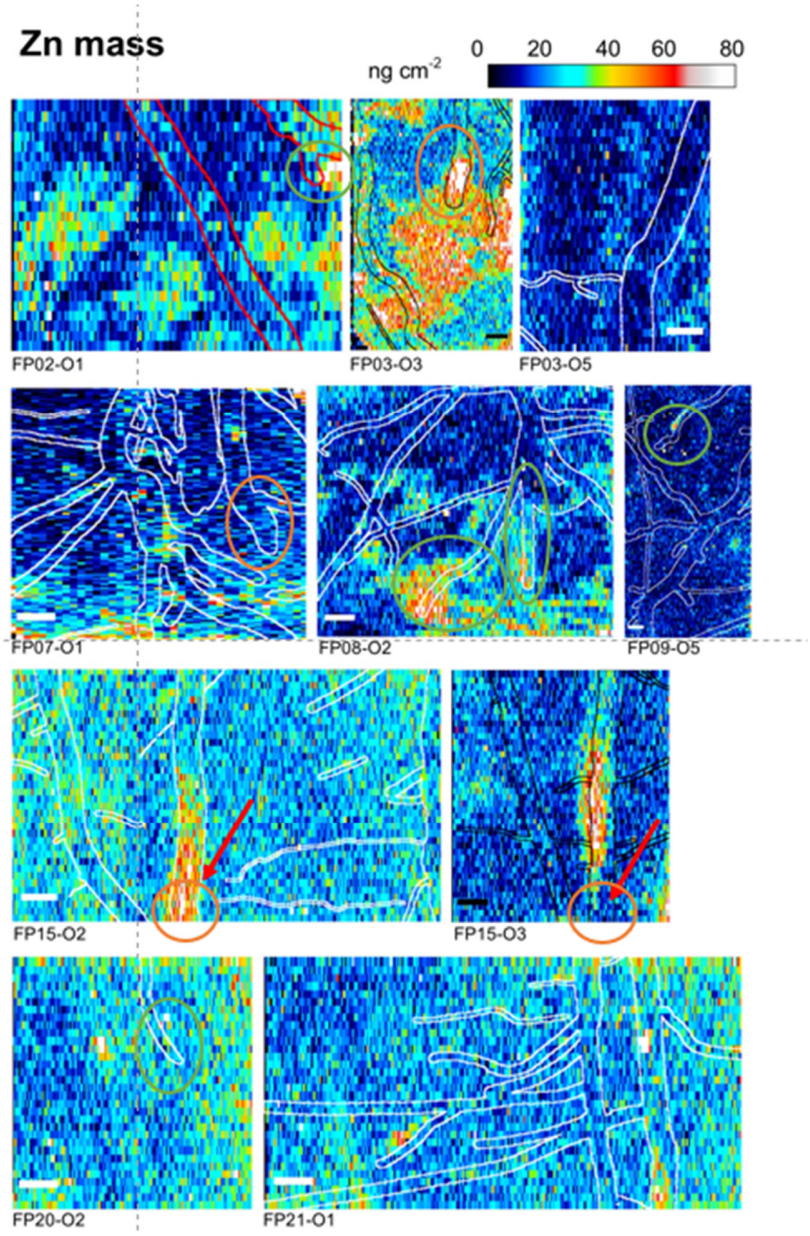

Figure S6. Labile zink (Zn) accumulated on DGT gels. Circles highlight root tips with a diameter > 1mm (orange) and ~0.5 mm (green). Red arrows show root tips that grew out of the ROI during DGT application.

Table S1. Two-way ANOVA and post-hoc Tukey test results for **averaged rhizosphere extents** (corresponding to data shown in Fig. 3) across treatments within each parameter (pH, phosphatase, P-flux, Mn-flux). Different letters **in columns** indicate significant (*p<0.05*) difference between treatments within each parameter.

Treatment	pH (a,b,c)	Phosphatase (k,l,m)	P-flux (no rhizoshere detected)	Mn-flux (x,y,z)
Loam-WT	a	k	n/a	x
Loam-*rth3*	a	kl	n/a	x
Sand-WT	a	l	n/a	x
Sand-*rth3*	a	kl	n/a	x
		p-values		
Substrate	*0.158*	***0.005*** **	-	*0.319*
Genotype	*0.657*	*0.977*	-	*0.160*
*Substrate*Genotype*	*0.916*	*0.306*	-	*0.717*

'***' *p<0.001*; '**' *p<0.01*; '*' *p<0.05*, '.' *p<0.10*.

Table S2. Two-way ANOVA and post-hoc Tukey test results for **average bulk, rhizosphere and root surface pH, acid phosphatase, P and Mn fluxes** across treatments within each spatial domain (corresponding to data shown in Fig. 4). Different letters **in column** indicate significant (*p<0.05*) difference between treatments within spatial domain. *P-values* are given *in italics* for each factor (Substrate, Genotype) and their interaction. Asterisks on the *P-values* indicate significant differences between soils, genotypes or their interactions. Significant factors (*p<0.05*) are marked **in bold**.

Treatment	**Root surface (a,b,c)**	**Individual rhizosphere (k,l,m)**	**Bulk soil (x,y,z)**	**Treatment**	**Root surface (a,b,c)**	**Individual rhizosphere (k,l,m)**	**Bulk soil (x,y,z)**
		pH				P-flux	
L-WT	a	k	x	L-WT	a	k	x
L-*rth3*	a	kl	y	L-rth3	a	k	x
S-WT	a	kl	y	S-WT	a	k	x
S-*rth3*	a	l	y	S-rth3	a	k	x
Substrate	*0.815*	*0.057.*	***0.001*** **	*Substrate*	*0.888*	*0.586*	*0.330*
Genotype	*0.139*	***0.037****	***0.004*** **	*Genotype*	*0.317*	*0.500*	*0.168*
*Substrate*Genotype*	*0.356*	*0.195*	*0.088 .*	*Substrate*Genotype*	*0.937*	*0.653*	*0.826*
		Acid phosphatase				Mn-flux	
L-WT	a	k	x	L-WT	a	k	x
L-*rth3*	a	k	x	L-rth3	a	k	x
S-WT	a	k	x	S-WT	a	k	x
S-*rth3*	a	k	x	S-rth3	a	k	x
Substrate	*0.373*	*0.422*	*0.552*	*Substrate*	*0.799*	*0.634*	*0.105*
Genotype	*0.436*	*0.256*	*0.721*	*Genotype*	*0.328*	*0.573*	*0.795*
*Substrate*Genotype*	*0.870*	*0.216*	*0.887*	*Substrate*Genotype*	*0.959*	*0.514*	*0.125*

*'***' p<0.001*; *'**' p<0.01*; *'*' p<0.05*, *'.' p<0.10*.

Table S3. Two-way ANOVA results comparing **hotspot coverage** (corresponding to data shown in Fig. 5) across treatments within each parameter (pH, phosphatase, P-flux, Mn-flux) and spatial domain (root surface, individual rhizosphere, bulk soil). Significant factors (p<0.05) are marked **in bold.**

Treatment	pH	Acid phosphatase	P-flux	Mn-flux
		Root surface		
Substrate	***0.040 ** **	***0.028 ** **	*0.587*	***0.054 . **
Genotype	*0.426*	*0.419*	*0.252*	*0.537*
*Substrate*Genotype*	*0.923*	*0.978*	*0.720*	*0.740*
		Individual rhizosphere		
Substrate	*0.449*	*0.926*	*0.176*	*0.213*
Genotype	*0.387*	*0.448*	*0.585*	*0.875*
*Substrate*Genotype*	*0.865*	*0.226*	*0.326*	*0.862*
		Bulk soil		
Substrate	*0.204*	*0.423*	*0.427*	*0.440*
Genotype	*0.195*	*0.751*	*0.296*	*0.584*
*Substrate*Genotype*	*0.140*	*0.720*	***0.058.**	*0.853*

'***' *p<0.001*; '**' *p<0.01*; '*' *p<0.05*, '.' *p<0.10*

Table S4. The results of one-way ANOVA and Tukey post-hoc test for comparison of **hotspot coverage in spatial domains (**root surface, individual rhizosphere, and bulk soil) **within each treatment** (corresponding to data shown in Fig. 5). *P-values* **in bold** indicate significant (*p<0.05*) difference between spatial domains. Different letters in rows indicate significant (*p<0.05*) differences between hotspot coverage of root surface, rhizosphere and bulk soil in each treatment.

Treatment	Root surface hotspot	Rhizosphere-hotspot	Bulk-hotspot	*p-value*
		pH		
Loam-WT	b	b	a	**0.002 ****
Loam-*rth3*	b	b	a	**0.002 ****
Sand-WT	b	b	a	**7e-05 *****
Sand-*rth3*	c	b	a	**3e-05 *****
		Acid phosphatase		
Loam-WT	b	b	a	**0.002 ****
Loam-*rth3*	b	ab	a	**0.010 ***
Sand-WT	b	b	a	**0.002 ****
Sand-*rth3*	b	b	a	**0.002 ****
		P-flux		
Loam-WT	a	a	a	0.409
Loam-*rth3*	a	a	a	0.898
Sand-WT	b	ab	a	**0.050 ***
Sand-*rth3*	a	a	a	0.792
		Mn-flux		
Loam-WT	a	a	a	0.168
Loam-*rth3*	a	a	a	0.191
Sand-WT	c	b	a	**0.002 ****
Sand-*rth3*	b	ab	a	**0.034 ***

'***' *p<0.001*; '**' *p<0.01*; '*' *p<0.05*, '.' *p<0.10*

Table S5. The results of *t-test* for paired means **comparison of overlap coefficient on root surface and in the standardized rhizosphere** (corresponding to data shown in Table 3). *P-values* **in bold** indicate significant (*p<0.05*) difference between overlap coefficients at root surface and in the rhizosphere in each treatment.

Parameters' interactions	Root surface vs. rhizosphere			
	Loam-WT	Loam-*rth3*	Sand-WT	Sand-*rth3*
pH-phosphatase	***0.001****	*0.108*	***0.001****	***0.010****
pH-P	*0.679*	*0.716*	*0.625*	*0.954*
pH-Mn	*0.168*	*0.155*	*0.142*	*0.154*
Phosphatase-P	*0.234*	*1.000*	*0.579*	*1.000*
Phosphatase-Mn	*0.157*	*0.141*	***0.031****	***0.014****
P-Mn	*0.140*	*0.576*	*0.806*	*0.687*

'***' *p<0.001*; '**' *p<0.01*; '*' *p<0.05*, '.' *p<0.10*

Table S6. The results of t-test for paired means comparison of **root surface young** (< 2cm from root cap) **and older root tissue** (> 4 cm from root cap), and older root tissues and bulk soil pH, acid phosphatase activity, P and Mn-fluxes (corresponding to data shown in Fig. 6). Significant differences (*p<0.1*) are shown in **bold**.

Treatment	Old vs. young root tissues	Old root tissues vs. bulk soil
	pH	
Loam-WT	***0.001****	*0.277*
Loam-rth3	***0.052 .***	*0.801*
Sand-WT	***0.001****	*0.182*
Sand-rth3	***0.034****	*0.130*
	Acid phosphatase	
Loam-WT	***0.068 .***	*0.090*
Loam-rth3	*0.406*	*0.624*
Sand-WT	*0.682*	***0.001****
Sand-rth3	***0.055 .***	***0.061 .***
	P-flux	
Loam-WT	*0.364*	*0.840*
Loam-rth3	*n/a*	*n/a*
Sand-WT	*0.481*	*0.674*
Sand-rth3	*0.405*	*0.208*
	Mn-flux	
Loam-WT	*0.261*	*0.656*
Loam-rth3	*n/a*	*n/a*
Sand-WT	*0.449*	***0.029 ****
Sand-rth3	*0.958*	*0.632*

'***' *p<0.001*; '**' *p<0.01*; '*' *p<0.05*, '.' *p<0.10*

2.5.9.2 References

Alva, A.K., Sumner, M.E., Miller, W.P., 1991. Relationship between ionic strength and electrical conductivity for soil solutions. Soil Science 152, 239–242. doi:10.1097/00010694-199110000-00001

Blossfeld, S., Gansert, D., 2007. A novel non-invasive optical method for quantitative visualization of pH dynamics in the rhizosphere of plants. Plant, Cell and Environment 30, 176–186. doi:10.1111/j.1365-3040.2006.01616.x

Guber, A., Kravchenko, A., Razavi, B.S., Uteau, D., Peth, S., Blagodatskaya, E., Kuzyakov, Y., 2018. Quantitative soil zymography: Mechanisms, processes of substrate and enzyme diffusion in porous media. Soil Biology and Biochemistry 127, 156–167. doi:10.1016/j.soilbio.2018.09.030

Kreuzeder, A., Santner, J., Prohaska, T., Wenzel, W.W., 2013. Gel for simultaneous chemical imaging of anionic and cationic solutes using diffusive gradients in thin films. Analytical Chemistry 85, 12028–12036. doi:10.1021/ac403050f

R Development Core Team, R., 2011. R: A Language and Environment for Statistical Computing. R Foundation for Statistical Computing, R Foundation for Statistical Computing. doi:10.1007/978-3-540-74686-7

Razavi, B.S., Zarebanadkouki, M., Blagodatskaya, E., Kuzyakov, Y., 2016. Rhizosphere shape of lentil and maize: Spatial distribution of enzyme activities. Soil Biology and Biochemistry 79, 229–237. doi:10.1016/j.soilbio.2016.02.020

Schindelin, J., Arganda-Carreras, I., Frise, E., Kaynig, V., Longair, M., Pietzsch, T., Preibisch, S., Rueden, C., Saalfeld, S., Schmid, B., Tinevez, J.-Y., White, D.J., Hartenstein, V., Eliceiri, K., Tomancak, P., Cardona, A., 2012. Fiji: an open-source platform for biological-image analysis. Nature Methods 9, 676–682. doi:10.1038/nmeth.2019

Spohn, M., Carminati, A., Kuzyakov, Y., 2013. Soil zymography - A novel in situ method for mapping distribution of enzyme activity in soil. Soil Biology and Biochemistry 58, 275–280. doi:10.1016/j.soilbio.2012.12.004

Tipping, E., Somerville, C.J., Luster, J., 2016. The C:N:P:S stoichiometry of soil organic matter. Biogeochemistry 130, 117–131. doi:10.1007/s10533-016-0247-z

Vetterlein, D., Lippold, E., Schreiter, S., Phalempin, M., Fahrenkampf, T., Hochholdinger, F., Marcon, C., Tarkka, M., Oburger, E., Ahmed, M., Javaux, M., Schlüter, S., 2021. Experimental platforms for the investigation of spatiotemporal patterns in the rhizosphere—Laboratory and field scale. Journal of Plant Nutrition and Soil Science 184, 35–50. doi:10.1002/jpln.202000079

2.6 Study 6. Water availability is more important than exudation for the spatial distribution of microbial activities under drought

Xuechen Zhang[a*], Nataliya Bilyera[b,c], Lichao Fan[d], Patrick Duddek[e,f], Mutez A. Ahmed[f], Andrea Carminati[e], Anders Kaestner[g], Michaela A. Dippold[h,i], Sandra Spielvogel[c], Bahar S. Razavi[b]

[a] College of Resources and Environment, Northwest A&F University, Yangling, 712100, China
[b] Department of Soil and Plant Microbiome, Institute of Phytopathology, Christian-Albrechts University of Kiel, Kiel, Germany
[c] Department of Soil Science, Institute of Plant Nutrition and Soil Science, Christian-Albrechts University of Kiel, Kiel, Germany.
[d] Department of Soil Science of Temperate Ecosystems, University of Göttingen, Göttingen, Germany
[e] Department of Environmental Systems Science, Physics of Soils and Terrestrial Ecosystems, ETH Zürich, Switzerland
[f] Division of Soil Physics, Bayreuth Center of Ecology and Environmental Research (BayCEER), University of Bayreuth, Bayreuth, Germany
[g] Laboratory for Neutron Scattering and Imaging, Paul Scherrer Institute, 5232 Villigen, Switzerland
[h] Biogeochemistry of Agroecosystems, University of Göttingen, Göttingen, Germany
[i] Geo-Biosphere Interactions, University of Tuebingen, Tuebingen, Germany

*Correspondence author: Xuechen Zhang (e-mail: Xueczhang@hotmail.com)

Status: *Under review in New Phytologist since 06.01.2022*

2.6.1 Summary

- Root hairs and soil water content play crucial roles in controlling the release and diffusion of root exudates and shaping profiles of biochemical properties in the rhizosphere. We still lack knowledge whether root hairs can offset the direct negative impacts of drought on microbial activity.
- Soil zymography, ^{14}C imaging and neutron radiography were coupled to identify how root hairs and soil moisture affect the spatial dependence of β-glucosidase activities on root exudates and soil water. To achieve this, we incubated two maize genotypes (wild type and root-hair defective mutant *rth3*) under ambient and drought conditions.
- Root hairs and optimal soil moisture increased hotspot area and rhizosphere extent of β-glucosidase activities. In contrast, drought enlarged the rhizosphere extent of root exudates and also of water content. Co-localization analysis showed that enzymatic hotspots were more co-localized with hotspots of root exudates under optimal moisture.

In contrast, enzyme hotspots showed higher dependency on water hotspots under the scarcity of both water and carbon.

- We conclude that both root hairs and soil moisture influenced spatial distribution of rhizosphere biochemical properties, but access to soil water was more important than the availability of root exudates for hydrolytic activity under drought.

Key words: *in-situ* imaging techniques, root morphology, spatial correlation, root hairs, rhizodeposition, enzyme activity, water scarcity

2.6.2 Introduction

The rhizosphere — a small volume of soil influnced by living roots — is a key hotspot of enzyme activities and plays an important role in carbon (C) cycling globally (Hinsinger *et al.*, 2009; Kuzyakov & Razavi, 2019). The spatial distribution of the rhizosphere with regards to enzyme activities highly depends on soil and plant properties, including soil moisture (Ahmadi *et al.*, 2018), root morphology and metabolites released by roots (Ma *et al.*, 2018; Zhang *et al.*, 2019).

Herbaceous plants release between 20% and 50% of their photosynthesized C as low or high molecular weight organic substances (Badri & Vivanco, 2009), through their roots into soil (Kuzyakov & Domanski, 2000; Kuzyakov *et al.*, 2003) – a process occurring via various mechanisms including secretion, diffusion and cell lysis (Jones *et al.*, 2009). Such a large input of C provides a significant energy source for microorganisms (Hinsinger *et al.*, 2009), thus inducing higher microbial abundance and activities (Oburger *et al.*, 2014) in the rhizosphere than in root-free soil (Burns, 1982). Detailed knowledge about the allocation and localization of photosynthetic C released from roots is an important prerequisite for understanding the complex interactions between plants and the rhizosphere microbiome.

The quantity, quality and spatial distribution of root exudates along the root and in the soil are strongly affected by root morphology (e.g. root hairs) (Nguyen, 2009; Datta *et al.*, 2011; Poirier *et al.*, 2018). Root hairs, an extension of the epidermal cells (Peterson & Farquhar, 1996), play a critical role in the resource exchange among soil, plants and soil microorganisms. The enlargement of root surface area by the extension of root hairs is a cost-effective morphological strategy of plants to acquire water and nutrients (Cailloux, 1972; Jungk, 2001; Carminati *et al.*, 2017). Because an important part of rhizodeposits may be released by root hairs, they act as a determinant of enzyme activity (Ma *et al.*, 2018) and microbial functioning, e.g. nutrient

mobilization, especially related to the spatial extent of root exudation and thus, enhanced microbial activity. However, we currently have only very limited understanding on the co-localization of root exudates and microbial activity such as enzyme activities.

In addition to root hairs, drought - a sub consequence of climate change (Hasibeder *et al.*, 2015) - commonly affects the quantity and alters the partitioning of root exudates (Preece & Peñuelas, 2016). Drought, likely up-regulates the belowground allocation of assimilated C to compensate negative effects of water limitation (Preece & Peñuelas, 2016). For example, an increase in the release of mucilage, a gel exuded at the root tip, not only facilitates root water uptake but also eases the root growth into dry soil (Ahmed *et al.*, 2014; Holz *et al.*, 2018b). However, the amount of root exudation is also projected to decline under severe drought, probably due to a lower photosynthetic activity as result of stomata closure or the C redirection to other vital processes (Gargallo-Garriga *et al.*, 2018). The presence of root hairs (e.g. more root exudates) may magnify the uncertainty in our understanding how drought affects root exudation and microbial functionality (e.g. enzyme activities). Apart from alterations in root exudation caused by drought, water depletion directly imposes osmotic pressure on both root and microbial cells, disconnects enzymes from substrate as well as microorganisms from nutrients, which can lead to microbial death and thus impair enzyme activities (Turner *et al.*, 2003; Holz *et al.*, 2019a). This suggests that the spatial distribution of enzyme activities may also shift based on the pattern of water content, especially if plants are exposed to drought stress. It is still unknown whether a higher root exudation can offset the direct negative impacts of water stress. Therefore, a process-based understanding is urgently needed to identify the role of root exudates and water content in the distribution of enzyme activities. Such knowledge is vital as it not only defines the soil volume actively used by plant and microorganisms, but also determine the soil volume where rhizosphere priming i.e. SOM decomposition as an important process in C cycling occurs (Kumar *et al.*, 2018). Hence, as the enzymatic decomposition of SOM is the rate-limiting step in C and nutrient cycling, its spatial respond to the drought stress in a world with changing climate is essential (Kuzyakov & Razavi, 2019).

Due to the spatial and chemical heterogeneity of soil structure, complexity of root morphology and rapid microbial incorporation of rhizodeposits, deciphering the spatial relation between enzyme activity and root exudation or water is highly challenging. Direct soil zymography - an *in situ* technique for two-dimensional (2D) imaging - allows to visualize and analyze the spatial distribution of extracellular enzymes (Spohn & Kuzyakov, 2013; Razavi *et al.*, 2016) at high resolution (Heitkötter & Marschner, 2018). The development of ^{14}C imaging has been applied to

visualize and quantify ^{14}C photosynthates in roots and soil at the microscale (Pausch & Kuzyakov, 2011; Spohn & Kuzyakov, 2013; Holz *et al.*, 2019b). Neutron radiography offers an opportunity to quantitatively image the soil water distribution around roots (Moradi *et al.*, 2009; Esser *et al.*, 2010; Zarebanadkouki *et al.*, 2018). Here, we combined enzyme kinetics and these three imaging techniques: soil zymography, radioisotope imaging (^{14}C imaging) and neutron radiography to: 1) estimate how root hairs and soil water content affect gradients of enzyme activities and photosynthates in the rhizosphere; 2) unravel whether the spatial linkage between enzyme activities and root exudates or between enzyme activities and soil water distribution depend on the overall soil moisture level. To achieve these objectives, two maize genotypes — wild type with root hairs and *rth3* root-hair defective mutant — were grown under drought conditions (30% of WHC) and at optimal water content (70% of WHC) for 3 weeks. Due to the great importance of β-glucosidase in cellulose degradation, cleaving cellobiose into glucose molecules, it has always been selected as the representative of C cycling related enzymes (German *et al.*, 2011; Zhang *et al.*, 2020). Apart from this, it is also sensitive to moisture stress and easily quantifiable (Padhy *et al.*, 2018). We hypothesized that: 1) root hairs and optimal soil moisture widen the rhizosphere extent of root exudates and consequently β-glucosidase activities; 2) the presence of root hairs at least partially buffers the negative impacts of drought on roots and microorganisms through the increased input of root exudation and thus higher enzyme activities; 3) the spatial pattern of enzyme activities is more closely co-localized with root exudates under optimal water content, while it is highly associated with water under drought.

2.6.3 Material and methods

2.6.3.1 Soil description and experimental set up

The loam soil substrate was collected from a Haplic Phaeozem close to Schladebach in Saxony Anhalt, Germany. The soil properties are described in detail in (Vetterlein *et al.*, 2021): organic C 8.5 g kg^{-1}, total N 0.8 g kg^{-1}, available P 32.7 mg kg^{-1}, pH ($CaCl_2$) 6.4. Prior to plant transplantation into rhizoboxes, NH_4NO_3-N, K_2SO_4-K, and $MgCl_2 \cdot 6\ H_2O$ as solution and $CaHPO_4$-P as powder were added to the soil to reach the contents: 50 mg N kg^{-1} soil, 50 mg K kg^{-1} soil, 40 mg P kg^{-1} soil and 25 mg Mg kg^{-1} soil, respectively.

Two maize (*Zea mays* L.) genotypes, the root-hair defective mutant *rth3* (showing root hair initiation but disturbed root hair elongation) (Hochholdinger *et al.*, 2008, 2018), and the corresponding wild-type sibling were grown for three weeks in rhizoboxes with an inner size of 10

× 21 × 0.6 cm. For a detailed description of the root-hair defective mutant *rth3*, please refer to Hochholdinger et al., (2018) and (2008).

Before transplanting the plants to the rhizoboxes, seeds were germinated on filter paper for 72 h. The rhizoboxes were kept at an angle of 45° to make sure the roots grow along the lower side. The soil water content was maintained at 70% water holding capacity (WHC) during the first two weeks. In the third week, the water content was kept at either 70% of WHC (optimal water content) or adjusted to 30% of WHC (drought). In total 12 rhizoboxes were planted: two genotypes of maize, two water content conditions, and 3 replicates for each treatment. All plants were grown under controlled conditions in a climate chamber with a constant temperature of 22 ± 1°C. The photoperiod was 12 h and the light intensity was 350 µM m^{-2} s^{-1}.

2.6.3.2 Plant labeling and ^{14}C imaging

After three weeks of maize growth, each plant was labeled with 0.5 MBq $^{14}CO_2$ at a target CO_2 concentration of 500 ppm, in an airtight chamber for six hours (Kuzyakov et al., 2006). Briefly, before labeling, the CO_2 inside the labeling chamber was reduced by cycling the air through 1 M NaOH for 8 hours with growth lights off. NaOH solution was then replaced by ^{14}C which was prepared as 3 MBq $Na_2{}^{14}CO_3$ solution (0.5 MBq × 6 plants) dissolved by 10 ml phosphoric acid (1 M H_3PO_4). The released $^{14}CO_2$ was pumped into the chamber for 6 h. During the labeling, all plants were kept under a growth light (350 µM m^{-2} s^{-1}) for highest photosynthetic activity. After labeling, the remaining $^{14}CO_2$ in the chamber was trapped with 1 M NaOH for 2 h. ^{14}C activities were determined by liquid scintillation counting on a Hidex 300SL Automatic Liquid Scintillation Counter (Hidex, Turku, Finland). 0.5 ml of NaOH was added to the 8 ml scintillation cocktail Rotiszint Eco plus (Carl Roth, Karlsruhe, Germany) and kept in the dark for 24 h for chemiluminescence to cease.

Directly after labeling, the rhizoboxes were transferred to a dark room. The rooted soil surfaces were exposed to storage phosphor screens (BAS-IP MS 2040 E, GE Healthcare, U.S.A.). All screens were erased for 10 min under the strong bright light before use, and were protected from moisture by transparent plastic bags (polypropylene, 40 µm thickness, density 0.95 g cm^{-3}, MDF Verpackungen GmbH, Bergisch Gladbach, Germany). The plate with plastic bag was attached to the rooted soil surface for 20 h in total darkness. Thereafter, the plates were scanned with a laser scanner for phosphor-imaging (650 nm excitation, FLA-7000, GE Healthcare, U.S.A.) with a spatial resolution of 25 µm (Banfield *et al.*, 2017) .

2.6.3.3 Direct soil zymography

Soil zymography was used to visualize the spatial distribution of β-glucosidase activity after ^{14}C imaging. The protocol we followed is described in detail in Razavi et al., (2016). Polyamide membranes (a pore size of 0.45 µm, Taoyuan, China) saturated with the 4-methylumbelliferyl -β-D-glucoside was applied to determine β-glucosidase activity on soil surfaces. The 4-methylumbelliferyl- (MUF) containing substrates become fluorescent when hydrolyzed by a substrate-specific enzyme. 4-methylumbelliferyl-β-D-glucoside was dissolved in the universal MES buffer at pH 6.5. All the chemicals were purchased from Sigma-Aldrich (Germany). After 1 h of incubation, the saturated membranes were lifted off the soil surface and the soil particles attached to the membranes were carefully removed using a soft brush.

A standard calibration was performed to link the β-glucosidase activity to the gray values obtained from the zymograms. Briefly, 9 pieces of 2 × 2 cm membranes were soaked in solutions of MUF with increasing concentrations (0, 0.01, 0.2, 0.5, 1, 2, 4, 6, and 10 mM). The amount of MUF needed for the saturation of each membrane pieces was based on a preliminary test. All the membranes used for rhizoboxes and calibration were placed in a dark room under UV lamps to be photographed.

2.6.3.4 Neutron radiography

Neutron radiography is a non-destructive method which is sensitive to hydrous materials (Moradi *et al.*, 2009; Ahmed *et al.*, 2016), and thus can quantify present water distribution in the rhizosphere (Oswald *et al.*, 2008; Holz *et al.*, 2018b; Zarebanadkouki *et al.*, 2018). The experiment was conducted at the ICON beam line (Kaestner *et al.*, 2011) at the Paul Scherrer Institute (PSI) in Switzerland. We used a CCD camera detector with an array of 1260 by 1260 pixels, a field of view of 15.75 cm by 15.75 cm, and a spatial resolution of 0.2 mm. 4 radiographs with marginal overlaps were scanned to cover the entire sample. The protocol for calculating water content from neutron radiography images were provided in earlier studies (Esser *et al.*, 2010).

2.6.3.5 Kinetics of enzyme activity

Kinetics parameters of β-glucosidase in the soil sampled from the rhizosphere of wild-type and *rth3* mutant maize under drought and optimal water content were measured using the fluorometric microplate assay based on the 4-methylumbelliferyl-β-D-glucoside (German *et al.*, 2011). β-glucosidase activities were determined at a range of substrate concentrations from 0, 5,

10, 20, 50, 100, 200 µmol L^{-1}. 0.5 g soil was homogenously mixed with 50 mL sterile water using the low-energy sonication. 50 µL soil suspension, 100 µL substrate solution and 50 µL MES buffer were added into a 96-well microplate. The fluorescence was measured using a Victor 1420-050 Multi label counter (PerkinElmer, USA) at 0, 20 min, 1 h and 2 h. Parameters of Michaelis-Menten kinetics for β-glucosidase activities were calculated with the following equation:

$$v = \frac{V_{max} \times [S]}{K_m + [S]}$$

where v is the reaction rate, V_{max} is the maximum enzyme activity, [S] is the substrate concentration, and K_m is the substrate concentration at half-maximum rate (Michaelis and Menten, 1913).

2.6.3.6 Image processing and analysis

Images obtained by zymography, ^{14}C imaging and neutron radiography were processed in ImageJ. First, the projected signals of the images were transformed to gray values (8-bit). The gray values were then converted either to enzyme activities or to water contents based on the corresponding calibration function.

To quantify the ^{14}C images, results were converted from a log into a linear system by applying the following equation (Banfield *et al.*, 2017):

$$PSL = (\frac{Res}{100})^2 \times \frac{4000}{S} \times 10^{L\,(\frac{QL}{G} - \frac{1}{2})}$$

where *PSL* (photo stimulated luminescence) is the quantified value of the image in linear scale and is an arbitrary unit describing the absorbed and corrected energy on the imaging plate) (Thu Hoang *et al.*, 2020). Res is the resolution of the image (µm; Res = 25 µm), S the sensitivity (S = 1000), L the latitude (L = 5) and G the gradation (G = 256).

We considered areas with gray values exceeding Mean + 2SD of the whole image as hotspots of β-glucosidase activity, ^{14}C activity and soil water content (Zhang *et al.*, 2020).

Root segments that did not overlap with other roots were randomly selected to calculate bidirectional rhizosphere extent for enzyme activities/^{14}C activities/water contents. Briefly, a vertical line was drawn through the root, and the gray values of this line were extracted. In total, between 14 and 83 lines (zymography: 15-47; ^{14}C images: 25-83; water images: 14-67) were performed of each image. To determine the extent, the average gray values of these replicates

were plotted against the distance in Sigmaplot 12.5. The distance at which the gray value increased from or dropped to the minimum asymptote was firstly visually taken as thresholds for bidirectional rhizosphere extent. Then we checked the significant difference between the gray values of five points lower and five points higher than the visual threshold. If the difference was significant at $p < 0.05$, we considered the visual thresholds as the real threshold.

The co-localization analysis between β-glucosidase activity and exudate hotspots or between β-glucosidase activity and water hotspots was performed by "Just another co-localization plugin" (JACoP) installed in Fiji (Bolte & Cordelières, 2006). Briefly, the images were adjusted to identical size. Then, the images were aligned/registered manually in Fiji using the plugin TrackEM2 (Cardona *et al.*, 2012). After the registration, the aligned images were used to analyze Manders' coefficients (M1 and M2, Manders et al., 1993) in JACoP.

$$M_1 = \frac{\sum_i R_{i,coloc}}{\sum_i R_i} \quad (1)$$

$$M_2 = \frac{\sum_i G_{i,coloc}}{\sum_i G_i} \quad (2)$$

where R_i and G_i are the grey values of each pixel of hotspot area of image R and G, respectively. $\sum_i R_{i,coloc}$ and $\sum_i G_{i,coloc}$ are the total co-localized grey values over the threshold for image R and G, respectively. $\sum_i R_i$ and $\sum_i G_i$ are the total grey values over the threshold for image R and G, respectively.

2.6.3.7 Statistical analysis

The Shapiro-Wilk test and Levene tests were performed to check normality and homogeneity of variances, respectively. Statistical analyses were performed in JMP and the significance of differences was tested using two-way ANOVA at a probability level of $p < 0.05$. If normality and homogeneity was not met, the Scheirer-Ray-Hare test was performed in R (version 3.6.3), at $p < 0.05$. If the effects of both genotype and water were significant, we calculated η^2 as a parameter to show the contribution of each factor to the total variation (effect size).

$$\eta^2 = \frac{SS_A}{SS_{total}} \quad (4)$$

where SS_A is the variance between treatments caused by factor A. SS_{total} was the total sum of squares.

2.6.4 Results

2.6.4.1 Spatial distribution and kinetics of β-glucosidase

The spatial distribution of β-glucosidase activity was strongly affected not only by root hairs but also by soil moisture (Fig. 1). Root hairs and optimal water content increased the activity and hotspot area of β-glucosidase (Fig 1, 2a & 3a). For both genotypes, the β-glucosidase hotspot area was mainly associated with roots (Fig. 1). The hotspot area of wild type was higher than that for mutant *rth3* by 20% at optimal soil water content and by 49% at drought (Fig. 2a). Similarly, the percentage of hotspot area for both wild type and mutant *rth3* decreased under drought compared with optimum water content (Fig. 2a).

The rhizosphere extent of β-glucosidase varied between drought and optimum water content (Fig. 2b). It was 37% and 60% broader under optimal water content conditions than that under drought for wild type and mutant *rth3*, respectively. Additionally, the rhizosphere extent of β-glucosidase activity was wider for roots of the wild-type maize than for those of mutant maize irrespective of soil water content (Fig. 2b, $p = 0.0039$).

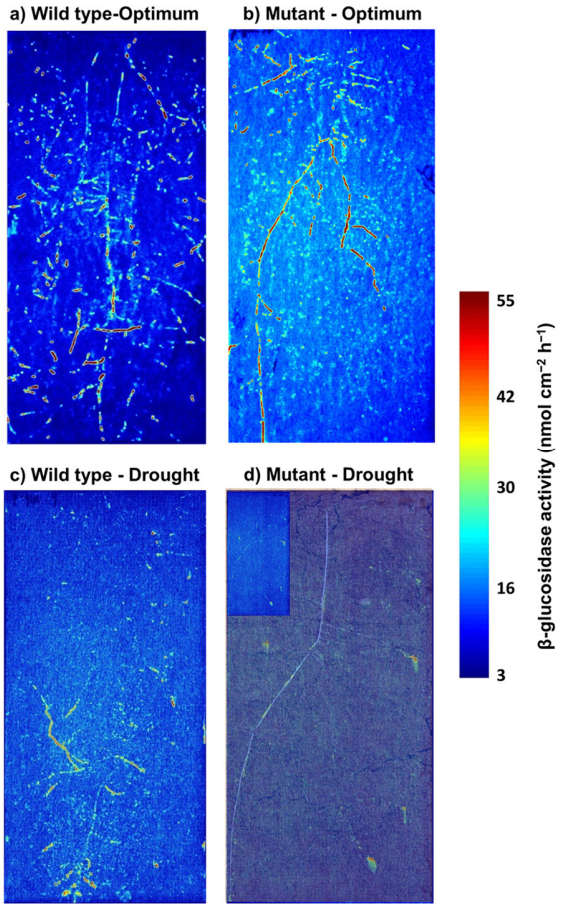

Figure 1. Spatial distribution of β-glucosidase activity for two maize genotypes (wild type and mutant *rth3*) under optimal water content (a & b) and drought conditions (c & d). The color scale is proportional to β-glucosidase activity (nmol cm^{-2} h^{-1}). *Note*: for Fig. 1d, a root photo was overlapped with zymogram to link root compartments with enzymatic hotspots, and the small figure in the upper left corner is original zymogram.

Compared to drought, optimal water content increased potential β-glucosidase activities (V_{max}) by 55% and 57% for wild type and mutant maize *rth3*, respectively (Fig. 3a). V_{max} in the rhizosphere soil of wild type was 27% and 29% higher than that for mutant *rth3* under optimal water content and drought, respectively (Fig. 3a). Similarly, water content and root hairs strongly increased both V_{max} and K_m of β-glucosidase activities (Fig. 3b). The effect size of an increased

water content on enzyme kinetics (η^2 = 0.74 for V_{max} and η^2 = 0.56 for K_m) was higher than that of the presence of root hairs (η^2 = 0.22 for V_{max} and η^2 = 0.28 for K_m) (Fig. 3).

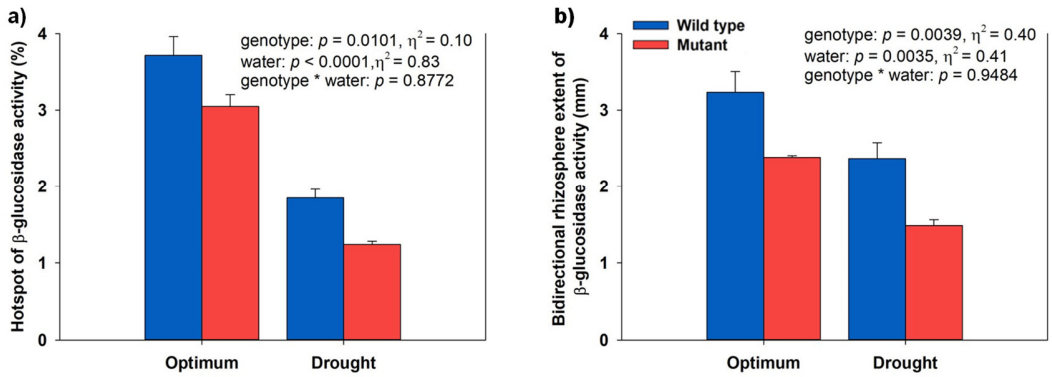

Figure 2 (a) Hotspot (%) and (b) bidirectional rhizosphere extent of β-glucosidase activity for two maize genotypes (wild type and mutant *rth3*) under optimal water content and drought conditions. *p* values were obtained after two-way ANOVA. η^2: effect size; genotype: wild type and mutant *rth3*; water: drought and optimal water content. Data are mean (n=3) and error bars represent standard deviation (SD).

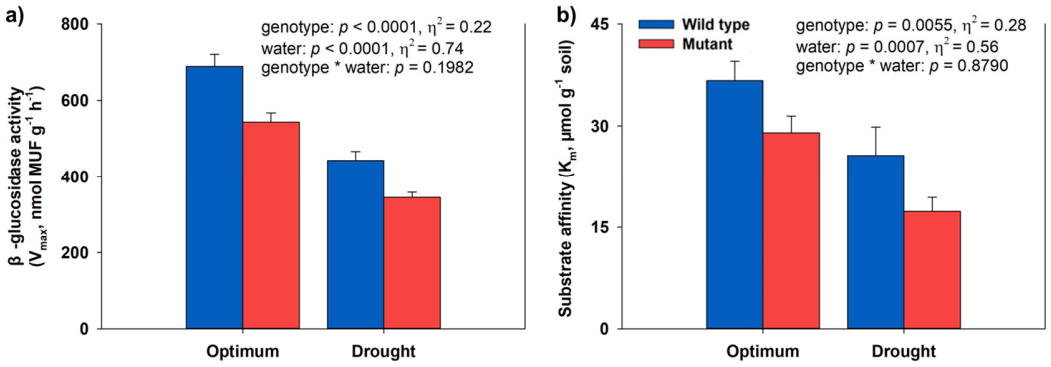

Figure 3 Michaelis–Menten kinetic parameters, i.e. (a) β-glucosidase activity (V_{max}, nmol g^{-1} h^{-1}) and (b) substrate affinity (K_m, µmol g^{-1} soil), of rhizosphere soil for two maize genotypes (wild type and mutant *rth3*) under optimal water content and drought conditions. *p* values were obtained after two-way ANOVA. η^2: effect size; genotype: wild type and mutant *rth3*; water: drought and optimal water content. Data are mean (n=3) and error bars represent standard deviation (SD).

Taken together, optimal water content contributed more to an increase in hotspot area, a broader rhizosphere extension and overall higher activities of β-glucosidase than root hairs did.

2.6.4.2 *Spatial distribution of ^{14}C exudates and water content*

Similar to the spatial distribution of enzyme activity, the distribution of photoassimilates showed a root-associated pattern, and the ^{14}C activity was higher under optimum water content than under drought (Fig. 4). Neither the presence of root hairs nor alterations of the soil water content changed the hotspot area of ^{14}C activity significantly (p > 0.05, Fig. 5a), but the trend was similar to β-glucosidase hotspots, i.e. larger hotspot area under optimal water content or in the rhizoboxes planted with wild-type maize. The bidirectional rhizosphere extent of root exudates increased by 27% for both genotypes under drought compared with that under optimal water content (Fig. 5b, p = 0.0069).

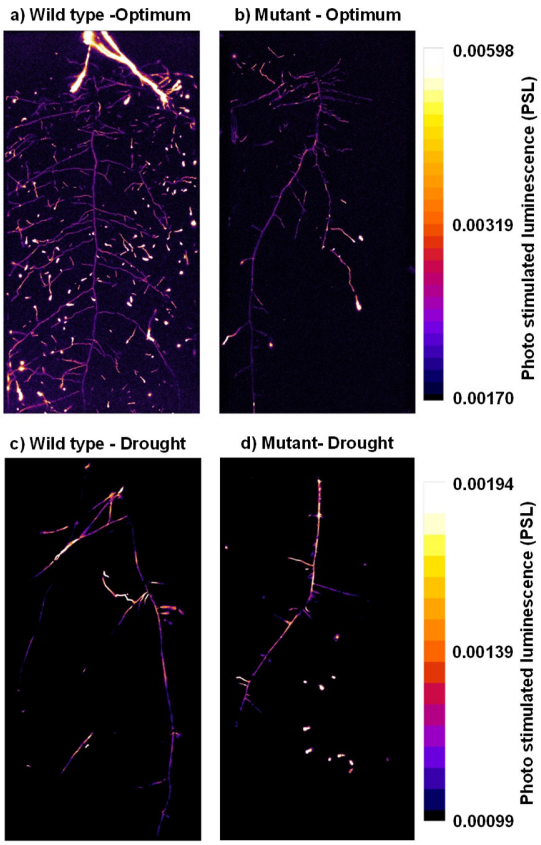

Figure 4 Spatial distribution of root exudates for two maize genotypes (wild type and mutant *rth3*) under optimal water content (a & b) and drought conditions (c & d). *Note:* different scales for drought and optimal water content.

The bidirectional rhizosphere extent of root exudates was broader for wild type (2.6 mm under optimal soil moisture vs. 3.3 mm under drought condition) than that for mutant *rth3* (2.1 mm under optimal soil moisture vs. 2.7 mm under drought condition) (Fig. 5b, p = 0.0013). The effect size of an increased water content on the rhizosphere extent of root exudates (η^2 = 0.42) was 10% higher than that of the presence of root hairs (η^2 = 0.32) (Fig. 5).

Remarkably, the distribution of exudates along the roots did not depend on the presence of root hairs and soil water content. In contrast, the activity of ^{14}C exudation hotspots was more affected by soil water content than by root hairs.

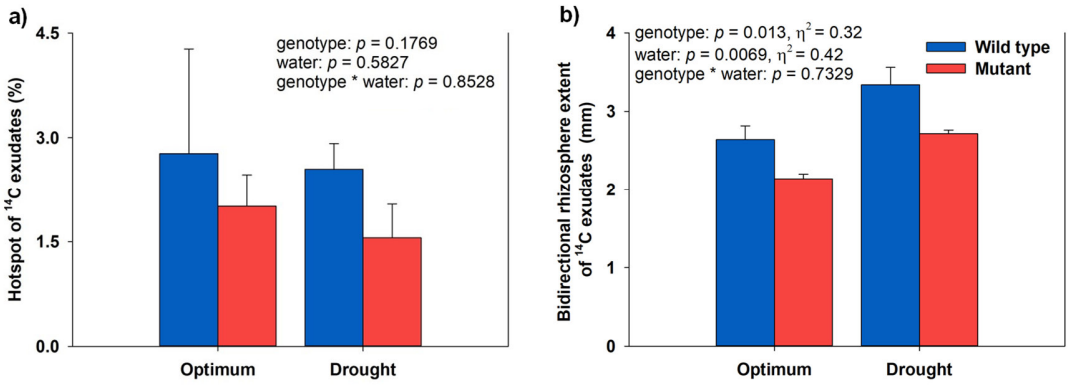

Figure 5 (a) Percentage of hotspot and (b) bidirectional rhizosphere extent of root exudates for two maize genotypes (wild type and *rth3* mutant) under optimal water content and drought conditions. *p* values were obtained after two-way ANOVA. η^2: effect size; genotype: wild type and mutant *rth3*; water: drought and optimal water content. Data are mean (n=3) and error bars represent standard deviation (SD).

The water content was higher in the rhizosphere compared to that in bulk soil (Fig. 6) under both drought and optimum water content and also for both wild-type and mutant maize. The water-rhizosphere extent, i.e. the range of a moist rhizosphere, was wider when the soil was under drought or when root hairs were present. The effect size of the decreased water (η^2 = 0.54) was much higher than that of the presence of root hairs (η^2 = 0.23) (Fig. 7).

2.6.4.3 Co-localization analysis

The effect of root hairs on the co-localization between hotspots of enzyme activity and root exudates was negligible (Fig. 8a). The fraction of enzyme hotspots that overlapped with exudate hotspots was larger under optimal conditions than under drought conditions (p = 0.0329, Fig. 8a).

The interaction of soil moisture and genotypes affected the part of enzyme activity hotspots co-localized with hotspots of water (p = 0.0077, Fig. 8b). The fraction of enzyme hotspots co-localized with water was highest under drought conditions in those rhizoboxes with the mutant *rth3*.

Hotspots of root exudates or water co-localized strongly with hotspots of enzyme activities under optimal water content but hardly under drought (p < 0.05) (Fig. 8).

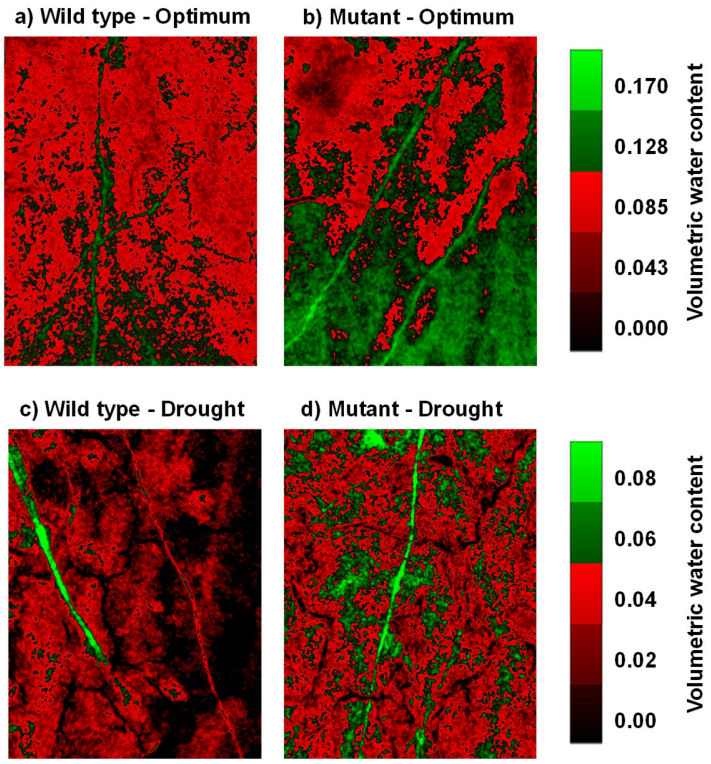

Figure 6. Region of interest (ROIs) of soil water spatial distribution for two maize genotypes (wild type and mutant *rth3*) under optimal water content (a & b) and drought conditions (c & d). Side color scale is proportional to volumetric water content.

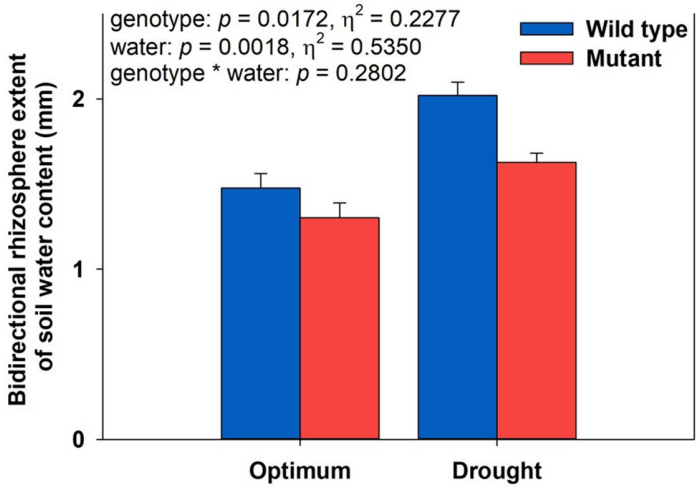

Figure 7 Bidirectional rhizosphere extent of soil water content for two maize genotypes (wild type and mutant *rth3*) under optimal water content and drought conditions. *p* values were obtained after two-way ANOVA. η^2: effect size; genotype: wild type and mutant *rth3*; water: drought and optimal water content. Data are mean (n=3) and error bars represent standard deviation (SD).

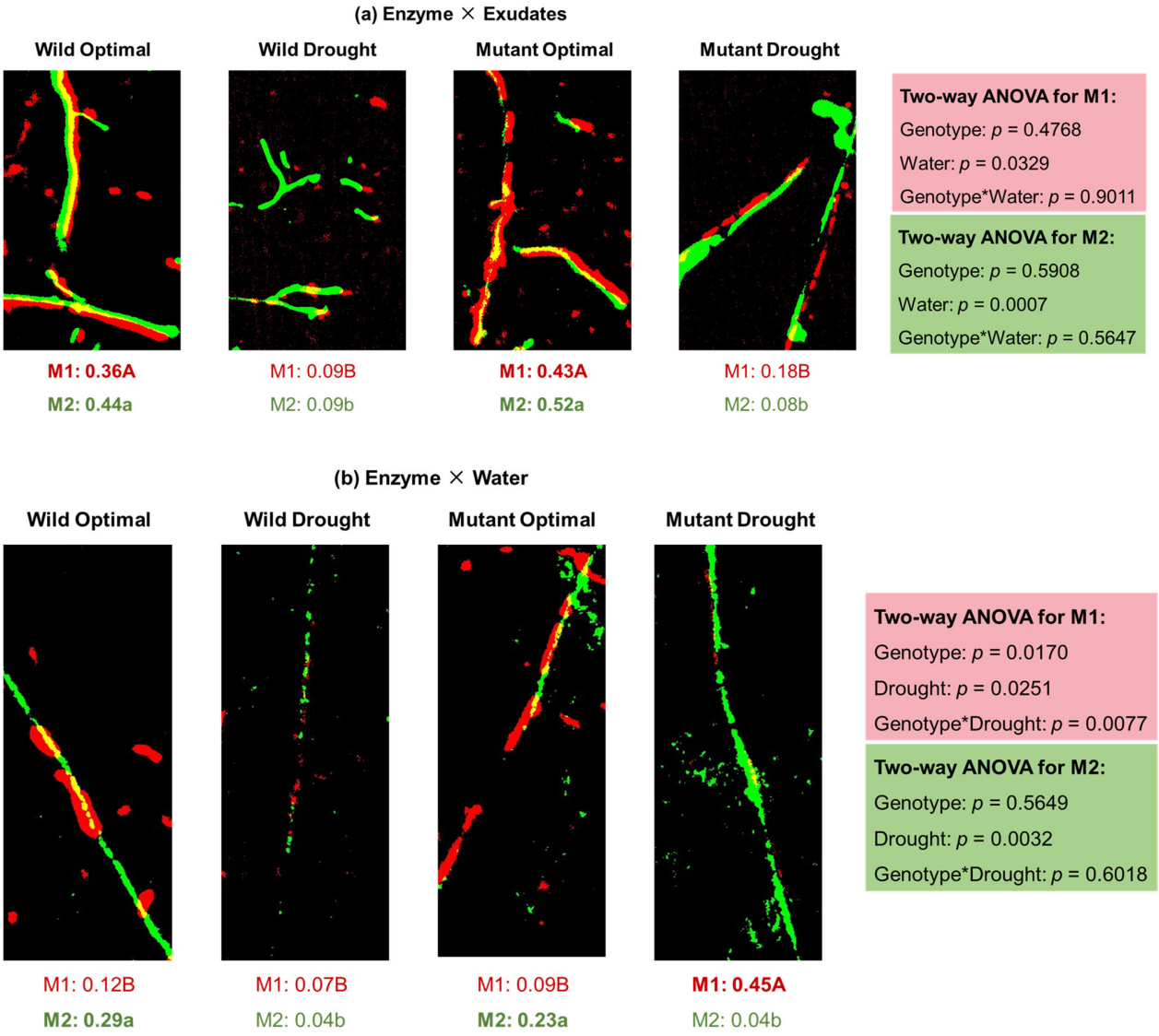

Figure 8 Colocalization analysis for region of interest (ROIs) of (a) hotspots between β-glucosidase activity (Enzyme) and ^{14}C exudates (Exudates), or (b) hotspots between β-glucosidase activity (Enzyme) and water content (Water). M1: Manders' coefficient, the fraction of Enzyme overlapping with Exudates or Water; M2: Manders' coefficient, the fraction of Exudates or Water overlapping with Enzyme; *p* values were obtained after two-way ANOVA. genotype: wild type and mutant *rth3*; water: drought and optimal water content. Upper case letters in (a): significant differences for M1 between optimal and drought conditions after two-way ANOVA and Student's t-test at $p < 0.05$. Upper case letters in (b): significant differences for M1 among four treatments after two-way ANOVA analysis and Tukey's HSD test at $p < 0.05$. Lower case letters in (a) and (b): significant differences for M2 between optimal and drought conditions after two-way ANOVA and Student's t-test at $p < 0.05$.

2.6.5 Discussion

2.6.5.1 Effects of root hairs and soil water content on rhizosphere biochemical properties

Higher β-glucosidase activities around roots (Fig. 1) occurred simultaneously with a higher allocation of photosynthesized C to root and rhizosphere as shown by ^{14}C imaging (Fig. 4). The activated and stimulated microbial activities induced by abundant labile C input (Wu *et al.*, 2017) and the direct enzyme release from roots (Asmar *et al.*, 1994) in the rhizosphere most likely drove the enzymatic hotspot there (Ma *et al.*, 2018). The effect of available substrate on the hotspot formation were more pronounced with the presence of root hairs. Root hairs, which released more root exudates (Fig. 4 , Pausch et al., 2016), enlarged the enzymatic hotspot area and extended the rhizosphere size (Fig. 1 and 2) as well as increased the enzyme activities (Fig. 3a). As the diffusion of enzymes is very limited (Guber et al., 2018), the direct enzyme release by roots is relevant only for the rhizoplane, and most of the rhizosphere enzymes are produced by microorganisms (which are stimulated by root exudates). Thus, the microbiome inhabiting the rhizosphere soil of the mutant *rth3* expressed efficient isoenzyme (reflected in higher substrate affinity) (Fig. 3b) to compensate for the absence of abundant root exudates (Zhang *et al.*, 2020).

Although root exudates directly relieved microbial C limitation, the importance of soil moisture offset root hairs in regulating the occurrence of enzyme hotspots. Drought reduced the hotspot area (Fig. 2a) and narrowed the rhizosphere extent of β-glucosidase activity (Fig. 2b). The larger hotspots area and wider rhizosphere extent of β-glucosidase activity were concurrent with optimal water content because the proper soil moisture is a prerequisite for higher root biomass. It has been strongly suggested as a compelling explanation for higher rhizodeposition (Preece and Peñuelas, 2016). Additionally, the optimal water content provides a suitable growth environment for microorganisms, and increased microbial access to nutrients and energy (Ahmed *et al.*, 2018), as well as an improved diffusion of root exudates into the extended soil volume (Holz *et al.*, 2019a). Consequently, β-glucosidase activities in wet soil were higher than under drought conditions (Fig. 3a). Such higher β-glucosidase activities were sufficient to maintain microbial activities and crucial functions, and thus the enzyme systems in dry soil were more efficient (Fig. 3b). Accordingly, we conclude that soil moisture is likely to contribute more than root morphology such as root hairs in controlling enzymatic hotspot and their distribution in the rhizosphere. Despite this, root hairs still play extremely important roles when plants face droughts. For example, root hairs tend to increase the hotspot area of root exudates, as well as significantly widen the rhizosphere extension of root exudates and water under drought (Fig. 5 & 7) meaning

24% - 37% increase of proportion of soil which can be mined by plant – a crucial root trait considering that the efficiency of gaining water and nutrients from a defined soil volume may strongly decrease under drought. These are likely to facilitate microbial activity and increase lubrication in the dry soil (Preece and Peñuelas, 2016; Holz *et al.*, 2018c), and thus enhance enzyme activity (Fig. 2 and 3) and hence, nutrient availability for plant.

2.6.5.2 The spatial control of root exudates or soil water on enzyme activity

Although the presence of root hairs showed positive effects on spatial distribution of β-glucosidase activity (Fig. 2 & 3), the relation between β-glucosidase and root exudates was unaffected by the presence or absence of root hairs (Fig. 8a). The co-localization of enzymatic hotspot and root exudates was strongly influenced by soil moisture (M1 and M2, Fig. 8a), i.e. it was weaker under drought than under optimal soil water content (Fig. 8a). Such discordance in the spatial distribution of enzyme activity hotspots (Fig. 1) and the concentrated localization of root exudates (Fig. 4) under drought could be explained by: 1) a lower enzyme production. Drought suppressed microbial activities (Huxman *et al.*, 2004; Dijkstra *et al.*, 2015) due to osmotic stresses (Turner *et al.*, 2003; Sanaullah *et al.*, 2011) and the lower substrate mobility (Schimel *et al.*, 2007). Thus, the released root exudates were likely to satisfy microbial living and maintenance but insufficient for enzyme production and expression. 2) the reduced translocation of easily available C to the rhizosphere (Fig. 4) because of the lower belowground C demand, the alteration in the allocation of recent photosynthates and the reduced diffusion of released C compounds (Ruehr *et al.*, 2009; Fuchslueger *et al.*, 2014; Hasibeder *et al.*, 2015). Consequently, this will decouple the spatial relation of root exudates, activation of microbes and enzyme activities. 3) Plant reduced direct enzyme release under drought. We assume that the portion of enzyme which were independent on root exudates were those existing in the soil previously or produced by microorganisms. Those enzymes functioned well under drying probably because enzymes and substrates are concentrating up in shrinking water films and small water-filled pores where the co-location of enzymes and substrates gets facilitated (Schimel, 2018). Hence, simultaneous analyzing the spatial distribution of root exudates, enzyme activities enable drawing conclusion that only the enzyme activities on the rhizoplane (root surface) or associated with root hairs originate directly from roots and a large amount of enzyme activity in the rhizosphere are drove by microorganisms.

Remarkably, the hotspot of β-glucosidase activity overlapped strongly with water hotspots under drought especially in rhizoboxes with the mutant *rth3* (M1 = 0.0077) (Fig. 8b). The co-

limitation of water and root exudates induced higher spatial dependency of enzymatic hotspots on water (Fig. 8b), but lower on root exudates (Fig. 8a). This suggests that water availability is more important than root exudates for a high catalytic activity in enzymatic hotspots under occurrence of a carbon and water co-limitations. This can be supported by the higher contribution of soil water hotspots to enzymatic hotspots under optimal soil moisture (values of M2, Fig. 8b). When soil water content decreases, the water films coating soil particle surfaces become thinner (Goebel *et al.*, 2011). This alteration of conducting liquid pathways decreases solute diffusion rates while increasing soil aeration (Ebrahimi & Or, 2016), (e.g. pattern valid for micropores, which are normally in anoxic conditions), and may change the chemical form of the elements (Makino *et al.*, 2000; Sardans & Peñuelas, 2007). Some of these elements are co-factors essential for cellular and enzyme functions (e.g. Tebo et al., 2005), so their bioavailability could improve microbial growth, activity and organic matter decomposition (Watanabe, et al., 2012). Similarly, when nutrient and enzyme diffusion is restricted under drought, nutrient availability to microorganisms is affected (Zarebanadkouki *et al.*, 2019), leading to starvation (Bär *et al.*, 2002). Therefore, many microorganisms were unable to thrive even though they inhabited microsites with high availability of C sources. Accordingly, root and their rhizosphere microbiome developed strategies to maintain a higher water content in the rhizosphere under drought. For example, the drought treatment widened the rhizosphere extent of root exudates irrespective of root hairs (Fig. 5) and thus at least partially compensates for the negative effects of drought. This wider extent might be attributed to the increased quantity of gel-like substance - mucilage -around the drought-stressed root (Carminati *et al.*, 2010; Sanaullah *et al.*, 2012), which accounted for 2-12% of total rhizodeposition (Dennis et al., 2010; Holz et al., 2018). Mucilage was shown to increase the water content at the root-soil interface during soil drying (McCully & Boyer, 1997; Carminati *et al.*, 2010). The presence of mucilage probably widened the area with high water extent close to the root especially under drought (Fig. 7) and thus induced faster diffusion rates of root exudate from root surface to soil (Kuzyakov & Razavi, 2019). Similar to the effect of mucilage, extracellular polymeric substances (EPS) produced by microorganism buffers moisture fluctuations in soil (Padhy *et al.*, 2018). Despite those beneficial microenvironments for rhizomicrobial growth, hotspots and rhizosphere extent of β-glucosidase activities were still lower under drought conditions than under optimal water content (Fig. 2).

2.6.6 Conclusions

Consequently, although biotic factors (e.g. root exudates) play an important role in the area and distributions of hydrolytic, SOM decomposing enzyme activities in soil, abiotic factors such

as soil moisture played a more important role for the formation of enzymatic hotspots, which are mainly located in the rhizosphere and define the rhizosphere extent. More in detail, the combination of three imaging methods (zymography, ^{14}C imaging and neutron radiography) pointed out that the co-localization between enzymatic hotspots and root exudates were only pronounced under optimal soil moisture where exudates are fueling the *de-novo* production of enzymes. While water availability limits the formation of enzyme hotspot areas under co-limitation of available C and water, the water films potentially supported by biogels such as mucilage and concentrated water films in micropores define the areas, where high enzyme activities can be maintained irrespective of a decrease in the average soil moisture (Fig. 9).

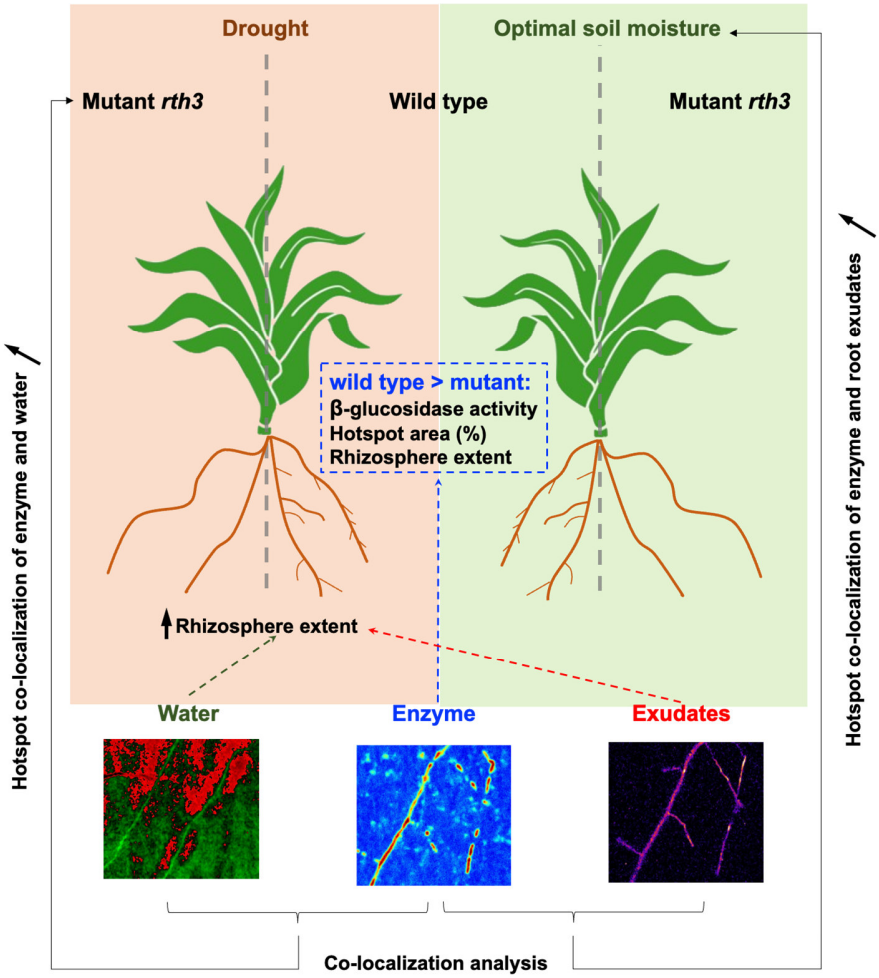

Figure 9 Root hairs induced larger hotspot area and broader rhizosphere extent of β-glucosidase activities, as well as higher potential β-glucosidase activities (V_{max}) than that for the maize mutant. Drought widened the rhizosphere extent of root exudates and soil water. Co-localization analysis showed that enzymatic hotspots are more co-localized with hotspots of root exudates under optimal water conditions. In contrast, enzyme hotspots showed higher dependency on water hotspots under the scarcity of both water and root exudates.

2.6.7 Acknowledgments

We gratefully acknowledge Jan Hovind from the ICON imaging station of the Paul Scherrer Institute (PSI), Villigen, Switzerland for their facilities and excellent technical support during the measurements with neutron radiography and providing us an imager (FLA-7000), and facilities for zymography installations. We greatly acknowledge. We acknowledge Caroline Marcon and Frank Hochholdinger (University of Bonn) for kindly providing seeds of maize mutant *rth3*. We greatly acknowledge Mohsen Zarebanadkouki for providing us his code to calculate water contents in the neutron images. This project was carried out in the framework of the priority programme 2089 “Rhizosphere spatiotemporal organization – a key to rhizosphere functions’ funded by the Deutsche Forschungsgemeinschaft (DFG, German Research Fundation) – Project numbers: 403670038 (BSR & SPP), 403670197 (MAA). M. Dippold and her PSI stay was financed by the Robert-Bosch Junior Professorship 2017. We gratefully acknowledge the China Scholarship Council (CSC) for financial support for Xuechen Zhang.

2.6.8 References

Ahmadi K, Razavi BS, Maharjan M, Kuzyakov Y, Kostka SJ, Carminati A, Zarebanadkouki M. 2018. Effects of rhizosphere wettability on microbial biomass, enzyme activities and localization. *Rhizosphere* 7: 35–42.

Ahmed MA, Kroener E, Holz M, Zarebanadkouki M, Carminati A. 2014. Mucilage exudation facilitates root water uptake in dry soils. *Functional Plant Biology* 41: 1129.

Ahmed MA, Sanaullah M, Blagodatskaya E, Mason-Jones K, Jawad H, Kuzyakov Y, Dippold MA. 2018. Soil microorganisms exhibit enzymatic and priming response to root mucilage under drought. *Soil Biology and Biochemistry* 116: 410–418.

Ahmed MA, Zarebanadkouki M, Kaestner A, Carminati A. 2016. Measurements of water uptake of maize roots: the key function of lateral roots. *Plant and Soil* 398: 59–77.

Asmar F, Eiland F, Nielsen NE. 1994. Effect of extracellular-enzyme activities on solubilization rate of soil organic nitrogen. *Biology and Fertility of Soils* 17: 32–38.

Badri DV, Vivanco JM. 2009. Regulation and function of root exudates. *Plant, Cell & Environment* 32: 666–681.

Banfield CC, Zarebanadkouki M, Kopka B, Kuzyakov Y. 2017. Labelling plants in the Chernobyl way: A new 137Cs and 14C foliar application approach to investigate rhizodeposition and biopore reuse. *Plant and Soil* 417: 301–315.

Bär M, Hardenberg J, Meron E, Provenzale A. 2002. Modelling the survival of bacteria in drylands: the advantage of being dormant. *Proceedings of the Royal Society of London. Series B: Biological Sciences* 269: 937–942.

Bilyera N, Zhang X, Duddek P, Fan L, Banfield CC, Schlüter S, Carminati A, Kaestner A, Ahmed MA, Kuzyakov Y. 2021. Maize genotype-specific exudation strategies: An adaptive mechanism to increase microbial activity in the rhizosphere. *Soil Biology and Biochemistry* 162: 108426.

Bolte S, Cordelières FP. 2006. A guided tour into subcellular colocalization analysis in light microscopy. *Journal of Microscopy* 224: 213–232.

Burns RG. 1982. Enzyme activity in soil: Location and a possible role in microbial ecology. *Soil Biology and Biochemistry* 14: 423–427.

Cailloux M. 1972. Metabolism and the absorption of water by root hairs. *Canadian Journal of Botany* 50: 557–573.

Cardona A, Saalfeld S, Schindelin J, Arganda-Carreras I, Preibisch S, Longair M, Tomancak P, Hartenstein V, Douglas RJ. 2012. TrakEM2 Software for Neural Circuit Reconstruction. *PLOS ONE* 7: e38011.

Carminati A, Moradi AB, Vetterlein D, Vontobel P, Lehmann E, Weller U, Vogel H-J, Oswald SE. 2010. Dynamics of soil water content in the rhizosphere. *Plant and Soil* 332: 163–176.

Carminati A, Passioura JB, Zarebanadkouki M, Ahmed MA, Ryan PR, Watt M, Delhaize E. 2017. Root hairs enable high transpiration

rates in drying soils. *New Phytologist* 216: 771–781.

Datta S, Kim CM, Pernas M, Pires ND, Proust H, Tam T, Vijayakumar P, Dolan L. 2011. Root hairs: development, growth and evolution at the plant-soil interface. *Plant and Soil* 346: 1–14.

Dennis PG, Miller AJ, Hirsch PR. 2010. Are root exudates more important than other sources of rhizodeposits in structuring rhizosphere bacterial communities? *FEMS Microbiology Ecology* 72: 313–327.

Dijkstra FA, He M, Johansen MP, Harrison JJ, Keitel C. 2015. Plant and microbial uptake of nitrogen and phosphorus affected by drought using 15N and 32P tracers. *Soil Biology and Biochemistry* 82: 135–142.

Ebrahimi A, Or D. 2016. Microbial community dynamics in soil aggregates shape biogeochemical gas fluxes from soil profiles – upscaling an aggregate biophysical model. *Global Change Biology* 22: 3141–3156.

Esser HG, Carminati A, Vontobel P, Lehmann EH, Oswald SE. 2010. Neutron radiography and tomography of water distribution in the root zone. *Journal of Plant Nutrition and Soil Science* 173: 757–764.

Fuchslueger L, Bahn M, Fritz K, Hasibeder R, Richter A. 2014. Experimental drought reduces the transfer of recently fixed plant carbon to soil microbes and alters the bacterial community composition in a mountain meadow. *New Phytologist* 201: 916–927.

Gargallo-Garriga A, Preece C, Sardans J, Oravec M, Urban O, Peñuelas J. 2018. Root exudate metabolomes change under drought and show limited capacity for recovery. *Scientific Reports* 8: 12696.

German DP, Weintraub MN, Grandy AS, Lauber CL, Rinkes ZL, Allison SD. 2011. Optimization of hydrolytic and oxidative enzyme methods for ecosystem studies. *Soil Biology and Biochemistry* 43: 1387–1397.

Goebel M-O, Bachmann J, Reichstein M, Janssens IA, Guggenberger G. 2011. Soil water repellency and its implications for organic matter decomposition – is there a link to extreme climatic events? *Global Change Biology* 17: 2640–2656.

Hasibeder R, Fuchslueger L, Richter A, Bahn M. 2015. Summer drought alters carbon allocation to roots and root respiration in mountain grassland. *New Phytologist* 205: 1117–1127.

Heitkötter J, Marschner B. 2018. Soil zymography as a powerful tool for exploring hotspots and substrate limitation in undisturbed subsoil. *Soil Biology and Biochemistry* 124: 210–217.

Hinsinger P, Bengough AG, Vetterlein D, Young IM. 2009. Rhizosphere: biophysics, biogeochemistry and ecological relevance. *Plant and Soil* 321: 117–152.

Hochholdinger F, Wen T-J, Zimmermann R, Chimot-Marolle P, da Costa e Silva O, Bruce W, Lamkey KR, Wienand U, Schnable PS. 2008. The maize (Zea mays L.) roothairless3 gene encodes a putative GPI-anchored, monocot-specific, COBRA-like protein that significantly affects grain yield. *The Plant Journal* 54: 888–898.

Hochholdinger F, Yu P, Marcon C. 2018. Genetic Control of Root System Development in Maize. *Trends in Plant Science* 23: 79–88.

Holz M, Leue M, Ahmed MA, Benard P, Gerke HH, Carminati A. 2018a. Spatial Distribution of Mucilage in the Rhizosphere Measured With Infrared Spectroscopy. *Frontiers in Environmental Science* 6.

Holz M, Zarebanadkouki M, Carminati A, Hovind J, Kaestner A, Spohn M. 2019a. Increased water retention in the rhizosphere allows for high phosphatase activity in drying soil. *Plant and Soil* 443: 259–271.

Holz M, Zarebanadkouki M, Carminati A, Kuzyakov Y. 2019b. Visualization and quantification of root exudation using 14C imaging: challenges and uncertainties. *Plant and Soil*.

Holz M, Zarebanadkouki M, Kaestner A, Kuzyakov Y, Carminati A. 2018b. Rhizodeposition under drought is controlled by root growth rate and rhizosphere water content. *Plant Soil* 423: 429–442.

Holz M, Zarebanadkouki M, Kuzyakov Y, Pausch J, Carminati A. 2018c. Root hairs increase rhizosphere extension and carbon input to soil. *Annals of Botany* 121: 61–69.

Huxman TE, Smith MD, Fay PA, Knapp AK, Shaw MR, Loik ME, Smith SD, Tissue DT, Zak JC, Weltzin JF, *et al.* 2004. Convergence across biomes to a common rain-use efficiency. *Nature* 429: 651–654.

Jones DL, Nguyen C, Finlay RD. 2009. Carbon flow in the rhizosphere: carbon trading at the soil–root interface. *Plant and Soil* 321: 5–33.

Jungk A. 2001. Root hairs and the acquisition of plant nutrients from soil. *Journal of Plant Nutrition and Soil Science* 164: 121–129.

Kaestner AP, Hartmann S, Kühne G, Frei G, Grünzweig C, Josic L, Schmid F, Lehmann EH. 2011. The ICON beamline – A facility for cold neutron imaging at SINQ. *Nuclear Instruments and Methods in Physics Research Section A: Accelerators, Spectrometers, Detectors and Associated Equipment* 659: 387–393.

Kumar A, Shahbaz M, Blagodatskaya E, Kuzyakov Y, Pausch J. 2018. Maize phenology alters the distribution of enzyme activities in soil: Field estimates. *Applied Soil Ecology*.

Kuzyakov Y, Domanski G. 2000. Carbon input by plants into the soil. Review. *Journal of Plant Nutrition and Soil Science* 163: 421–431.

Kuzyakov Y, Raskatov A, Kaupenjohann M. 2003. Turnover and distribution of root exudates of Zea mays. *Plant and Soil* 254: 317–327.

Kuzyakov Y, Razavi BS. 2019. Rhizosphere size and shape: Temporal dynamics and spatial stationarity. *Soil Biology and Biochemistry*: S0038071719301452.

Kuzyakov Y, Shevtzova E, Pustovoytov K. 2006. Carbonate re-crystallization in soil revealed by 14C labeling: Experiment, model and significance for paleo-environmental reconstructions. *Geoderma* 131: 45–58.

Ma X, Zarebanadkouki M, Kuzyakov Y, Blagodatskaya E, Pausch J, Razavi BS. 2018. Spatial patterns of enzyme activities in the rhizosphere: Effects of root hairs and root radius. *Soil Biology and Biochemistry* 118: 69–78.

Michaelis, L, Menten, ML. 1913. Kinetik der Invertinwirkung. Biochem. Zeitung 49: 333–369.

Makino T, Hasegawa S, Sakurai Y, Ohno S, Utagawa H, Maejima Y, Momohara K. 2000. Influence of soil-drying under field conditions on exchangeable manganese, cobalt, and copper contents. *Soil Science and Plant Nutrition* 46: 581–590.

Manders EMM, Verbeek FJ, Aten JA. 1993. Measurement of co-localization of objects in dual-colour confocal images. *Journal of Microscopy* 169: 375–382.

McCully ME, Boyer JS. 1997. The expansion of maize root-cap mucilage during hydration. 3. Changes in water potential and water content. *Physiologia Plantarum* 99: 169–177.

Moradi AB, Conesa HM, Robinson B, Lehmann E, Kuehne G, Kaestner A, Oswald S, Schulin R. 2009. Neutron radiography as a tool for revealing root development in soil: capabilities and limitations. *Plant and Soil* 318: 243–255.

Nguyen C. 2009. Rhizodeposition of Organic C by Plant: Mechanisms and Controls. In: Lichtfouse E, Navarrete M, Debaeke P, Véronique S, Alberola C, eds. Sustainable Agriculture. Dordrecht: Springer Netherlands, 97–123.

Oburger E, Gruber B, Schindlegger Y, Schenkeveld WDC, Hann S, Kraemer SM, Wenzel WW, Puschenreiter M. 2014. Root exudation of phytosiderophores from soil-grown wheat. *New Phytologist* 203: 1161–1174.

Oswald SE, Menon M, Carminati A, Vontobel P, Lehmann E, Schulin R. 2008. Quantitative Imaging of Infiltration, Root Growth, and Root Water Uptake via Neutron Radiography. *Vadose Zone Journal* 7: 1035–1047.

Padhy SR, Nayak S, Dash PK, Das M, Roy KS, Nayak AK, Neogi S, Bhattacharyya P. 2018. Elevated carbon dioxide and temperature imparted intrinsic drought tolerance in aerobic rice system through enhanced exopolysaccharide production and rhizospheric activation. *Agriculture, Ecosystems & Environment* 268: 52–60.

Pausch J, Kuzyakov Y. 2011. Photoassimilate allocation and dynamics of hotspots in roots visualized by C-14 phosphor imaging. *Journal of Plant Nutrition and Soil Science* 174: 12–19.

Pausch J, Loeppmann S, Kühnel A, Forbush K, Kuzyakov Y, Cheng W. 2016. Rhizosphere priming of barley with and without root hairs. *Soil Biology and Biochemistry* 100: 74–82.

Peterson RL, Farquhar ML. 1996. Root hairs: Specialized tubular cells extending root surfaces. *The Botanical Review* 62: 1–40.

Poirier V, Roumet C, Munson AD. 2018. The root of the matter: Linking root traits and soil organic matter stabilization processes. *Soil Biology and Biochemistry* 120: 246–259.

Preece C, Peñuelas J. 2016. Rhizodeposition under drought and consequences for soil communities and ecosystem resilience. *Plant and Soil* 409: 1–17.

Razavi BS, Zarebanadkouki M, Blagodatskaya E, Kuzyakov Y. 2016. Rhizosphere shape of lentil and maize: Spatial distribution of enzyme activities. *Soil Biology and Biochemistry* 96: 229–237.

Ruehr NK, Offermann CA, Gessler A, Winkler JB, Ferrio JP, Buchmann N, Barnard RL. 2009. Drought effects on allocation of recent carbon: from beech leaves to soil CO2 efflux. *New Phytologist* 184: 950–961.

Sanaullah M, Blagodatskaya E, Chabbi A, Rumpel C, Kuzyakov Y. 2011. Drought effects on microbial biomass and enzyme activities in the rhizosphere of grasses depend on plant community composition. *Applied Soil Ecology* 48: 38–44.

Sanaullah M, Chabbi A, Rumpel C, Kuzyakov Y. 2012. Carbon allocation in grassland communities under drought stress followed by 14C pulse labeling. *Soil Biology and Biochemistry* 55: 132–139.

Sardans J, Peñuelas J. 2007. Drought changes the dynamics of trace element accumulation in a Mediterranean Quercus ilex forest. *Environmental Pollution* 147: 567–583.

Schimel JP. 2018. Life in Dry Soils: Effects of Drought on Soil Microbial Communities and Processes. *Annual Review of Ecology, Evolution, and Systematics* 49: 409–432.

Schimel J, Balser TC, Wallenstein M. 2007. Microbial Stress-Response Physiology and Its Implications for Ecosystem Function. *Ecology* 88: 1386–1394.

Spohn M, Kuzyakov Y. 2013. Distribution of microbial- and root-derived phosphatase activities in the rhizosphere depending on P availability and C allocation – Coupling soil zymography with 14C imaging. *Soil Biology and Biochemistry* 67: 106–113.

Tebo BM, Johnson HA, McCarthy JK, Templeton AS. 2005. Geomicrobiology of manganese(II) oxidation. *Trends in Microbiology* 13: 421–428.

Thu Hoang DT, Maranguit D, Kuzyakov Y, Razavi BS. 2020. Accelerated microbial activity, turnover and efficiency in the drilosphere is depth dependent. *Soil Biology and Biochemistry* 147: 107852.

Turner BL, Driessen JP, Haygarth PM, Mckelvie ID. 2003. Potential contribution of lysed bacterial cells to phosphorus solubilisation in two rewetted Australian pasture soils. *Soil Biology and Biochemistry* 35: 187–189.

Vetterlein D, Lippold E, Schreiter S, Phalempin M, Fahrenkampf T, Hochholdinger F, Marcon C, Tarkka M, Oburger E, Ahmed M, *et al.* 2021. Experimental platforms for the investigation of spatiotemporal patterns in the rhizosphere—Laboratory and field scale. *Journal of Plant Nutrition and Soil Science* 184: 35–50.

Watanabe M, van der Veen S, Nakajima H, Abee T. 2012. Effect of respiration and manganese on oxidative stress resistance of Lactobacillus plantarum WCFS. 158: 293–300.

Wu X, Ge T, Yan W, Zhou J, Wei X, Chen L, Chen X, Nannipieri P, Wu J. 2017. Irrigation management and phosphorus addition alter the abundance of carbon dioxide-fixing autotrophs in phosphorus-limited paddy soil. *FEMS Microbiology Ecology* 93.

Zarebanadkouki M, Ahmed M, Hedwig C, Benard P, Kostka SJ, Kastner A, Carminati A. 2018. Rhizosphere hydrophobicity limits root water uptake after drying and subsequent rewetting. *Plant and Soil* 428: 265–277.

Zarebanadkouki M, Fink T, Benard P, Banfield CC. 2019. Mucilage Facilitates Nutrient Diffusion in the Drying Rhizosphere. *Vadose Zone Journal* 18: 1–13.

Zhang X, Dippold MA, Kuzyakov Y, Razavi BS. 2019. Spatial pattern of enzyme activities depends on root exudate composition. *Soil Biology and Biochemistry* 133: 83–93.

Zhang X, Kuzyakov Y, Zang H, Dippold MA, Shi L, Spielvogel S, Razavi BS. 2020. Rhizosphere hotspots: Root hairs and warming control microbial efficiency, carbon utilization and energy production. *Soil Biology and Biochemistry*: 107872.

2.6.9 Supplementary materials

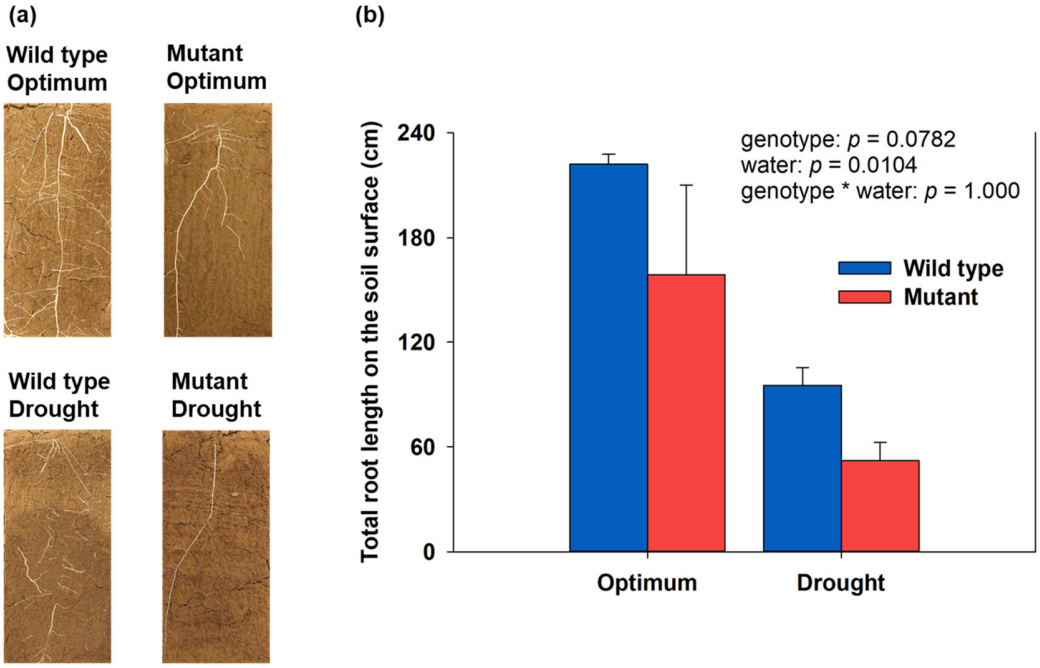

Figure S1. (a) root images and (b) total root length on the soil surface for two maize genotypes (wild type and mutant *rth3*) under optimal water content and drought conditions. *p* values were obtained after Scheirer-Ray-Hare test. genotype: wild type and mutant *rth3*; water: drought and optimal water content. Data are mean (n=3) and error bars represent standard deviation (SD).

2.7 Study 7. Effect of root hairs and benzoxazinoids on maize microbiome and its enzymatic activity in the rhizosphere hot- and coldspots

Nataliya Bilyera[a,b], Jan Waelchli[c], Lingling Shi[d,e,f], Veronica Caggia[g], Xuechen Zhang[e], Klaus Shlaeppi[c,g], Michaela A. Dippold[e,f], Bahar S. Razavi[a], Sandra Spielvogel[b]

[a] *Department of Soil and Plant Microbiome, Christian-Albrechts-University of Kiel, Kiel, Germany*
[b] *Department of Soil Science, Christian-Albrechts-University of Kiel, Kiel, Germany*
[c] *Plant Microbe Interactions, Department of Environmental Sciences, University of Basel, Basel, Switzerland*
[d] *Key Laboratory of Economic Plants and Biotechnology, Kunming Institute of Botany, Chinese Academy of Sciences, Kunming, China*
[e] *Department of Biogeochemistry of Agroecosystems, University of Göttingen, Göttingen, Germany*
[f] *Geo-Biosphere Interactions, University of Tuebingen, Tuebingen, Germany*
[g] *Institute of Plant Sciences, University of Bern, Bern, Switzerland*

*Corresponding author Bahar S. Razavi, Email: brazavi@phytomed.uni-kiel.de

Status: *Unpublished, In preparation*

2.7.1 Abstract

Root morphology and the composition of root exudates shape the spatial organization and various processes in the rhizosphere. For instance, root hairs are essential for plant nutrition, while secondary plant metabolites (i.e. benzoxazinoids) ensure plant defence from herbivore and fungal infection. Nevertheless, it is still unknown to which extent root hairs and benzoxazinoids may change the microbiome and enzymatic activities, as well as formation of rhizosphere hot- and coldspots.

To study the effect of root hairs and benzoxasinoids on the rhizosphere microbiome structure and its enzymatic activities we compared mutants with defective root hairs *rth3* or with reduced benzoxazinoids *bx1* with the corresponding wild-type (WT) maize.

Root hairs increased acid phosphatase activity by 80% promoting mineralization of organic phosphorus sources to available forms in the hotspots. In the coldspots, broken root hairs in WT facilitated the intensive microbial hotspots with up to two times higher β-glucosidase and chitinase activities, compared to *rth3*.

The presence of benzoxazinoids in root exudates strongly supported plant defence against pathogenic fungi (i.e., genus *Fusarium* and *Gibberella*) while the total microbial biomass remained unaffected. In response to the presence of pathogenic fungi, *bx1* exuded 70% more chitinase for defence purpose to partly compensate for benzoxazinoids deficiency, which was however, less efficient against pathogens than the presence of benzoxazinoids.

Overall, we conclude that: i) root hairs facilitate better plant nutrition at the shortage of available nutrients (i.e., coldspots), while; ii) the presence of benzoxazinoids in exudates protect plant from pathogenic microorganisms. This two root traits are promising for plant breeding of genotypes suitable for sustainable agriculture and organic farming.

Keywords: enzyme activity; substrate affinity; plant defence, secondary metabolites, DNA sequencing.

2.7.2 Introduction

Spatial organization of the rhizosphere plays and important role for its functioning, as roots attract microbes via exudation to form specific soil rhizosphere microbiome which contribute to plant nutrition (Berg and Smalla, 2009; Bonkowski et al., 2021; Vetterlein et al., 2020). The enzymes released by root and produced by microorganisms are the main players of biochemical cycle in the rhizosphere able mineralizing soil organic matter (SOM) to mine for limiting nutrients (Sinsabaugh and Follstad Shah, 2012). An increased enzyme activity in the rhizosphere reflects microbial nutrients demand (Allison and Vitousek, 2005), and could be maintained temporally due to strong competition for available nutrients between roots and microorganism (Kuzyakov and Xu, 2013).

The application of soil zymography – *in situ* imaging method of soil enzymatic activities – allows mapping the gradient of enzyme activities in the rhizosphere (Heitkötter and Marschner, 2018; Razavi et al., 2019; Spohn et al., 2013). Thus, numerous soil zymography studies revealed the formation of microbial hotspot of increased β-glucosidase, cellobiohydrolase, acid phosphatase, chitinase, leucine aminopeptidase, activities in the rhizosphere (Ge et al., 2017; Giles et al., 2018; Greenfield et al., 2021; Holz et al., 2020; Hummel et al., 2021; Ma et al., 2018, 2017; Rakotoson et al., 2020; Razavi et al., 2016b; Tian et al., 2020). However, the enzymatic hotspots are not always homogeneously distributed in the rhizosphere (Tian et al., 2020) and may coincide there with the recently described coldspots – the microsites with activities in the range

of bulk soil but localized within the rhizosphere (Zhang et al., 2021). The microorganisms in the rhizosphere hotspots have a greater enzyme activity, lower affinity for the substrates and lower catalytic efficiency (Sanaullah et al., 2016; Tian et al., 2020), but the enzyme kinetics parameters in the coldspots remains less studied.

The different spatial patterns (hotspots or coldspots) may be formed and could be efficient only at the presence of substrates. Thus, hotspots are located mainly along the active root parts with locally induced N limitation and high input of primary metabolites as a substrate for maintaining high enzyme activities. Additionally, microbial community in the hotspots are generally characterized by a lower alpha diversity (Peiffer et al., 2013), but different groups of microorganisms have more relationships between each other's (Zhang et al., 2021). In contrast to hotspots, microorganisms in the coldspots could be less affected by root activity being located in zones with low nutrients adsorption capacity, and consequently, according to microbial economic theory, enzyme production will be lower if nutrients acquisition is decreased (Koch, 1985). Besides, microbiome in the coldspots could be more diverse (Peiffer et al., 2013), but less connected in between groups than in the hotspots (Zhang et al., 2021).

Root morphology (i.e. root hairs) and exudate composition (i.e. benzoxazinoids) are the root traits that may modify the formation and distribution of hot- and coldspots in the rhizosphere, as well as alter their microbiome and influence their hydrolytic properties. On one hand, the presence of root hairs ensures larger root surface in contact with soil resulting in higher nutrients absorption and leading to depletion zone formation (Haling et al., 2013; Hummel et al., 2021; Silberbush and Barber, 1983). Later, after the break and lysis of the root hairs the formed rhizodeposits may serve as a substrate for microorganisms promoting their activity and increasing the portion of active microbial biomass (Jungk, 2001, Zhang et al., 2020). On the other hand, plant compansate the absence of root hairs by higher exudation rates from the whole root system if compared to mainly root tip exudation of maize with root hairs (Bilyera at al., 2021). Moreover, low molecular substances released with exudates are more availalble for microoorganisms, than root hair residues, which require additional energy and sources to degrade. Thus, it is still unknown to which extend the presence of root hairs may facilitate or inhibit the formation of rhizosphere hotspot and coldspot, and which effect they may have on the microbiome structure and its diversity.

During the growing period, maize experiences not only nutrients limitation, but also faces herbivores and fungal damage. In response to this damage, plant synthesizes and releases

benzoxazinoids (BXs) – the defensive secondary metabolites (Dick et al., 2012; Erb and Kliebenstein, 2020; Frey et al., 1997; Seybold et al., 2020). Despite an important plant protective function, benzoxazinoids were found to reduce maize yield in the field experiment (Hu et al., 2018) probably due to the inhibition of beneficial microorganisms, which in turn increase nutrients availability (Berendsen et al., 2012; Hu et al., 2018). Thus, the inhibitory effects of benzoxasinoids could, on one hand, promote higher nutrients demand and formation of enzymatic hotspots, and on the other hand, benzoxazinoids may inactivate some part of enzyme-producing microorganisms, decrease their alpha diversity and thus hamper enzymatic hotspots formation. These possible contradictory effects caused by benzoxazinoids reiquire detailed studies on rhizosphere microbiome and its enzyme kinetic parameters in the hot- and coldspots.

To study the effects of root hairs and benzoxazinoids on the enzyme kinetics parameters and microbiome structure and diversity in the rhizosphere hot- and coldspots, we compared maize mutant with defective root hairs *rth3* and mutant with reduced benzoxazinoids in exudates *bx1* with the corresponding wild-type (WT) maize (B73) (Table 1). We hypothesized, that (i) the rhizosphere coldspots are formed in low substrate region, which induces C limitation and higher alpha diversity of microbiome, (ii) the presence of root hairs increases microbial biomass and decreases C limitation (iii) the total microbial biomass and biodiversity (alpha) is higher in the absence of benzoxazinoids, as they act as defensive secondary metabolites and suppress microbial activity. To test these hypotheses, we applied soil zymography at 21-days old maize of three genotypes (WT, *rth3*, *bx1*) grown under laboratory conditions to localize rhizosphere hot- and coldspots of β-glucosidase activity – an enzyme important for SOM mineralization. Further, we measured kinetics parameters of C-cycle (β-glucosidase), P-cycle (acid phosphatase) and N-cycle (chitinase and leucine aminopeptidase) enzymes, and conducted DNA extraction and sequencing in the soil from hot and coldspots of rhizosphere.

Table 1. Root traits of the maize genotypes (wild-type (WT), *rth3* and *bx1*) and their role for microbial activity in the rhizosphere and plant nutrition

Root traits	Genotypes			Role
	bx1*	**WT**	***rth3*****	
Root-hairs	+	+	-	Higher adsorption surface, large extent for exudates release, broken root hairs as additional source of OM.
Benzoxazinoids	-	+	+	Suppress microbial biomass; act as a defensive metabolite

*90% reduced amount of benzoxazinoids in exudates (Frey et al., 1997)
** 90% reduced and defective root-hairs (Hochholdinger et al., 2008)

2.7.3 Materials and methods

2.7.3.1 Rhizobox experiment

We used a Haplic Phaeozem soil substrate with a loamy texture, consisting of sand – 33%, silt – 48%, and clay – 19% (Vetterlein et al., 2021). The soil pH ($CaCl_2$) was 6.4, total C and N were 8.5 and 0.8 g kg^{-1}, respectively; available P and K were 32.7, and 28.5 mg kg^{-1}, respectively (Vetterlein et al., 2021). The following nutrients were added to the soil before packing rhizoboxes: 50 mg kg^{-1} N as NH_4NO_3, 50 mg kg^{-1} K as K_2SO_4, 25 mg kg^{-1} Mg as $MgCl_26H_2O$, and 40 mg kg^{-1} P as $CaHPO_4$. The 1 mm sieved soil was homogenously packed into rhizoboxes of 10 x 21.2 x 0.6 cm avoiding formation of layers. The mass of soil was about 161-162 g per rhizobox, assuring a homogenous bulk density of 1.27 g cm^{-3}.

Three maize (*Zea mays* L.) genotypes – wild type (WT, B73), root-hair defective (>90%) mutant (*rth3)* (Hochholdinger et al., 2008; Wen and Schnable, 1994) and benzoxazinoids (BXs) deficit (>90%) mutant (*bx1)* (Frey et al., 1997) – were grown in the rhizoboxes. After 3 days of germination, the pre-germinated seedlings of each genotype were planted in four replicates into separate rhizoboxes and all plants were grown for 21 days. The rhizoboxes were placed under the angle of approx. 45° to ensure roots growing towards the lower side. About 20 – 22% of volumetric water content (VWC) was kept by watering the soil regularly from the top. Plants were grown in the climate chamber with a controlled temperature of 22 °C during the day and 18 °C during the night, a set photoperiod of 12 h dark, 12 h light cycle, relative air humidity of 65% and a light source (LED Grow Light, GrowLED, France) intensity of 350 µM m^{-2} s^{-1} of photosynthetically active radiation at the top of the rhizobox.

2.7.3.2 Hotspot and coldspot identification and soil sampling

The direct soil zymography (Razavi et al., 2019, 2016b) was used to define and map the areas of hot and cold spots of β-glucosidase activities (Razavi et al., 2016b; Tian et al., 2020). The β-glucosidase activity was visualized using polyamide membranes (0.45 µm mesh size, Tao Yuan, China) saturated with 4-methylumbelliferyl-β-D-glucoside (Sigma-Aldrich, Germany). The substrate was completely dissolved in MES buffer ($C_6H_{13}NO_4SNa_{0.5}$) (pH:6.5) (Sigma-Aldrich, Germany) by shaking to reach the concentration of 1 g L^{-1} (Sanaullah et al., 2016) which corresponds to 3.5 mM. Polyamide membrane filters with a size of 20×20 cm and a pore size of 0.45 µm were cut to 10×20 cm to fit the size of the rhizobox. Each membrane was saturated with 5 ml of the substrate solution by covering it completely with the solution in a flat box for 10 sec. The rhizoboxes were opened from the rooted side, and the saturated membranes were applied

directly to the soil surface (Razavi et al., 2016b). After 1 h incubation at root-soil interface, the membranes were carefully lifted off, and few attached soil particles were gently removed using tweezers and a soft-thin paintbrush. The membranes were placed in a dark room under ultraviolet (UV) light with an excitation wavelength of 355 nm. Photos were taken by a digital camera Canon EOS 6D with a Canon lens EF 94 mm 1: 4L IS. The aperture and shutter speed were set to f/5.6 and 1/30 s, respectively. The areas of high (=hotspot) and low fluorescence (=coldspot) were determined on zymograms visually and marked with the pencil.

A composite sample of 0.65 – 0.7 g of soil was collected from hot- and coldspot of β-glucosidase activity in the rhizosphere of each rhizobox using the micro-spatula and needle (Zhang et al., 2021). The tools were rinsed by 80-% ethanol before each sampling to avoid microbial contamination between samples. One portion of ~0.5 g soil was placed in the first Eppendorf tube and stored at +4 ^{0}C for enzyme assay, a second portion of ~0.2 – 0.25 g soil was placed to the second Eppendorf tube and freezed at -70 ^{0}C for DNA extraction and sequencing.

2.7.3.3 Enzymes kinetics

Activities of β-glucosidase (BG), acid phosphomonoesterase (AP), N-acetyl-β-glucosaminidase (NAG) and leucine aminopeptidase (LAP) in hotspots and coldspots were measured using fluorogenically labelled substrates as described in Razavi et al. (2016). Briefly, three fluorogenic substrates based on 4-methylumbelliferone (MUF), namely, 4-methylumbelliferyl-β-D-glucoside, 4-methylumbelliferyl- phosphate, and 4-methylumbelliferyl-N-acetyl-β-D-glucosaminide; and one based on 7-amino-4-methylcoumarin (AMC), namely, L-Leucine-7-amino-4-methyl coumarin were used to detect activity of β-glucosidase, acid phosphomonoesterase and N-acetyl-β-glucosaminidase, leucine aminopiptidase activity, respectively. All substrates and chemicals were purchased from Sigma-Aldrich (Germany).

Suspensions of 0.5 g soil with 50 mL sterile water (Nannipieri et al., 2012) were prepared separately for each in 4 replicates using low-energy sonication (40 J s^{-1} output energy) for 2 min. Fifty microliters of soil solutions, 50 µL 0.1 M MES (pH 6.1), used as buffer, and 100 µL of substrate solution (in the concentrations 0, 5, 10, 20, 50, 100, 200 µmol L^{-1}. were pipetted in a 96-well microplate (black, Brand pureGrade, Germany). Plates were kept at room temperature, agitated and measured fluorometrically (excitation 360 nm; emission 450 nm) after 0, 30 min, 1h and 2 h incubation with an automated plate-reader (Victor^{3} 1420-050 Multi label Counter; Perkin Elmer, USA). Parameters of Michaelis-Menten kinetics for enzyme activities were calculated with the following equation:

$$v = \frac{V_{max} \times [S]}{K_m + [S]} \quad (1)$$

where v is the reaction rate, V_{max} is the maximum enzyme activity, [S] is the substrate concentration, K_m is the substrate concentration at half-maximal rate.

The catalytic efficiency of enzymes (K_a) was determined as the ratio between V_{max} and K_m (Koshland, 2002; Moscatelli et al., 2012). The catalytic efficiency reflects the total enzyme catalytic process combining enzyme substrate complex dissociation (V_{max}) and the rate of enzyme substrate complex formation (K_m). The K_a serves as an indicator to reflect the functional changes of microbial communities. The higher K_a indicates better catalytic properties of the enzyme (Moscatelli et al., 2012).

The substrate turnover time (T_s, hours) was calculated according to the following equation (Panikov et al., 1992):

$$T_s = (K_m + S)/V_{max} \quad (2)$$

where S is the substrate concentration. The substrate turnover time was calculated at substrate concentration for the situations corresponding to the lack of substrate, as $S = K_m/10$ (Tian et al., 2020).

2.7.3.4 Microbiome analysis and bioinformatics

DNA was extracted using the QIAGEN DNeasy PowerSoil Pro kit (QIAGEN, Germany) for soil following the manufacturer's instructions with 200 mg rhizosphere soil from hot or coldspots as input material. DNA was quantified using a AccuClear™ Ultra High Sensitivity dsDNA Quantitation Kit with 7 DNA standards (Biotium, CA USA) on Tecan spectrometer (Tecan group AG, Switzerland).

We sequence several different experiments in a single MiSeq run and the qPCR products of this study were included in a run of which the sequences were deposited previously (Hu et al., 2018). The V3–V4 region of 16S rRNA was amplified with the primers 515F (Parada) and 806R (Apprill). The sequences of the qPCR samples can be extracted from the raw data based on the barcodes and primers indicated in Table S1.

Firstly, the raw read data were quality checked with FastQC (Andrews, 2010) and demultiplexed using cutadapt (Martin, 2011). Than we followed the DADA2 pipeline from Callahan et al., (2016) using the R package dada2 (v3.10). Instead of clustering the sequences in operational taxonomic units (OTUs), the DADA2 pipeline produces amplicon sequence variants

(ASVs), which replace OTUs as the units of analysis (Callahan et al., 2017). The sequences were quality filtered (max. expected errors: 2, min length: forward reads: 240bp, reverse reads: 160bp, discard reads that match phiX), truncated (after 140 bp or at the first instance of a quality score ≤ 2), and dereplicated. A parametric error model was learned by the DADA algorithm to correct sequencing errors.

The forward and reverse reads were merged based on identical overlap sequences of at least twelve bases. Finally, a count table was constructed, chimeras were removed, and taxonomies assigned with a naive Bayesian classifier using the DADA2 formatted 16S region with a DADA2 training set from the SILVA database for bacteria (Callahan, 2018) or ITS region with used the dynamic general fasta release from UNITE database for fungi (Abarenkov et al., 2020).

2.7.3.5 Calculations

Limitations of carbon (C), phosphorus (P) or nitrogen (N) were assessed using activity proportions of C-, P- and N-cycles enzymes. Vector length abled to provide the evidence of the relative C limitation vs. nutrient limitation was calculated using the Eq.3 (Moorhead et al., 2016):

$$\text{Length} = \sqrt{x^2 + y^2} \tag{3}$$

The angle of vector provides the evidence on relative P or N limitation. P limitation is reflected by the steepness of the vector over 45^0, while N limitation is reflected by the steepness of the vector under 45^0 (Moorhead et al., 2016).

$$\text{Angle} = \text{DEGREES(ATAN2(x, y))} \tag{4}$$

where x represents the relative C vs. P acquiring activities and calculated as the ratio BG/(BG+AP); y represents the relative C vs. N acquiring activities and calculated as the ratio BG/(BG+LAP+NAG).

DNA-based microbial biomass C was calculated by applying conversion factor of 4.4 (Semenov et al., 2018) to the values obtained from previously extracted and quantified dsDNA per soil mass (see section 2.4).

2.7.3.6 Statistical analysis

All data are presented as mean ± standard error of four replicate rhizoboxes. All analyses were performed using R software, Version 3.6.1 (R Development Core Team, 2011) at significance level of α = 0.05. Prior to statistical test all data were checked for outliers. The outlier test was performed in R using *rstatix* package. A Shapiro-Wilk test was performed for residues of means to check for normality, and the Bartlett test was applied to check the homogeneity of variances. If data meet normality and homogeneity, two-way ANOVA and Tukey's HSD post hoc test were performed for 'Genotype' and 'Spot', as the factors. One-way ANOVA and Tukey's HSD post hoc test were also performed for coldspots and hotspots separately for factor 'Genotype'. Welsh two sample test was performed to compare cold- and hotspot within each genotype.

2.7.4 Results

2.7.4.1 Enzyme kinetics and substrate turnover in cold – and hotspots

Maximum potential activity (V_{max}) were generally 42-265% higher (*p<0.05*) in the hotspots, than in coldspots for all enzymes, except for chitinase and β-glucosidase in *bx1*, where we observed 30-51% lower V_{max} values (*p<0.1*, Fig.1). The genotype and spot were significant factors for V_{max} variability of all tested enzymes (Fig.1).

In opposite to V_{max}, K_m values generally increased in coldspots compared to hotspots and especially up to 3.5-6 folds in *bx1* for N-cycling enzymes (chitinase and leucine-aminopeptidase) (Fig. 2). The genotype factor was significant in coldspots for chitinase and leucine-aminopeptidase, but in hotspots for β-glucosidase and acid phosphatase (Fig. 2).

Catalytic efficiency or K_a values were 2-4.5 times higher (*p<0.05*) in hotspots than in coldspots for all enzymes except β-glucosidase in *bx1* and except leucine aminopeptidase in *rth3* (Fig. 3). K_a values remained similar in the hotspots and coldspots of WT for all tested enzymes (Fig. 3).

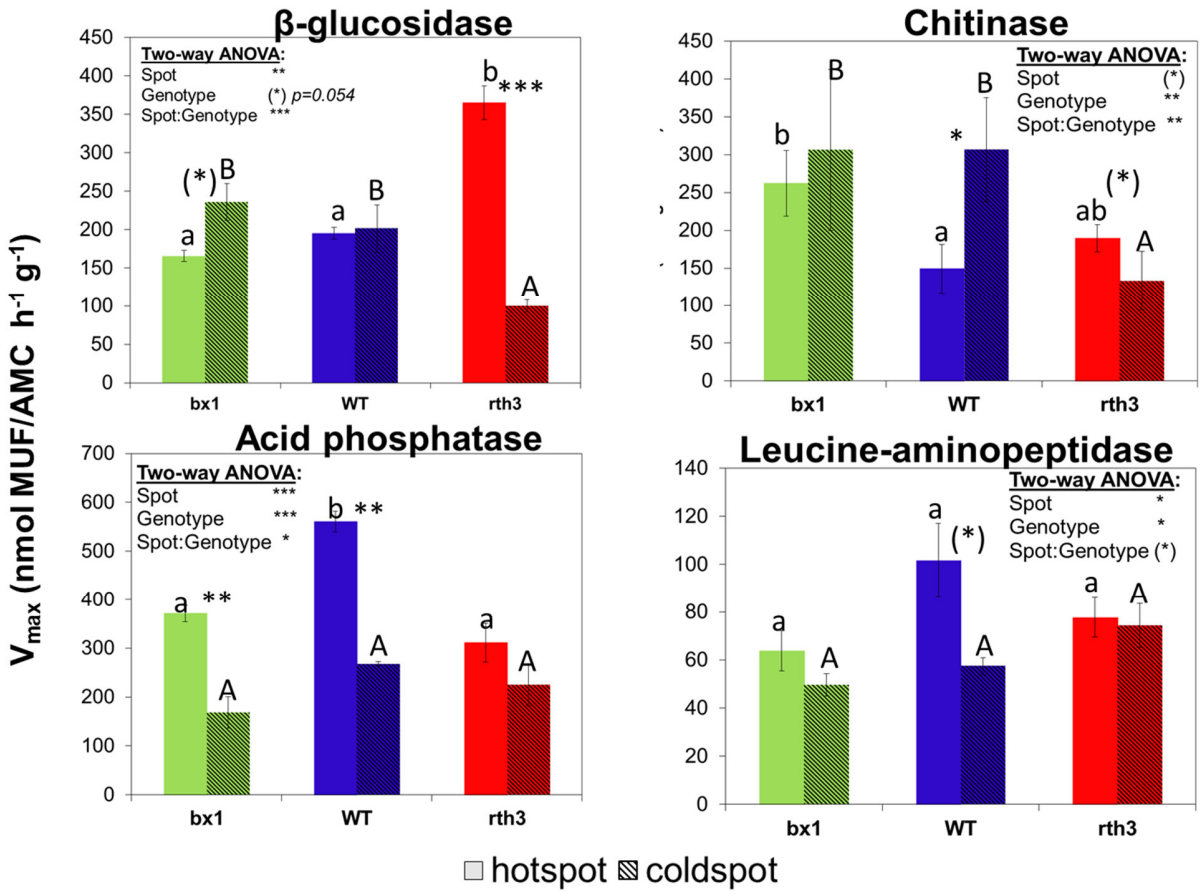

Figure 1. Maximum enzyme activity (V_{max}) of β-glucosidase, acid phosphatase, chitinase and leucine aminopeptidase. Data are means for each genotype (*bx1,* WT, and *rth3)* (n=4), error bars indicate standard error. Different capital letters indicate significant difference among the genotypes in colspots, while lower case letters indicate significant differences among the genotypes in hotspot at *P<0.05*. Asterisks above the bars indicate significant differences between cold- and hotspot for each genotype ('***' *P*<0.001; '**' *P*<0.01; '*' *P*<0.05, '(*)' *P*<0.1).

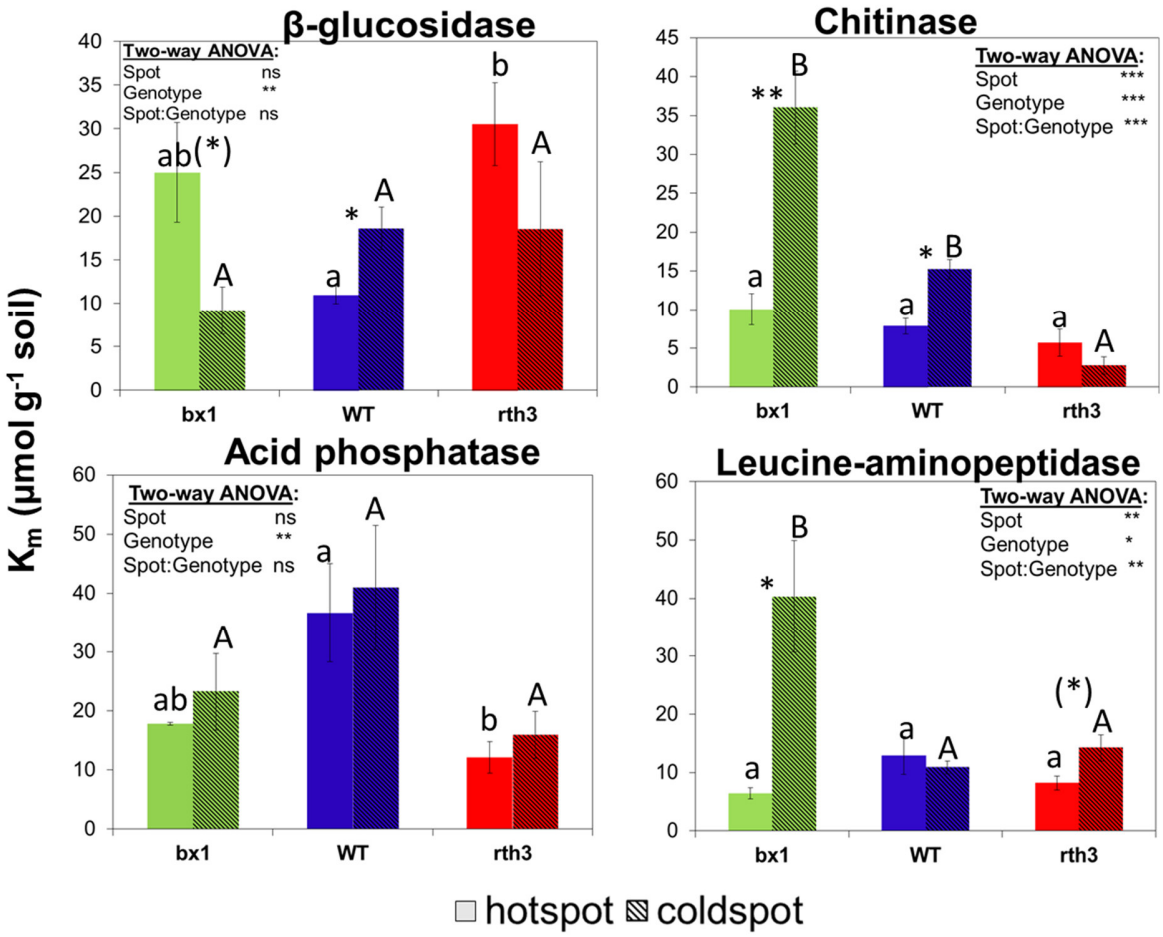

Figure 2. K_m values of β-glucosidase, acid phosphatase, chitinase and leucine aminopeptidase. Data are means for each genotype (*bx1,* WT, and *rth3)* (n=4), error bars indicate standard error. Different capital letters indicate significant difference among the genotypes in coldspots, while lower case letters indicate significant differences among the genotypes in hotspot at *P<0.05*. Asterisks above the bars indicate significant differences between cold- and hotspot for each genotype ('***' *P*<0.001; '**' *P*<0.01; '*' *P*<0.05, '(*)' *P*<0.1).

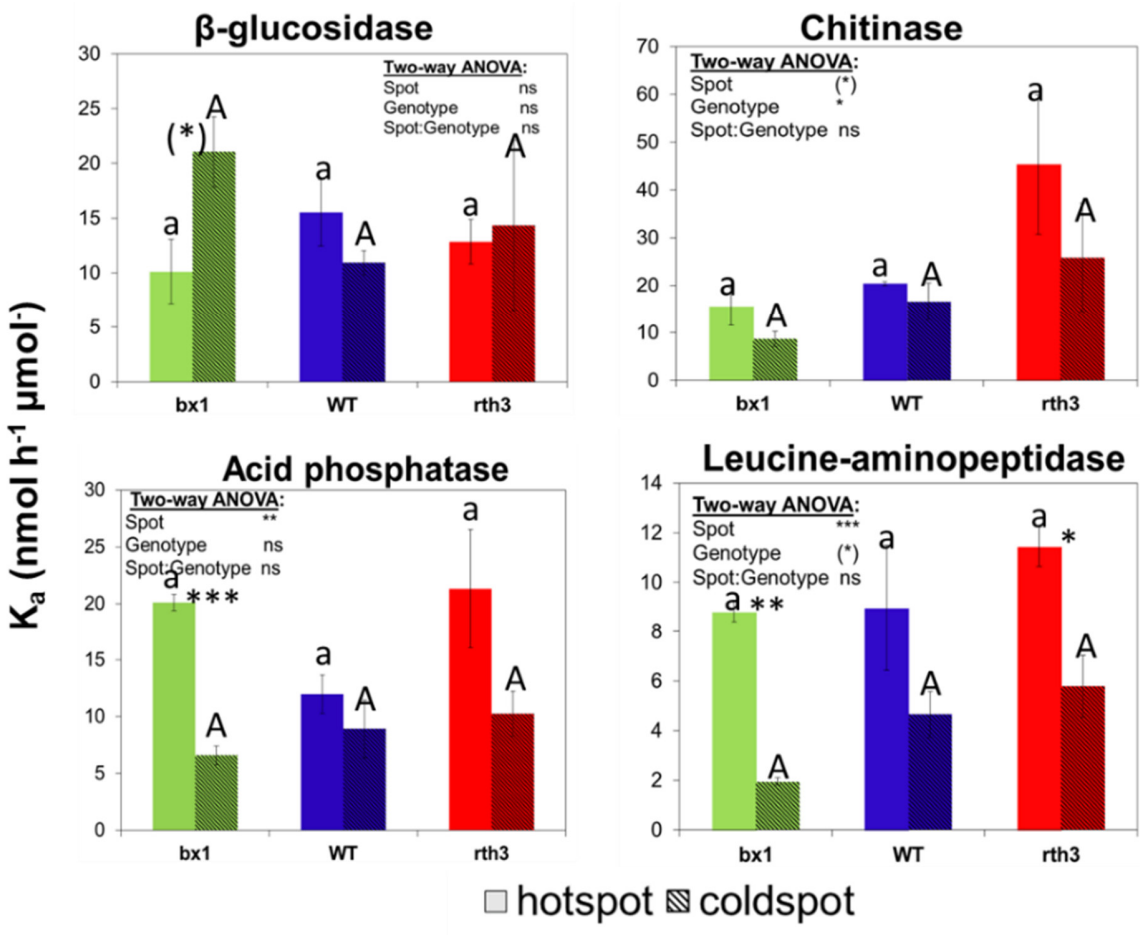

Figure 3. Catalytic efficiency (K_a) of β-glucosidase, acid phosphatase, chitinase and leucine aminopeptidase. Data are means for each genotype (*bx1,* WT, and *rth3)* (n=4), error bars indicate standard error. Different capital letters indicate significant difference among the genotypes in colspots, while lower case letters indicate significant differences among the genotypes in hotspot at *P<0.05.* Asterisks above the bars indicate significant differences between cold- and hotspot for each genotype ('***' *P*<0.001; '**' *P*<0.01; '*' *P*<0.05, '(*)' *P*<0.1).

The turnover time of all enzymes in hotspot were 1.3-4.6 times shorter than in the coldspot, except β-glucosidase in *bx1*, were it was 3.7 folds longer in hotspot than in the coldspot. The turnover time for acid phosphatase, chitinase and leucine aminopeptidase showed no significant differences between the hotspots and coldspots in WT and *rth3* (Fig. 4).

Calculated C limitation was similar for the hotspots and coldspots in WT, increased in *rth3* from coldspots to hotspot or decreased in *bx1* from coldspots to hotspots (Table 2). Generally, for all genotypes, N limitation (angles from 31 to 43) was detected in hotspots, while phosphorus limitation (angles from 45 to 53) was found in coldspots (Table 2).

Table 2. Vector length and vector angle for the ration of enzyme activities in the hotspot and coldspot of three maize genotypes (WT, *rth3* and *bx1*). Different capital letters indicate significant difference among the genotypes in the colspots, while lower case letters indicate significant differences among the genotypes in the hotspots at *P<0.05*. Asterisks indicate significant differences between cold- and hotspot for each genotype ('***' *P*<0.001; '**' *P*<0.01; '*' *P*<0.05, '(*)' *P*<0.1; 'ns' *P*>0.1).

Spot	Genotype	Vector length§		Vector angle§§	
		Mean	**SE**	**Mean**	**SE**
Hotspot	WT	0.51^{ns}a	0.05	31^{**}a	3
	*rth*3	0.79^{***}b	0.06	43^{ns}b	3
	*bx*1	0.46^{*}a	0.06	$42^{(*)}$b	2
Coldspot	WT	0.51A	0.04	50A	4
	*rth*3	0.50A	0.02	45A	1
	*bx*1	0.73B	0.10	53A	7
Two-way ANOVA	***Factor***	***p-value***		***p-value***	
	Spot	*0.34582*		***4.21e-05***	
	Genotype	***0.00174***		***0.02466***	
	*Spot*Genotype*	***5.15e-06***		***0.00445***	

§*The vector length* ($\sqrt{(\mathrm{BG}/(\mathrm{BG}+\mathrm{AP})^2 + \mathrm{BG}/(\mathrm{BG}+\mathrm{LAP}+\mathrm{NAG})^2}$ *provides the evidence of the relative C limitation vs. nutrient (N and P) limitation (Moorhead et al., 2016);*

§§ *The angle of vector* (DEGREES(ATAN2((BG/(BG+AP), BG/(BG+LAP+NAG)) *provides the evidence of relative P (the steepness of the vector over 45^0) or N limitation (the steepness of the vector over 45^0) (Moorhead et al., 2016).*

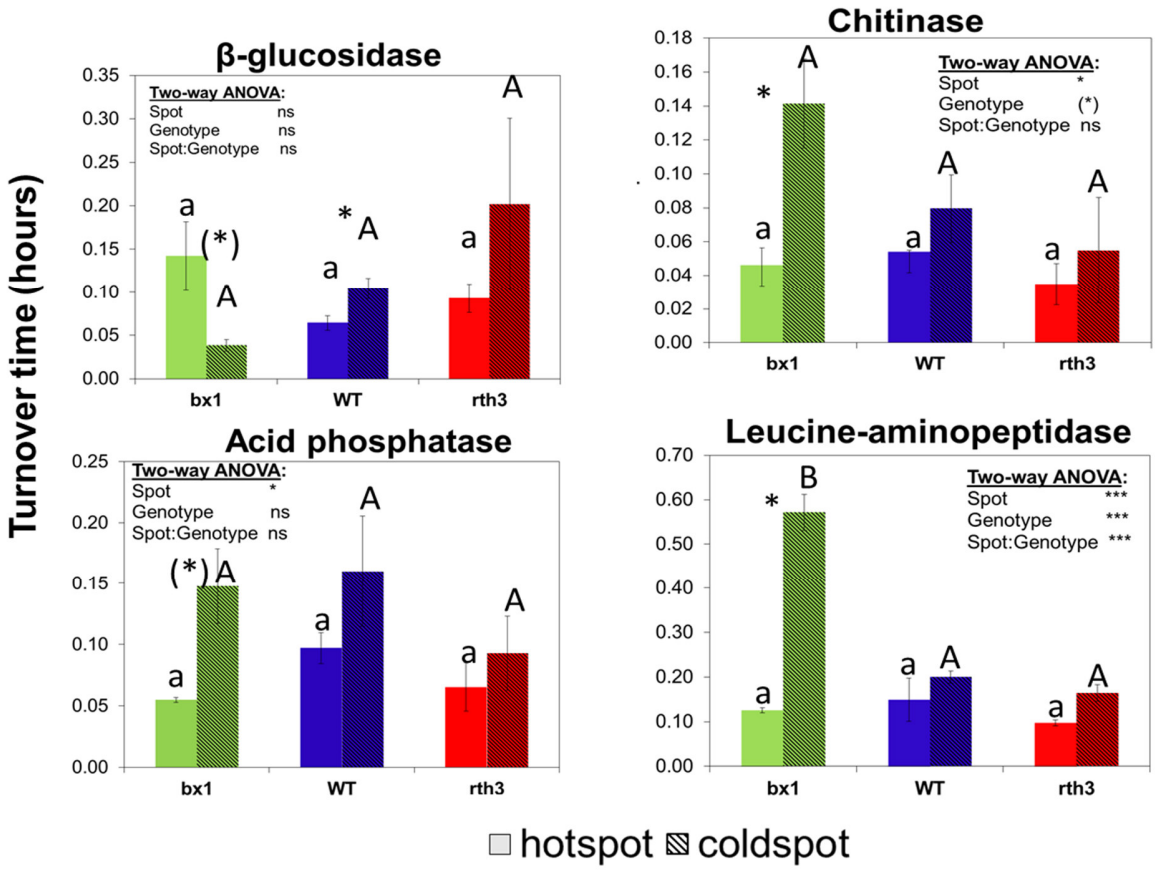

Figure 4. Turnover time at the lack of substrate of four enzymes: β-glucosidase, acid phosphatase, chitinase and leucine aminopeptidase. Data are means for each genotype (*bx1,* WT, and *rth3)* (n=4), error bars indicate standard error. Different capital letters indicate significant difference among the genotypes in colspots, while lower case letters indicate significant differences among the genotypes in hotspot at *P<0.05*. Asterisks above the bars indicate significant differences between cold- and hotspot for each genotype ('***' *P*<0.001; '**' *P*<0.01; '*' *P*<0.05, '(*)' *P*<0.1).

2.7.4.2 Microbial biomass and microbiome analysis

Total microbial biomass in the hotspots was 14 and 22% higher (*p<0.01*) than in the coldspots for WT and *bx1*, respectively (Fig. 5a). Shannon Diversity for fungi was up to two-folds lower than for bacteria being similar in the hotspot and coldspots for WT and *rth3,* but higher in the coldspots than in the hotspots for bacteria microbiome in *bx1* (Fig. 5 b). Fungal microbiome slightly differ between WT and *rth3* (P=0.075), but was similar in hot and coldspots (Table S1, Fig. S3 and S4). In contrast, bacterial microbiome did not differ between genotypes (P=0.195),

but varied between hot – and coldspots in WT and *bx1* (Table S1, Fig. S3), as well as in *rth3* for constrained ordination of beta-diversity (Fig. S4b).

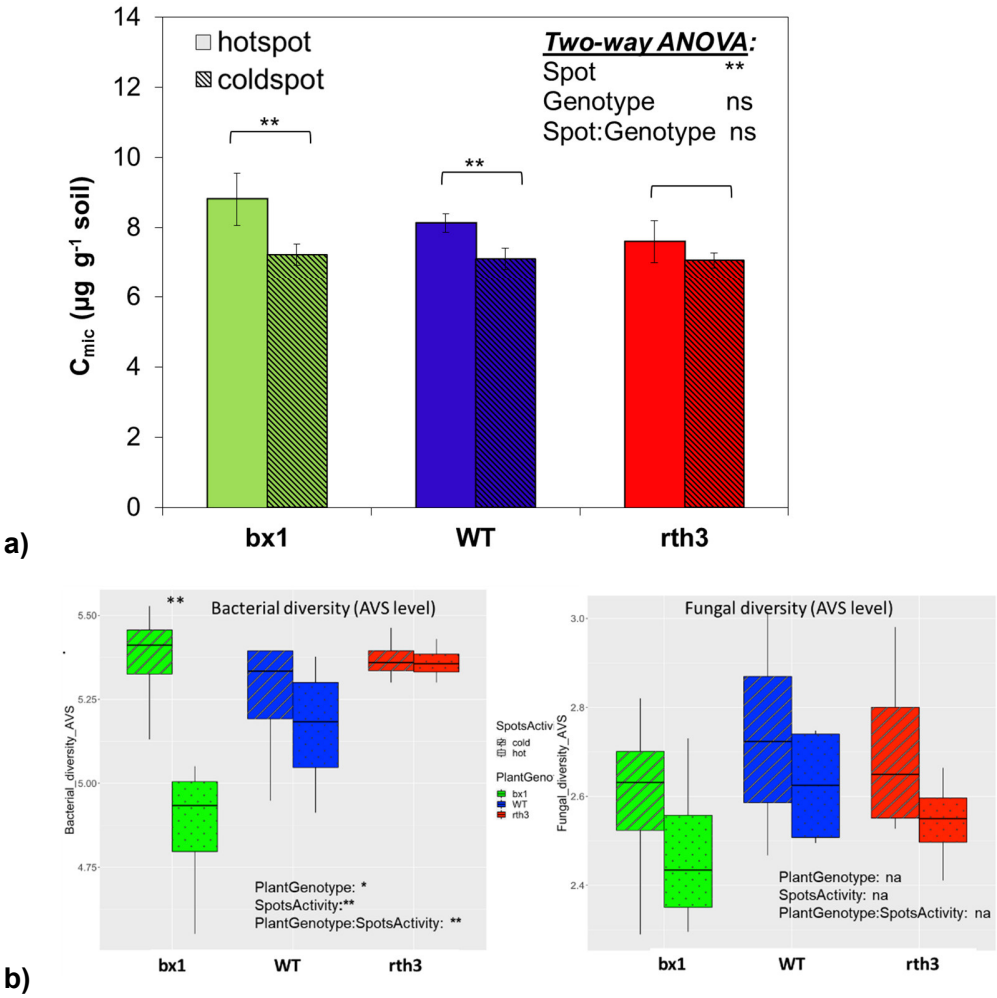

Figure 5. Microbial biomass carbon (C_{mic}) (a) and Shannon diversity for bacterial and fungal diversity (b). Data are means for each genotype (*bx1,* WT, and *rth3)* (n=4), error bars indicate standard error. Different capital letters indicate significant difference among the genotypes in colspots, while lower case letters indicate significant differences among the genotypes in hotspot at *P<0.05*. Asterisks above the bars indicate significant differences between cold- and hotspot for each genotype ('***' *P*<0.001; '**' *P*<0.01; '*' *P*<0.05, '(*)' *P*<0.1).

The most dominant bacterial genus out of top 20 detected were *Sphingomonas, Candidatus Uldaeobacter, Massilia, Lysobacter, Bradyrhizobium* (Fig. 6a). For fungal microbiome the most abundant were *Mortierella, Solicoccozyma, Acremonium*, and also *Fusarium* and *Giberella* for *bx1* (Fig. 6b).

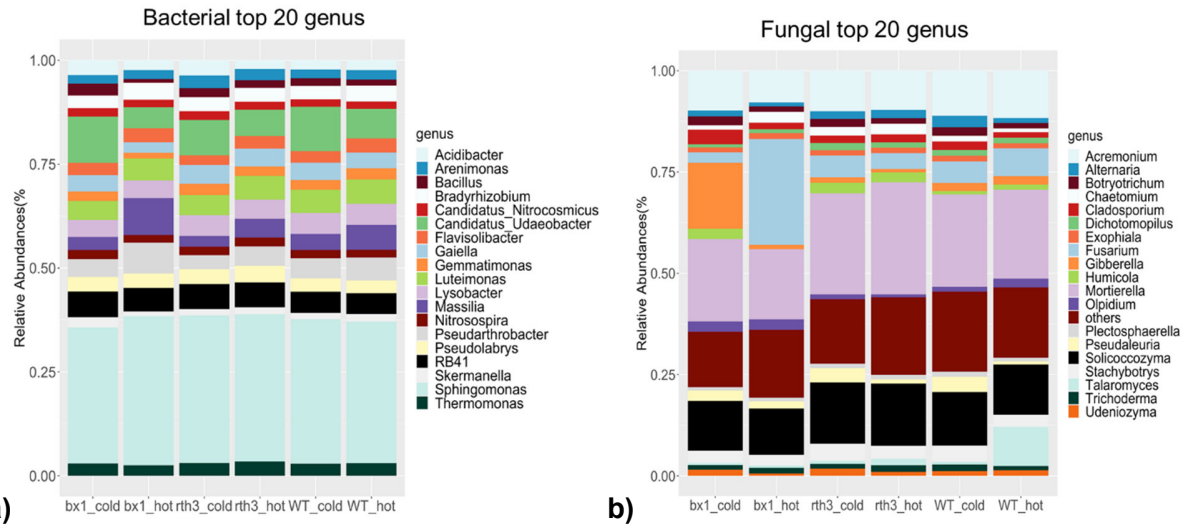

Figure 6. Relative abundance of top soil bacterial (a) and fungal (b) communities at genus level in the soil from the cold- and hotspots of three maize genotypes (WT, *rth3, bx1*). Data are mean of four replicates, except two replicates for *bx1* coldspots.

2.7.5 Discussion

2.7.5.1 Effect of root hairs on rhizosphere microbiome and its enzymatic activities

Microorganisms in the hotspots of root-hair defective *rth3* had significantly higher C limitation (1.55 times larger vector length, Table 2), than root-hair forming WT. This also was reflected in up to two time's higher maximum potential activity (V_{max}) and up to three times higher K_m of β-glucosidase (Fig. 1 and 2). The opposite trend was reported by Zhang et al. (2020), who found significantly higher K_m and V_{max} in the hotspots of WT than *rth3* at 30 ^{0}C. This difference in the results may be attributed to the different temperatures during our experiments, as Q_{10} was found to be an important factor for the shift in enzymatic system (Nottingham et al., 2016; Razavi et al., 2016a). Nevertheless, such an increase in C-cycle enzyme activities along with detected C limitation may by caused by the absence of root hairs. For example, the absence of root hairs decreases rhizosphere extent for β-glucosidase by at least 35% (Bilyera et al., 2021b) and thus, requiring higher enzyme activity (V_{max}) and substrate affinity (K_m) to reach the same overall hydrolytic efficiency in the reduced soil volume. Furthermore, previously detected exudation mainly via root tips in WT and from the whole root in *rth3* (Bilyera et al., 2021b) may also explain higher β-glucosidase activities in *rth3*, as root exudates belong to more easily available substrates for enzymes than broken root hairs, whereas the amount of easily available substrate determines microbial activity (Kandeler, 1990; Loeppmann et al., 2016). However, catalytic efficiency (K_a), as

well as turnover time remained similar for β-glucosidase activity in the hotspots with and without root hairs (Fig. 3 and 4). Very probably, that enzyme mediated catalysis depended on water content in the rhizosphere hotspot (Saleh and Kalodimos, 2017), and had a similar efficiency because of the same water content levels in the rhizosphere of WT and *rth3* (Bilyera et al., 2021b).

In contrast to β-glucosidase, P cycle enzyme activity increased in the hotspots due to the presence of root hairs. The formation of P depletion zones around the roots and especially with the presence of root hairs (Hummel et al., 2021) induced up to 80% higher acid phosphatase activity (Fig. 1) to mineralize organic P to plant available forms. It should be also noted, that hotspot microorganisms themselves did not experience P limitation as calculated from enzyme activity data (Table 2).

The presence of root hairs leads to 2.3 folds higher V_{max} and 5.5 folds higher K_m for chitinase activity in the coldspots only (Fig. 1 and 2). It seems, that spatial distribution of hotspots varies for different enzymes and those for chitinase do not follow β-glucosidase, which we used for precise soil sampling. This is especially relevant for WT, in which former root hairs regions could be generally rich in microbial biomass including chitin from fungal cell walls, which serves as a substrate for chitinases (Hanzlíková et al., 1989). In contrast, leucine aminopeptidase activity as well as its kinetic parameters did not differ between WT and *rth3* (Fig. 1-4). This is in line with Greenfield et al., (2021) who found similar leucine aminopeptidase activities in the rhizosphere of barley with and without root hairs after destructive sampling.

Generally, root hairs facilitated contrasting maximum enzyme activity (V_{max}) and substrate affinity (K_m) to all four enzymes in hot- and coldspots (Fig. 1 and 2). Similar trend was observed in poor soils, but hot- and coldspots in fertile soils did not differ significantly (Tian et al., 2020). The soil of our experiment with the less than 1% of soil organic matter content (Vetterlein et al., 2021) is rather poor and the broken root hairs may facilitate here the intensive microbial hotspots due to the input of additional rhizodeposits. Despite the hotspots were defined based on the β-glucosidase zymograms, the maximum potential β-glucosidase activity *ex situ* was similar in hot- and coldspots. This is a shortcoming of 2D zymography methods, which may measure activities in the very top layer (few mm) and thus detect only up to 20% of the actual enzyme activity (Guber et al., 2018). This calls always for accompanying sampling and *en situ* enzyme measurements (Greenfield et al., 2021; Guber et al., 2018). An increased abundance of *Candidatus* Udaeocacter in coldspots compared to hotspots of WT and *rth3* may indicate that microbiome altered toward the species acquiring also more energy demanding amino acids and vitamins instead of soil

organic carbon (Brewer et al., 2017). An increase of *Acidibacter* abundance in a hotspot of root deficient *rth3* if compared to WT may be also related to C-cycle. *Acidibacter* is oligotroph and was found to produce β-glucosidase, therefore its higher abundance in the soils with very low C resource availability is reasonable for root-hair defective *rth3* (Kielak et al., 2016).

2.7.5.2 Role of benzoxazinoids on rhizosphere microbiome and its enzymatic activities

Despite an important role of benzoxazinoids (BXs) for plant protection (Erb and Kliebenstein, 2020; Schlaeppi et al., 2021), they also may perform suppressive effect on enzymatic activity of beneficial soil microorganism (Bilyera et al., 2021b). However, the absence of BXs in exudates did not significantly increase the total soil microbial biomass (Fig. 5a), but changed its bacterial microbiome structure and decreased bacterial diversity in the hotspots (Fig. S3, Fig. 5b). Unlike bacterial, fungal microbiome of hotspots was not affected by BXs in our study (Fig. S3), what differs from the results of Hu et al. (2018) on another soils, who detected the changes in both bacterial and fungal microbiome structure, but no change of alpha diversity from BXs. This inconsistency in microorganisms' feedback to benzoxazinoids in different soils was recently studied by Cadot at al. (2021) and linked to the contrasting soil fertility effect. In poor soils like in our experiment, microorganisms actively produce enzymes to mine for nutrients, which is less expressed in fertile soils. The calculated much higher microbial C limitation in coldspots of *bx1* than in WT (Table 2) could only partly indicate actual C starvation in microbiome. The other possible reason is the release β-glucosidase to catalyse the activation of chemical plant defence (Vassão et al., 2018), which is especially relevant when BXs are not presented in exudates. This β-glucosidase could be produced by *bx1* maize or rhizosphere soil microbiome that was significantly altered, as discussed above.

Similarly, to C, the increased N limitation in the hotspots of *bx1* than WT (Table 2) was not solely related to the actual N demand. Both enzymes of N-cycle (leucine aminopeptidase and chitinase) may also acts as the natural protection substances for plant to defend it against pathogens (Flach et al., 1992; Henrissat, 1991; Scranton et al., 2012). Such increase in chitinase activity may partly compensate for BXs deficiency. Nevertheless, it seems that chitinases were not as effective against pathogenic fungi as benzoxazinoids. The latter was proved by dramatically increased abundance of plant pathogenic fungi of genus *Fusarium* and *Gibberella* (Fig. 6), which causes Gibberella stalk and ear rot or root rot diseases on maize (Goswami and Kistler, 2004; Okello et al., 2019; Zhao et al., 2021). Typically, plants synthesize BXs in response to infection and regulate the release of based on the media, they grow in, and thus modify its

concentration in the rhizosphere (Hazrati et al., 2020; Seybold et al., 2020), which is not relevant for BXs deficient genotype *bx1*. Many studies suggested beneficial effects of benzoxazinoids (i.e. anticancer, antimicrobial) on animal and human health, while only some reported putative toxicological properties (i.e. mutagenic effects) (Adhikari et al., 2015; Schlaeppi et al., 2021). This calls for the increasing of BXs concentration per plant biomass in plant breeding to benefit from consuming natural antimicrobial substances by animals and humans or having stronger defence from pathogenic organisms. Overall, the absence of benzoxazinoids in root exudation promotes higher abundance of pathogenic fungi, which could lead to plant infection on the latter stages of growth inducing the loss of crop productivity and maize grain contamination with a i.e. mycotoxins, as a by-products of pathogenic fungi development.

2.7.5.3 Why the rhizosphere coldspots are formed?

Generally, there was a trend of an increased turnover time and Shannon fungal and bacterial biodiversity, but lower total microbial C biomass in the coldspots over hotspots (Fig. 4 and 5). Thus, more diverse microbiome could potentially perform diverse functional roles in coldspots, but at the same time the majority of microbes are in the dormant state there (Blagodatskaya and Kuzyakov, 2013; Joergensen and Wichern, 2018). Non-activated dormant microorganisms tend to support similar enzyme activities per unit of microbial biomass to maintain their existence (Bilyera et al., 2021a). When the portion of active growing microorganisms increased, they perform more intensive hydrolytic properties, which is a case of hotspots (Tian et al., 2020; Zhang et al., 2020). Meanwhile, enzyme catalytic efficiency in hot- and coldspots remains similar (Fig. 3), which was in line with Tian et al. (2020) who previously reported no changes in **c**atalytic efficiency in the hotspots and bulk soil. The comparable **c**atalytic efficiency in hot and cold spots indicate that at least active parts of bacteria and fungi belong to the same functional groups, otherwise **c**atalytic efficiency could varied within two orders of magnitude (Hall, 1999; Henrissat, 1991).

One possible reason of coldspots formation may be their reduced dependency on the root exudates despite being in the same proximity to root as hotspots. If this were a case, a reduced input of available C would lead to higher C limitation, which was relevant for *bx1* only. As was already mentioned, some enzymes may be released for plant defence in *bx1* to compensate for BXs deficiency and taking into account that both – plant- and microbially-derived enzymes – are presented in the rhizosphere, the calculated limitations could not fully represent nutrient status in cold- and hotspots, as hypothesized. In contrast to C, N limitation in hotspots and P limitation in

coldspots were clearly showed for all genotypes (Table 2). Frequently reported N limitation in root affected soil (Loeppmann et al., 2016; Vitousek and Howarth, 1990) and P limitation in bulk soil (Hinsinger, 2001) may prove that hotspots are more root dependent, then coldspots.

Another reason of coldspots formation may be related to contrasting patterns of exudation along the roots. For instance, recently showed rather patchy acidification features of rhizosphere in maize (Bilyera et al., 2022) could spatially alter enzyme activities, as they may vary up to three folds due to changes in pH values from 6 to 8 (Foster et al., 2018).

Besides, it is very probable that bimodal distribution of rhizosphere properties and related non-homogeneous root water uptake lead to hydraulic isolation of some rhizosphere regions (Carminati and Vetterlein, 2013). Thus, having less water availability microorganisms of this isolated microenvironments may perform less enzyme activities. However, to test this assumption, further studies and more spatially resolved analysis of enzyme activities and water availability around the root are required.

2.7.6 Conclusions

Root hairs contributed to 80% higher acid phosphatase activity to resupply phosphate uptake by plants via mineralization of organic phosphorus sources to available forms. Broken root hairs in WT facilitated the intensive microbial hotspots due to additional input of rhizodeposits and increased β-glucosidase and chitinase activities up to two times, compared to *rth3*. The lack of organic matter input in root-hair defective *rth3* resulted in a higher abundance of *Acidobacter*, oligotroph able to acquire energy from low C soil.

The presence of benzoxazinoids in root exudates did not significantly reduce microbial biomass, but strongly supported the plant defence against pathogenic fungi (i.e., genus *Fusarium* and *Gibberella*), which, however, could not be fully substituted by an increased exudation and activities of enzymes) with plant protection function (i.e. chitinase, β-glucosidase) in *bx1*.

Overall, root hairs facilitate better plant nutrition at the shortage of available nutrients (i.e., coldspots), while the presence of benzoxazinoids in exudates protect plant from pathogenic microorganisms and thus prevent deceases. Therefore, root hairs and benzoxazinoids are the most promising genotype root traits for sustainable productivity and phytosanitary measures to protect soil from fungal hotspots as well as associated food contamination with mycotoxins. These root traits are of special interest for efficient organic farming.

2.7.7 Acknowledgements

We acknowledge Caroline Marcon and Frank Hochholdinger (University of Bonn) for kindly providing seeds of maize mutant *rth3*. This project was carried out in the framework of the priority program 2089 “Rhizosphere spatiotemporal organization – a key to rhizosphere functions’ funded by the Deutsche Forschungsgemeinschaft (DFG, German Research Foundation) – Project number 403670038 (BSR & SPP). The work was funded by the Interfaculty Research Cooperation (IRC) “One Health” at University of Bern, Sub-Project 4. We gratefully acknowledge the China Scholarship Council (CSC) for the financial support of Xuechen Zhang, and the Robert Bosch Foundation for supporting Michaela Dippold and this study via the Robert Bosch Junior Professorship 2017.

References

Abarenkov, K., Zirk, A., Piirmann, T., Pöhönen, R., Ivanov, F., Nilsson, R. H., Kõljalg, U. 2020. UNITE general FASTA release for Fungi. Version 04.02.2020. UNITE Community. doi:10.15156/BIO/786368

Adhikari, K.B., Tanwir, F., Gregersen, P.L., Steffensen, S.K., Jensen, B.M., Poulsen, L.K., Nielsen, C.H., Høyer, S., Borre, M., Fomsgaard, I.S., 2015. Benzoxazinoids: Cereal phytochemicals with putative therapeutic and health-protecting properties. Molecular Nutrition & Food Research 59, 1324–1338. doi:10.1002/mnfr.201400717

Allison, S.D., Vitousek, P.M., 2005. Responses of extracellular enzymes to simple and complex nutrient inputs. Soil Biology and Biochemistry 37, 937–944. doi:10.1016/j.soilbio.2004.09.014

Andrews, S., 2010. FASTQC. A quality control tool for high throughput sequence data.

Berendsen, R.L., Pieterse, C.M.J., Bakker, P.A.H.M., 2012. The rhizosphere microbiome and plant health. Trends in Plant Science 17, 478–486. doi:10.1016/j.tplants.2012.04.001

Berg, G., Smalla, K., 2009. Plant species and soil type cooperatively shape the structure and function of microbial communities in the rhizosphere. FEMS Microbiology Ecology 68, 1–13. doi:10.1111/j.1574-6941.2009.00654.x

Bilyera, N., Dippold, M.A., Bleicher, J., Maranguit, D., Kuzyakov, Y., Blagodatskaya, E., 2021a. Microbial tradeoffs in internal and external use of resources regulated by phosphorus and carbon availability. European Journal of Soil Biology 106, 103353. doi:10.1016/j.ejsobi.2021.103353

Bilyera, N., Hummel, C., Daudin, G., Santangeli, M., Zhang, X., Santner, J., Lippold, E., Schlüter, S., Bertrand, I., Wenzel, W., Razavi, B.S., Oburger, E., 2022. Co-localised phosphorus mobilization processes in the rhizosphere of field-grown maize jointly contribute to plant nutrition. Soil Biology and Biochemistry 165. doi:10.1016/j.soilbio.2021.108497

Bilyera, N., Zhang, X., Duddek, P., Fan, L., Banfield, C.C., Schlüter, S., Carminati, A., Kaestner, A., Ahmed, M.A., Kuzyakov, Y., Dippold, M.A., Spielvogel, S., Razavi, B.S., 2021b. Maize genotype-specific exudation strategies: an adaptive mechanism to increase microbial activity in the rhizosphere. Soil Biology and Biochemistry 162, 108426. doi:10.1016/j.soilbio.2021.108426

Blagodatskaya, E., Kuzyakov, Y., 2013. Active microorganisms in soil: Critical review of estimation criteria and approaches. Soil Biology and Biochemistry. doi:10.1016/j.soilbio.2013.08.024

Bonkowski, M., Tarkka, M., Razavi, B.S., Schmidt, H., Blagodatskaya, E., Koller, R., Yu, P., Knief, C., Hochholdinger, F., Vetterlein, D., 2021. Spatiotemporal Dynamics of Maize (Zea mays L.) Root Growth and Its Potential Consequences for the Assembly of the Rhizosphere Microbiota. Frontiers in Microbiology 12. doi:10.3389/fmicb.2021.619499

Brewer, T.E., Handley, K.M., Carini, P., Gilbert, J.A., Fierer, N., 2017. Genome reduction in an abundant and ubiquitous soil bacterium ‘Candidatus Udaeobacter copiosus.’ Nature Microbiology 2, 16198. doi:10.1038/nmicrobiol.2016.198

Cadot, S., Guan, H., Bigalke, M., Walser, J., Jander, G., Erb, M., Heijden, M.G.A. Van Der, Schlaeppi, K., 2021. Specific and conserved patterns of microbiota-structuring by maize benzoxazinoids in the field 1–19.

Callahan, B.J., McMurdie, P.J., Holmes, S.P., 2017. Exact sequence variants should replace operational taxonomic units in marker-

gene data analysis. The ISME Journal 11, 2639–2643. doi:10.1038/ismej.2017.119

Callahan, B.J., McMurdie, P.J., Rosen, M.J., Han, A.W., Johnson, A.J.A., Holmes, S.P., 2016. DADA2: High-resolution sample inference from Illumina amplicon data. Nature Methods 13, 581–583. doi:10.1038/nmeth.3869

Carminati, A., Vetterlein, D., 2013. Plasticity of rhizosphere hydraulic properties as a key for efficient utilization of scarce resources. Annals of Botany 112, 277–290. doi:10.1093/aob/mcs262

Dick, R., Rattei, T., Haslbeck, M., Schwab, W., Gierl, A., Frey, M., 2012. Comparative analysis of benzoxazinoid biosynthesis in monocots and dicots: Independent recruitment of Stabilization and activation functions. Plant Cell 24, 915–928. doi:10.1105/tpc.112.096461

Erb, M., Kliebenstein, D.J., 2020. Plant Secondary Metabolites as Defenses, Regulators, and Primary Metabolites: The Blurred Functional Trichotomy. Plant Physiology 184, 39–52. doi:10.1104/pp.20.00433

Flach, J., Pilet, P.-E., Jollès, P., 1992. What's new in chitinase research? Experientia 48, 701–716. doi:10.1007/BF02124285

Foster, E., Fogle, E., Cotrufo, M., 2018. Sorption to Biochar Impacts β-Glucosidase and Phosphatase Enzyme Activities. Agriculture 8, 158. doi:10.3390/agriculture8100158

Frey, M., Chomet, P., Glawischnig, E., Stettner, C., Grün, S., Winklmair, A., Eisenreich, W., Bacher, A., Meeley, R.B., Briggs, S.P., Simcox, K., Gierl, A., 1997. Analysis of a chemical plant defense mechanism in grasses. Science 277, 696–699. doi:10.1126/science.277.5326.696

Ge, T., Wei, X., Razavi, B.S., Zhu, Z., Hu, Y., Kuzyakov, Y., Jones, D.L., Wu, J., 2017. Stability and dynamics of enzyme activity patterns in the rice rhizosphere: Effects of plant growth and temperature. Soil Biology and Biochemistry 113, 108–115. doi:10.1016/j.soilbio.2017.06.005

Giles, C.D., Dupuy, L., Boitt, G., Brown, L.K., Condron, L.M., Darch, T., Blackwell, M.S.A., Menezes-Blackburn, D., Shand, C.A., Stutter, M.I., Lumsdon, D.G., Wendler, R., Cooper, P., Wearing, C., Zhang, H., Haygarth, P.M., George, T.S., 2018. Root development impacts on the distribution of phosphatase activity: Improvements in quantification using soil zymography. Soil Biology and Biochemistry 116, 158–166. doi:10.1016/j.soilbio.2017.08.011

Goswami, R.S., Kistler, H.C., 2004. Heading for disaster: Fusarium graminearum on cereal crops. Molecular Plant Pathology 5, 515–525. doi:10.1111/j.1364-3703.2004.00252.x

Greenfield, L.M., Razavi, B.S., Bilyera, N., Zhang, X., Jones, D.L., 2021. Root hairs and protein addition to soil promote leucine aminopeptidase activity of Hordeum vulgare L. Rhizosphere 18, 100329. doi:10.1016/j.rhisph.2021.100329

Guber, A., Kravchenko, A., Razavi, B.S., Uteau, D., Peth, S., Blagodatskaya, E., Kuzyakov, Y., 2018. Quantitative soil zymography: Mechanisms, processes of substrate and enzyme diffusion in porous media. Soil Biology and Biochemistry 127, 156–167. doi:10.1016/j.soilbio.2018.09.030

Haling, R.E., Brown, L.K., Bengough, A.G., Young, I.M., Hallett, P.D., White, P.J., George, T.S., 2013. Root hairs improve root penetration, root–soil contact, and phosphorus acquisition in soils of different strength. Journal of Experimental Botany 64, 3711–3721. doi:10.1093/jxb/ert200

Hall, B.G., 1999. Experimental evolution of Ebg enzyme provides clues about the evolution of catalysis and to evolutionary potential. FEMS Microbiology Letters 174, 1–8. doi:10.1016/S0378-1097(99)00096-8

Hanzlíková, A., Šotolová, I., Jandera, A., 1989. Chitinase in the Rhizosphere and on Plant Roots. Developments in Soil Science 18, 293–299. doi:10.1016/S0166-2481(08)70228-9

Hazrati, H., Fomsgaard, I.S., Kudsk, P., 2020. Root-Exuded Benzoxazinoids : Uptake and Translocation in Neighboring Plants. doi:10.1021/acs.jafc.0c04245

Heitkötter, J., Marschner, B., 2018. Soil zymography as a powerful tool for exploring hotspots and substrate limitation in undisturbed subsoil. Soil Biology and Biochemistry 124, 210–217. doi:10.1016/j.soilbio.2018.06.021

Henrissat, B., 1991. A classification of glycosyl hydrolases based on amino acid sequence similarities. Biochemical Journal 280, 309–316. doi:10.1042/bj2800309

Hinsinger, P., 2001. Bioavailability of soil inorganic P in the rhizosphere as affected by root-induced chemical changes: A review, in: Plant and Soil. pp. 173–195. doi:10.1023/A:1013351617532

Hochholdinger, F., Wen, T.-J., Zimmermann, R., Chimot-Marolle, P., da Costa e Silva, O., Bruce, W., Lamkey, K.R., Wienand, U., Schnable, P.S., 2008. The maize (Zea mays L.) roothairless3 gene encodes a putative GPI-anchored, monocot-specific, COBRA-like protein that significantly affects grain yield. The Plant Journal 54, 888–898.

Holz, M., Zarebanadkouki, M., Carminati, A., Becker, J.N., Spohn, M., 2020. The effect of root hairs on rhizosphere phosphatase activity. Journal of Plant Nutrition and Soil Science 000, 1–7. doi:10.1002/jpln.201900426

Hu, L., Robert, C.A.M., Cadot, S., Zhang, X., Ye, M., Li, B., Manzo, D., Chervet, N., Steinger, T., Van Der Heijden, M.G.A., Schlaeppi, K., Erb, M., 2018. Root exudate metabolites drive plant-soil feedbacks on growth and defense by shaping the rhizosphere microbiota. Nature Communications 9, 1–13. doi:10.1038/s41467-018-05122-7

Hummel, C., Boitt, G., Santner, J., Lehto, N.J., Condron, L., Wenzel, W.W., 2021. Co-occurring increased phosphatase activity and labile P depletion in the rhizosphere of Lupinus angustifolius assessed with a novel, combined 2D-imaging approach. Soil Biology and Biochemistry 153. doi:10.1016/j.soilbio.2020.107963

Joergensen, R.G., Wichern, F., 2018. Alive and kicking: Why dormant soil microorganisms matter. Soil Biology and Biochemistry 116, 419–430. doi:10.1016/j.soilbio.2017.10.022

Kandeler, E., 1990. Characterization of free and adsorbed phosphatases in soils. Biology and Fertility of Soils 9, 199–202. doi:10.1007/BF00335808

Kielak, A.M., Barreto, C.C., Kowalchuk, G.A., van Veen, J.A., Kuramae, E.E., 2016. The ecology of Acidobacteria: Moving beyond genes and genomes. Frontiers in Microbiology 7, 1–16. doi:10.3389/fmicb.2016.00744

Koch, A.L., 1985. The macroeconomics of bacterial growth, in: Fletcher, M., Floodgate, G.D. (Eds.), Bacteria in Their Natural Environments. Academic Press, London, pp. 1–42.

Koshland, D.E., 2002. The Application and Usefulness of the Ratio kcat/KM. Bioorganic Chemistry 30, 211–213. doi:10.1006/bioo.2002.1246

Kuzyakov, Y., Xu, X., 2013. Competition between roots and microorganisms for nitrogen: Mechanisms and ecological relevance. New Phytologist 198, 656–669. doi:10.1111/nph.12235

Loeppmann, S., Blagodatskaya, E., Pausch, J., Kuzyakov, Y., 2016. Substrate quality affects kinetics and catalytic efficiency of exo-enzymes in rhizosphere and detritusphere. Soil Biology and Biochemistry 92, 111–118. doi:10.1016/j.soilbio.2015.09.020

Ma, X., Razavi, B.S., Holz, M., Blagodatskaya, E., Kuzyakov, Y., 2017. Warming increases hotspot areas of enzyme activity and shortens the duration of hot moments in the root-detritusphere. Soil Biology and Biochemistry 107, 226–233. doi:10.1016/j.soilbio.2017.01.009

Ma, X., Zarebanadkouki, M., Kuzyakov, Y., Blagodatskaya, E., Pausch, J., Razavi, B.S., 2018. Spatial patterns of enzyme activities in the rhizosphere: Effects of root hairs and root radius. Soil Biology and Biochemistry 118, 69–78. doi:10.1016/j.soilbio.2017.12.009

Martin, M., 2011. Cutadapt removes adapter sequences from high-throughput sequencing reads. EMBnet.Journal 17, 10. doi:10.14806/ej.17.1.200

Moorhead, D.L., Sinsabaugh, R.L., Hill, B.H., Weintraub, M.N., 2016. Vector analysis of ecoenzyme activities reveal constraints on coupled C, N and P dynamics. Soil Biology and Biochemistry 93, 1–7. doi:10.1016/j.soilbio.2015.10.019

Moscatelli, M.C., Lagomarsino, A., Garzillo, A.M.V., Pignataro, A., Grego, S., 2012. β-Glucosidase kinetic parameters as indicators of soil quality under conventional and organic cropping systems applying two analytical approaches. Ecological Indicators 13, 322–327. doi:10.1016/j.ecolind.2011.06.031

Nannipieri, P., Giagnoni, L., Renella, G., Puglisi, E., Ceccanti, B., Masciandaro, G., Fornasier, F., Moscatelli, M.C., Marinari, S., 2012. Soil enzymology: classical and molecular approaches. Biology and Fertility of Soils 48, 743–762. doi:10.1007/s00374-012-0723-0

Nottingham, A.T., Turner, B.L., Whitaker, J., Ostle, N., Bardgett, R.D., McNamara, N.P., Salinas, N., Meir, P., 2016. Temperature sensitivity of soil enzymes along an elevation gradient in the Peruvian Andes. Biogeochemistry 127, 217–230.

Okello, P.N., Petrović, K., Kontz, B., Mathew, F.M., 2019. Eight species of Fusarium cause root rot of corn (Zea mays) in South Dakota. Plant Health Progress 20, 38–43. doi:10.1094/PHP-11-18-0075-RS

Panikov, N.S., Blagodatsky, S.A., Blagodatskaya, J. V., Glagolev, M. V., 1992. Determination of microbial mineralization activity in soil by modified Wright and Hobbie method. Biology and Fertility of Soils 14, 280–287. doi:10.1007/BF00395464

Peiffer, J.A., Spor, A., Koren, O., Jin, Z., Green, S., Dangl, J.L., 2013. Diversity and heritability of the maize rhizosphere microbiome under field conditions. doi:10.1073/pnas.1302837110/-/DCSupplemental.www.pnas.org/cgi/doi/10.1073/pnas.1302837110

R Development Core Team, R., 2011. R: A Language and Environment for Statistical Computing. R Foundation for Statistical Computing, R Foundation for Statistical Computing. doi:10.1007/978-3-540-74686-7

Rakotoson, T., Holz, M., Wissuwa, M., 2020. Rhizosphere Phosphorus de fi ciency tolerance in Oryza sativa : Root and rhizosphere traits. Rhizosphere 14, 28–30. doi:10.1016/j.rhisph.2020.100198

Razavi, B.S., Blagodatskaya, E., Kuzyakov, Y., 2016a. Temperature selects for static soil enzyme systems to maintain high catalytic efficiency. Soil Biology and Biochemistry 97, 15–22. doi:10.1016/j.soilbio.2016.02.018

Razavi, B.S., Zarebanadkouki, M., Blagodatskaya, E., Kuzyakov, Y., 2016b. Rhizosphere shape of lentil and maize: Spatial distribution of enzyme activities. Soil Biology and Biochemistry 79, 229–237. doi:10.1016/j.soilbio.2016.02.020

Razavi, B.S., Zhang, X., Bilyera, N., Guber, A., Zarebanadkouki, M., 2019. Soil zymography: Simple and reliable? Review of current knowledge and optimization of the method. Rhizosphere. doi:10.1016/j.rhisph.2019.100161

Saleh, T., Kalodimos, C.G., 2017. Enzymes at work are enzymes in motion. Science 355, 247–248. doi:10.1126/science.aal4632

Sanaullah, M., Razavi, B.S., Blagodatskaya, E., Kuzyakov, Y., 2016. Spatial distribution and catalytic mechanisms of β-glucosidase activity at the root-soil interface. Biology and Fertility of Soils 52, 505–514. doi:10.1007/s00374-016-1094-8

Schlaeppi, K., Gross, J.J., Hapfelmeier, S., Erb, M., 2021. Plant chemistry and food web health. New Phytologist 231, 957–962.

Scranton, M.A., Yee, A., Park, S., Walling, L.L., 2012. Plant Leucine Aminopeptidases Moonlight as Molecular Chaperones to Alleviate Stress-induced Damage * □. Journal of Biological Chemistry 287, 18408–18417. doi:10.1074/jbc.M111.309500

Semenov, M., Blagodatskaya, E., Stepanov, A., Kuzyakov, Y., 2018. DNA-based determination of soil microbial biomass in alkaline and carbonaceous soils of semi-arid climate. Journal of Arid Environments 150, 54–61. doi:10.1016/j.jaridenv.2017.11.013

Seybold, H., Demetrowitsch, T.J., Hassani, M.A., Szymczak, S., Reim, E., Haueisen, J., Lübbers, L., Rühlemann, M., Franke, A., Schwarz, K., Stukenbrock, E.H., 2020. A fungal pathogen induces systemic susceptibility and systemic shifts in wheat metabolome and microbiome composition. Nature Communications 11, 1910. doi:10.1038/s41467-020-15633-x

Silberbush, M., Barber, S.A., 1983. Sensitivity of simulated phosphorus uptake to parameters used by a mechanistic-mathematical model. Plant and Soil 74, 93–100. doi:10.1007/BF02178744

Sinsabaugh, R.L., Follstad Shah, J.J., 2012. Ecoenzymatic Stoichiometry and Ecological Theory. Annual Review of Ecology, Evolution, and Systematics 43, 313–343. doi:10.1146/annurev-ecolsys-071112-124414

Spohn, M., Carminati, A., Kuzyakov, Y., 2013. Soil zymography - A novel in situ method for mapping distribution of enzyme activity in soil. Soil Biology and Biochemistry 58, 275–280. doi:10.1016/j.soilbio.2012.12.004

Tian, P., Razavi, B.S., Zhang, X., Wang, Q., Blagodatskaya, E., 2020. Microbial growth and enzyme kinetics in rhizosphere hotspots are modulated by soil organics and nutrient availability. Soil Biology and Biochemistry 141. doi:10.1016/j.soilbio.2019.107662

Vassão, D.G., Wielsch, N., Gomes, A.M. de M.M., Gebauer-Jung, S., Hupfer, Y., Svatoš, A., Gershenzon, J., 2018. Plant defensive β-Glucosidases resist digestion and sustain activity in the gut of a lepidopteran herbivore. Frontiers in Plant Science 9, 1–13. doi:10.3389/fpls.2018.01389

Vetterlein, D., Carminati, A., Kögel-Knabner, I., Bienert, G.P., Smalla, K., Oburger, E., Schnepf, A., Banitz, T., Tarkka, M.T., Schlüter, S., 2020. Rhizosphere spatiotemporal organisation - a key to rhizosphere functions. Frontiers in Agronomy 2, 8.

Vetterlein, D., Lippold, E., Schreiter, S., Phalempin, M., Fahrenkampf, T., Hochholdinger, F., Marcon, C., Tarkka, M., Oburger, E., Ahmed, M., Javaux, M., Schlüter, S., 2021. Experimental platforms for the investigation of spatiotemporal patterns in the rhizosphere—Laboratory and field scale. Journal of Plant Nutrition and Soil Science 184, 35–50. doi:10.1002/jpln.202000079

Vitousek, P.M., Howarth, R.W., 1990. Nitrogen limitation on land and in the sea : How can it occur ? 87–115.

Wen, T.-J., Schnable, P.S., 1994. Analyses of Mutants of Three Genes that Influence Root Hair Development in Zea mays (Gramineae) Suggest that Root Hairs are Dispensable. American Journal of Botany 81, 833. doi:10.2307/2445764

Zhang, X., Kuzyakov, Y., Zang, H., Dippold, M.A., Shi, L., Spielvogel, S., Razavi, B.S., 2020. Rhizosphere hotspots: Root hairs and warming control microbial efficiency, carbon utilization and energy production. Soil Biology and Biochemistry 107872. doi:10.1016/j.soilbio.2020.107872

Zhang, X., Myrold, D.D., Shi, L., Kuzyakov, Y., Dai, H., Thi, D., Hoang, T., Dippold, M.A., Meng, X., Song, X., Li, Z., Zhou, J., Razavi, B.S., 2021. Resistance of microbial community and its functional sensitivity in the rhizosphere hotspots to drought. Soil Biology and Biochemistry 161, 108360. doi:10.1016/j.soilbio.2021.108360

Zhao, Y., Fu, W., Hu, C., Chen, G., Xiao, Z., Chen, Y., Wang, Z., Cheng, H., 2021. Variation of rhizosphere microbial community in continuous mono-maize seed production. Scientific Reports 11, 1–13. doi:10.1038/s41598-021-81228-1

Supporting information

Table S1. Barcode to sample assignments

Primer*	Padding	Barcode	Primer Sequence	Oligo Sequence 5' > 3'	Length
FORWARD PRIMER					
515F			GTGYCAGCMGCCGCGGTAA	GTGYCAGCMGCCGCGGTAA	20
F1_515F	GGTAG	**ACCTCAGT**	GTGYCAGCMGCCGCGGTAA	GGTAGACCTCAGTGTGYCAGCMGCCGCGGTAA	33
F2_515F	GGTAG	**CTGATGAG**	GTGYCAGCMGCCGCGGTAA	GGTAGCTGATGAGGTGYCAGCMGCCGCGGTAA	33
F3_515F	GGTAG	**TATCGCGA**	GTGYCAGCMGCCGCGGTAA	GGTAGTATCGCGAGTGYCAGCMGCCGCGGTAA	33
F4_515F	GGTAG	**GATTGTCC**	GTGYCAGCMGCCGCGGTAA	GGTAGGATTGTCCGTGYCAGCMGCCGCGGTAA	33
F5_515F	GGTAG	**AATCGCTG**	GTGYCAGCMGCCGCGGTAA	GGTAGAATCGCTGGTGYCAGCMGCCGCGGTAA	33
F6_515F	GGTAG	**CGAATTGC**	GTGYCAGCMGCCGCGGTAA	GGTAGCGAATTGCGTGYCAGCMGCCGCGGTAA	33
F7_515F	GGTAG	**GGCATTCT**	GTGYCAGCMGCCGCGGTAA	GGTAGGGCATTCTGTGYCAGCMGCCGCGGTAA	33
F8_515F	GGTAG	**TTCGAAGC**	GTGYCAGCMGCCGCGGTAA	GGTAGTTCGAAGCGTGYCAGCMGCCGCGGTAA	33
REVERSE PRIMER					
806R			GGACTACNVGGGTWTCTAAT	GGACTACNVGGGTWTCTAAT	20
R1_806R	GGTAG	**TGTCAGTG**	GGACTACNVGGGTWTCTAAT	GGTAGTGTCAGTGGGACTACNVGGGTWTCTAAT	33
R2_806R	GGTAG	**GTGTCCTT**	GGACTACNVGGGTWTCTAAT	GGTAGGTGTCCTTGGACTACNVGGGTWTCTAAT	33
R3_806R	GGTAG	**CTATGCCT**	GGACTACNVGGGTWTCTAAT	GGTAGCTATGCCTGGACTACNVGGGTWTCTAAT	33
R4_806R	GGTAG	**AAGCGACT**	GGACTACNVGGGTWTCTAAT	GGTAGAAGCGACTGGACTACNVGGGTWTCTAAT	33
R5_806R	GGTAG	**ATCTGACC**	GGACTACNVGGGTWTCTAAT	GGTAGATCTGACCGGACTACNVGGGTWTCTAAT	33
R6_806R	GGTAG	**CGTAGATG**	GGACTACNVGGGTWTCTAAT	GGTAGCGTAGATGGGACTACNVGGGTWTCTAAT	33

**Earth microbiome project (EMP) primers (updated 16S V4 Primers 515F (Parada)–806R (Apprill))*

***Table S2**. Beta diversity by PERMANOVA analysis. Significant (Pr<0.1) values are marked in bold.*

	Df	Sum of Sqs	R^2	F	Pr (>F)
Fungi			All genotypes		
Spot	1	0.1514	0.07	1.181	0.212
Genotype	2	0.3735	0.16	1.457	**0.075**
Spot*Genotype	1	0.1059	0.05	0.8259	0.747
Residual	13	1.666	0.72	NA*	NA
Total	17	2.297	1	NA	NA
			WT		
Spot	1	0.1782	0.15	1.03	0.428
Residua	6	1.038	0.85	NA	NA
Total	7	1.216	1	NA	NA
l			*rth3*		
Spot	1	0.05596	0.10	0.7026	0.973
Residua	6	0.4779	0.90	NA	NA
Total	7	0.5338	1	NA	NA
Bacteria			All genotypes		
Spot	1	0.266	0.14	3.636	**0.005**
Genotype	2	0.1786	0.10	1.221	0.195
Spot*Genotype	2	0.1587	0.09	1.085	0.31
Residual	17	1.244	0.67	NA	NA
Total	22	1.847	1	NA	NA
			WT		
Spot	1	0.09522	0.20	1.476	**0.023**
Residua	6	0.3871	0.80	NA	NA
Total	7	0.4823	1	NA	NA
			rth3		
Spot	1	0.07297	0.15	1.082	0.229
Residua	6	0.4048	0.85	NA	NA
Total	7	0.4777	1	NA	NA
			bx1		
Spot	1	0.1358	0.30	2.137	**0.032**
Residua	5	0.3178	0.70	NA	NA
Total	6	0.4536	1	NA	NA

**NA – non available.*

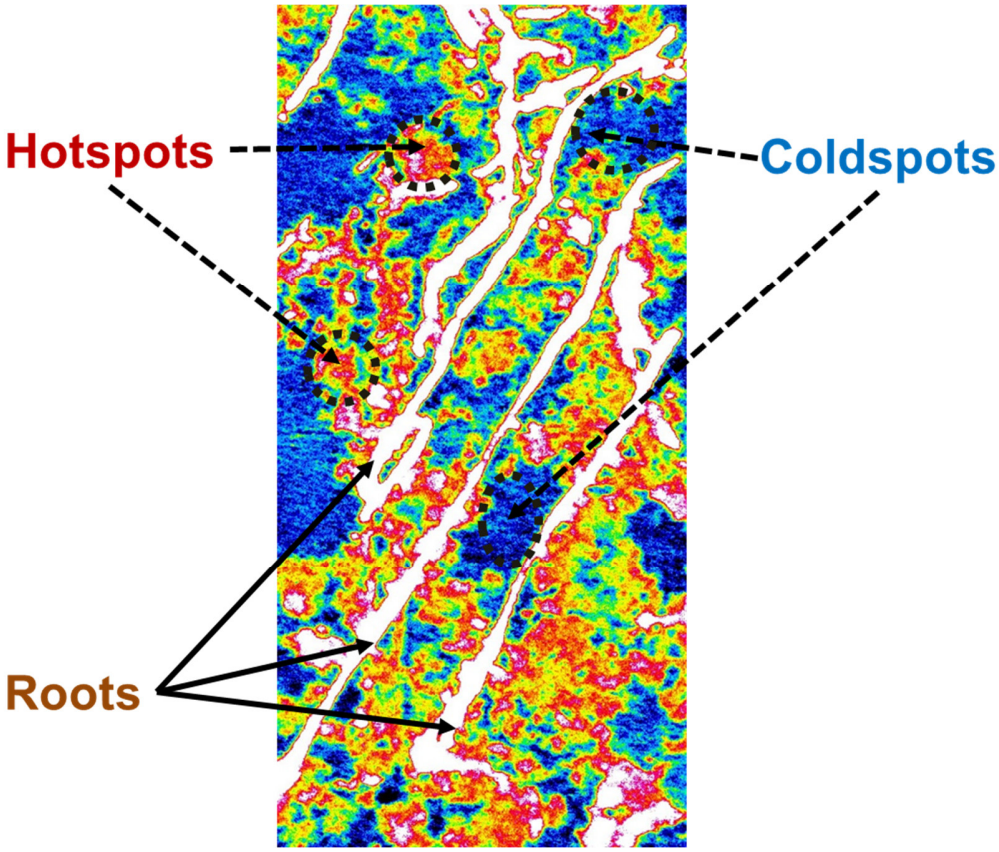

Figure S1. An exemplary image of the hot- and coldspot localization of β-glucosidase activity in the rhizosphere.

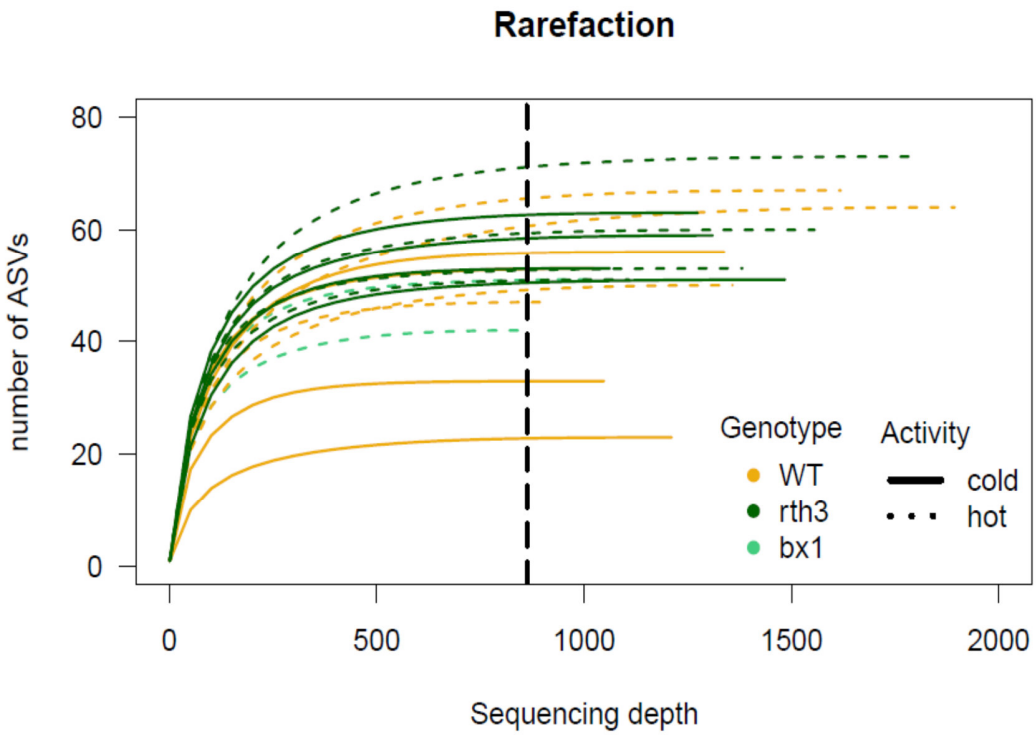

a)

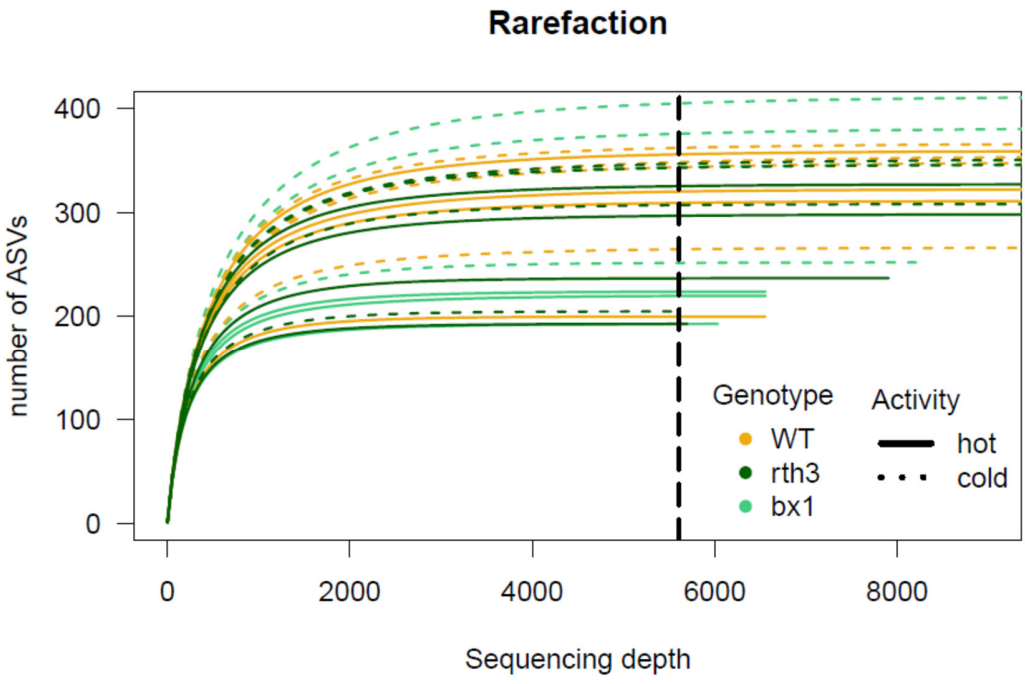

b)

Figure S2. Rarefaction analysis of the soil hot- and coldspot fungal (a) and bacterial (b) microbiome. The sampling intensity plot shows the detected ASVs number (y-axis) depending on the sequencing depth-(x-axis). When the curves reach plateau at sequencing depth, they were sufficiently deeply sequenced. Vertical black line marks the sample with the smallest number of sequences across all samples.

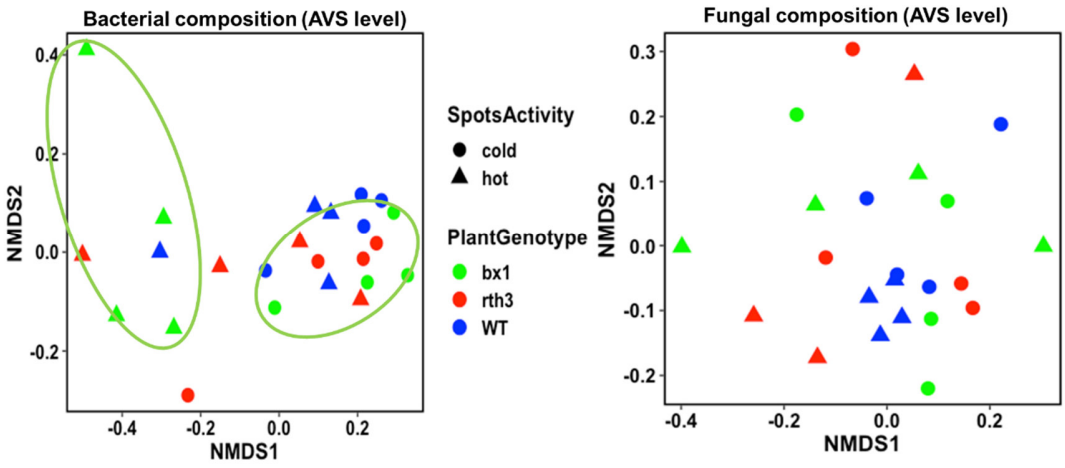

Figure S3. Non-metric multidimensional scaling (NMDS) plot of the bacterial and fungal community structure associated with rhizosphere hot or coldspots of the maize genotypes (WT, *rth3, bx1*).

3 Acknowledgements

I would like to thank many people who kindly supported me on the way to doctoral degree, and without whom this PhD study would not been done.

First of all, I sincerely thank Jun.-Prof. Dr. Bahar S. Razavi for accepting me as her doctoral student and giving this great chance to participate in an exciting research project, the opportunity to develop my own ideas, as well as for being always supportive and available for any advice at each step and during the whole period of this journey. I further thank Prof. Dr. Sandra Spielvogel and Prof. Dr. Michaela A. Dippold for their great support of my scientific work and very valuable input to the studies. Thanks for many suggestions to my manuscripts that made me think and dig deeper into the topic. Prof. Dr. Yakov Kuzyakov and Dr. Irina Kuzyakova supported me greatly on the topic of statistical analysis of soil images, which appears because of my curiosity and strong willingness to find a better way. Thank you very much for your encouragement and kind help in this challenging topic.

I acknowledge DFG for financial support of the project (403670038) within the framework of the priority program 2089 ‘Rhizosphere Spatiotemporal Organization – a Key to Rhizosphere Functions’ and also the Interfaculty Research Cooperation “One Health” at University of Bern for funding Sub-Project 4. Further I acknowledge the ICON imaging station of the Paul Scherrer Institute, Villigen, Switzerland for their facilities.

It was my pleasure to work closely with the groups from Uni Bayreuth/ Uni Zurich (DE/CH) (Patrick Dudek, Dr. Mutez Ahmed and Prof. Dr. Andrea Carminaty), from BOKU, Vienna (AT) (Dr. Eva Oburger and Christina Hummel), Uni Göttingen (DE) (Dr. Lichao Fan, Dr. Callum C. Banfield), Uni Bern/Basel (CH) (Prof. Dr. Klaus Schlaeppi, Veronica Caggia and Jan Waelchli), INRAE, Montpellier (FR) (Gabriele Daudin), Uni Michigan (USA) (Dr. Andrey Guber), Bangor Uni (UK) (Dr. Lucy Greenfield), UFZ, Halle (DE) (Eva Lippold, Dr. Steffen Schlütter and Prof. Dr. Doris Vetterlein). I would like to thank all of you for valuable input, always useful and constructive comments, and multidisciplinary insight into our join studies. I have learnt a lot about new methods from you!

I thank Xuechen Zhang who was always with me during many trips, fieldwork and experiments. My further thanks goes to Christina Hummel who was my colleague for field imaging experiment and my virtual officemate during lockdowns. I am very thankful for our long and fruitful scientific (and other) discussions, as well as for her great help with the German version of the

summary. Christina and Xuechen, your presence in my PhD life is very much appreciated. I was also very lucky to share my office with amazing Sara Loftus and Nina Hennings, who became my friends. Thanks for your German communication lessons during the breaks, for always-helpful advices on many aspects of scientific and social life and for creating the best environment in our office, I can ever wish.

Finally, I thank my son Rodion, husband, mother, brother, and parents in law for their sincere support of my willingness to obtain the doctoral degree. Especially I appreciate their love, non-stop encouragement and kind help with everything I needed during the PhD study.

خیلی ممنونم. Vielen Dank! Thank you! Merci!

謝謝！ Большое спасибо! Щиро дякую! Gracie!

4 Declarations

I hereby declare that

i. apart from the supervisor's guidance the content and design of the thesis is all my own work;

ii. the thesis has not been submitted either partially or wholly as part of a doctoral degree to another examining body and it has not been published or submitted for publication;

iii. the thesis has been prepared with regard to the Rules of Good Scientific Practice of the German Research Foundation;

iv. an academic degree has never been withdrawn.

Kiel,_____ (date) _____ (signature)